Lecture 4

Detonation simulation

Course *Block-structured Adaptive Finite Volume Methods for Shock-Induced Combustion Simulation*

Ralf Deiterding
German Aerospace Center (DLR)
Institute for Aerodynamics and Flow Technology
Bunsenstr. 10, Göttingen, Germany

E-mail: ralf.deiterding@dlr.de

Outline

Outline

Outline

Planar ZND Structure

Steady situation under Galilean transformation:

$$\frac{\partial}{\partial x'}(\rho u') = 0$$

$$\frac{\partial}{\partial x'}(\rho u'^2 + p) = 0$$

$$\frac{\partial}{\partial x'}(u' \rho H) = 0$$

$$\frac{\partial Y_i}{\partial x'} = \frac{W_i \dot{\omega}_i \left(\rho \frac{Y_1}{W_1}, \ldots, \rho \frac{Y_K}{W_K}, T\right)}{\rho u'}$$

CJ-detonation of $\mathrm{H_2} : \mathrm{O_2} : \mathrm{Ar}$ with molar ratios $2 : 1 : 7$ at $T_0 = 298\,\mathrm{K}$ and $p_0 = 6.67\,\mathrm{kPa}$, $d_{CJ} \approx 1627\,\mathrm{m/s}$.

$t_{ig} \approx 3.55\,\mu\mathrm{s}$, $u'_{vN} \approx 395.5\,\mathrm{m/s}$, $l_{ig} \approx 0.14\,\mathrm{cm}$.

Cf. vtf/amroc/clawpack/applications/euler_chem/1d/ModelDetonation

Planar ZND Structure

Steady situation under Galilean transformation:

$$\frac{\partial}{\partial x'}(\rho u') = 0$$

$$\frac{\partial}{\partial x'}(\rho u'^2 + p) = 0$$

$$\frac{\partial}{\partial x'}(u' \rho H) = 0$$

$$\frac{\partial Y_i}{\partial x'} = \frac{W_i \dot{\omega}_i \left(\rho \frac{Y_1}{W_1}, \ldots, \rho \frac{Y_K}{W_K}, T\right)}{\rho u'}$$

CJ-detonation of $\mathrm{H_2} : \mathrm{O_2} : \mathrm{Ar}$ with molar ratios $2 : 1 : 7$ at $T_0 = 298\,\mathrm{K}$ and $p_0 = 6.67\,\mathrm{kPa}$, $d_{CJ} \approx 1627\,\mathrm{m/s}$.

$t_{ig} \approx 3.55\,\mu\mathrm{s}$, $u'_{vN} \approx 395.5\,\mathrm{m/s}$, $l_{ig} \approx 0.14\,\mathrm{cm}$.

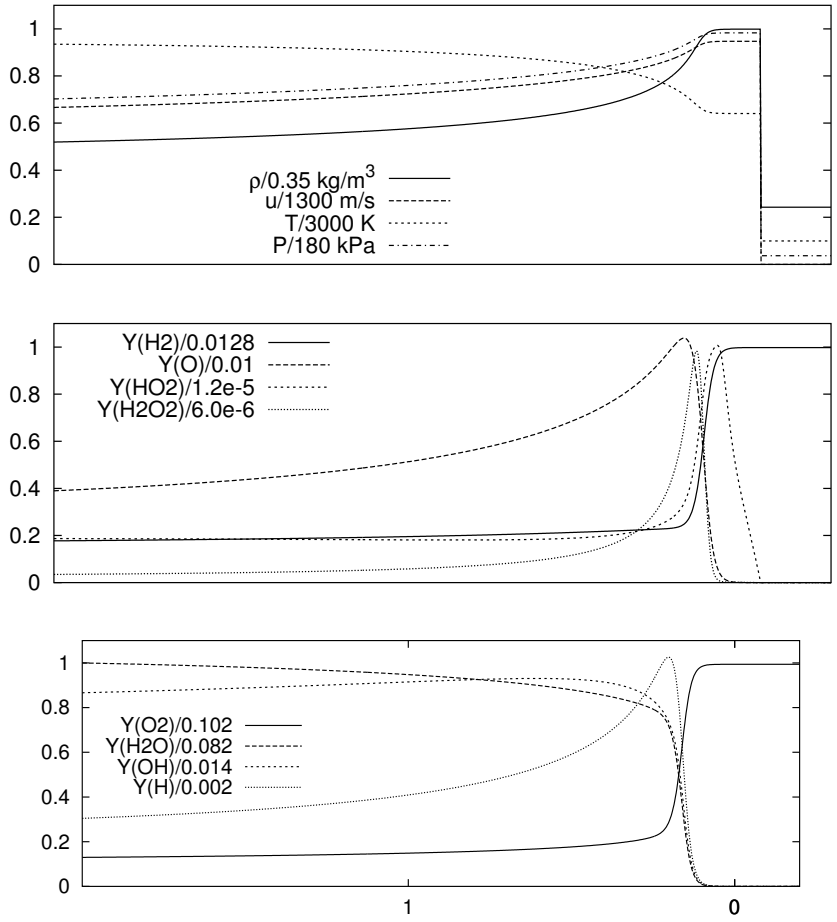

Cf. vtf/amroc/clawpack/applications/euler_chem/1d/ModelDetonation

Detonation cell structure in 2D - Regular instability

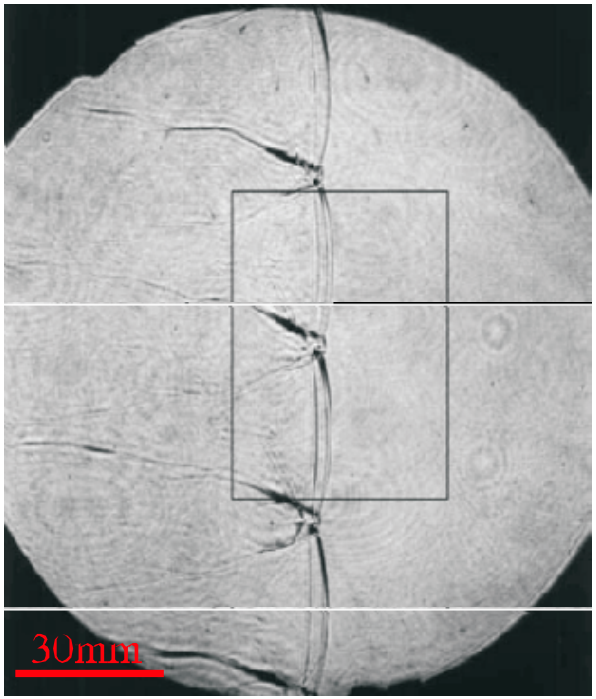

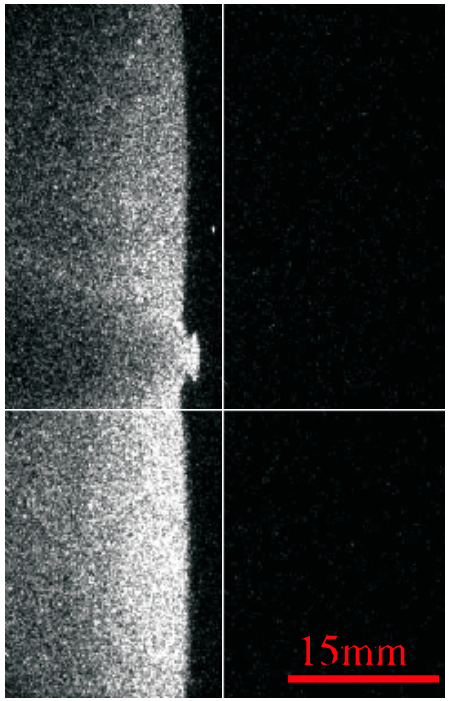

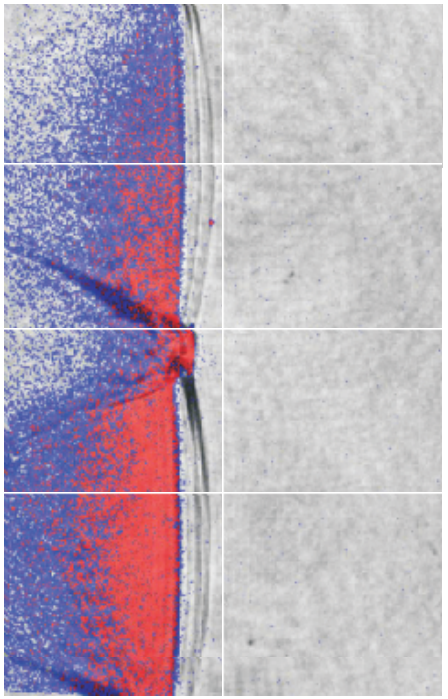

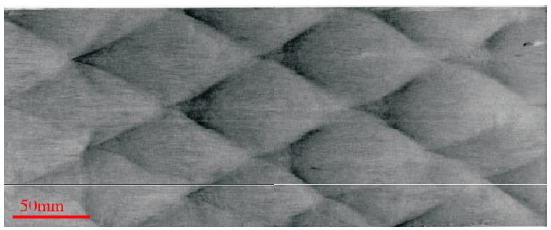

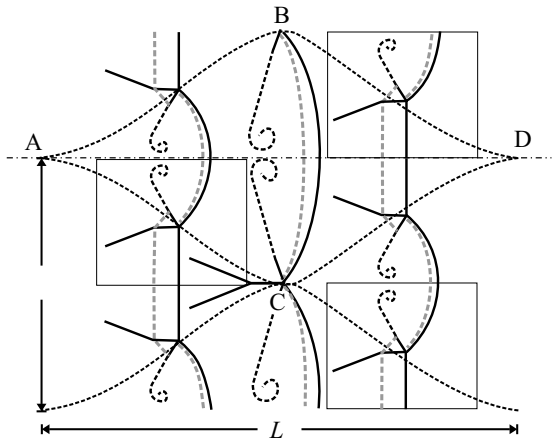

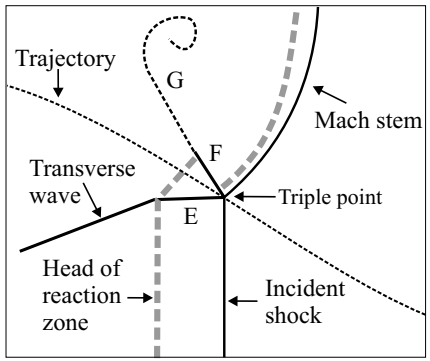

E: Reflected shock. F: Slip line. G: Diffusive extension of slip line.

Transverse detonation structure - irregular instability

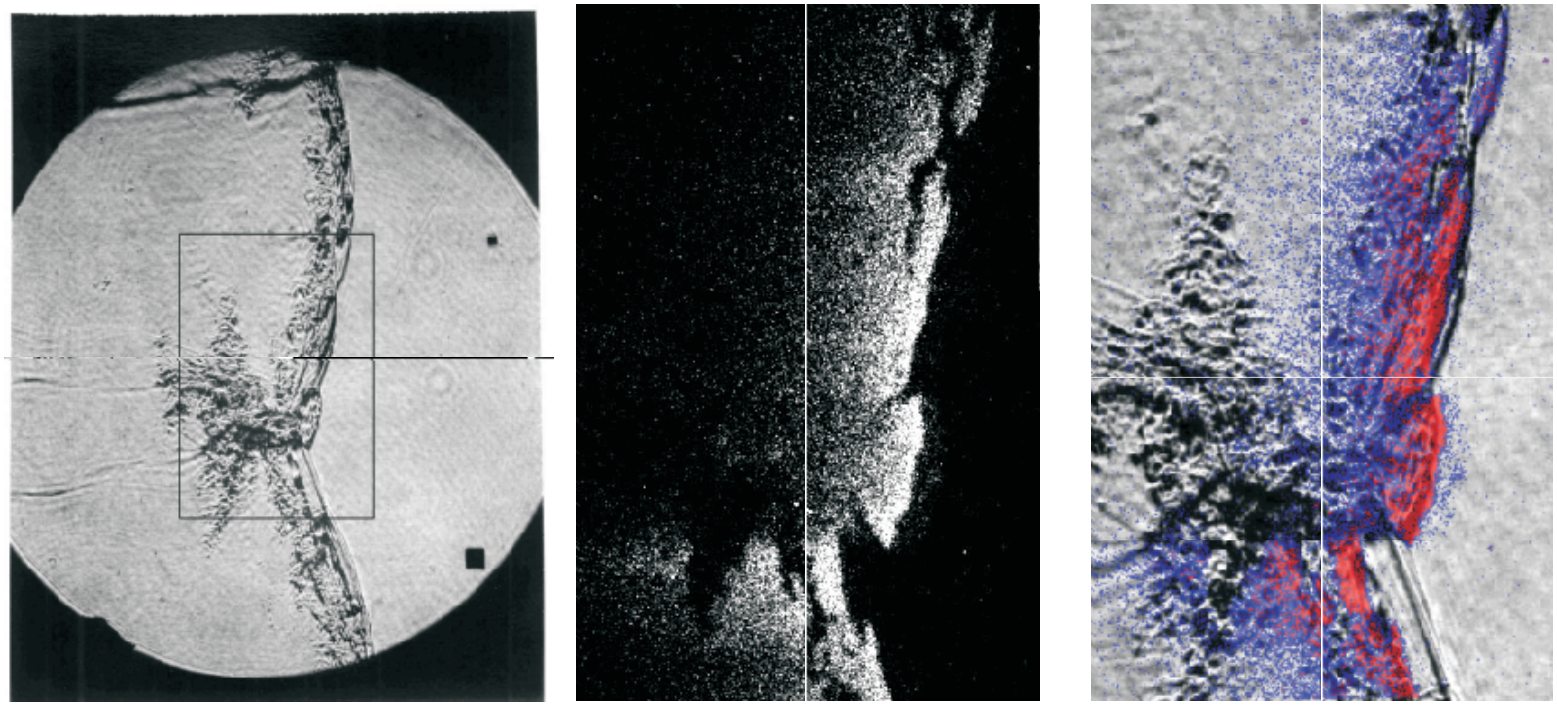

Simulation of regular structures

- CJ detonation for $H_2 : O_2 : Ar$ (2:1:7) at $T_0 = 298\,\mathrm{K}$ and $p_0 = 10\,\mathrm{kPa}$, cell width $1.6\,\mathrm{cm}$
- Perturb 1d ZND solution with unreacted high-pressure pocket behind front
- Triple point trajectories by tracking max $|\omega|$ on auxiliary mesh shifted through grid with CJ velocity. $\omega = \frac{\partial v}{\partial x} - \frac{\partial u}{\partial y}$
- SAMR simulation with 4 additional levels (2,2,2,4), $67.6\,\mathrm{Pts}/l_{ig}$
- Configuration similar to Oran et al., J. Combustion and Flame 113, 1998.

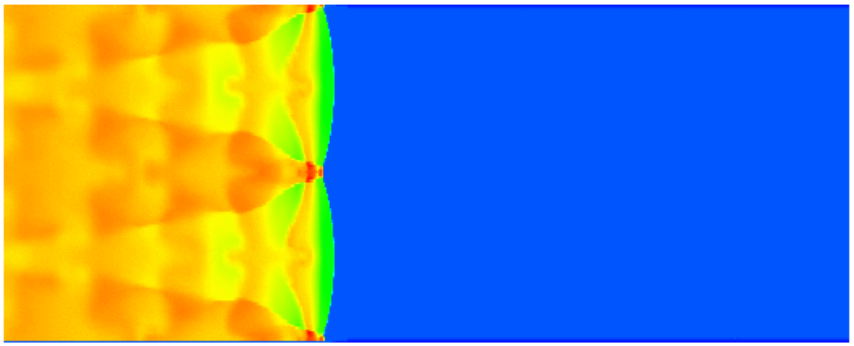

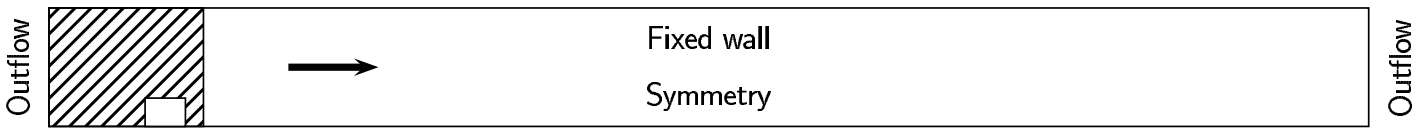

Simulation of regular structures

- CJ detonation for $H_2 : O_2 : Ar$ (2:1:7) at $T_0 = 298\,\mathrm{K}$ and $p_0 = 10\,\mathrm{kPa}$, cell width $1.6\,\mathrm{cm}$
- Perturb 1d ZND solution with unreacted high-pressure pocket behind front
- Triple point trajectories by tracking max $|\omega|$ on auxiliary mesh shifted through grid with CJ velocity. $\omega = \frac{\partial v}{\partial x} - \frac{\partial u}{\partial y}$
- SAMR simulation with 4 additional levels (2,2,2,4), $67.6\,\mathrm{Pts}/l_{ig}$
- Configuration similar to Oran et al., J. Combustion and Flame 113, 1998.

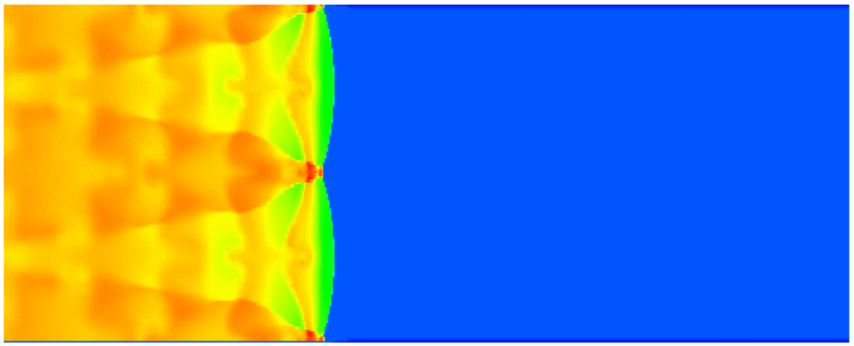

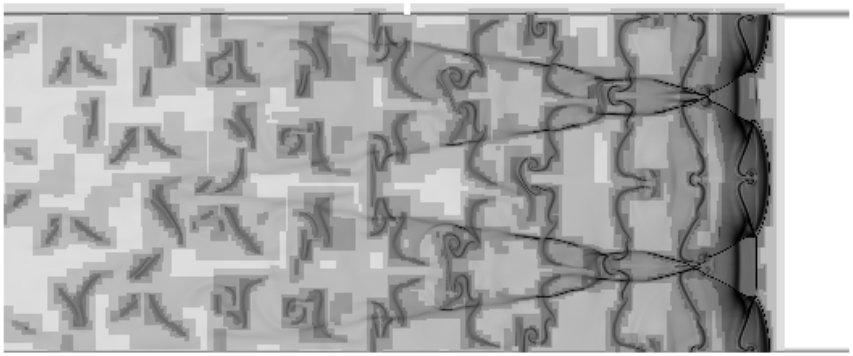

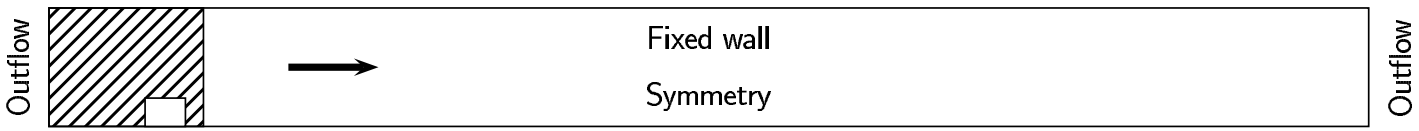

Simulation of regular structures

- CJ detonation for $H_2 : O_2 : Ar$ (2:1:7) at $T_0 = 298\,\mathrm{K}$ and $p_0 = 10\,\mathrm{kPa}$, cell width $1.6\,\mathrm{cm}$
- Perturb 1d ZND solution with unreacted high-pressure pocket behind front
- Triple point trajectories by tracking max $|\omega|$ on auxiliary mesh shifted through grid with CJ velocity. $\omega = \frac{\partial v}{\partial x} - \frac{\partial u}{\partial y}$
- SAMR simulation with 4 additional levels (2,2,2,4), $67.6\,\mathrm{Pts}/l_{ig}$
- Configuration similar to Oran et al., J. Combustion and Flame 113, 1998.

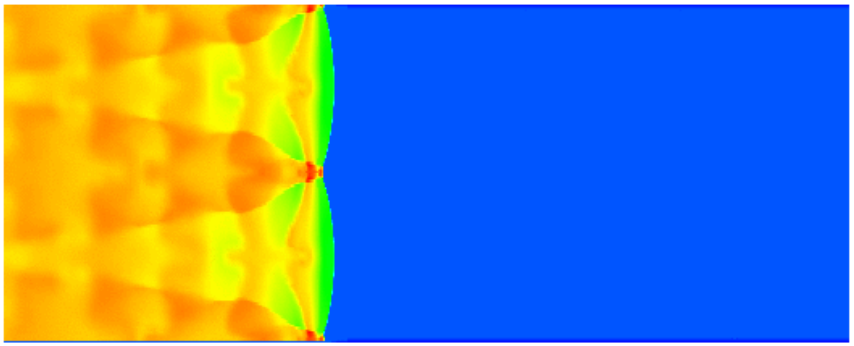

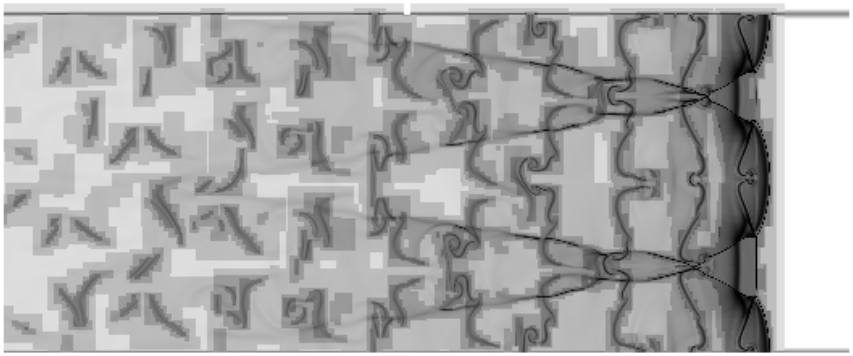

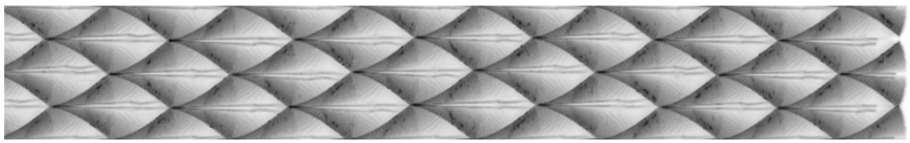

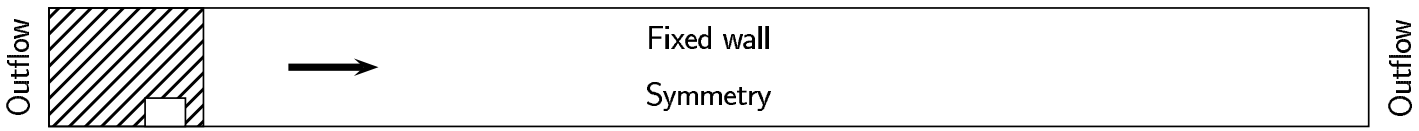

Simulation of regular structures

- CJ detonation for $H_2 : O_2 : Ar$ (2:1:7) at $T_0 = 298\,\mathrm{K}$ and $p_0 = 10\,\mathrm{kPa}$, cell width $1.6\,\mathrm{cm}$
- Perturb 1d ZND solution with unreacted high-pressure pocket behind front
- Triple point trajectories by tracking max $|\omega|$ on auxiliary mesh shifted through grid with CJ velocity. $\omega = \dfrac{\partial v}{\partial x} - \dfrac{\partial u}{\partial y}$
- SAMR simulation with 4 additional levels (2,2,2,4), $67.6\,\mathrm{Pts}/l_{ig}$
- Configuration similar to Oran et al., J. Combustion and Flame 113, 1998.

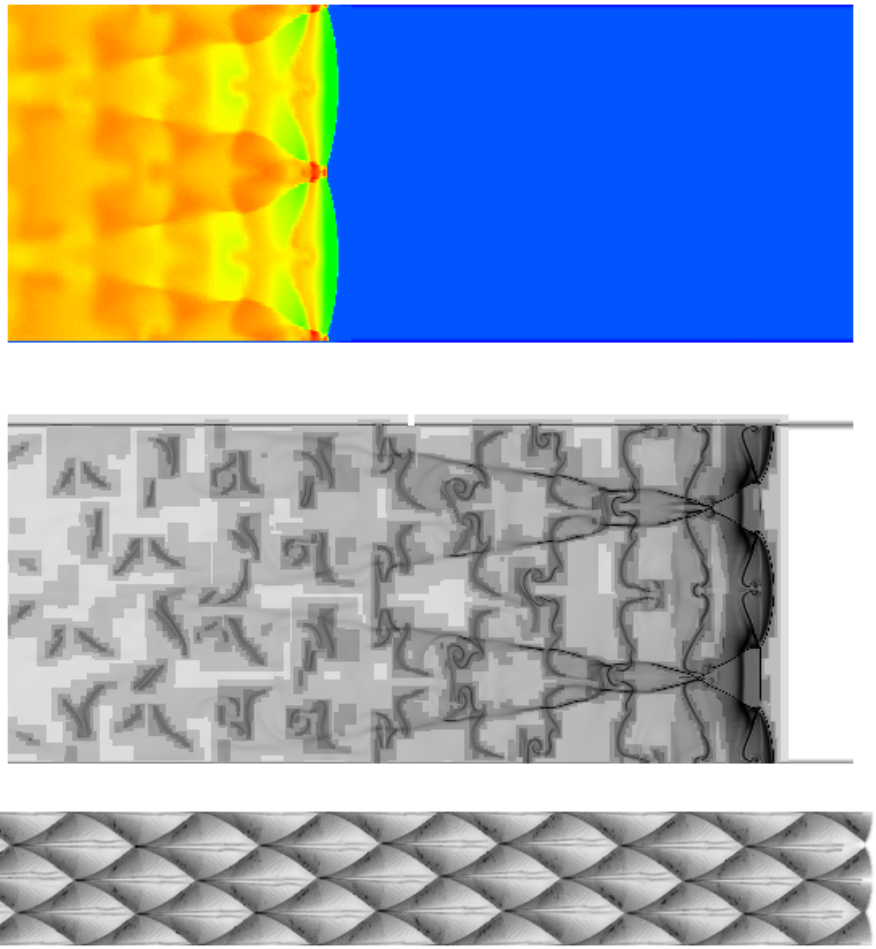

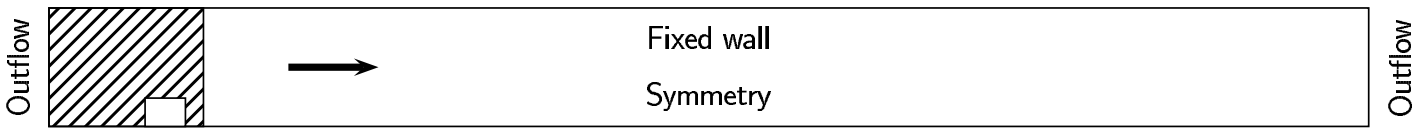

vtf/amroc/clawpack/applications/euler_chem/2d/StrehlowH2O2/StatDet

Detonation diffraction

- CJ detonation for $H_2 : O_2 : Ar/2 : 1 : 7$ at $T_0 = 298\,\mathrm{K}$ and $p_0 = 10\,\mathrm{kPa}$. Cell width $\lambda_c = 1.6\,\mathrm{cm}$
- Adaption criteria (similar as before):
  1. Scaled gradients of ρ and p
  2. Error estimation in Y_i by Richardson extrapolation
- $25\,\mathrm{Pts}/l_{ig}$. 5 refinement levels (2,2,2,4).
- Adaptive computations use up to $\sim 2.2\,\mathrm{M}$ instead of $\sim 150\,\mathrm{M}$ cells (uniform grid)
- $\sim 3850\,\mathrm{h}$ CPU ($\sim 80\,\mathrm{h}$ real time) on 48 nodes Athlon 1.4GHz

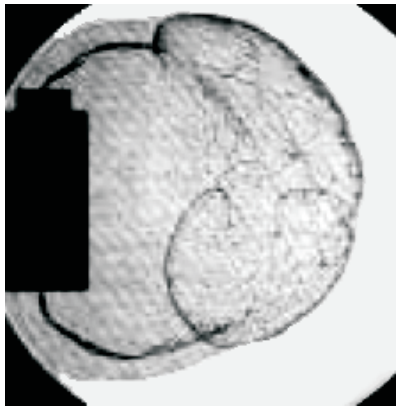

E. Schultz. *Detonation diffraction through an abrupt area expansion*. PhD thesis, California Institute of Technology, Pasadena, California, April 2000.

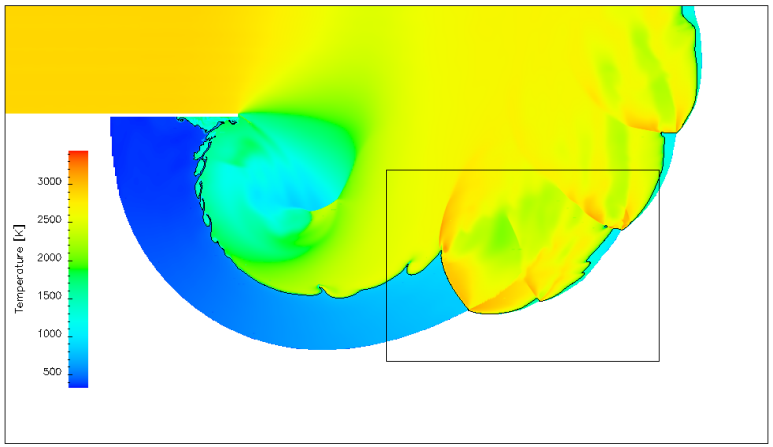

Detonation diffraction - adaptation

Final distribution to 48 nodes and density distribution on four refinement levels

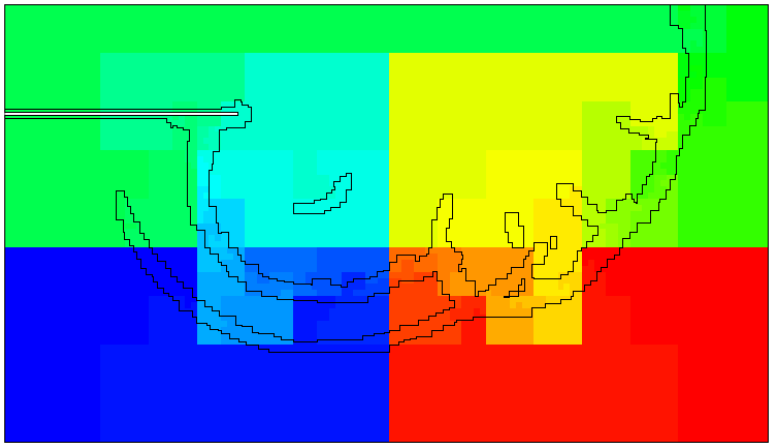

Detonation diffraction - adaptation

Final distribution to 48 nodes and density distribution on four refinement levels

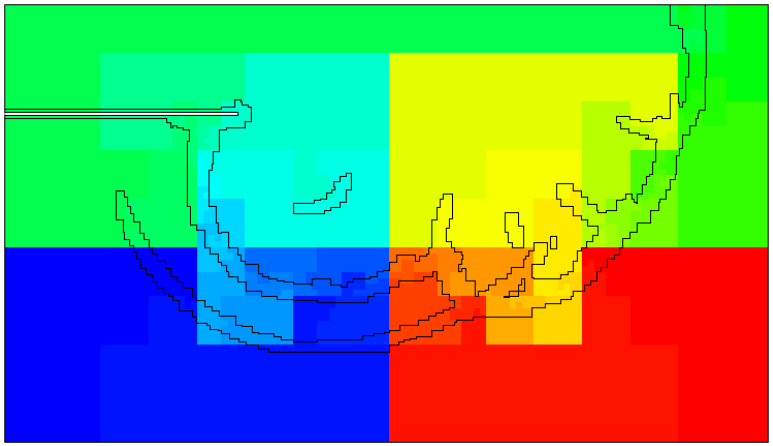

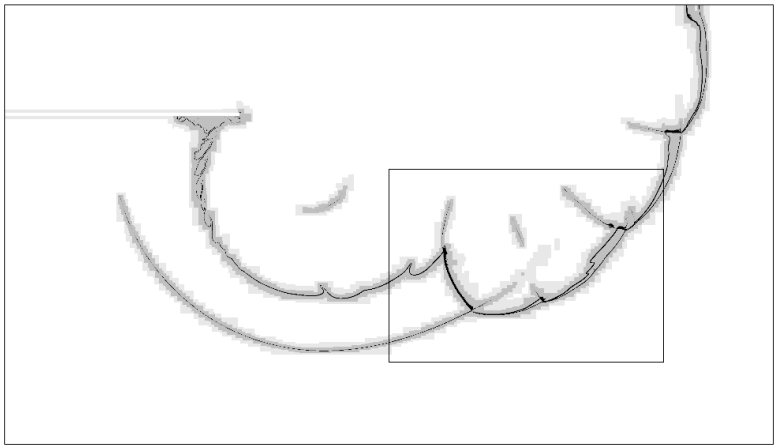

Detonation diffraction - adaptation

Final distribution to 48 nodes and density distribution on four refinement levels

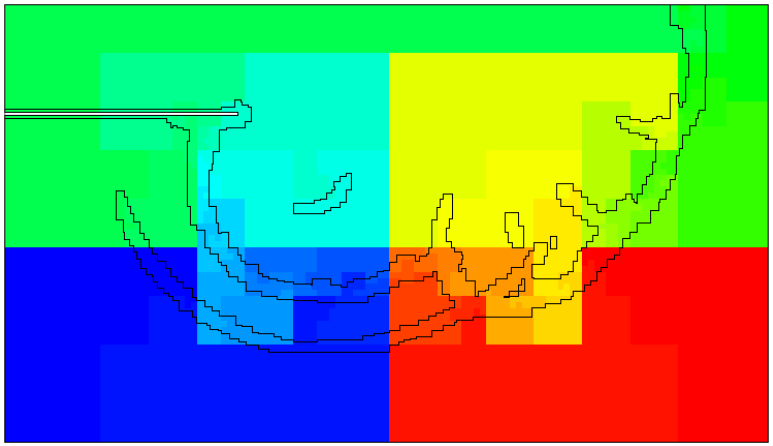

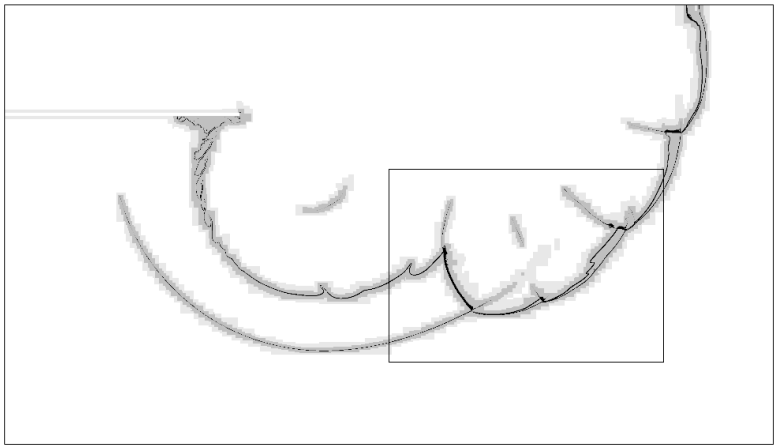

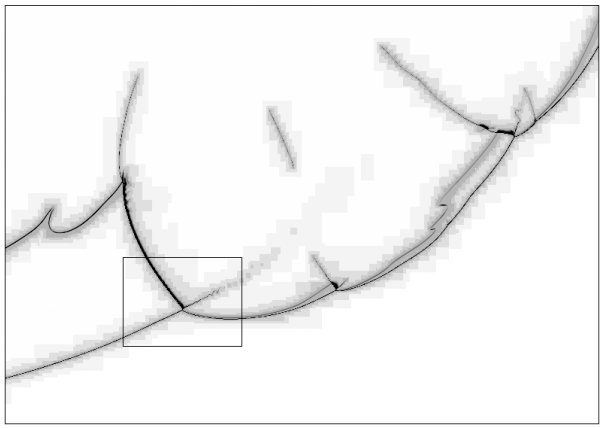

Detonation diffraction - adaptation

Final distribution to 48 nodes and density distribution on four refinement levels

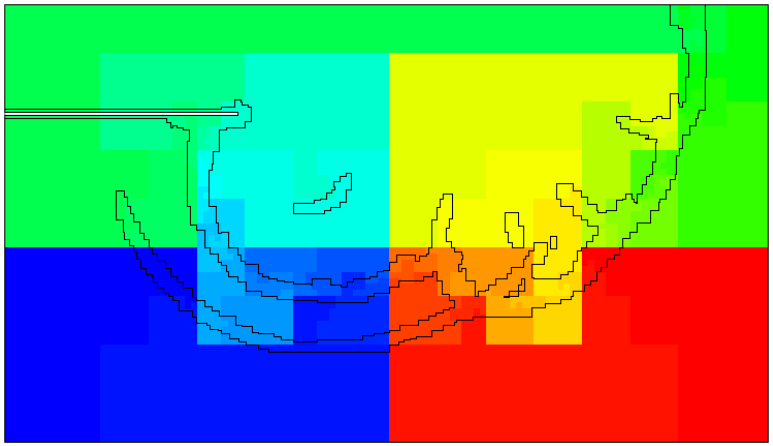

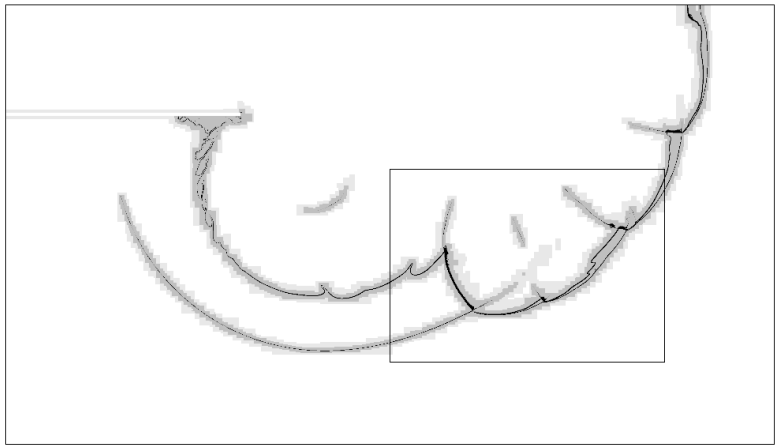

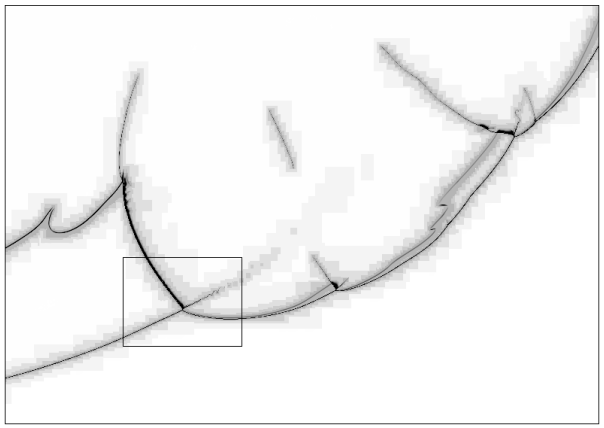

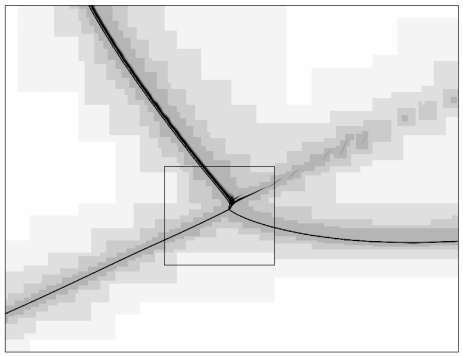

Detonation diffraction - adaptation

Final distribution to 48 nodes and density distribution on four refinement levels

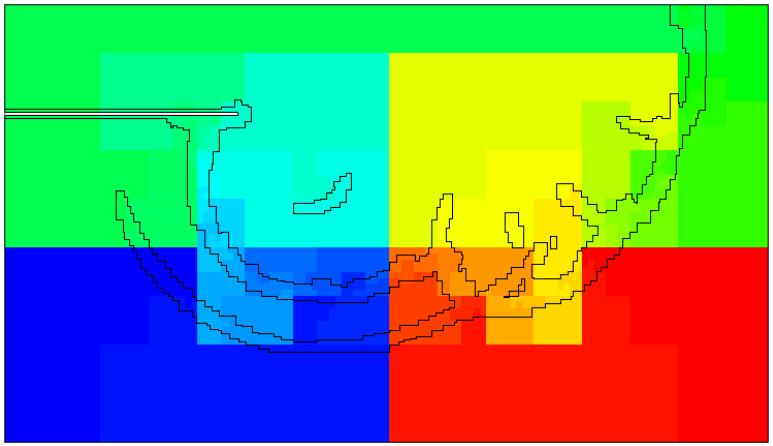

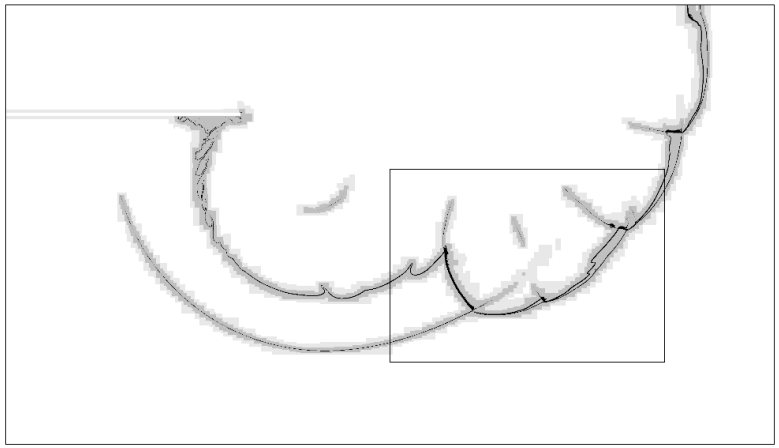

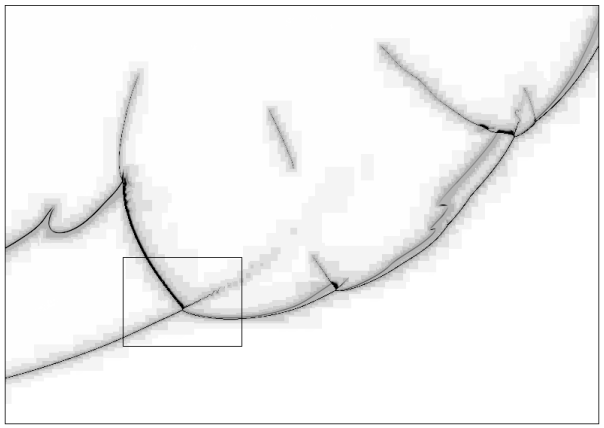

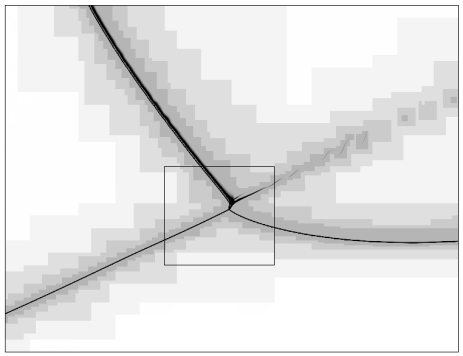

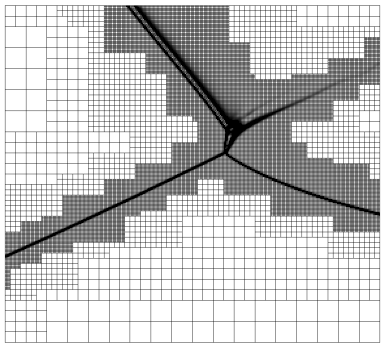

Detonation diffraction - adaptation

Final distribution to 48 nodes and density distribution on four refinement levels

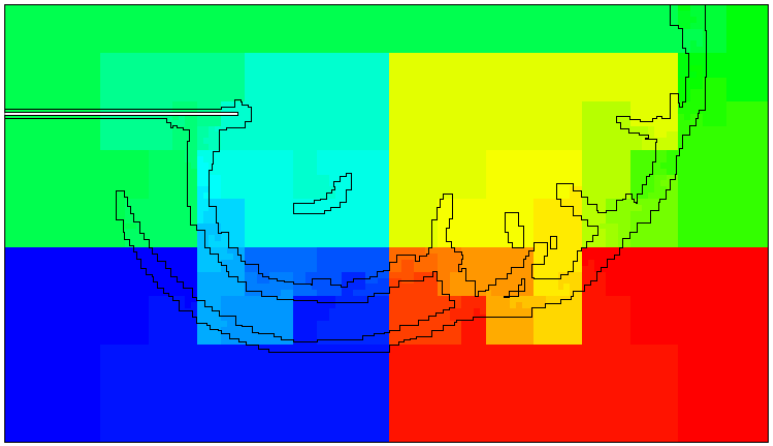

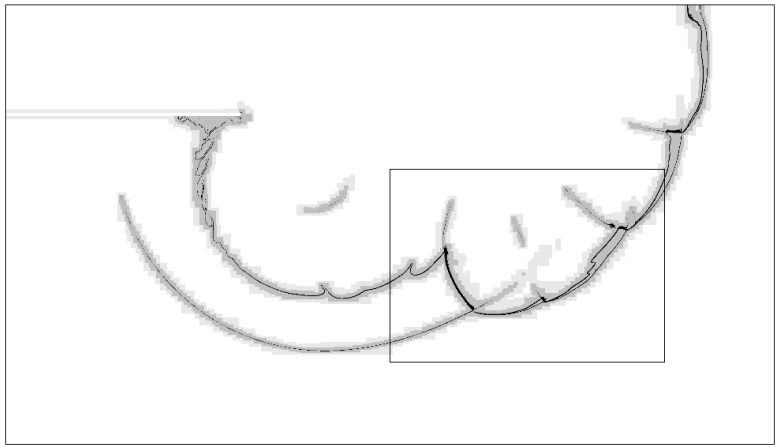

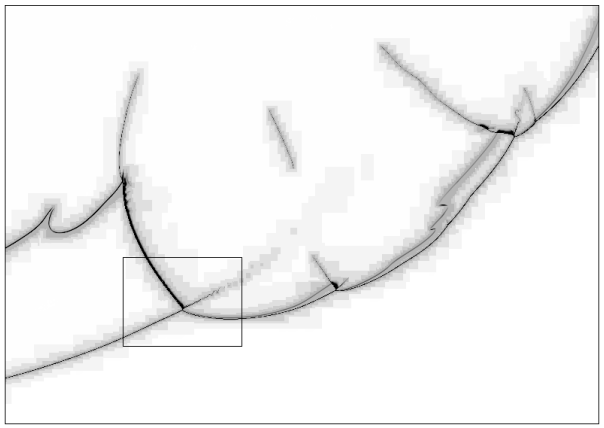

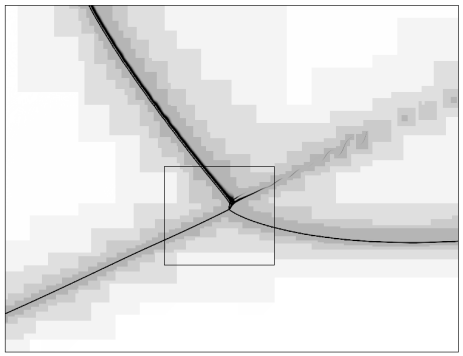

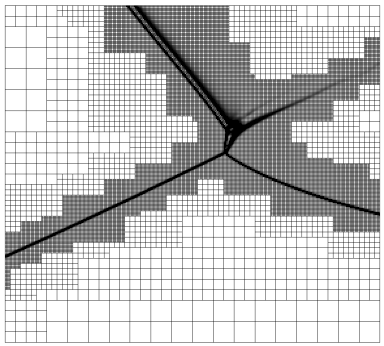

vtf/amroc/clawpack/applications/euler_chem/2d/Diffraction

Triple point analysis

Double Mach reflection structure shortly before the next collision

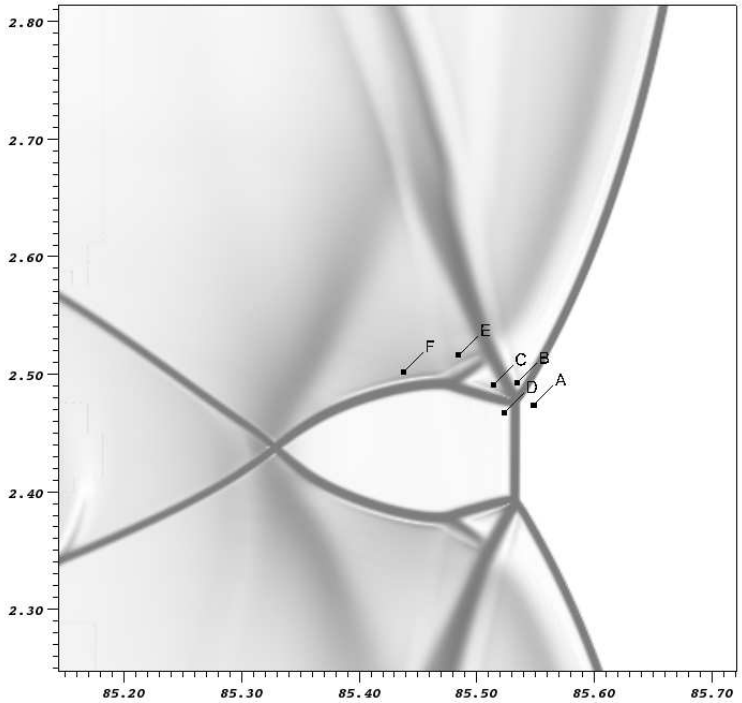

	p/p_0	ρ/ρ_0	T [K]	u[m/s]	M
A	1.00	1.00	298	1775	5.078
B	31.45	4.17	2248	447	0.477
C	31.69	5.32	1775	965	1.153
D	19.17	3.84	1487	1178	1.533
E	35.61	5.72	1856	901	1.053
F	40.61	6.09	1987	777	0.880

Triple point analysis

Double Mach reflection structure shortly before the next collision

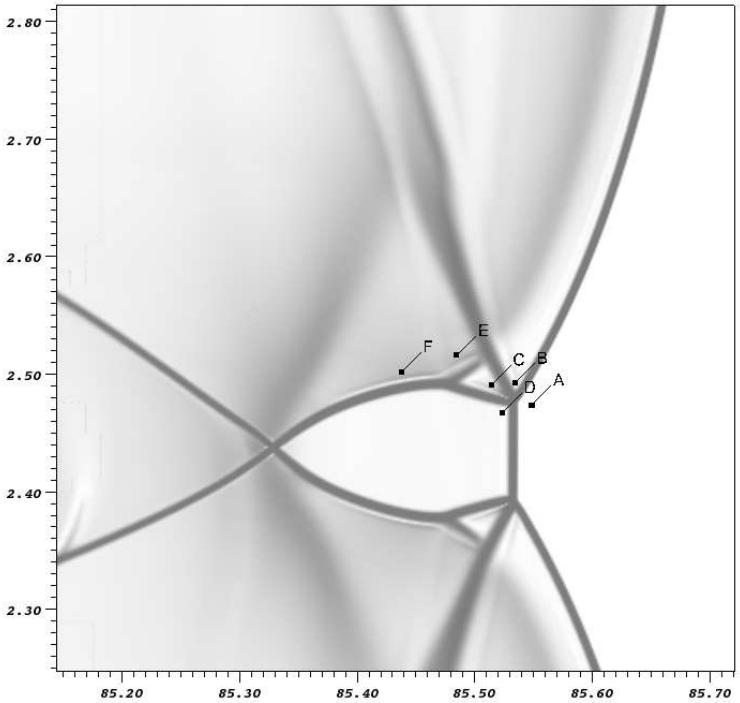

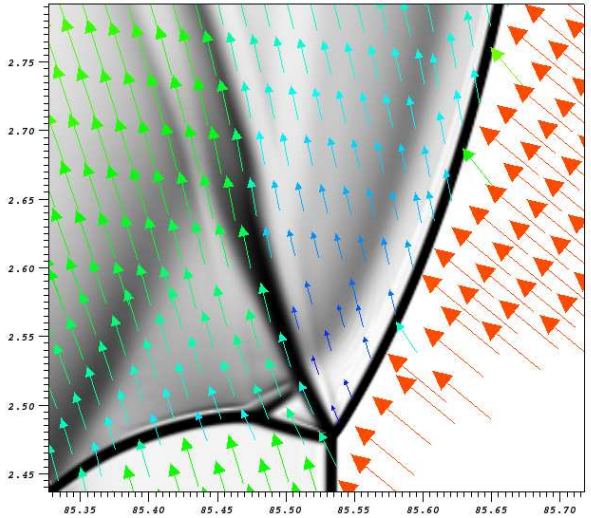

	p/p_0	ρ/ρ_0	T [K]	u[m/s]	M
A	1.00	1.00	298	1775	5.078
B	31.45	4.17	2248	447	0.477
C	31.69	5.32	1775	965	1.153
D	19.17	3.84	1487	1178	1.533
E	35.61	5.72	1856	901	1.053
F	40.61	6.09	1987	777	0.880

Triple point analysis

Double Mach reflection structure shortly before the next collision

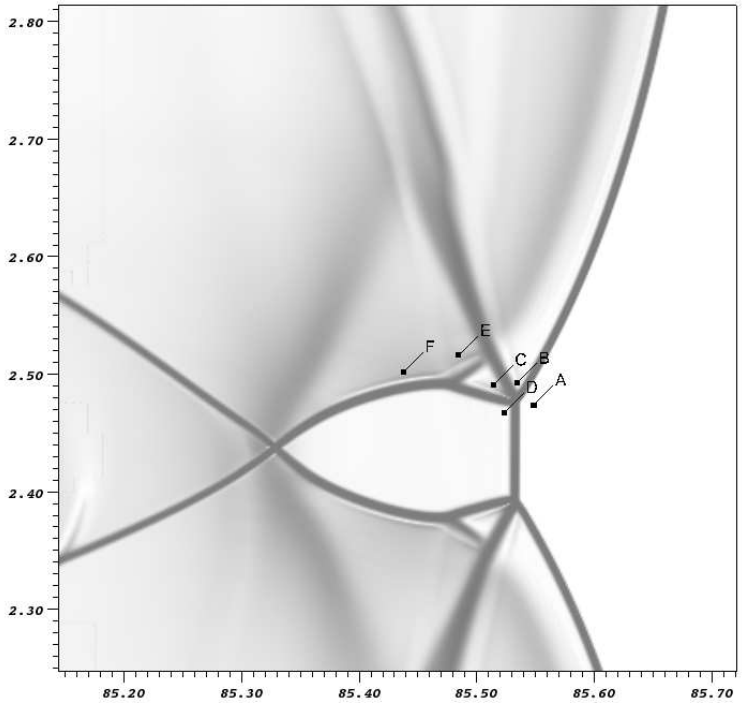

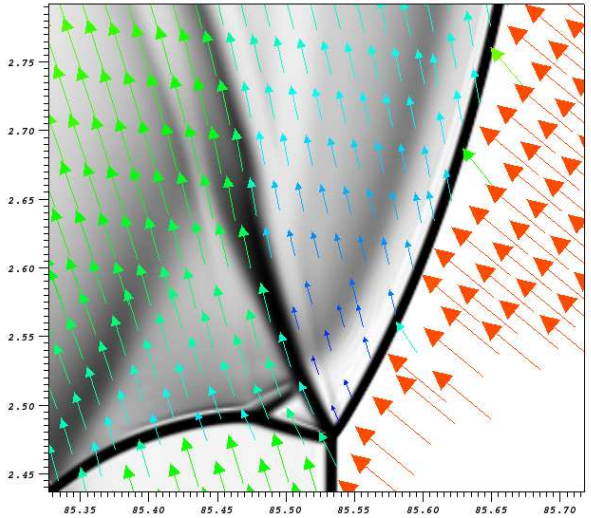

	p/p_0	ρ/ρ_0	T [K]	u[m/s]	M
A	1.00	1.00	298	1775	5.078
B	31.45	4.17	2248	447	0.477
C	31.69	5.32	1775	965	1.153
D	19.17	3.84	1487	1178	1.533
E	35.61	5.72	1856	901	1.053
F	40.61	6.09	1987	777	0.880

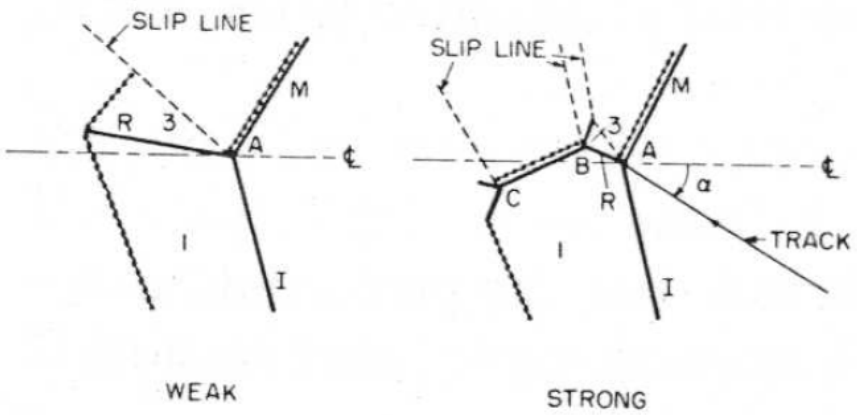

Shock polar analysis of triple points in detonations

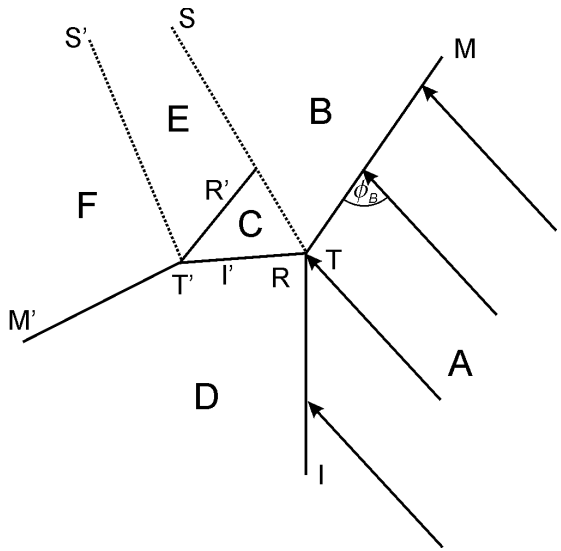

Shock polar analysis of triple points in detonations

- Neglect reaction, but consider $c_{pi}(T)$
- Data extracted point-wise from simulation

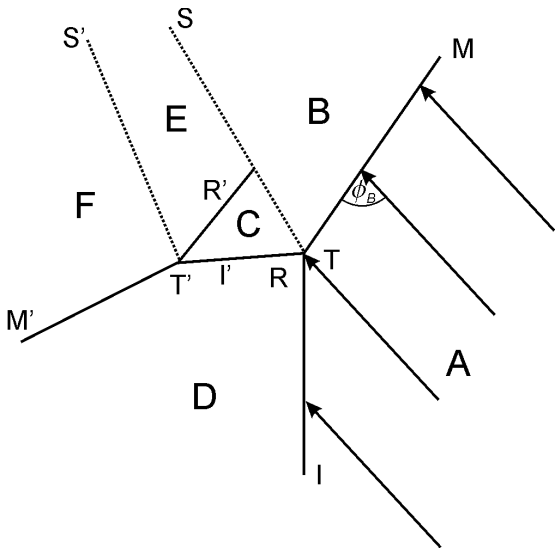

Shock polar analysis of triple points in detonations

- Neglect reaction, but consider $c_{pi}(T)$
- Data extracted point-wise from simulation
- Primary triple point T travels exactly at tip of Mach stem $\rightarrow$ use oblique shock relations between A and B

$$\begin{aligned} \rho_A u_A \sin(\phi_B) &= \rho_B u_B \sin(\phi_B - \theta_B)\,, \\ p_A + \rho_A u_A^2 \sin^2(\phi_B) &= p_B + \rho_B u_B^2 \sin^2(\phi_B - \theta_B) \end{aligned}$$

to evaluate inflow velocity as $u_A = \dfrac{1}{\sin\phi_B}\sqrt{\dfrac{\rho_B(p_B - p_A)}{\rho_A(\rho_B - \rho_A)}}$

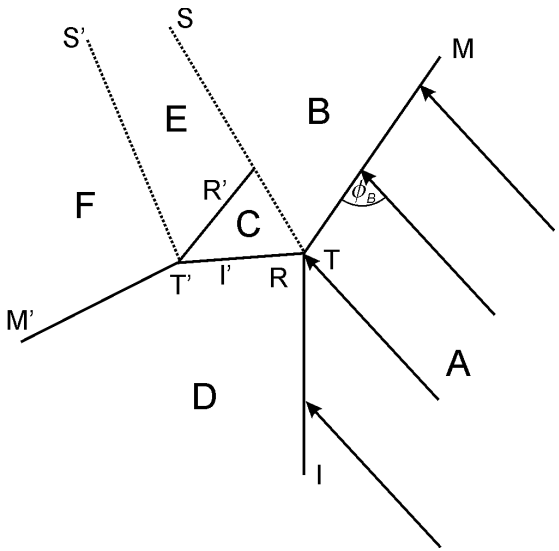

Shock polar analysis of triple points in detonations

- Neglect reaction, but consider $c_{pi}(T)$
- Data extracted point-wise from simulation
- Primary triple point T travels exactly at tip of Mach stem $\rightarrow$ use oblique shock relations between A and B

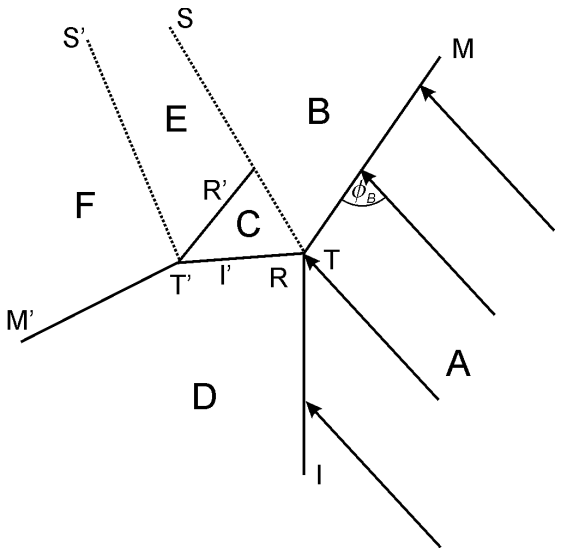

$$\begin{aligned} \rho_A u_A \sin(\phi_B) &= \rho_B u_B \sin(\phi_B - \theta_B)\,, \\ p_A + \rho_A u_A^2 \sin^2(\phi_B) &= p_B + \rho_B u_B^2 \sin^2(\phi_B - \theta_B) \end{aligned}$$

to evaluate inflow velocity as $u_A = \dfrac{1}{\sin\phi_B}\sqrt{\dfrac{\rho_B(p_B - p_A)}{\rho_A(\rho_B - \rho_A)}}$

- Measure inflow angle ϕ_B between Mach stem and triple point trajectory

Shock polar analysis of triple points in detonations

- Neglect reaction, but consider $c_{pi}(T)$
- Data extracted point-wise from simulation
- Primary triple point T travels exactly at tip of Mach stem $\rightarrow$ use oblique shock relations between A and B

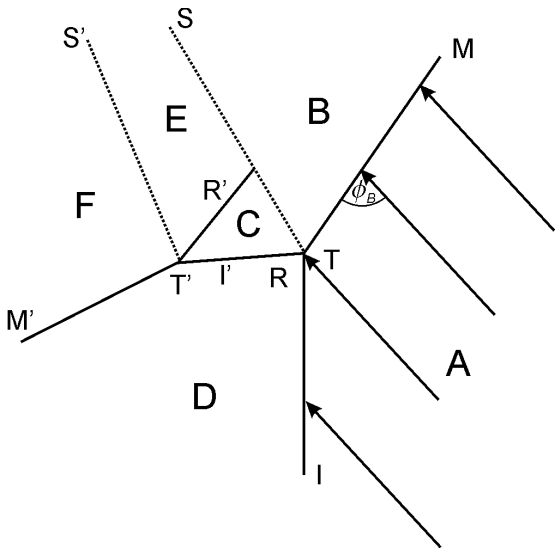

$$\begin{aligned} \rho_A u_A \sin(\phi_B) &= \rho_B u_B \sin(\phi_B - \theta_B)\,, \\ p_A + \rho_A u_A^2 \sin^2(\phi_B) &= p_B + \rho_B u_B^2 \sin^2(\phi_B - \theta_B) \end{aligned}$$

to evaluate inflow velocity as $u_A = \dfrac{1}{\sin\phi_B}\sqrt{\dfrac{\rho_B(p_B - p_A)}{\rho_A(\rho_B - \rho_A)}}$

- Measure inflow angle ϕ_B between Mach stem and triple point trajectory
- Velocity $\mathbf{a}$ of T' relative to T cannot be derived that easily: Oblique shock relations across C and D hold true both in frame of reference for T and T'

$$\begin{aligned} \rho_C u_{C,n} &= \rho_D u_{D,n} \\ p_C + \rho_C u_{C,n}^2 &= p_D + \rho_D u_{D,n}^2 \\ u_{C,t} &= u_{D,t} \\ h_C + \frac{1}{2} u_{C,n}^2 &= h_D + \frac{1}{2} u_{D,n}^2 \end{aligned}$$

Shock polar analysis of triple points in detonations

- Neglect reaction, but consider $c_{pi}(T)$
- Data extracted point-wise from simulation
- Primary triple point T travels exactly at tip of Mach stem $\rightarrow$ use oblique shock relations between A and B

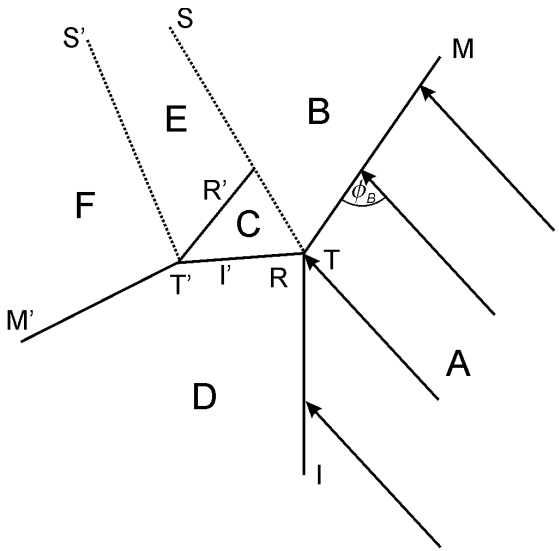

$$\begin{aligned} \rho_A u_A \sin(\phi_B) &= \rho_B u_B \sin(\phi_B - \theta_B)\,, \\ p_A + \rho_A u_A^2 \sin^2(\phi_B) &= p_B + \rho_B u_B^2 \sin^2(\phi_B - \theta_B) \end{aligned}$$

to evaluate inflow velocity as $u_A = \dfrac{1}{\sin\phi_B}\sqrt{\dfrac{\rho_B(p_B - p_A)}{\rho_A(\rho_B - \rho_A)}}$

- Measure inflow angle ϕ_B between Mach stem and triple point trajectory
- Velocity $\mathbf{a}$ of T' relative to T cannot be derived that easily: Oblique shock relations across C and D hold true both in frame of reference for T and T'

$$\begin{aligned} \rho_C \left(u_{C,n} - a_n\right) &= \rho_D \left(u_{D,n} - a_n\right) \\ p_C + \rho_C \left(u_{C,n} - a_n\right)^2 &= p_D + \rho_D \left(u_{D,n} - a_n\right)^2 \\ u_{C,t} - a_t &= u_{D,t} - a_t \\ h_C + \frac{1}{2}\left(u_{C,n} - a_n\right)^2 &= h_D + \frac{1}{2}\left(u_{D,n} - a_n\right)^2 \end{aligned}$$

Shock polar analysis of triple points in detonations

- Neglect reaction, but consider $c_{pi}(T)$
- Data extracted point-wise from simulation
- Primary triple point T travels exactly at tip of Mach stem $\rightarrow$ use oblique shock relations between A and B

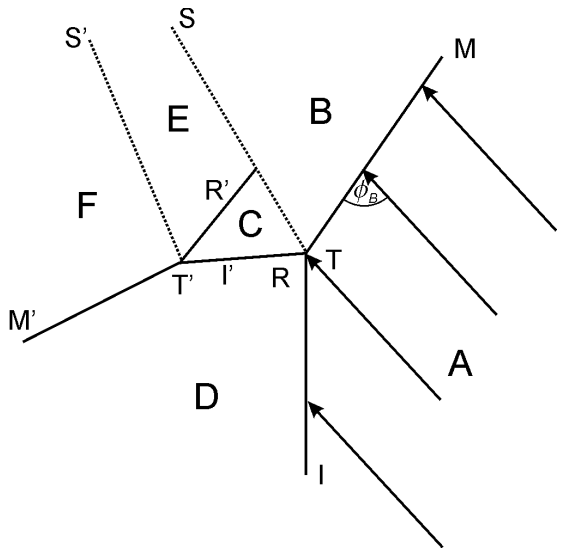

$$\begin{aligned} \rho_A u_A \sin(\phi_B) &= \rho_B u_B \sin(\phi_B - \theta_B)\,, \\ p_A + \rho_A u_A^2 \sin^2(\phi_B) &= p_B + \rho_B u_B^2 \sin^2(\phi_B - \theta_B) \end{aligned}$$

to evaluate inflow velocity as $u_A = \dfrac{1}{\sin\phi_B}\sqrt{\dfrac{\rho_B(p_B - p_A)}{\rho_A(\rho_B - \rho_A)}}$

- Measure inflow angle ϕ_B between Mach stem and triple point trajectory
- Velocity $\mathbf{a}$ of T' relative to T cannot be derived that easily: Oblique shock relations across C and D hold true both in frame of reference for T and T'

$$\begin{aligned} \rho_C\left(u_{C,n} - a_n\right) &= \rho_D\left(u_{D,n} - a_n\right) \\ p_C + \rho_C\left(u_{C,n} - a_n\right)^2 &= p_D + \rho_D\left(u_{D,n} - a_n\right)^2 \\ u_{C,t} - a_t &= u_{D,t} - a_t \\ h_C + \frac{1}{2}\left(u_{C,n} - a_n\right)^2 &= h_D + \frac{1}{2}\left(u_{D,n} - a_n\right)^2 \end{aligned}$$

$\rightarrow a_n = 0$, a_t arbitrary

Estimate $a_t = \dfrac{L_R}{t_{\text{init}}}$

Detonation propagation through pipe bends

- 2D Simulation of CJ detonation for $\mathrm{H_2} : \mathrm{O_2} : \mathrm{Ar}/2 : 1 : 7$ at $T_0 = 298\,\mathrm{K}$ and $p_0 = 10\,\mathrm{kPa}$. Tube width of 5 detonation cells
- AMR base grid 1200×992. 4 additional refinement levels (2,2,2,4). $67.6\,\mathrm{Pts}/l_{ig}$
- Adaptive computations use up to $7.1 \cdot 10^6$ cells ($4.8 \cdot 10^6$ on highest level) instead of $1.22 \cdot 10^9$ cells (uniform grid)
- $\sim 70,000\,\mathrm{h}$ CPU on 128 CPUs Pentium-4 2.2GHz

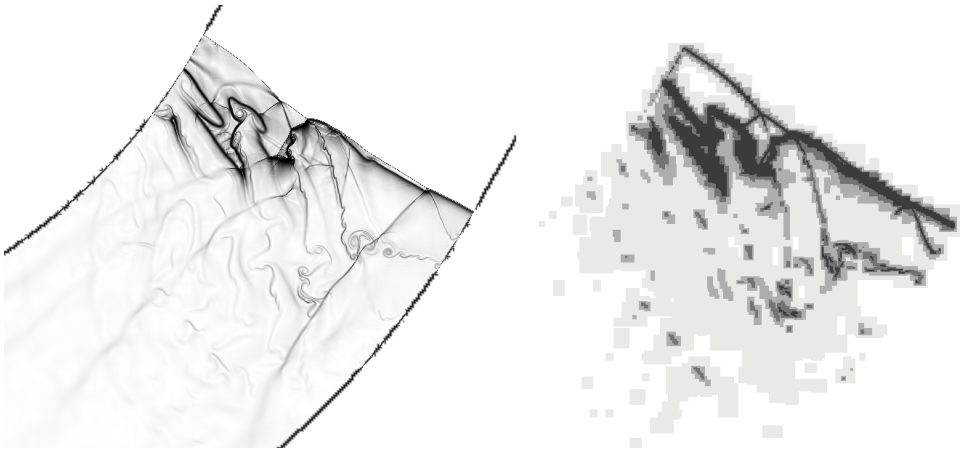

Detonation propagation through pipe bends

- 2D Simulation of CJ detonation for $\mathrm{H_2} : \mathrm{O_2} : \mathrm{Ar}/2 : 1 : 7$ at $T_0 = 298\,\mathrm{K}$ and $p_0 = 10\,\mathrm{kPa}$. Tube width of 5 detonation cells
- AMR base grid 1200×992. 4 additional refinement levels (2,2,2,4). $67.6\,\mathrm{Pts}/l_{ig}$
- Adaptive computations use up to $7.1 \cdot 10^6$ cells ($4.8 \cdot 10^6$ on highest level) instead of $1.22 \cdot 10^9$ cells (uniform grid)
- $\sim 70,000\,\mathrm{h}$ CPU on 128 CPUs Pentium-4 2.2GHz

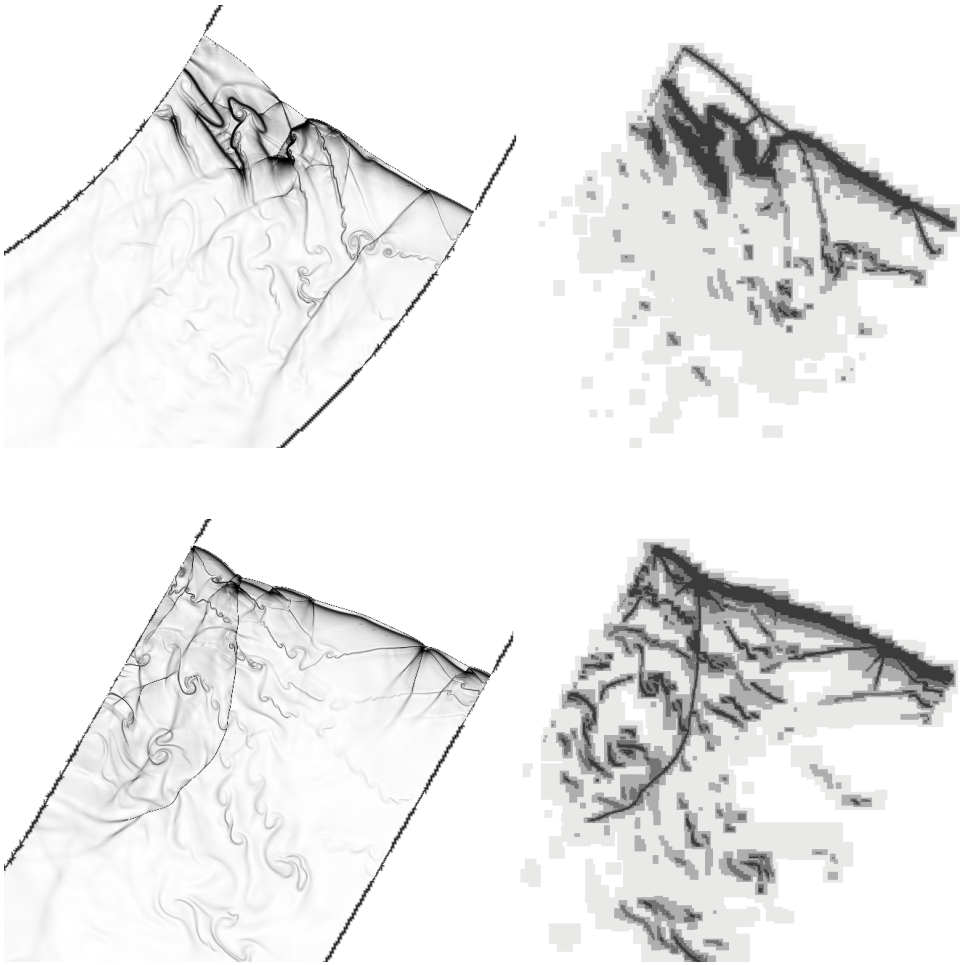

Detonation propagation through pipe bends

- 2D Simulation of CJ detonation for $\mathrm{H_2} : \mathrm{O_2} : \mathrm{Ar}/2 : 1 : 7$ at $T_0 = 298\,\mathrm{K}$ and $p_0 = 10\,\mathrm{kPa}$. Tube width of 5 detonation cells
- AMR base grid 1200×992. 4 additional refinement levels (2,2,2,4). $67.6\,\mathrm{Pts}/l_{ig}$
- Adaptive computations use up to $7.1 \cdot 10^6$ cells ($4.8 \cdot 10^6$ on highest level) instead of $1.22 \cdot 10^9$ cells (uniform grid)
- $\sim 70,000\,\mathrm{h}$ CPU on 128 CPUs Pentium-4 2.2GHz

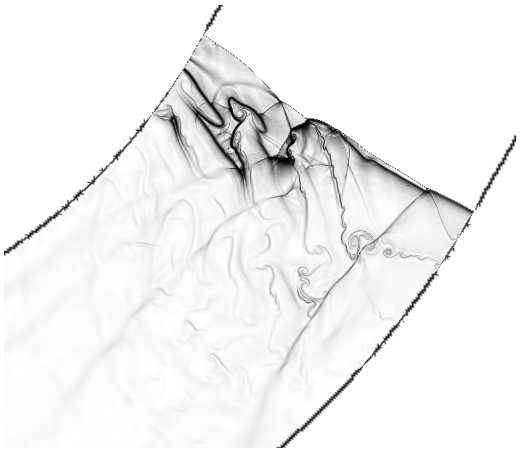

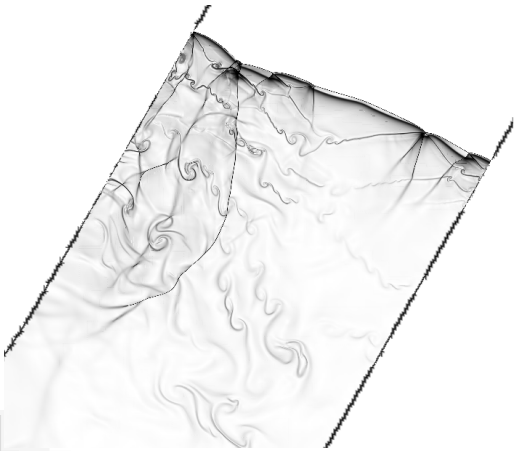

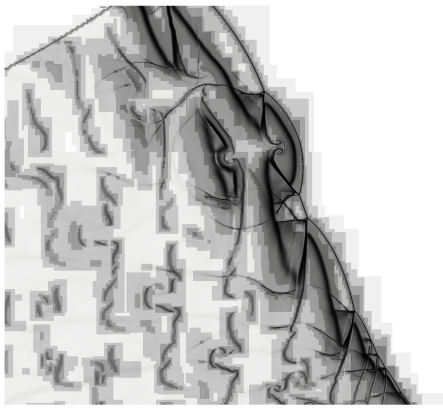
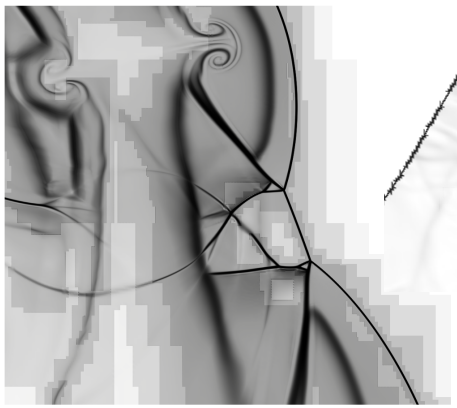

Triple point tracks

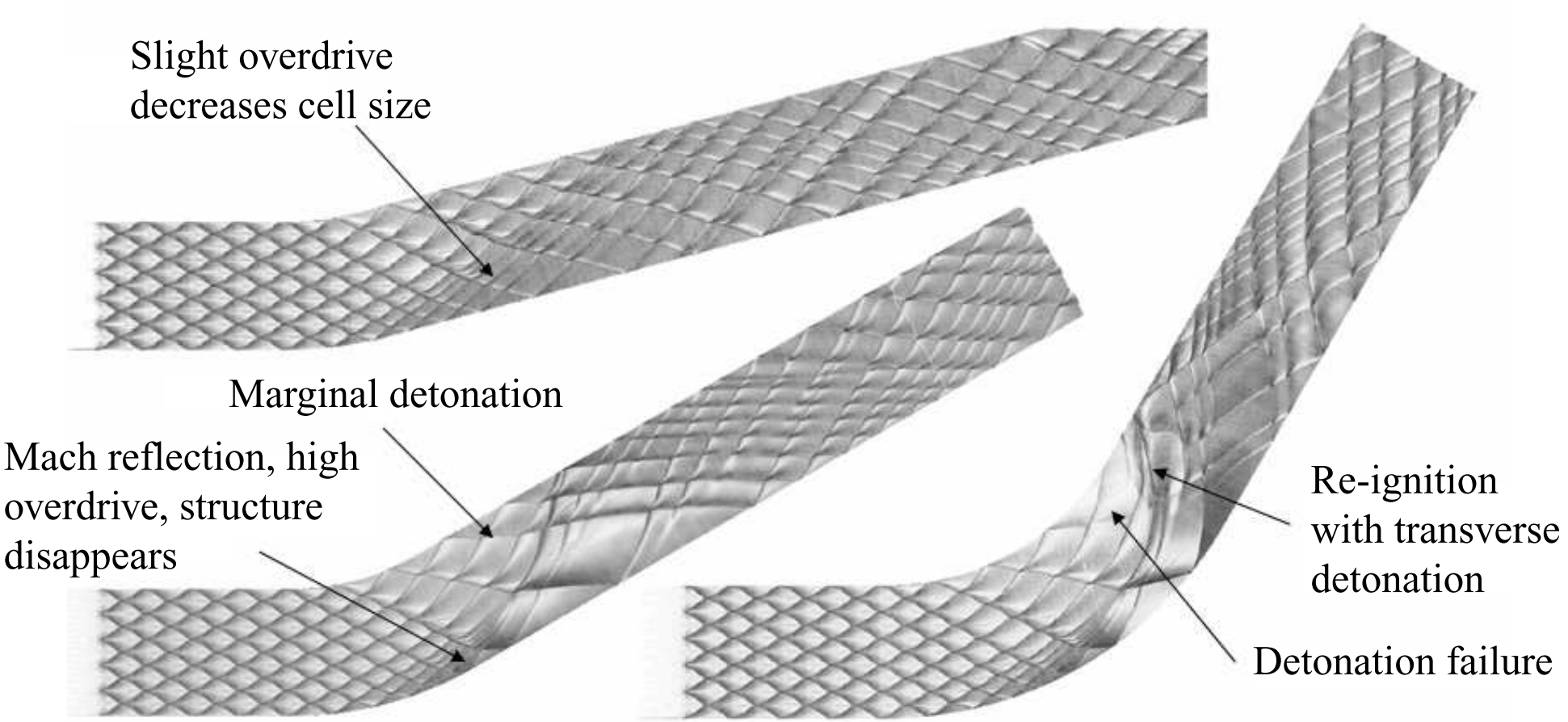

$\varphi = 15^{\circ}$ (left, top), $\varphi = 30^{\circ}$ (left, bottom), and $\varphi = 60^{\circ}$ (right)

vtf/amroc/clawpack/applications/euler_chem/2d/PipeBend

Triple point structures – $\varphi = 15^{\mathrm{o}}$

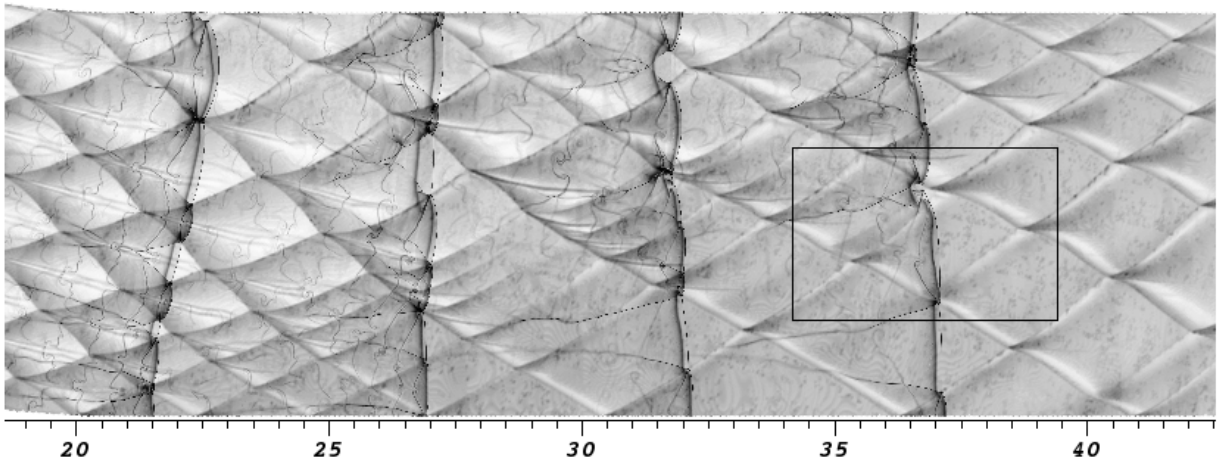

Triple point structures – $\varphi = 15^{\mathrm{o}}$

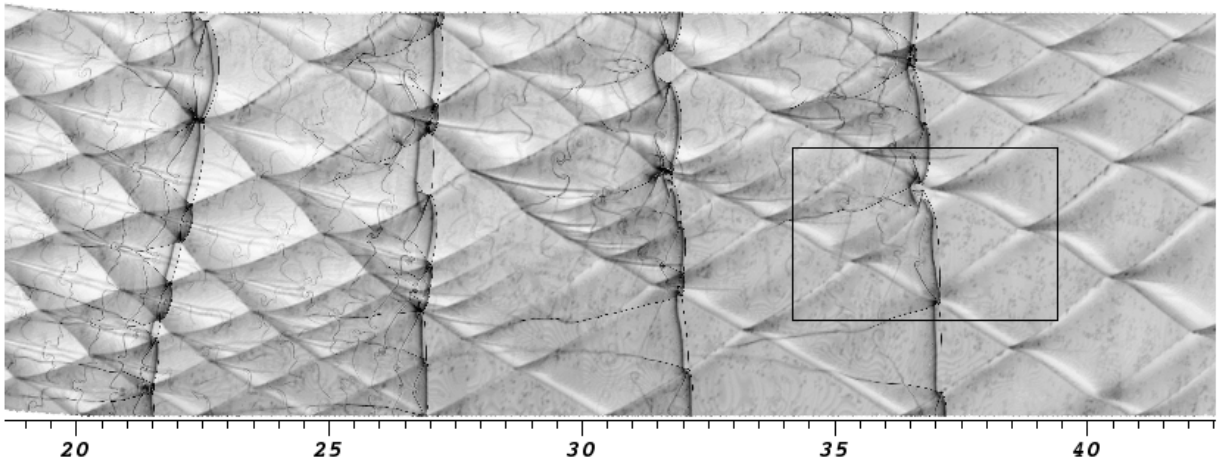

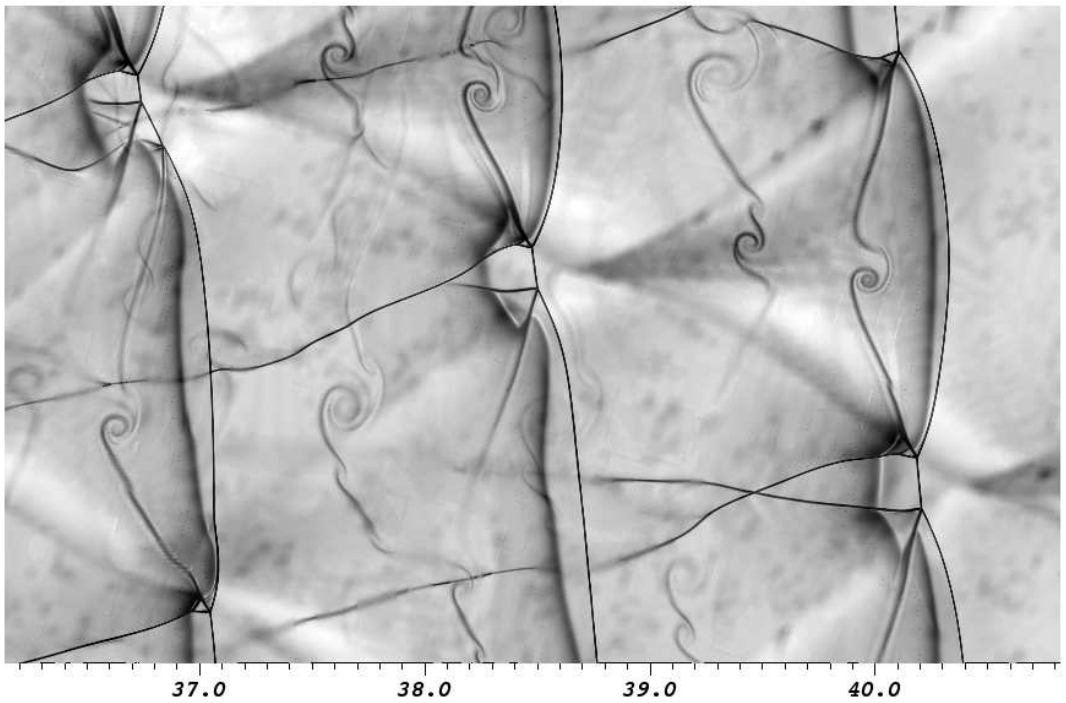

Triple point structures – $\varphi = 15^{\circ}$

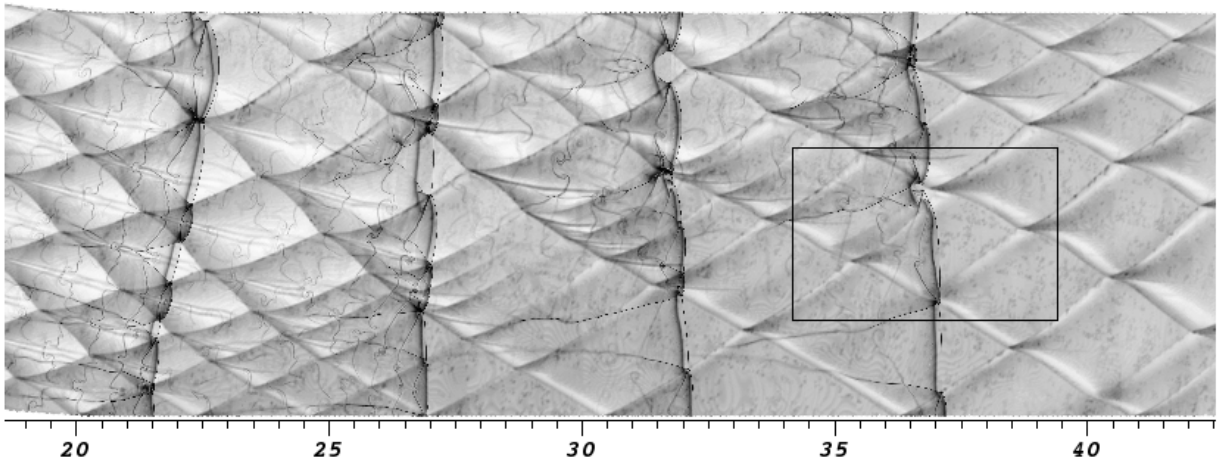

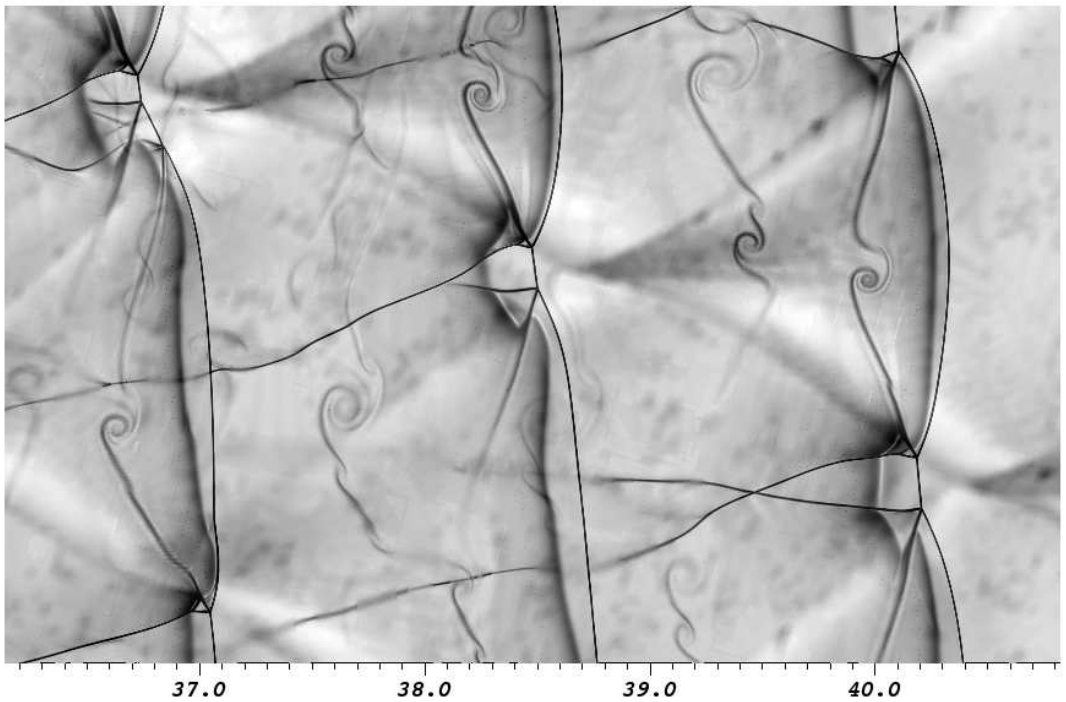

- Triple point re-initiation after bend with change from transitional to Double Mach reflection

Triple point structures – $\varphi = 30^{\circ}$

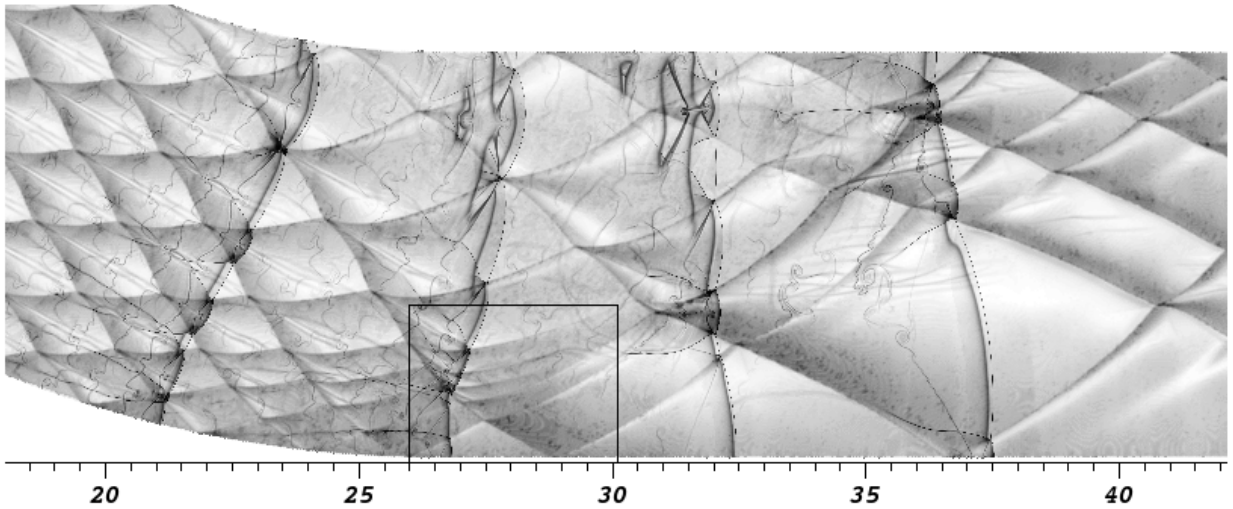

Triple point structures – $\varphi = 30^{\circ}$

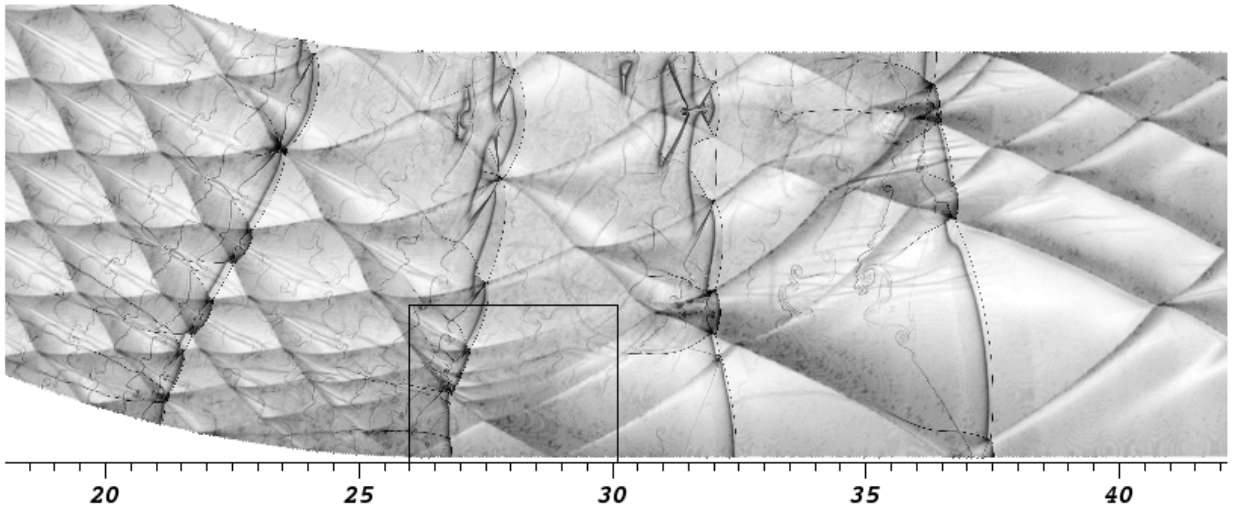

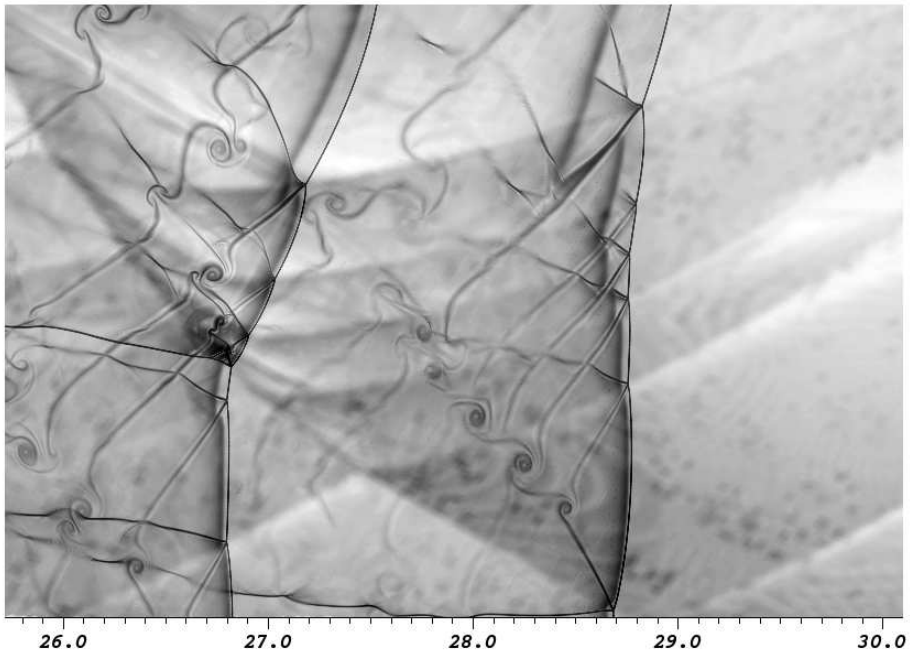

Triple point structures – $\varphi = 30^{\circ}$

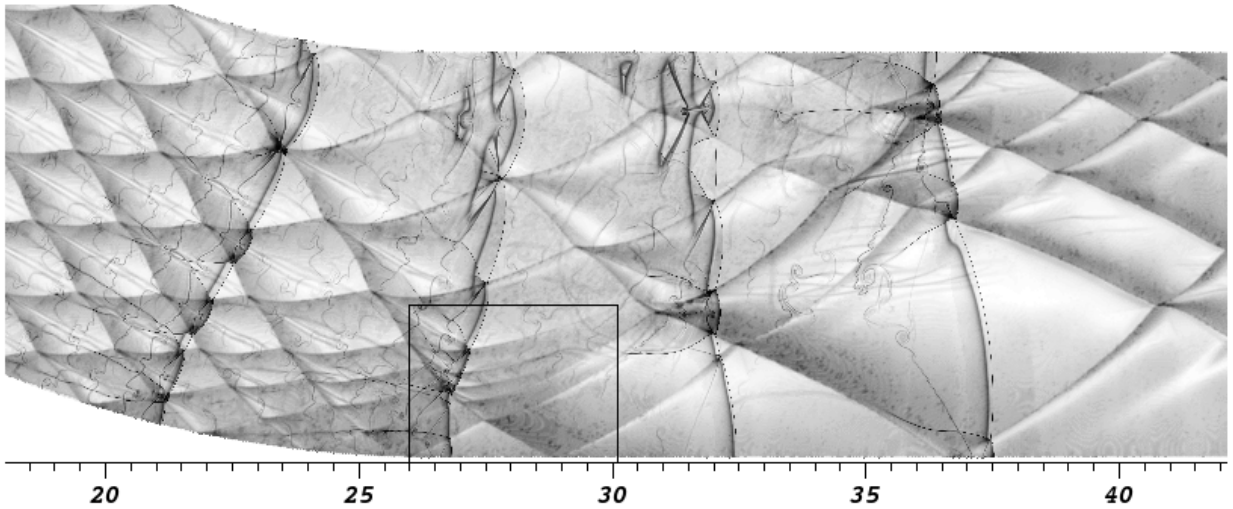

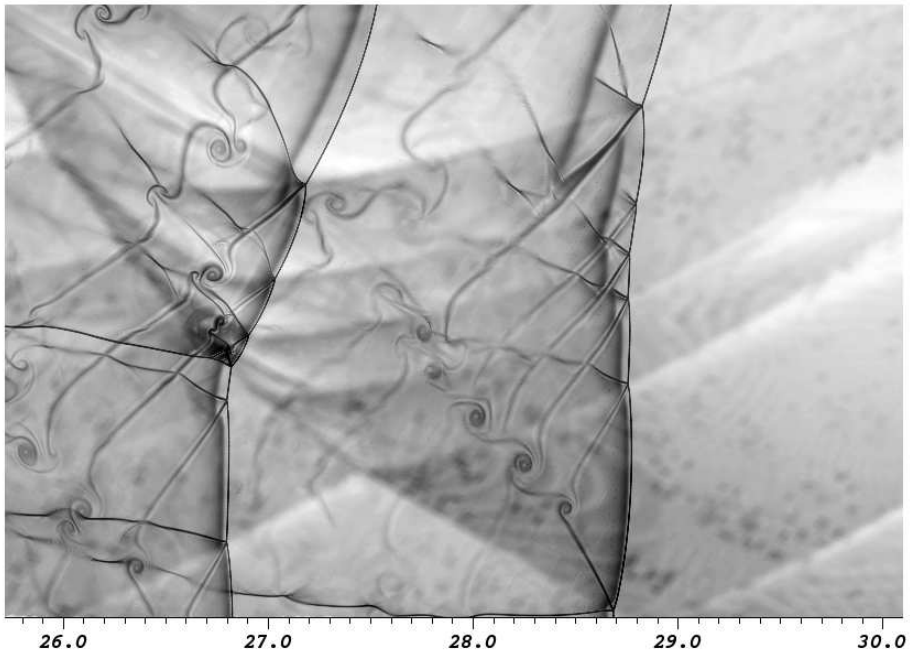

- Triple point quenching and failure as single Mach reflection

Transition criteria

Solve system of oblique shock relations numerically and determine transition boundaries [Ben-Dor, 2007].

- Regular reflection (RR): $M_B^T < 1$
- Single Mach reflection (SMR): $M_C^T < 1$ and $M_B^T > 1$
- Transitional Mach reflection: $M_C^{T'} < 1$ and $M_C^T > 1$
- Double Mach reflection: $M_C^{T'} > 1$ and $M_C^T > 1$

Transition criteria

Solve system of oblique shock relations numerically and determine transition boundaries [Ben-Dor, 2007].

- Regular reflection (RR): $M_B^T < 1$
- Single Mach reflection (SMR): $M_C^T < 1$ and $M_B^T > 1$
- Transitional Mach reflection: $M_C^{T'} < 1$ and $M_C^T > 1$
- Double Mach reflection: $M_C^{T'} > 1$ and $M_C^T > 1$
- Here: Nonreactive $\mathrm{H_2} : \mathrm{O_2} : \mathrm{Ar}$ mixture at initially $298\,\mathrm{K}$ and $10\,\mathrm{kPa}$

For detonations:

$$S := \frac{p_C - p_D}{p_D}$$

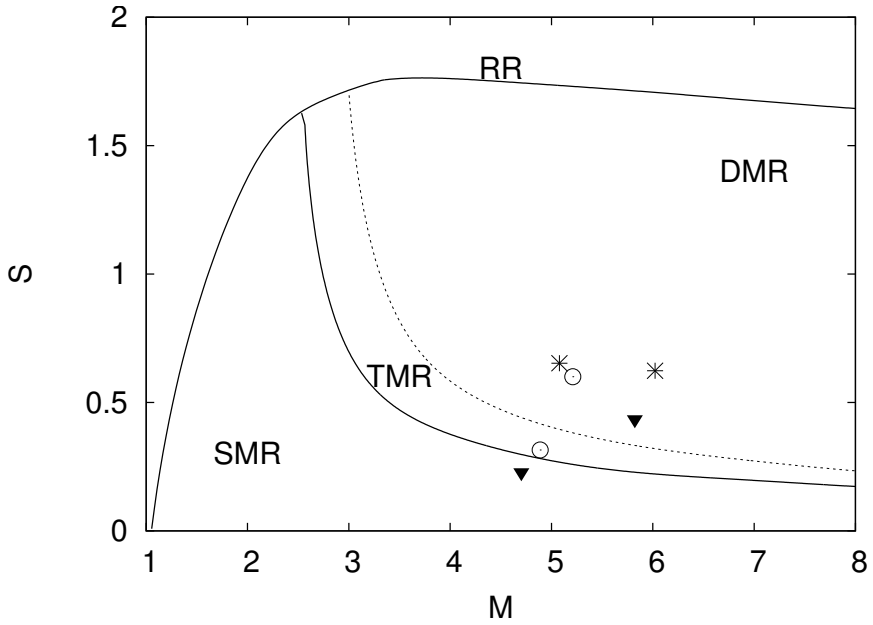

TMR/DMR transition for $a_t = 100\,\mathrm{m/s}$

Transition criteria

Solve system of oblique shock relations numerically and determine transition boundaries [Ben-Dor, 2007].

- Regular reflection (RR): $M_B^T < 1$
- Single Mach reflection (SMR): $M_C^T < 1$ and $M_B^T > 1$
- Transitional Mach reflection: $M_C^{T'} < 1$ and $M_C^T > 1$
- Double Mach reflection: $M_C^{T'} > 1$ and $M_C^T > 1$
- Here: Nonreactive $\mathrm{H_2} : \mathrm{O_2} : \mathrm{Ar}$ mixture at initially $298\,\mathrm{K}$ and $10\,\mathrm{kPa}$

For detonations:

$$S := \frac{p_C - p_D}{p_D}$$

[Deiterding, 2011]

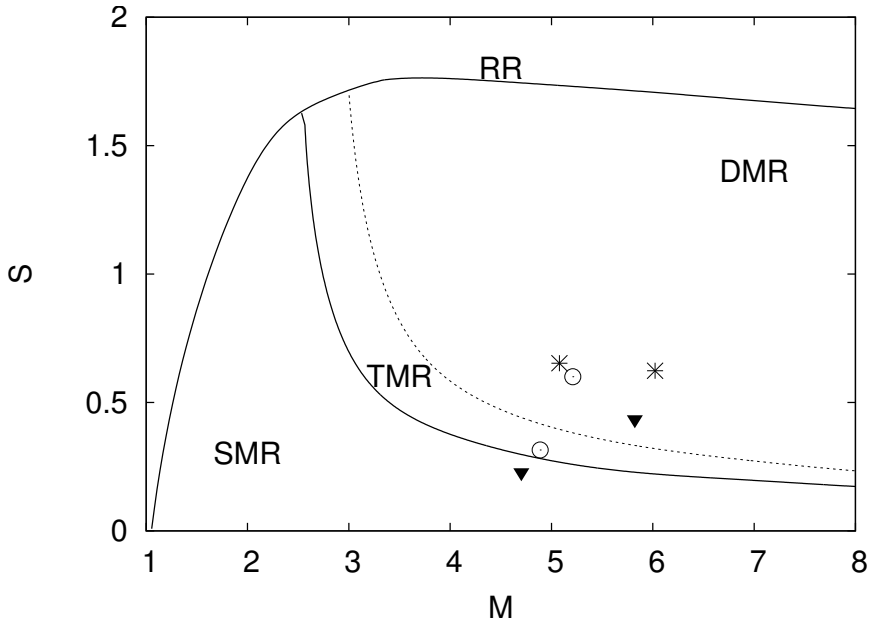

TMR/DMR transition for $a_t = 100\,\mathrm{m/s}$

- Non-reactive shock wave reflection theory seems applicable to predict local triple point structure and stability
- Triple point type is determined solely by S and M. Useful to determine type in underresolved situations.

Triple point structures, $\varphi = 15$

Strong DMR structure in diffraction region behind bend, $S = 1.062$

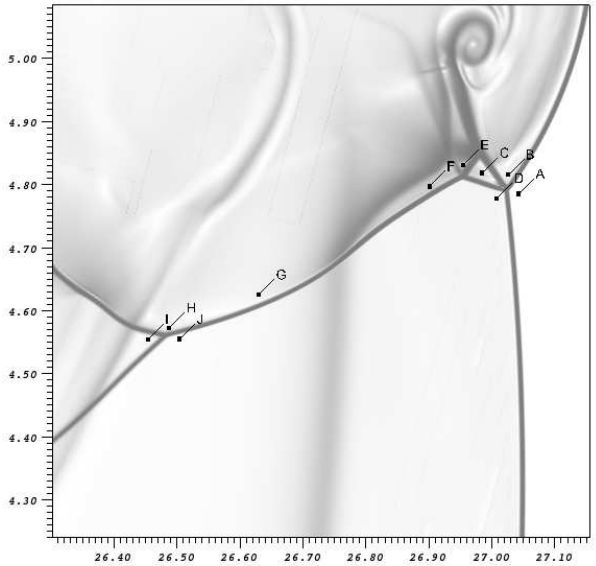

	p/p_A	r/r_A	T [K]	v[m/s]	M
A	1.00	1.00	298	1835	5.249
B	33.77	4.33	2326	447	0.469
C	33.12	5.80	1701	1111	1.355
D	16.06	3.67	1304	1363	1.889
E	66.90	9.10	2191	758	0.818
F	57.94	7.64	2259	668	0.710
G	35.28	3.41	3235	699	
H	38.98	3.41	3589	593	
I	23.66	2.37	3149	969	
J	13.58	1.67	2570	1347	

Triple point structures, $\varphi = 15$

Strong DMR structure in diffraction region behind bend, $S = 1.062$

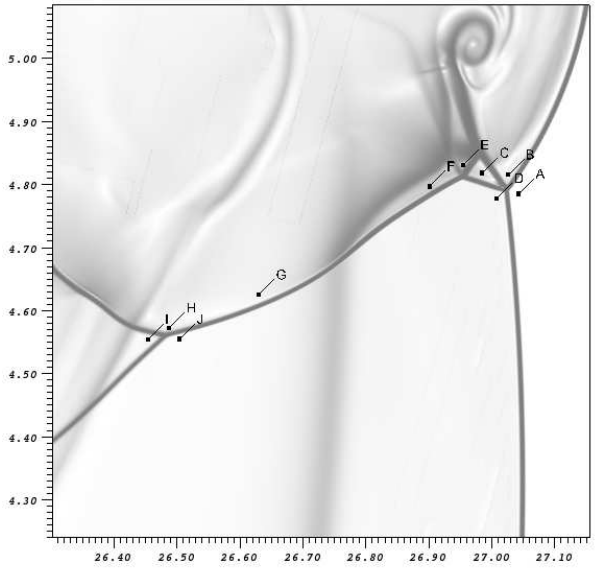

	p/p_A	r/r_A	T [K]	v[m/s]	M
A	1.00	1.00	298	1835	5.249
B	33.77	4.33	2326	447	0.469
C	33.12	5.80	1701	1111	1.355
D	16.06	3.67	1304	1363	1.889
E	66.90	9.10	2191	758	0.818
F	57.94	7.64	2259	668	0.710
G	35.28	3.41	3235	699	
H	38.98	3.41	3589	593	
I	23.66	2.37	3149	969	
J	13.58	1.67	2570	1347	

TMR structure in compression region shortly behind bend, $S = 0.338$

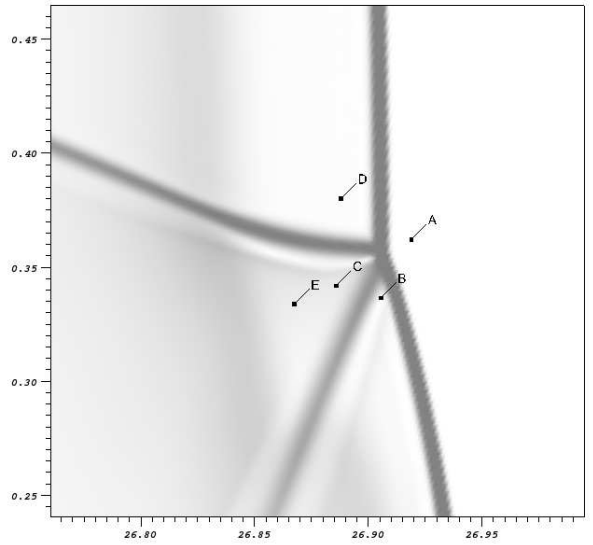

	p/p_A	r/r_A	T [K]	v[m/s]	M
A	1.00	1.00	298	1908	5.459
B	34.14	4.21	2418	647	0.666
C	35.49	4.95	2135	929	1.015
D	26.53	4.09	1934	1085	1.243
E	34.91	4.88	2134	938	1.025

Triple point structures

TMR structure in marginal region near limit of detonability, $\varphi = 30$, $S = 0.338$

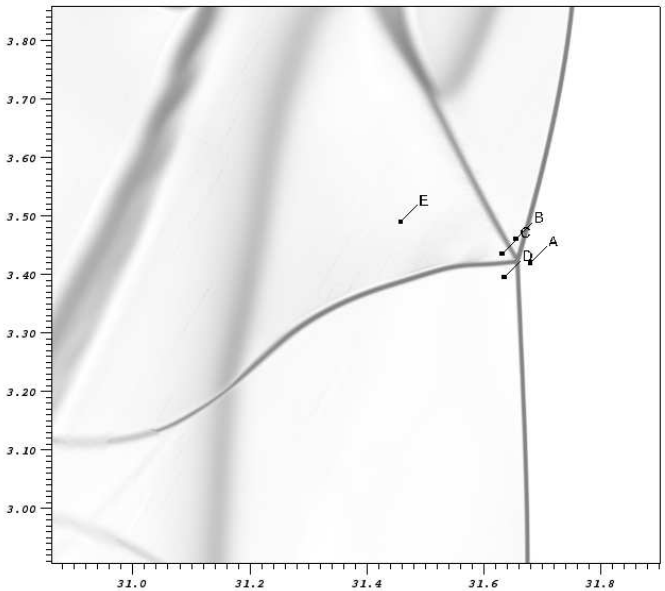

	p/p_A	r/r_A	T [K]	v[m/s]	M
A	1.00	1.00	298	1424	4.073
B	18.97	3.83	1475	502	0.656
C	18.73	4.30	1297	726	1.009
D	14.00	3.58	1167	848	1.240
E	19.08	4.20	1352	744	1.014

Triple point structures

TMR structure in marginal region near limit of detonability, $\varphi = 30$, $S = 0.338$

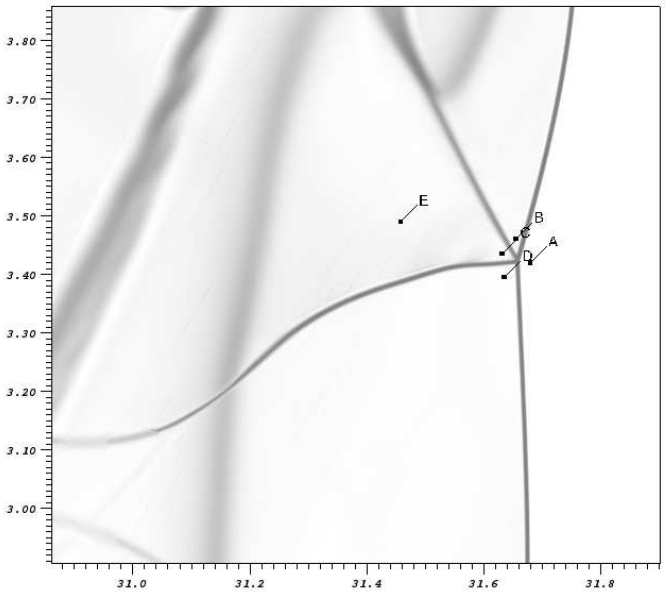

	p/p_A	r/r_A	T [K]	v[m/s]	M
A	1.00	1.00	298	1424	4.073
B	18.97	3.83	1475	502	0.656
C	18.73	4.30	1297	726	1.009
D	14.00	3.58	1167	848	1.240
E	19.08	4.20	1352	744	1.014

Re-ignition with strong DMR and transverse detonation, $\varphi = 45$, $S = 1.377$

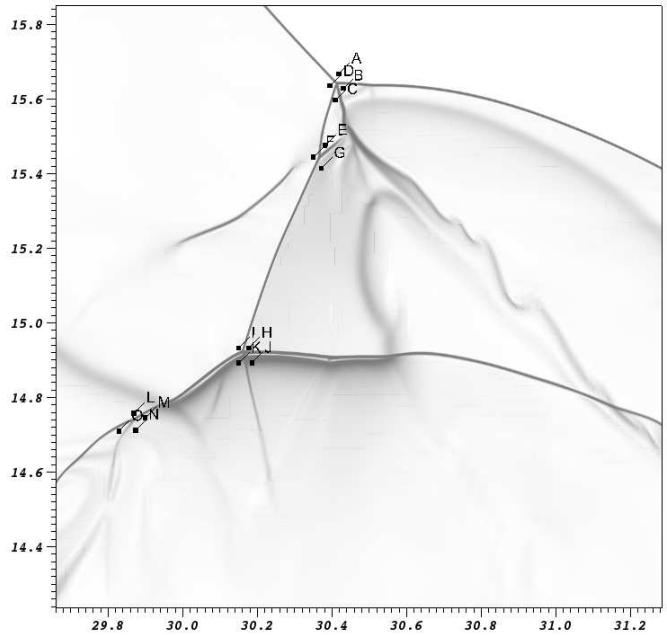

	p/p_A	r/r_A	T [K]	v[m/s]	M
A	1.00	1.00	298	1812	5.186
B	32.58	4.27	2272	456	0.483
C	33.23	6.21	1594	1156	1.454
D	13.98	3.58	1162	1446	2.119
E	31.54	6.30	1492	1208	1.569
F	16.13	4.14	1161	1393	2.042
G	41.63	7.45	1665	1034	1.274
H	30.57	6.31	1443	1180	1.557
I	14.11	3.85	1092	1431	2.161
J	77.31	9.08	2610	756	
K	78.85	8.59	2812	521	

Detonation cell structure in 3D

- Simulation of only one quadrant
- 44.8 Pts/l_{ig} for $\mathrm{H_2} : \mathrm{O_2} : \mathrm{Ar}$ CJ detonation
- SAMR base grid 400x24x24, 2 additional refinement levels (2, 4)
- Simulation uses $\sim 18\,\mathrm{M}$ cells instead of $\sim 118\,\mathrm{M}$ (unigrid)
- $\sim 51,000\,\mathrm{h}$ CPU on 128 CPU Compaq Alpha. $\mathcal{H}$: 37.6 %, $\mathcal{S}$: 25.1 %

Schlieren and isosurface of Y_{OH}

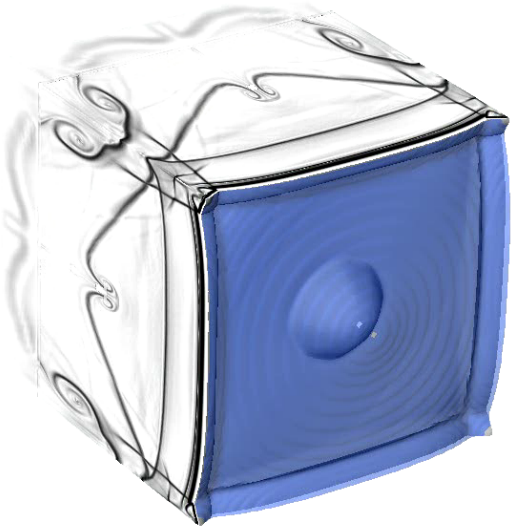

Detonation cell structure in 3D

- Simulation of only one quadrant
- 44.8 Pts/l_{ig} for $\mathrm{H_2} : \mathrm{O_2} : \mathrm{Ar}$ CJ detonation
- SAMR base grid 400x24x24, 2 additional refinement levels (2, 4)
- Simulation uses $\sim 18\,\mathrm{M}$ cells instead of $\sim 118\,\mathrm{M}$ (unigrid)
- $\sim 51,000\,\mathrm{h}$ CPU on 128 CPU Compaq Alpha. $\mathcal{H}$: 37.6 %, $\mathcal{S}$: 25.1 %

Schlieren on refinement levels

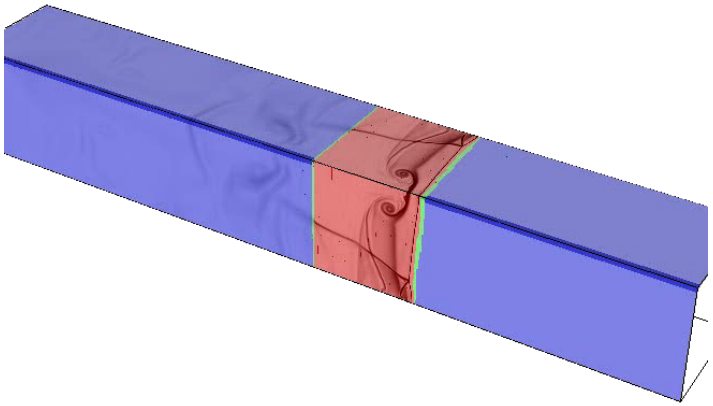

Schlieren and isosurface of Y_{OH}

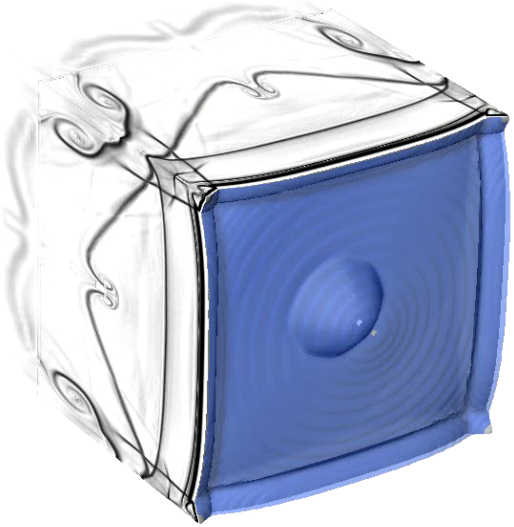

Detonation cell structure in 3D

- Simulation of only one quadrant
- 44.8 Pts/l_{ig} for $\mathrm{H_2} : \mathrm{O_2} : \mathrm{Ar}$ CJ detonation
- SAMR base grid 400x24x24, 2 additional refinement levels (2, 4)
- Simulation uses $\sim 18\,\mathrm{M}$ cells instead of $\sim 118\,\mathrm{M}$ (unigrid)
- $\sim 51,000\,\mathrm{h}$ CPU on 128 CPU Compaq Alpha. $\mathcal{H}$: 37.6 %, $\mathcal{S}$: 25.1 %

Schlieren and isosurface of Y_{OH}

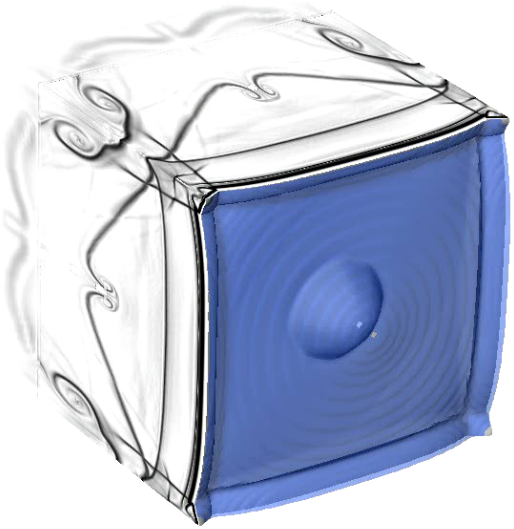

Schlieren on refinement levels

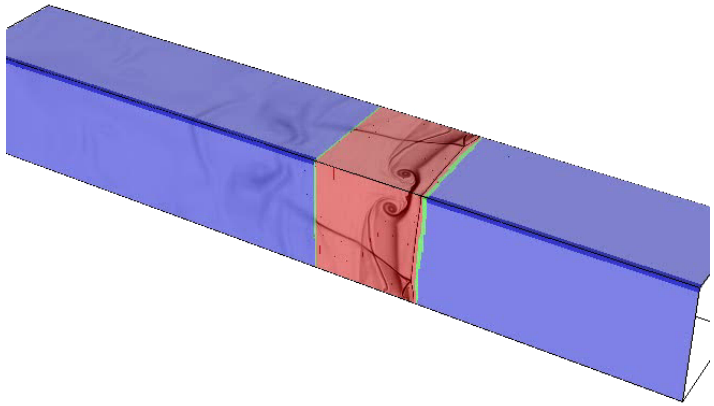

Distribution to 128 processors

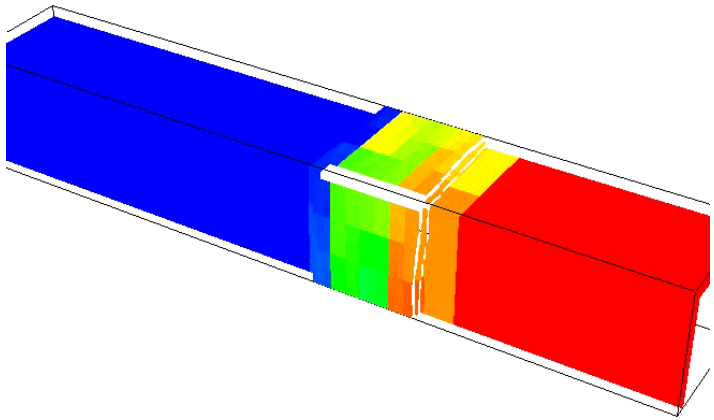

Detonation cell structure in 3D - II

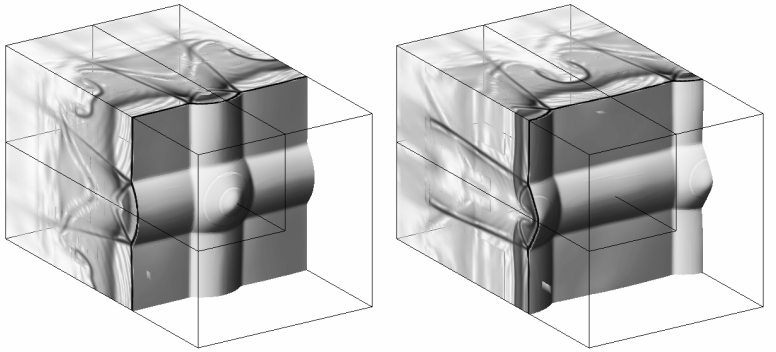

Schlieren plots of density, mirrored for visualization

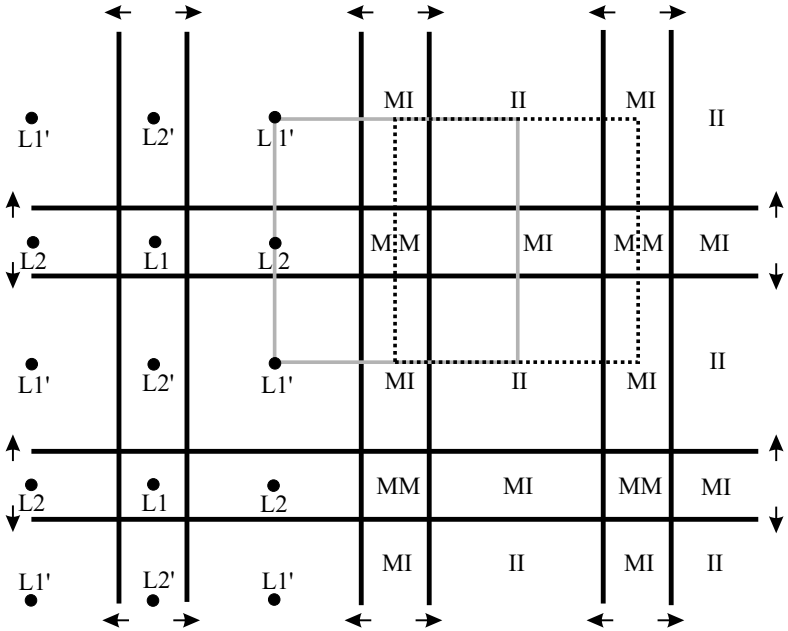

Schematic front view of the periodic triple point line structure right plot at the same time.

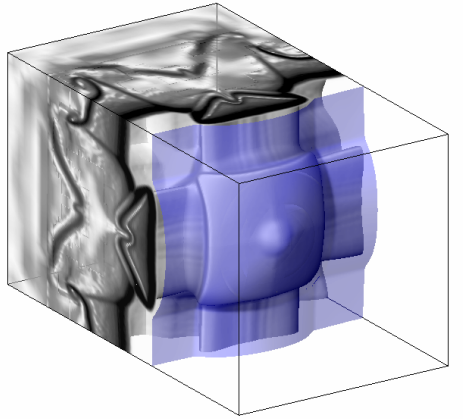

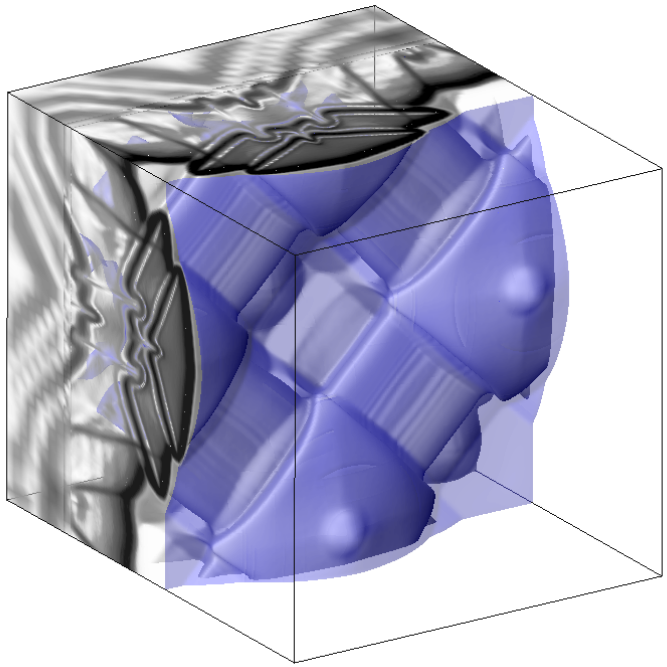

Schlieren plots of Y_{OH}

vtf/amroc/clawpack/applications/euler_chem/3d/StrehlowH2O2/StatDet

vtf/amroc/clawpack/applications/euler_chem/3d/StatDetPeriodic

Temporal Development of Detonation Velocity

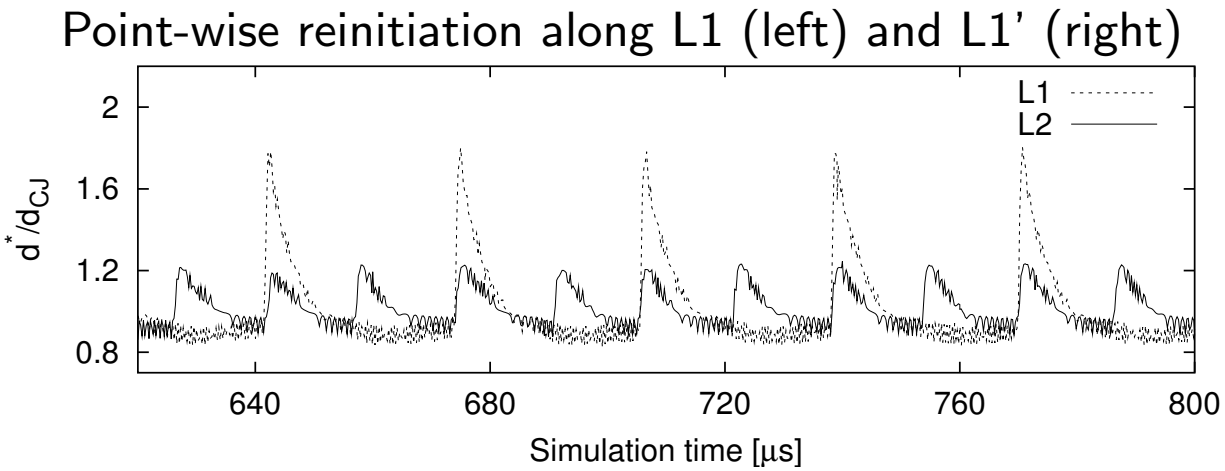

Temporal Development of Detonation Velocity

Point-wise reinitiation along L1 (left) and L1' (right)

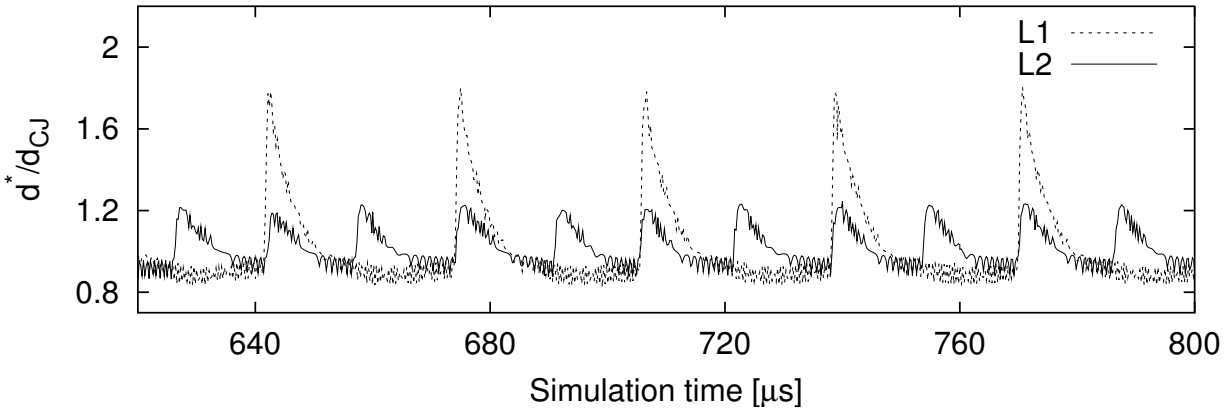

Comparison with 2D Simulation

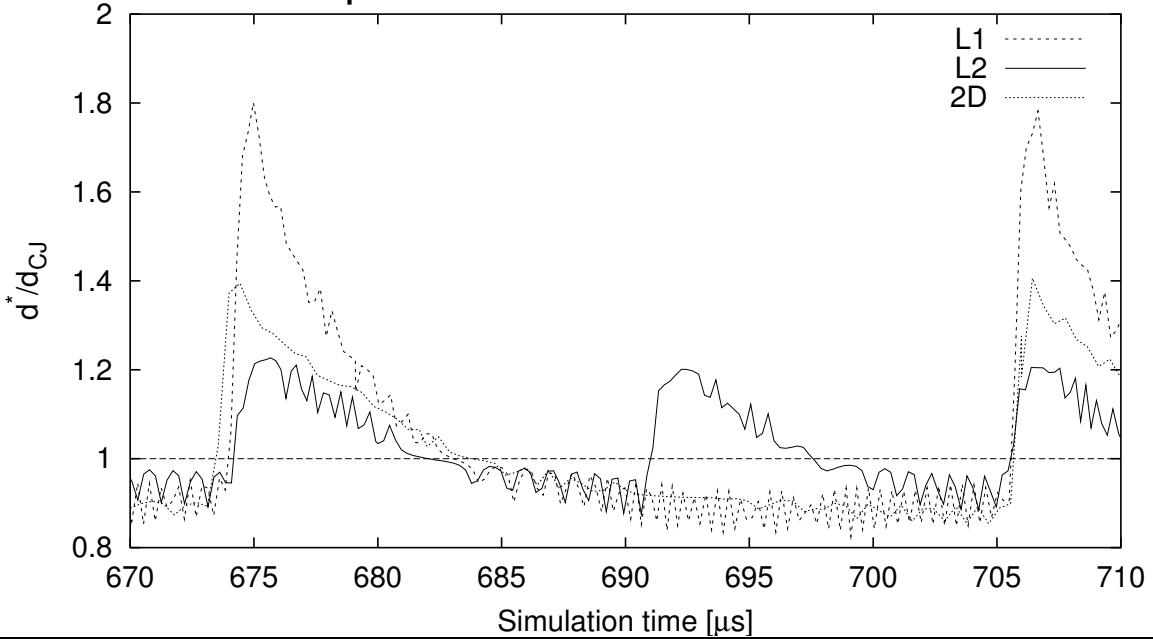

Axisymmetric Navier-Stokes equations with chemical reaction

$$\frac{\partial \mathbf{q}}{\partial t} + \frac{\partial (\mathbf{f} - \mathbf{f}_v)}{\partial x} + \frac{\partial (\mathbf{g} - \mathbf{g}_v)}{\partial y} = \frac{\alpha}{y}(\mathbf{c} - \mathbf{g} + \mathbf{g}_v) + \mathbf{s}$$

$$\mathbf{q} = \begin{bmatrix} \rho_i \\ \rho u \\ \rho v \\ \rho E \end{bmatrix}, \ \mathbf{f} = \begin{bmatrix} \rho_i u \\ \rho u^2 + p \\ \rho uv \\ u(\rho E + p) \end{bmatrix}, \ \mathbf{g} = \begin{bmatrix} \rho_i v \\ \rho uv \\ \rho v^2 + p \\ v(\rho E + p) \end{bmatrix}, \ \mathbf{c} = \begin{bmatrix} 0 \\ 0 \\ p - \tau_{\theta\theta} \\ 0 \end{bmatrix}, \ \mathbf{s} = \begin{bmatrix} \dot{\omega}_i \\ 0 \\ 0 \\ 0 \end{bmatrix}$$

Axisymmetric Navier-Stokes equations with chemical reaction

$$\frac{\partial \mathbf{q}}{\partial t} + \frac{\partial (\mathbf{f} - \mathbf{f}_v)}{\partial x} + \frac{\partial (\mathbf{g} - \mathbf{g}_v)}{\partial y} = \frac{\alpha}{y}(\mathbf{c} - \mathbf{g} + \mathbf{g}_v) + \mathbf{s}$$

$$\mathbf{q} = \begin{bmatrix} \rho_i \\ \rho u \\ \rho v \\ \rho E \end{bmatrix}, \ \mathbf{f} = \begin{bmatrix} \rho_i u \\ \rho u^2 + p \\ \rho uv \\ u(\rho E + p) \end{bmatrix}, \ \mathbf{g} = \begin{bmatrix} \rho_i v \\ \rho uv \\ \rho v^2 + p \\ v(\rho E + p) \end{bmatrix}, \ \mathbf{c} = \begin{bmatrix} 0 \\ 0 \\ p - \tau_{\theta\theta} \\ 0 \end{bmatrix}, \ \mathbf{s} = \begin{bmatrix} \dot{\omega}_i \\ 0 \\ 0 \\ 0 \end{bmatrix}$$

$$\mathbf{f}_v = \begin{bmatrix} \rho D_i \dfrac{\partial Y_i}{\partial x} \\ \tau_{xx} \\ \tau_{xy} \\ k\dfrac{\partial T}{\partial x} + \rho \sum h_j D_j \dfrac{\partial Y_j}{\partial x} + u\tau_{xx} + v\tau_{xy} \end{bmatrix}$$

$$\mathbf{g}_v = \begin{bmatrix} \rho D_i \dfrac{\partial Y_i}{\partial y} \\ \tau_{xy} \\ \tau_{yy} \\ k\dfrac{\partial T}{\partial y} + \rho \sum h_j D_j \dfrac{\partial Y_j}{\partial y} + u\tau_{xy} + v\tau_{yy} \end{bmatrix}$$

$$\tau_{xx} = -\frac{2}{3}\mu(\nabla \cdot \mathbf{v}) + 2\mu\frac{\partial u}{\partial x}$$

$$\tau_{yy} = -\frac{2}{3}\mu(\nabla \cdot \mathbf{v}) + 2\mu\frac{\partial v}{\partial y}$$

$$\tau_{\theta\theta} = -\frac{2}{3}\mu(\nabla \cdot \mathbf{v}) + 2\mu\frac{v}{y}$$

$$\tau_{xy} = \mu\left(\frac{\partial u}{\partial y} + \frac{\partial v}{\partial x}\right)$$

$$\nabla \cdot \mathbf{v} = \left(\frac{\partial u}{\partial x} + \frac{\partial v}{\partial y} + \alpha\frac{v}{y}\right)$$

Chemistry and transport properties

Arrhenius-kinetics:

$$\dot{\omega}_i = \sum_{j=1}^{M} (\nu_{ji}^r - \nu_{ji}^f) \left[k_j^f \prod_{n=1}^{K} \left(\frac{\rho_n}{W_n} \right)^{\nu_{jn}^f} - k_j^r \prod_{n=1}^{K} \left(\frac{\rho_n}{W_n} \right)^{\nu_{jn}^r} \right] \quad i = 1, \ldots, K$$

Chemistry and transport properties

Arrhenius-kinetics:

$$\dot{\omega}_i = \sum_{j=1}^{M} (\nu_{ji}^r - \nu_{ji}^f) \left[k_j^f \prod_{n=1}^{K} \left(\frac{\rho_n}{W_n} \right)^{\nu_{jn}^f} - k_j^r \prod_{n=1}^{K} \left(\frac{\rho_n}{W_n} \right)^{\nu_{jn}^r} \right] \quad i = 1, \ldots, K$$

- Parsing of mechanisms and evaluation of $\dot{\omega}_i$ with Chemkin-II
- $c_{pi}(T)$ and $h_i(T)$ tabulated, linear interpolation between values

Chemistry and transport properties

Arrhenius-kinetics:

$$\dot{\omega}_i = \sum_{j=1}^{M} (\nu_{ji}^r - \nu_{ji}^f) \left[k_j^f \prod_{n=1}^{K} \left(\frac{\rho_n}{W_n} \right)^{\nu_{jn}^f} - k_j^r \prod_{n=1}^{K} \left(\frac{\rho_n}{W_n} \right)^{\nu_{jn}^r} \right] \quad i = 1, \ldots, K$$

- Parsing of mechanisms and evaluation of $\dot{\omega}_i$ with Chemkin-II
- $c_{pi}(T)$ and $h_i(T)$ tabulated, linear interpolation between values

Mixture viscosity $\mu = \mu(T, Y_i)$ with Wilke formula

$$\mu = \sum_{i=1}^{K} \frac{Y_i \mu_i}{W_i \sum_{m=1}^{K} Y_m \Phi_{im} / W_m} \text{ with } \Phi_{im} = \frac{1}{\sqrt{8}} \left(1 + \frac{W_i}{W_m} \right)^{-\frac{1}{2}} \left(1 + \left(\frac{\mu_i}{\mu_m} \right)^{\frac{1}{2}} \left(\frac{W_m}{W_j} \right)^{\frac{1}{4}} \right)^2$$

Chemistry and transport properties

Arrhenius-kinetics:

$$\dot{\omega}_i = \sum_{j=1}^{M} (\nu_{ji}^r - \nu_{ji}^f) \left[k_j^f \prod_{n=1}^{K} \left(\frac{\rho_n}{W_n} \right)^{\nu_{jn}^f} - k_j^r \prod_{n=1}^{K} \left(\frac{\rho_n}{W_n} \right)^{\nu_{jn}^r} \right] \quad i = 1, \ldots, K$$

- Parsing of mechanisms and evaluation of $\dot{\omega}_i$ with Chemkin-II
- $c_{pi}(T)$ and $h_i(T)$ tabulated, linear interpolation between values

Mixture viscosity $\mu = \mu(T, Y_i)$ with Wilke formula

$$\mu = \sum_{i=1}^{K} \frac{Y_i \mu_i}{W_i \sum_{m=1}^{K} Y_m \Phi_{im} / W_m} \text{ with } \Phi_{im} = \frac{1}{\sqrt{8}} \left(1 + \frac{W_i}{W_m} \right)^{-\frac{1}{2}} \left(1 + \left(\frac{\mu_i}{\mu_m} \right)^{\frac{1}{2}} \left(\frac{W_m}{W_j} \right)^{\frac{1}{4}} \right)^2$$

Mixture thermal conductivity $k = k(T, Y_i)$ following Mathur

$$k = \frac{1}{2} \left(W \sum_{i=1}^{K} \frac{Y_i k_i}{W_i} + \frac{1}{W \sum_{i=1}^{K} Y_i / (W_i k_i)} \right)$$

Chemistry and transport properties

Arrhenius-kinetics:

$$\dot{\omega}_i = \sum_{j=1}^{M} (\nu_{ji}^r - \nu_{ji}^f) \left[k_j^f \prod_{n=1}^{K} \left(\frac{\rho_n}{W_n} \right)^{\nu_{jn}^f} - k_j^r \prod_{n=1}^{K} \left(\frac{\rho_n}{W_n} \right)^{\nu_{jn}^r} \right] \quad i = 1, \ldots, K$$

- Parsing of mechanisms and evaluation of $\dot{\omega}_i$ with Chemkin-II
- $c_{pi}(T)$ and $h_i(T)$ tabulated, linear interpolation between values

Mixture viscosity $\mu = \mu(T, Y_i)$ with Wilke formula

$$\mu = \sum_{i=1}^{K} \frac{Y_i \mu_i}{W_i \sum_{m=1}^{K} Y_m \Phi_{im} / W_m} \text{ with } \Phi_{im} = \frac{1}{\sqrt{8}} \left(1 + \frac{W_i}{W_m} \right)^{-\frac{1}{2}} \left(1 + \left(\frac{\mu_i}{\mu_m} \right)^{\frac{1}{2}} \left(\frac{W_m}{W_j} \right)^{\frac{1}{4}} \right)^2$$

Mixture thermal conductivity $k = k(T, Y_i)$ following Mathur

$$k = \frac{1}{2} \left(W \sum_{i=1}^{K} \frac{Y_i k_i}{W_i} + \frac{1}{W \sum_{i=1}^{K} Y_i / (W_i k_i)} \right)$$

Mixture diffusion coefficients $D_i = D_i(T, p, Y_i)$ from binary diffusion $D_{mi}(T, p)$ as

$$D_i = \frac{1 - Y_i}{W \sum_{m \neq i} Y_m / (W_m D_{mi})}$$

- Evaluation with Chemkin-II Transport library

Splitting method

$$\partial_t \mathbf{q} + \partial_x(\mathbf{f} - \mathbf{f}_v) + \partial_y(\mathbf{g} - \mathbf{g}_v) = \frac{\alpha}{y}(\mathbf{c} - \mathbf{g} + \mathbf{g}_v) + \mathbf{s}$$

Splitting method

$$\partial_t \mathbf{q} + \partial_x(\mathbf{f} - \mathbf{f}_v) + \partial_y(\mathbf{g} - \mathbf{g}_v) = \frac{\alpha}{y}(\mathbf{c} - \mathbf{g} + \mathbf{g}_v) + \mathbf{s}$$

Dimensional splitting for PDE

$$\mathcal{X}^{(\Delta t)}: \quad \partial_t \mathbf{q} + \partial_x(\mathbf{f}(\mathbf{q}) - \mathbf{f}_v(\mathbf{q})) = 0\,, \qquad \text{IC: } \mathbf{Q}(t_m) \overset{\Delta t}{\Longrightarrow} \tilde{\mathbf{Q}}^{1/2}$$

$$\mathcal{Y}^{(\Delta t)}: \quad \partial_t \mathbf{q} + \partial_y(\mathbf{g}(\mathbf{q}) - \mathbf{g}_v(\mathbf{q})) = 0\,, \qquad \text{IC: } \tilde{\mathbf{Q}}^{1/2} \overset{\Delta t}{\Longrightarrow} \tilde{\mathbf{Q}}$$

Splitting method

$$\partial_t \mathbf{q} + \partial_x(\mathbf{f} - \mathbf{f}_v) + \partial_y(\mathbf{g} - \mathbf{g}_v) = \frac{\alpha}{y}(\mathbf{c} - \mathbf{g} + \mathbf{g}_v) + \mathbf{s}$$

Dimensional splitting for PDE

$$\mathcal{X}^{(\Delta t)}: \quad \partial_t \mathbf{q} + \partial_x(\mathbf{f}(\mathbf{q}) - \mathbf{f}_v(\mathbf{q})) = 0\,, \qquad \text{IC: } \mathbf{Q}(t_m) \overset{\Delta t}{\Longrightarrow} \tilde{\mathbf{Q}}^{1/2}$$

$$\mathcal{Y}^{(\Delta t)}: \quad \partial_t \mathbf{q} + \partial_y(\mathbf{g}(\mathbf{q}) - \mathbf{g}_v(\mathbf{q})) = 0\,, \qquad \text{IC: } \tilde{\mathbf{Q}}^{1/2} \overset{\Delta t}{\Longrightarrow} \tilde{\mathbf{Q}}$$

Treat right-hand side as source term

$$\mathcal{C}^{(\Delta t)}: \quad \partial_t \mathbf{q} = \tfrac{\alpha}{y}(\mathbf{c}(\mathbf{q}) - \mathbf{g}(\mathbf{q}) + \mathbf{g}_v(\mathbf{q}))\,, \qquad \text{IC: } \tilde{\mathbf{Q}} \overset{\Delta t}{\Longrightarrow} \bar{\mathbf{Q}}$$

Splitting method

$$\partial_t \mathbf{q} + \partial_x(\mathbf{f} - \mathbf{f}_v) + \partial_y(\mathbf{g} - \mathbf{g}_v) = \frac{\alpha}{y}(\mathbf{c} - \mathbf{g} + \mathbf{g}_v) + \mathbf{s}$$

Dimensional splitting for PDE

$$\mathcal{X}^{(\Delta t)}: \quad \partial_t \mathbf{q} + \partial_x(\mathbf{f}(\mathbf{q}) - \mathbf{f}_v(\mathbf{q})) = 0\,, \qquad \text{IC: } \mathbf{Q}(t_m) \overset{\Delta t}{\Longrightarrow} \tilde{\mathbf{Q}}^{1/2}$$

$$\mathcal{Y}^{(\Delta t)}: \quad \partial_t \mathbf{q} + \partial_y(\mathbf{g}(\mathbf{q}) - \mathbf{g}_v(\mathbf{q})) = 0\,, \qquad \text{IC: } \tilde{\mathbf{Q}}^{1/2} \overset{\Delta t}{\Longrightarrow} \tilde{\mathbf{Q}}$$

Treat right-hand side as source term

$$\mathcal{C}^{(\Delta t)}: \quad \partial_t \mathbf{q} = \tfrac{\alpha}{y}(\mathbf{c}(\mathbf{q}) - \mathbf{g}(\mathbf{q}) + \mathbf{g}_v(\mathbf{q}))\,, \qquad \text{IC: } \tilde{\mathbf{Q}} \overset{\Delta t}{\Longrightarrow} \bar{\mathbf{Q}}$$

Chemical source term

$$\mathcal{S}^{(\Delta t)}: \quad \partial_t \mathbf{q} = \mathbf{s}(\mathbf{q})\,, \qquad \text{IC: } \bar{\mathbf{Q}} \overset{\Delta t}{\Longrightarrow} \mathbf{Q}(t_m + \Delta t)$$

Splitting method

$$\partial_t \mathbf{q} + \partial_x(\mathbf{f} - \mathbf{f}_v) + \partial_y(\mathbf{g} - \mathbf{g}_v) = \frac{\alpha}{y}(\mathbf{c} - \mathbf{g} + \mathbf{g}_v) + \mathbf{s}$$

Dimensional splitting for PDE

$$\mathcal{X}^{(\Delta t)}: \quad \partial_t \mathbf{q} + \partial_x(\mathbf{f}(\mathbf{q}) - \mathbf{f}_v(\mathbf{q})) = 0\,, \qquad \text{IC: } \mathbf{Q}(t_m) \overset{\Delta t}{\Longrightarrow} \tilde{\mathbf{Q}}^{1/2}$$

$$\mathcal{Y}^{(\Delta t)}: \quad \partial_t \mathbf{q} + \partial_y(\mathbf{g}(\mathbf{q}) - \mathbf{g}_v(\mathbf{q})) = 0\,, \qquad \text{IC: } \tilde{\mathbf{Q}}^{1/2} \overset{\Delta t}{\Longrightarrow} \tilde{\mathbf{Q}}$$

Treat right-hand side as source term

$$\mathcal{C}^{(\Delta t)}: \quad \partial_t \mathbf{q} = \tfrac{\alpha}{y}(\mathbf{c}(\mathbf{q}) - \mathbf{g}(\mathbf{q}) + \mathbf{g}_v(\mathbf{q}))\,, \qquad \text{IC: } \tilde{\mathbf{Q}} \overset{\Delta t}{\Longrightarrow} \bar{\mathbf{Q}}$$

Chemical source term

$$\mathcal{S}^{(\Delta t)}: \quad \partial_t \mathbf{q} = \mathbf{s}(\mathbf{q})\,, \qquad \text{IC: } \bar{\mathbf{Q}} \overset{\Delta t}{\Longrightarrow} \mathbf{Q}(t_m + \Delta t)$$

Formally 1st-order algorithm

$$\mathbf{Q}(t_m + \Delta t) = \mathcal{S}^{(\Delta t)}\mathcal{C}^{(\Delta t)}\mathcal{Y}^{(\Delta t)}\mathcal{X}^{(\Delta t)}(\mathbf{Q}(t_m))$$

but all sub-operators 2nd-order accurate or higher.

Finite volume discretization

Time discretization $t_n = n\Delta t$, discrete volumes $I_{jk} = [x_j - \frac{1}{2}\Delta x, x_j + \frac{1}{2}\Delta x[\times[y_k - \frac{1}{2}\Delta y, y_k + \frac{1}{2}\Delta y[\times =: [x_{j-1/2}, x_{j+1/2}[\times[y_{k-1/2}, y_{k+1/2}[$

Approximation $\mathbf{Q}_{jk}(t) \approx \frac{1}{|I_{jk}|} \int_{I_{jk}} \mathbf{q}(\mathbf{x}, t)\, dx$ and numerical fluxes

$$\mathbf{F}\left(\mathbf{Q}_{jk}(t), \mathbf{Q}_{j+1,k}(t)\right) \approx \mathbf{f}(\mathbf{q}(x_{j+1/2}, y_k, t)),$$

$$\mathbf{F}_v\left(\mathbf{Q}_{jk}(t), \mathbf{Q}_{j+1,k}(t)\right) \approx \mathbf{f}_v(\mathbf{q}(x_{j+1/2}, y_k, t), \nabla\mathbf{q}(x_{j+1/2}, y_k, t))$$

yield (for simplicity)

$$\mathbf{Q}_{jk}^{n+1} = \mathbf{Q}_{kj}^{n} - \frac{\Delta t}{\Delta x}\left[\mathbf{F}\left(\mathbf{Q}_{jk}^{n}, \mathbf{Q}_{j+1,k}^{n}\right) - \mathbf{F}\left(\mathbf{Q}_{j-1,k}^{n}, \mathbf{Q}_{jk}^{n}\right)\right] + \frac{\Delta t}{\Delta x}\left[\mathbf{F}_v\left(\mathbf{Q}_{jk}^{n}, \mathbf{Q}_{j+1,k}^{n}\right) - \mathbf{F}_v\left(\mathbf{Q}_{j-1,k}^{n}, \mathbf{Q}_{jk}^{n}\right)\right]$$

Finite volume discretization

Time discretization $t_n = n\Delta t$, discrete volumes $I_{jk} = [x_j - \frac{1}{2}\Delta x, x_j + \frac{1}{2}\Delta x[\times[y_k - \frac{1}{2}\Delta y, y_k + \frac{1}{2}\Delta y[\times =: [x_{j-1/2}, x_{j+1/2}[\times[y_{k-1/2}, y_{k+1/2}[$

Approximation $\mathbf{Q}_{jk}(t) \approx \frac{1}{|I_{jk}|} \int_{I_{jk}} \mathbf{q}(\mathbf{x}, t)\, dx$ and numerical fluxes

$$\mathbf{F}\left(\mathbf{Q}_{jk}(t), \mathbf{Q}_{j+1,k}(t)\right) \approx \mathbf{f}(\mathbf{q}(x_{j+1/2}, y_k, t)),$$

$$\mathbf{F}_v\left(\mathbf{Q}_{jk}(t), \mathbf{Q}_{j+1,k}(t)\right) \approx \mathbf{f}_v(\mathbf{q}(x_{j+1/2}, y_k, t), \nabla\mathbf{q}(x_{j+1/2}, y_k, t))$$

yield (for simplicity)

$$\mathbf{Q}_{jk}^{n+1} = \mathbf{Q}_{kj}^{n} - \frac{\Delta t}{\Delta x}\left[\mathbf{F}\left(\mathbf{Q}_{jk}^{n}, \mathbf{Q}_{j+1,k}^{n}\right) - \mathbf{F}\left(\mathbf{Q}_{j-1,k}^{n}, \mathbf{Q}_{jk}^{n}\right)\right] + \frac{\Delta t}{\Delta x}\left[\mathbf{F}_v\left(\mathbf{Q}_{jk}^{n}, \mathbf{Q}_{j+1,k}^{n}\right) - \mathbf{F}_v\left(\mathbf{Q}_{j-1,k}^{n}, \mathbf{Q}_{jk}^{n}\right)\right]$$

- Riemann solver to approximate $\mathbf{F}\left(\mathbf{Q}_{jk}^{n}, \mathbf{Q}_{j+1,k}^{n}\right)$

Finite volume discretization

Time discretization $t_n = n\Delta t$, discrete volumes $I_{jk} = [x_j - \frac{1}{2}\Delta x, x_j + \frac{1}{2}\Delta x[\times[y_k - \frac{1}{2}\Delta y, y_k + \frac{1}{2}\Delta y[\times =: [x_{j-1/2}, x_{j+1/2}[\times[y_{k-1/2}, y_{k+1/2}[$

Approximation $\mathbf{Q}_{jk}(t) \approx \frac{1}{|I_{jk}|} \int_{I_{jk}} \mathbf{q}(\mathbf{x}, t)\, dx$ and numerical fluxes

$$\mathbf{F}\left(\mathbf{Q}_{jk}(t), \mathbf{Q}_{j+1,k}(t)\right) \approx \mathbf{f}(\mathbf{q}(x_{j+1/2}, y_k, t)),$$

$$\mathbf{F}_v\left(\mathbf{Q}_{jk}(t), \mathbf{Q}_{j+1,k}(t)\right) \approx \mathbf{f}_v(\mathbf{q}(x_{j+1/2}, y_k, t), \nabla\mathbf{q}(x_{j+1/2}, y_k, t))$$

yield (for simplicity)

$$\mathbf{Q}_{jk}^{n+1} = \mathbf{Q}_{kj}^n - \frac{\Delta t}{\Delta x}\left[\mathbf{F}\left(\mathbf{Q}_{jk}^n, \mathbf{Q}_{j+1,k}^n\right) - \mathbf{F}\left(\mathbf{Q}_{j-1,k}^n, \mathbf{Q}_{jk}^n\right)\right] + \frac{\Delta t}{\Delta x}\left[\mathbf{F}_v\left(\mathbf{Q}_{jk}^n, \mathbf{Q}_{j+1,k}^n\right) - \mathbf{F}_v\left(\mathbf{Q}_{j-1,k}^n, \mathbf{Q}_{jk}^n\right)\right]$$

- Riemann solver to approximate $\mathbf{F}\left(\mathbf{Q}_{jk}^n, \mathbf{Q}_{j+1,k}^n\right)$
- 1st-order finite differences for $\mathbf{F}_v\left(\mathbf{Q}_{jk}^n, \mathbf{Q}_{j+1,k}^n\right)$ yield 2nd-order accurate central differences in $(*)$

Finite volume discretization

Time discretization $t_n = n\Delta t$, discrete volumes $I_{jk} = [x_j - \frac{1}{2}\Delta x, x_j + \frac{1}{2}\Delta x[\times[y_k - \frac{1}{2}\Delta y, y_k + \frac{1}{2}\Delta y[\times =: [x_{j-1/2}, x_{j+1/2}[\times[y_{k-1/2}, y_{k+1/2}[$

Approximation $\mathbf{Q}_{jk}(t) \approx \frac{1}{|I_{jk}|} \int_{I_{jk}} \mathbf{q}(\mathbf{x}, t)\, dx$ and numerical fluxes

$$\mathbf{F}\left(\mathbf{Q}_{jk}(t), \mathbf{Q}_{j+1,k}(t)\right) \approx \mathbf{f}(\mathbf{q}(x_{j+1/2}, y_k, t)),$$

$$\mathbf{F}_v\left(\mathbf{Q}_{jk}(t), \mathbf{Q}_{j+1,k}(t)\right) \approx \mathbf{f}_v(\mathbf{q}(x_{j+1/2}, y_k, t), \nabla\mathbf{q}(x_{j+1/2}, y_k, t))$$

yield (for simplicity)

$$\mathbf{Q}_{jk}^{n+1} = \mathbf{Q}_{kj}^{n} - \frac{\Delta t}{\Delta x}\left[\mathbf{F}\left(\mathbf{Q}_{jk}^{n}, \mathbf{Q}_{j+1,k}^{n}\right) - \mathbf{F}\left(\mathbf{Q}_{j-1,k}^{n}, \mathbf{Q}_{jk}^{n}\right)\right] + \frac{\Delta t}{\Delta x}\left[\mathbf{F}_v\left(\mathbf{Q}_{jk}^{n}, \mathbf{Q}_{j+1,k}^{n}\right) - \mathbf{F}_v\left(\mathbf{Q}_{j-1,k}^{n}, \mathbf{Q}_{jk}^{n}\right)\right]$$

- Riemann solver to approximate $\mathbf{F}\left(\mathbf{Q}_{jk}^{n}, \mathbf{Q}_{j+1,k}^{n}\right)$
- 1st-order finite differences for $\mathbf{F}_v\left(\mathbf{Q}_{jk}^{n}, \mathbf{Q}_{j+1,k}^{n}\right)$ yield 2nd-order accurate central differences in $(*)$

Stability condition used:

$$\max_{i,j,k}\left\{\frac{\Delta t}{\Delta x}(|u_{jk}| + c_{jk}) + \frac{8}{3}\frac{\mu_{jk}\Delta t}{\rho_{jk}\Delta x^2}, \frac{\Delta t}{\Delta x}(|u_{jk}| + c_{jk}) + \frac{2k_j\Delta t}{c_{v,jk}\rho_j\Delta x^2}, \frac{\Delta t}{\Delta x}(|u_{jk}| + c_{jk}) + D_{i,jk}\frac{\Delta t}{\Delta x^2}\right\} \leq 1$$

Finite volume discretization – cont.

Symmetry source term $\mathcal{C}^{(\Delta t)}$: Use

$$\mathbf{Q}_{jk}^{n+1} = \mathbf{Q}_{jk}^{n} + \Delta t \left(\frac{\alpha}{y} (\mathbf{c}(\mathbf{Q}_{jk}^{n}) - \mathbf{g}(\mathbf{Q}_{jk}^{n}) + \frac{1}{2} \left(\mathbf{G}_v \left(\mathbf{Q}_{jk}^{n}, \mathbf{Q}_{j,k+1}^{n} \right) + \mathbf{G}_v \left(\mathbf{Q}_{j,k-1}^{n}, \mathbf{Q}_{jk}^{n} \right) \right) \right)$$

within explicit 2nd-order accurate Runge-Kutta method

- Gives 2nd-order central difference approximation of $\mathbf{G}_v$

Finite volume discretization – cont.

Symmetry source term $\mathcal{C}^{(\Delta t)}$: Use

$$\mathbf{Q}_{jk}^{n+1} = \mathbf{Q}_{jk}^{n} + \Delta t \left(\frac{\alpha}{y} (\mathbf{c}(\mathbf{Q}_{jk}^{n}) - \mathbf{g}(\mathbf{Q}_{jk}^{n}) + \frac{1}{2} \left(\mathbf{G}_v \left(\mathbf{Q}_{jk}^{n}, \mathbf{Q}_{j,k+1}^{n} \right) + \mathbf{G}_v \left(\mathbf{Q}_{j,k-1}^{n}, \mathbf{Q}_{jk}^{n} \right) \right) \right)$$

within explicit 2nd-order accurate Runge-Kutta method

- Gives 2nd-order central difference approximation of $\mathbf{G}_v$
- Transport properties μ, k, D_i are stored in vector of state $\mathbf{Q}$ and kept constant throughout entire time step

Finite volume discretization – cont.

Symmetry source term $\mathcal{C}^{(\Delta t)}$: Use

$$\mathbf{Q}_{jk}^{n+1} = \mathbf{Q}_{jk}^{n} + \Delta t \left(\frac{\alpha}{y} (\mathbf{c}(\mathbf{Q}_{jk}^{n}) - \mathbf{g}(\mathbf{Q}_{jk}^{n}) + \frac{1}{2} \left(\mathbf{G}_v \left(\mathbf{Q}_{jk}^{n}, \mathbf{Q}_{j,k+1}^{n} \right) + \mathbf{G}_v \left(\mathbf{Q}_{j,k-1}^{n}, \mathbf{Q}_{jk}^{n} \right) \right) \right)$$

within explicit 2nd-order accurate Runge-Kutta method

- Gives 2nd-order central difference approximation of $\mathbf{G}_v$
- Transport properties μ, k, D_i are stored in vector of state $\mathbf{Q}$ and kept constant throughout entire time step

Chemical source term $\mathcal{S}^{(\cdot)}$:

- 4th-order accurate semi-implicit ODE-solver subcycles within each cell
- ρ, e, u, v remain unchanged!

$$\partial_t \rho_i = W_i \dot{\omega}_i(\rho_1, \ldots, \rho_K, T) \qquad i = 1, \ldots, K$$

Lehr's ballistic range experiments

- Spherical-nosed projectile of radius $1.5\,\mathrm{mm}$ travels with constant velocity through stoichiometric $\mathrm{H_2} : \mathrm{O_2} : \mathrm{N_2}$ mixture (molar ratios 2:1:3.76) at $42.663\,\mathrm{kPa}$ and $T = 293\,\mathrm{K}$ [Lehr, 1972]
- Mechanism by [Jachimowski, 1988]: 19 equilibrium reactions, 9 species. Chapman Jouguet velocity $\sim 1957\,\mathrm{m/s}$.

Lehr's ballistic range experiments

- Spherical-nosed projectile of radius $1.5\,\mathrm{mm}$ travels with constant velocity through stoichiometric $\mathrm{H_2} : \mathrm{O_2} : \mathrm{N_2}$ mixture (molar ratios 2:1:3.76) at $42.663\,\mathrm{kPa}$ and $T = 293\,\mathrm{K}$ [Lehr, 1972]
- Mechanism by [Jachimowski, 1988]: 19 equilibrium reactions, 9 species. Chapman Jouguet velocity $\sim 1957\,\mathrm{m/s}$.
- Axisymmetric Navier-Stokes and Eulers simulations on AMR base mesh of 400×200 cells, physical domain size $6\,\mathrm{cm} \times 3\,\mathrm{cm}$
- 4-level computations with refinement factors 2,2,4 to final time $t = 170\,\mu\mathrm{s}$. Refinement downstream removed.

Lehr's ballistic range experiments

- Spherical-nosed projectile of radius $1.5\,\mathrm{mm}$ travels with constant velocity through stoichiometric $\mathrm{H_2} : \mathrm{O_2} : \mathrm{N_2}$ mixture (molar ratios 2:1:3.76) at $42.663\,\mathrm{kPa}$ and $T = 293\,\mathrm{K}$ [Lehr, 1972]
- Mechanism by [Jachimowski, 1988]: 19 equilibrium reactions, 9 species. Chapman Jouguet velocity $\sim 1957\,\mathrm{m/s}$.
- Axisymmetric Navier-Stokes and Eulers simulations on AMR base mesh of 400×200 cells, physical domain size $6\,\mathrm{cm} \times 3\,\mathrm{cm}$
- 4-level computations with refinement factors 2,2,4 to final time $t = 170\,\mu\mathrm{s}$. Refinement downstream removed.
- Main configurations
  - Velocity $v_I = 1931\,\mathrm{m/s}$ ($M = 4.79$), $\sim 40\,\mathrm{Pts}/l_{ig}$
  - Velocity $v_I = 1806\,\mathrm{m/s}$ ($M = 4.48$), $\sim 60\,\mathrm{Pts}/l_{ig}$
- Various previous studies with not entirely consistent results. E.g. [Yungster and Radhakrishnan, 1996], [Axdahl et al., 2011]

Lehr's ballistic range experiments

- Spherical-nosed projectile of radius $1.5\,\mathrm{mm}$ travels with constant velocity through stoichiometric $\mathrm{H_2} : \mathrm{O_2} : \mathrm{N_2}$ mixture (molar ratios 2:1:3.76) at $42.663\,\mathrm{kPa}$ and $T = 293\,\mathrm{K}$ [Lehr, 1972]
- Mechanism by [Jachimowski, 1988]: 19 equilibrium reactions, 9 species. Chapman Jouguet velocity $\sim 1957\,\mathrm{m/s}$.
- Axisymmetric Navier-Stokes and Eulers simulations on AMR base mesh of 400×200 cells, physical domain size $6\,\mathrm{cm} \times 3\,\mathrm{cm}$
- 4-level computations with refinement factors 2,2,4 to final time $t = 170\,\mu\mathrm{s}$. Refinement downstream removed.
- Main configurations
  - Velocity $v_l = 1931\,\mathrm{m/s}$ ($M = 4.79$), $\sim 40\,\mathrm{Pts}/l_{ig}$
  - Velocity $v_l = 1806\,\mathrm{m/s}$ ($M = 4.48$), $\sim 60\,\mathrm{Pts}/l_{ig}$
- Various previous studies with not entirely consistent results. E.g. [Yungster and Radhakrishnan, 1996], [Axdahl et al., 2011]
- Stagnation point location and pressure tracked in every time step

Lehr's ballistic range experiments

- Spherical-nosed projectile of radius $1.5\,\mathrm{mm}$ travels with constant velocity through stoichiometric $\mathrm{H_2} : \mathrm{O_2} : \mathrm{N_2}$ mixture (molar ratios 2:1:3.76) at $42.663\,\mathrm{kPa}$ and $T = 293\,\mathrm{K}$ [Lehr, 1972]
- Mechanism by [Jachimowski, 1988]: 19 equilibrium reactions, 9 species. Chapman Jouguet velocity $\sim 1957\,\mathrm{m/s}$.
- Axisymmetric Navier-Stokes and Eulers simulations on AMR base mesh of 400×200 cells, physical domain size $6\,\mathrm{cm} \times 3\,\mathrm{cm}$
- 4-level computations with refinement factors 2,2,4 to final time $t = 170\,\mu\mathrm{s}$. Refinement downstream removed.
- Main configurations
  - Velocity $v_l = 1931\,\mathrm{m/s}$ ($M = 4.79$), $\sim 40\,\mathrm{Pts}/l_{ig}$
  - Velocity $v_l = 1806\,\mathrm{m/s}$ ($M = 4.48$), $\sim 60\,\mathrm{Pts}/l_{ig}$
- Various previous studies with not entirely consistent results. E.g. [Yungster and Radhakrishnan, 1996], [Axdahl et al., 2011]
- Stagnation point location and pressure tracked in every time step
- All computations were on 32 cores requiring $\sim 1500\,\mathrm{h}$ CPU each

Lehr's ballistic range experiments

- Spherical-nosed projectile of radius $1.5\,\mathrm{mm}$ travels with constant velocity through stoichiometric $H_2 : O_2 : N_2$ mixture (molar ratios 2:1:3.76) at $42.663\,\mathrm{kPa}$ and $T = 293\,\mathrm{K}$ [Lehr, 1972]
- Mechanism by [Jachimowski, 1988]: 19 equilibrium reactions, 9 species. Chapman Jouguet velocity $\sim 1957\,\mathrm{m/s}$.
- Axisymmetric Navier-Stokes and Eulers simulations on AMR base mesh of 400×200 cells, physical domain size $6\,\mathrm{cm} \times 3\,\mathrm{cm}$
- 4-level computations with refinement factors 2,2,4 to final time $t = 170\,\mu\mathrm{s}$. Refinement downstream removed.
- Main configurations
  - Velocity $v_l = 1931\,\mathrm{m/s}$ ($M = 4.79$), $\sim 40\,\mathrm{Pts}/l_{ig}$
  - Velocity $v_l = 1806\,\mathrm{m/s}$ ($M = 4.48$), $\sim 60\,\mathrm{Pts}/l_{ig}$
- Various previous studies with not entirely consistent results. E.g. [Yungster and Radhakrishnan, 1996], [Axdahl et al., 2011]
- Stagnation point location and pressure tracked in every time step
- All computations were on 32 cores requiring $\sim 1500\,\mathrm{h}$ CPU each

vtf/amroc/clawpack/applications/euler_chem/2d/SphereLehr

vtf/amroc/clawpack/applications/euler_chem/2d/SphereLehrNav

Viscous case – $M = 4.79$

- 5619 iterations with CFL=0.9 to $t = 170\,\mu\mathrm{s}$
- Oscillation frequency in last $20\,\mu\mathrm{s}$: $\sim 722\,\mathrm{kHz}$ (viscous), $\sim 737\,\mathrm{kHz}$ (inviscid)
- Experimental value: $\sim 720\,\mathrm{kHz}$

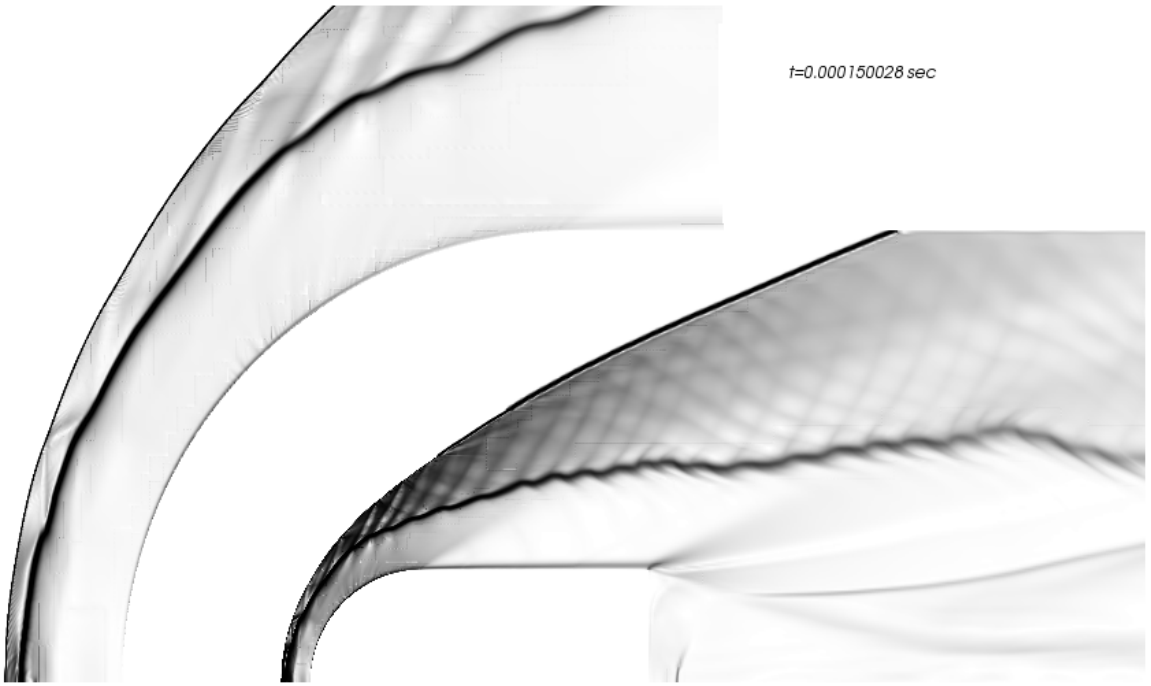

Schlieren plot of density

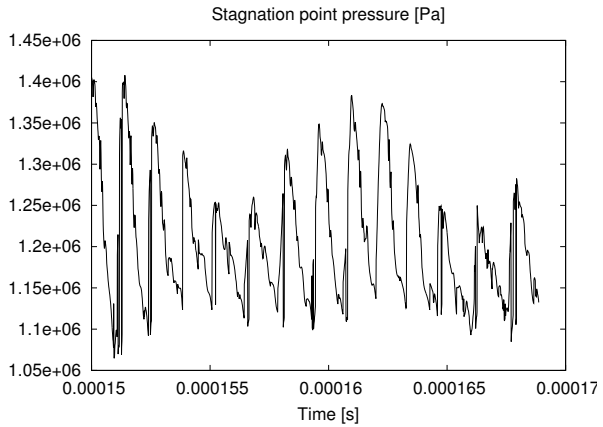

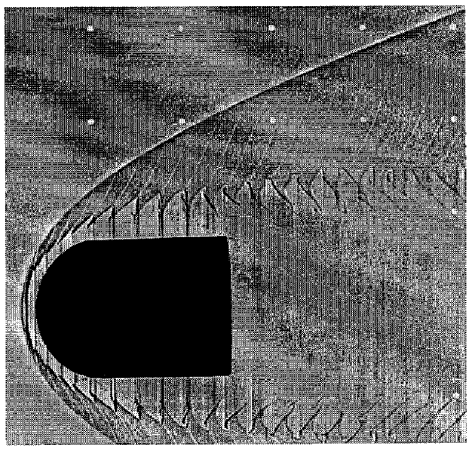

Viscous case – $M = 4.79$ – mesh adaptation

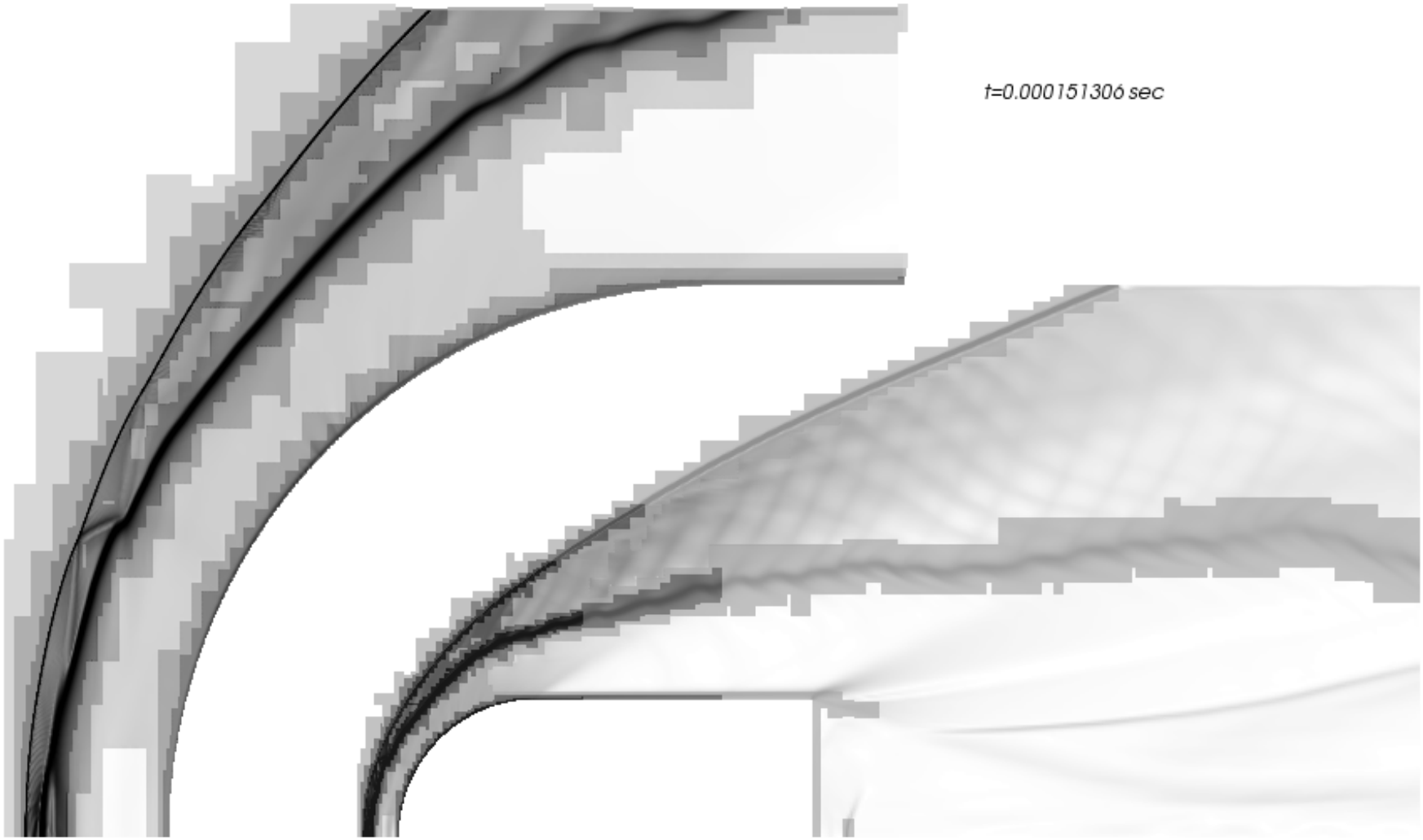

Comparison of temperature field

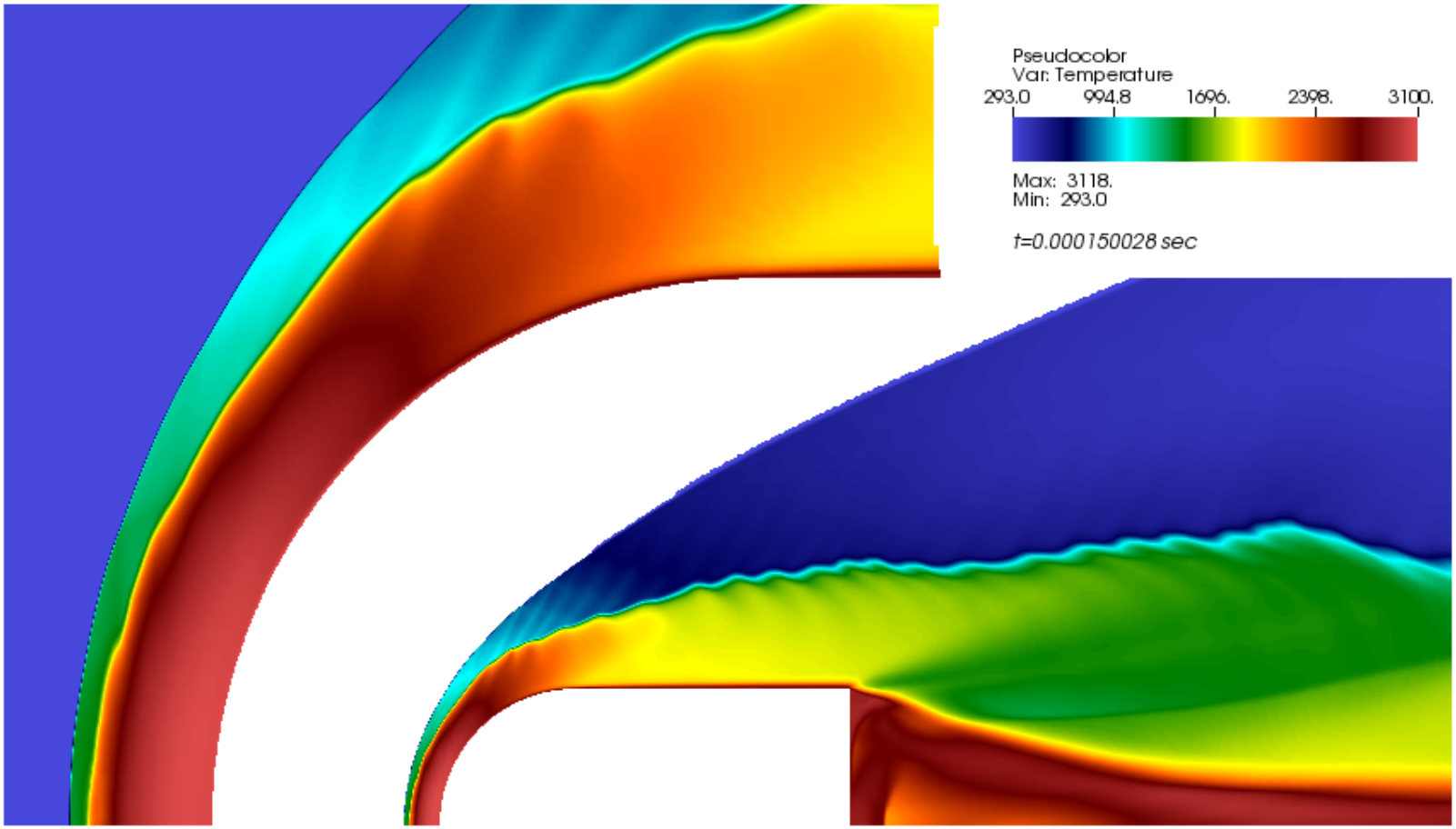

Viscous

Comparison of temperature field

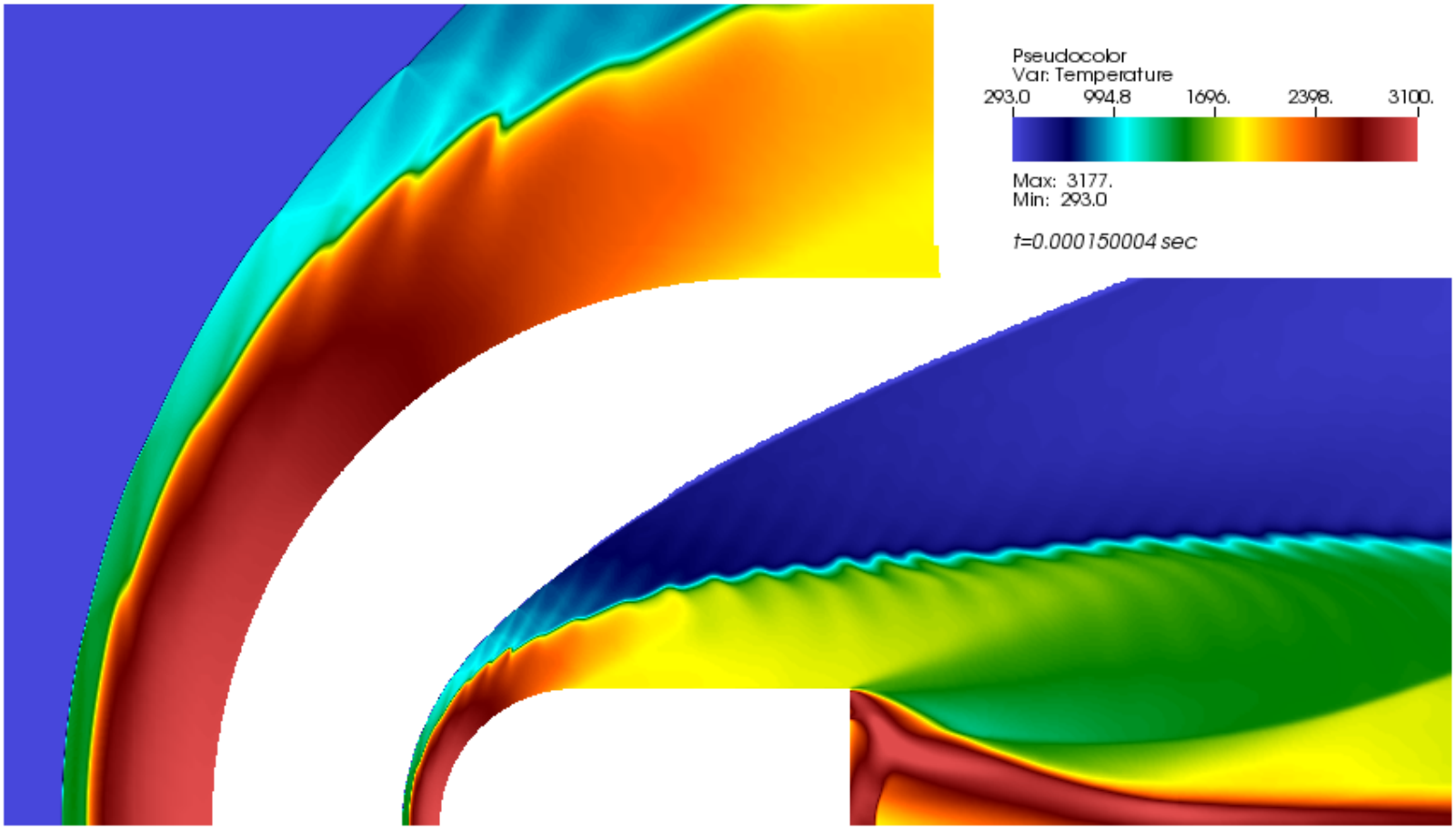

Inviscid

Viscous case – $M = 4.48$

- 5432 iterations with CFL=0.9 to $t = 170\,\mu\mathrm{s}$
- Oscillation frequency in last $20\,\mu\mathrm{s}$: $\sim 417\,\mathrm{kHz}$
- Experimental value: $\sim 425\,\mathrm{kHz}$

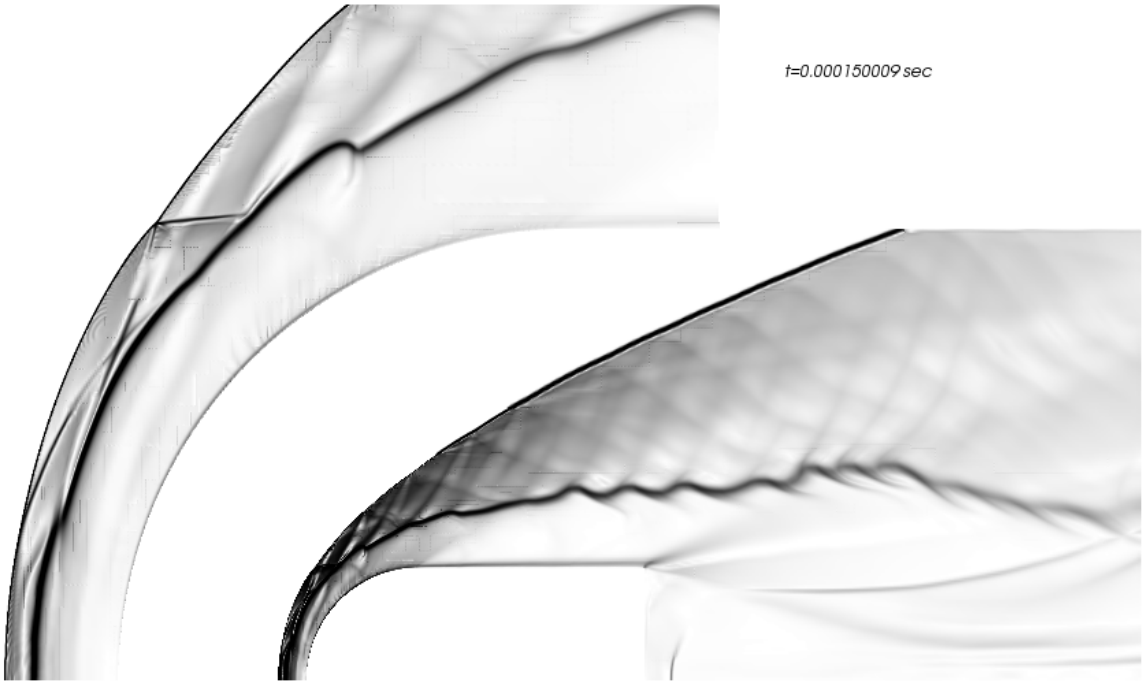

Schlieren plot of density

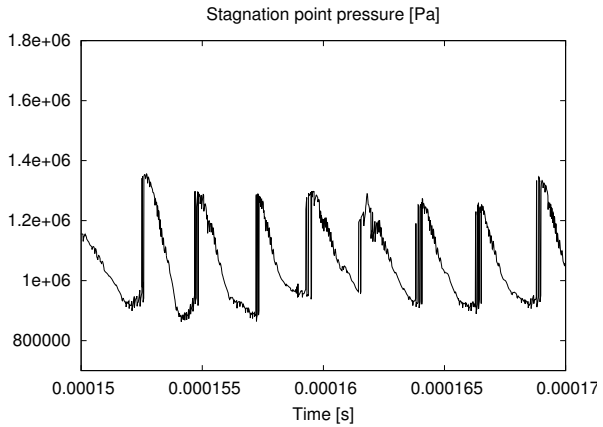

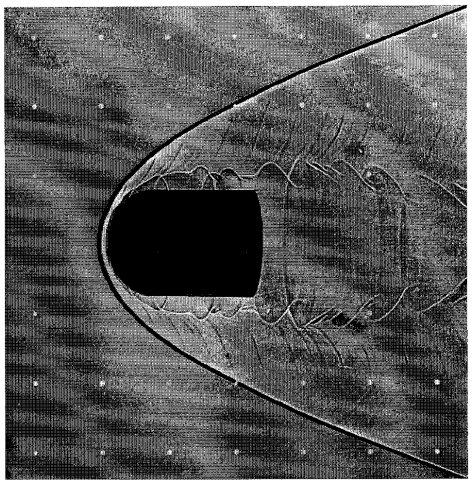

Oscillation mechanism

Schlieren of density

Temperature

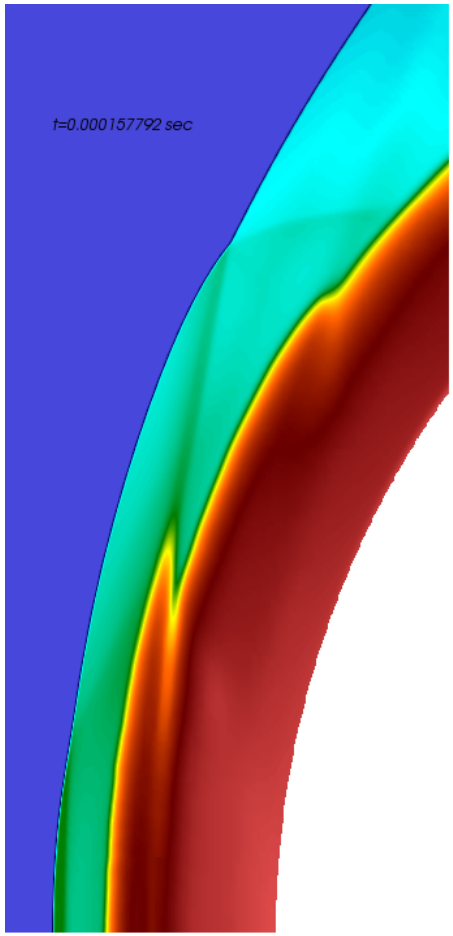

Mass fraction OH

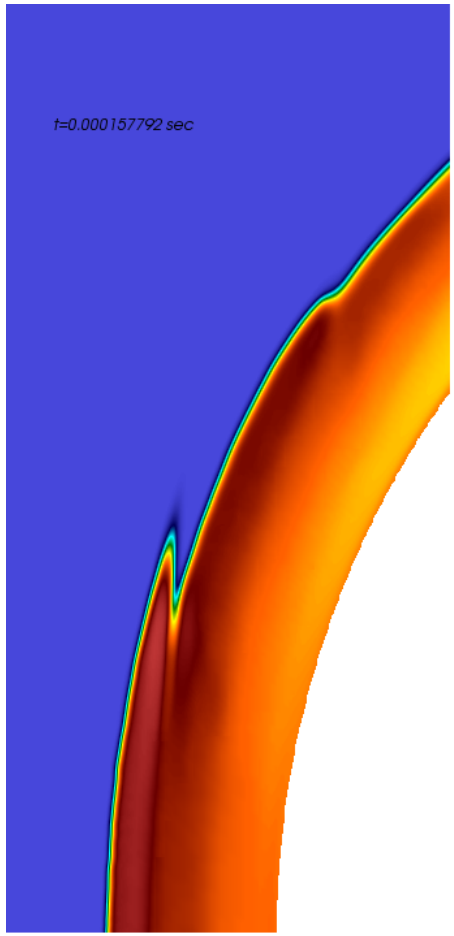

Pressure

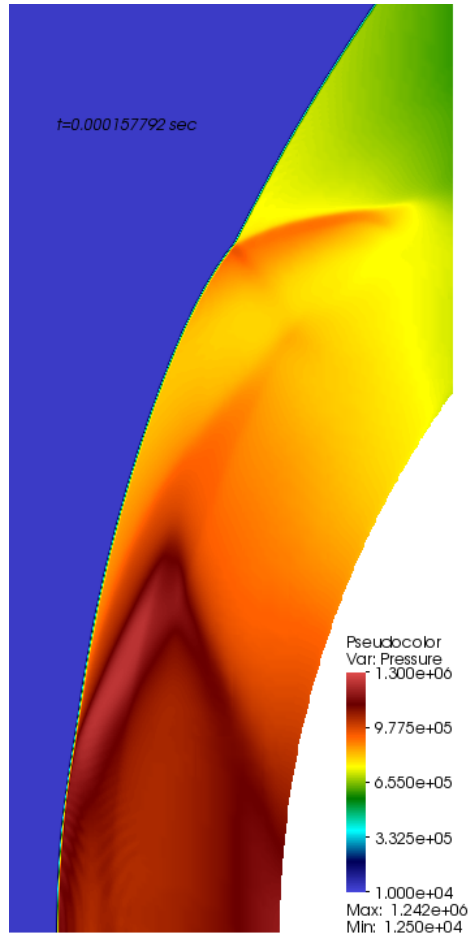

Oscillation mechanism

Schlieren of density

Temperature

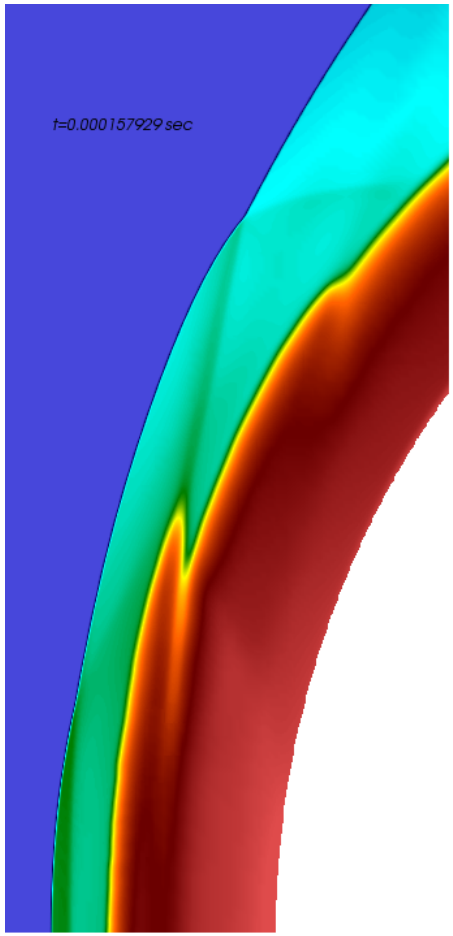

Mass fraction OH

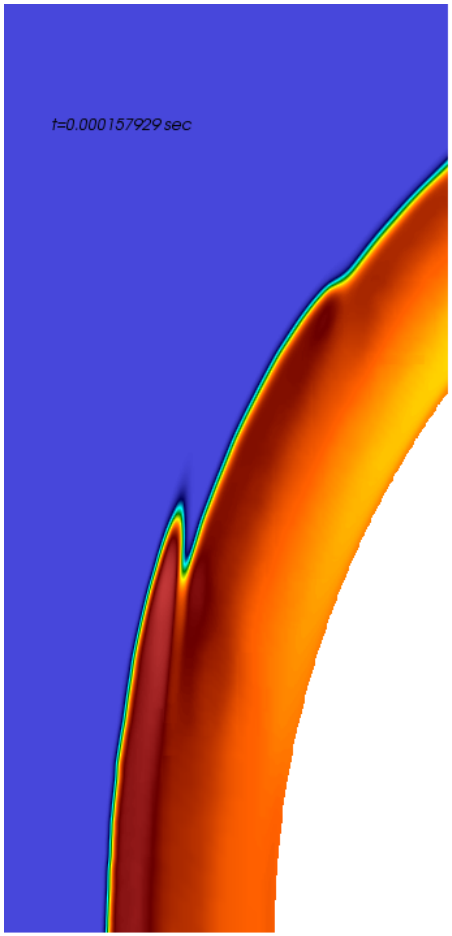

Pressure

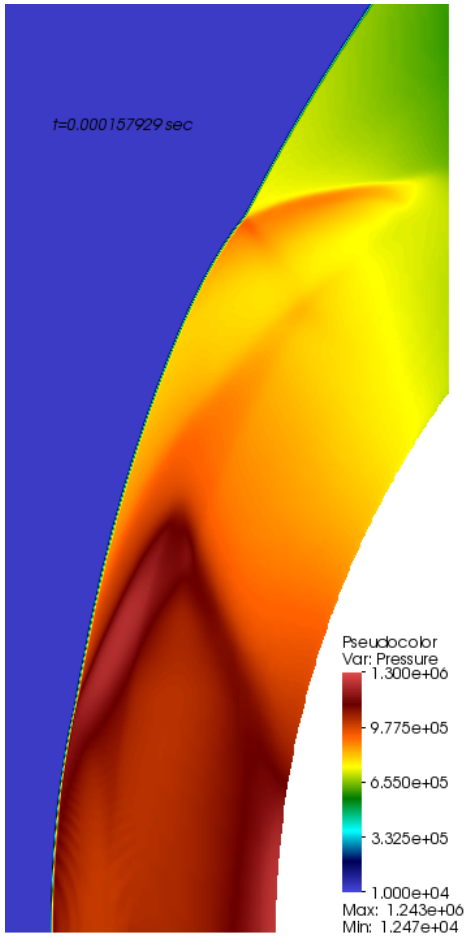

Oscillation mechanism

Schlieren of density

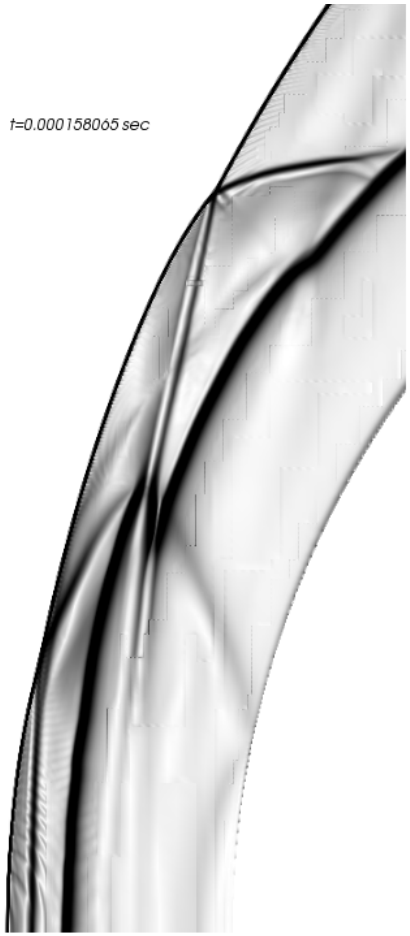

Temperature

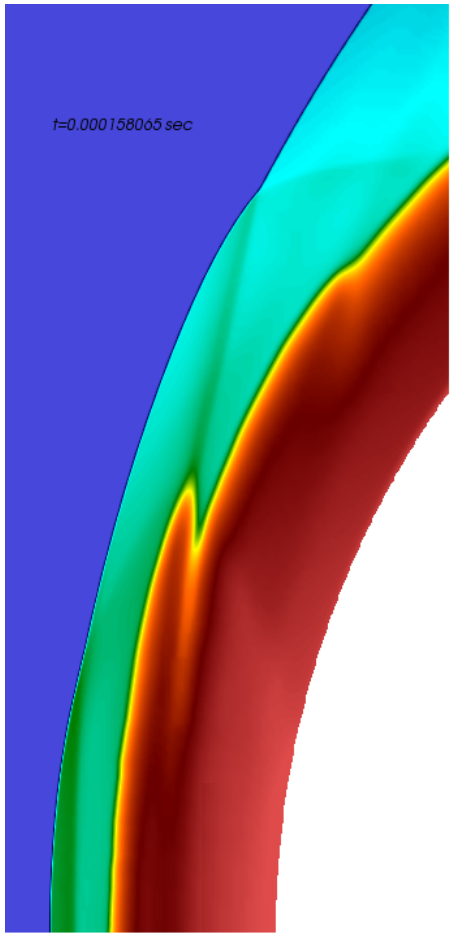

Mass fraction OH

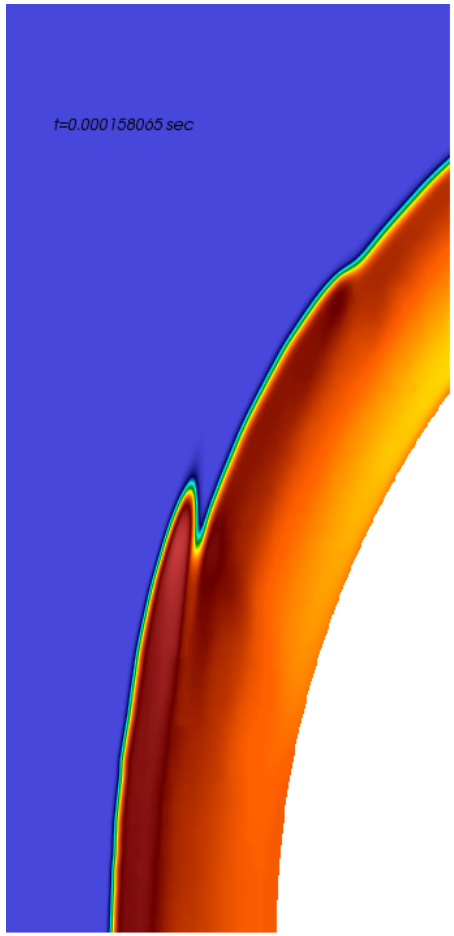

Pressure

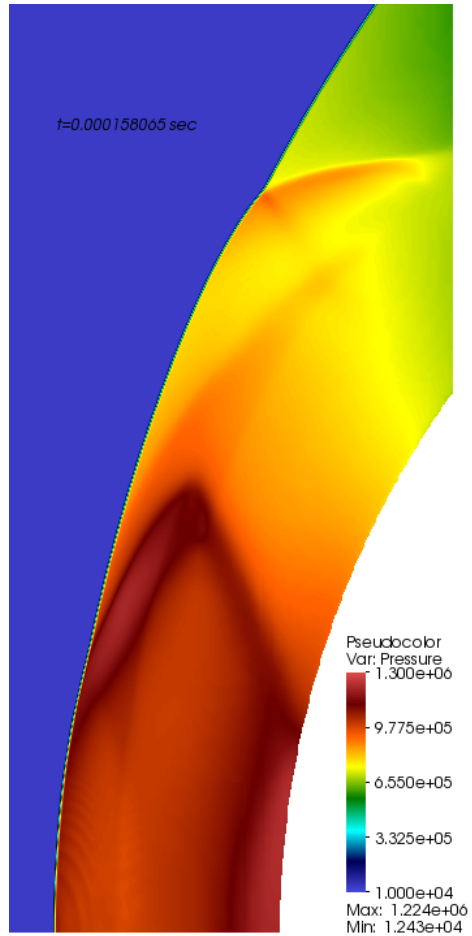

Oscillation mechanism

Schlieren of density

Temperature

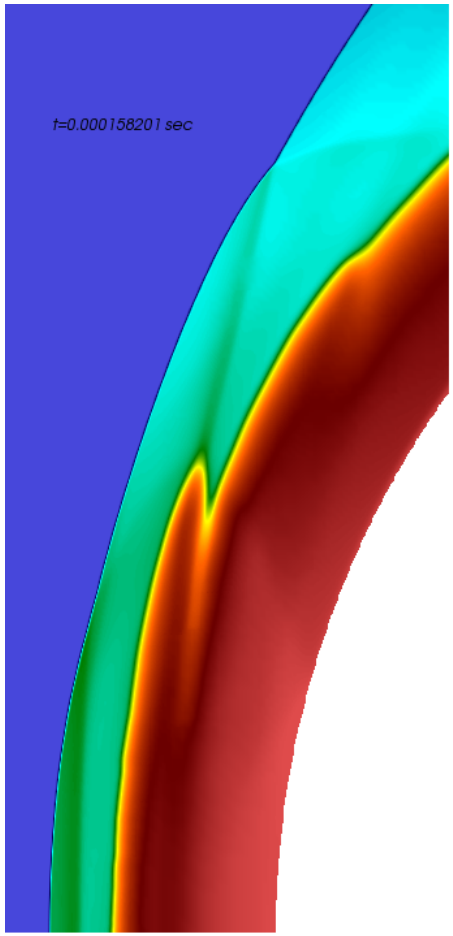

Mass fraction OH

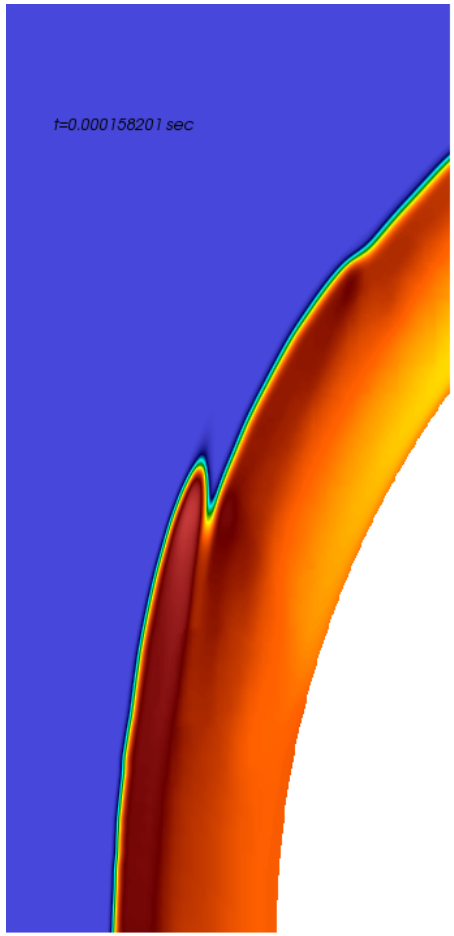

Pressure

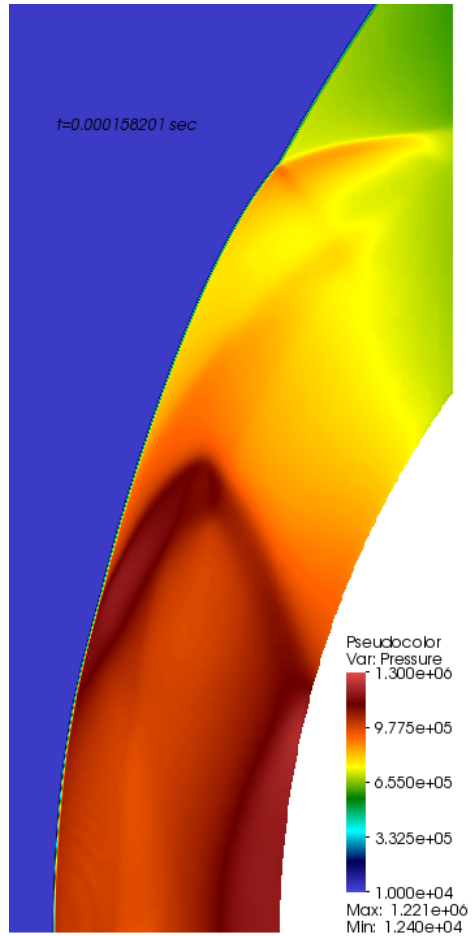

Oscillation mechanism

Schlieren of density

Temperature

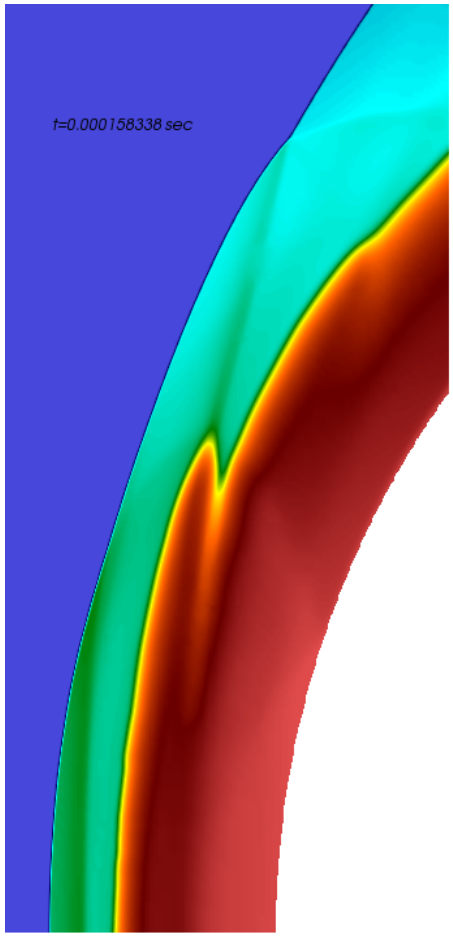

Mass fraction OH

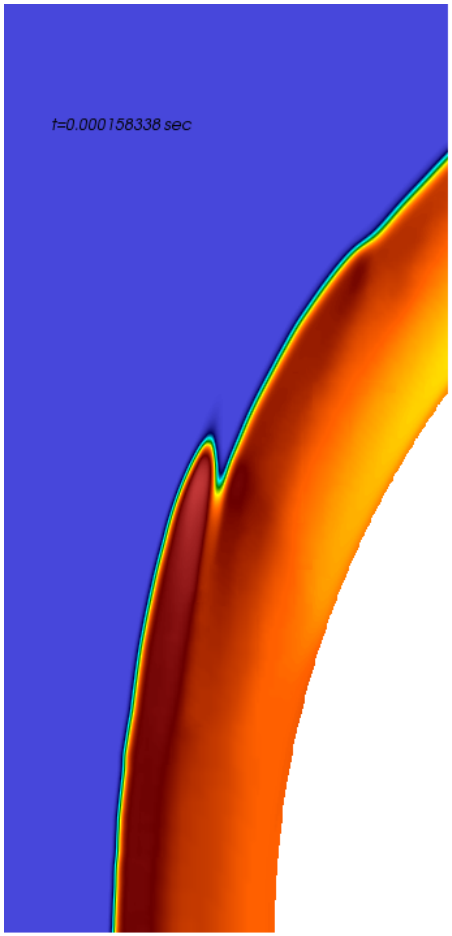

Pressure

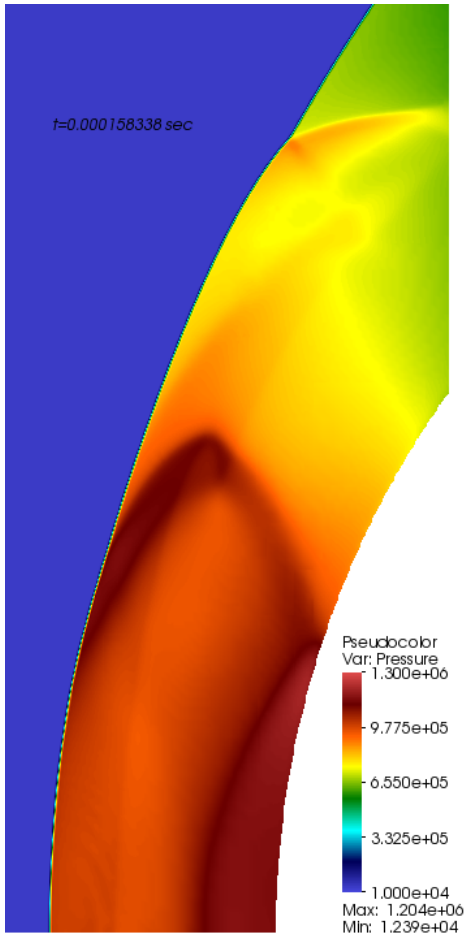

Oscillation mechanism

Schlieren of density

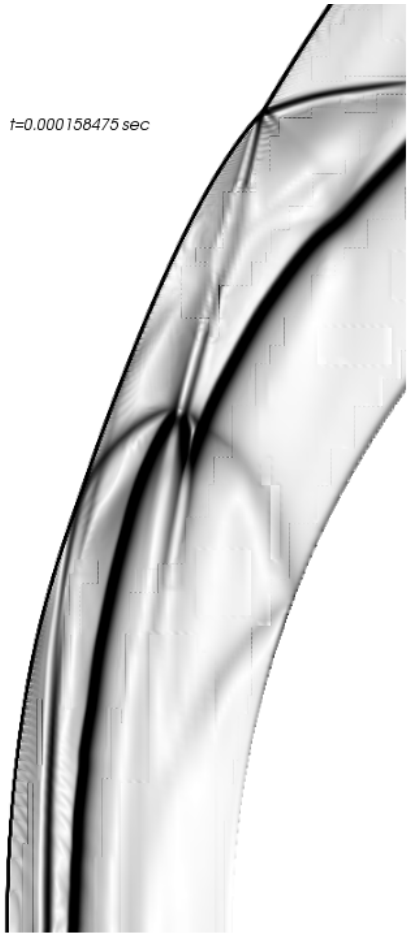

Temperature

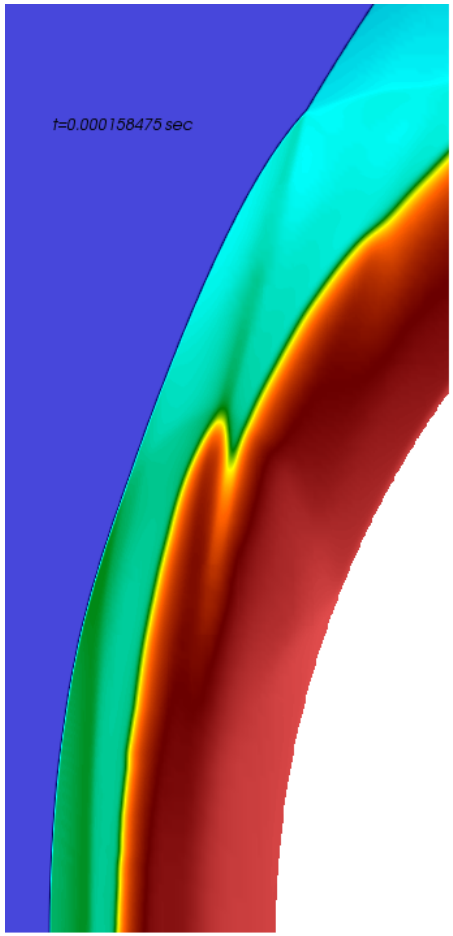

Mass fraction OH

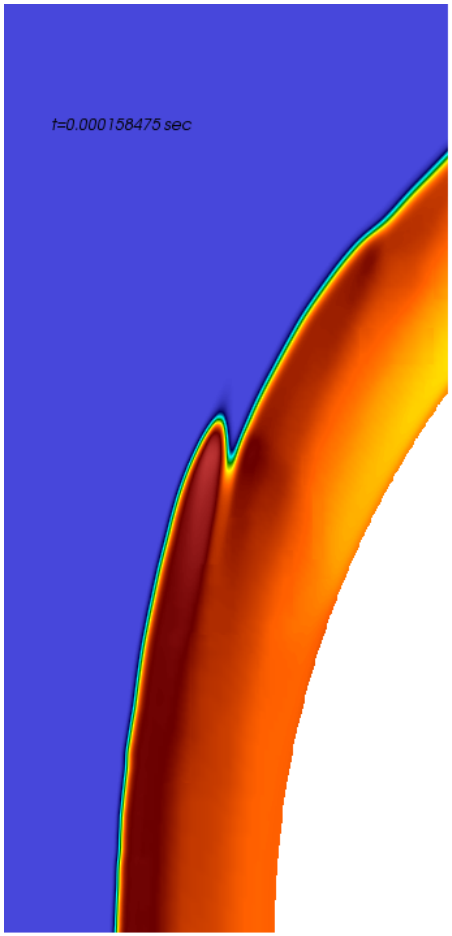

Pressure

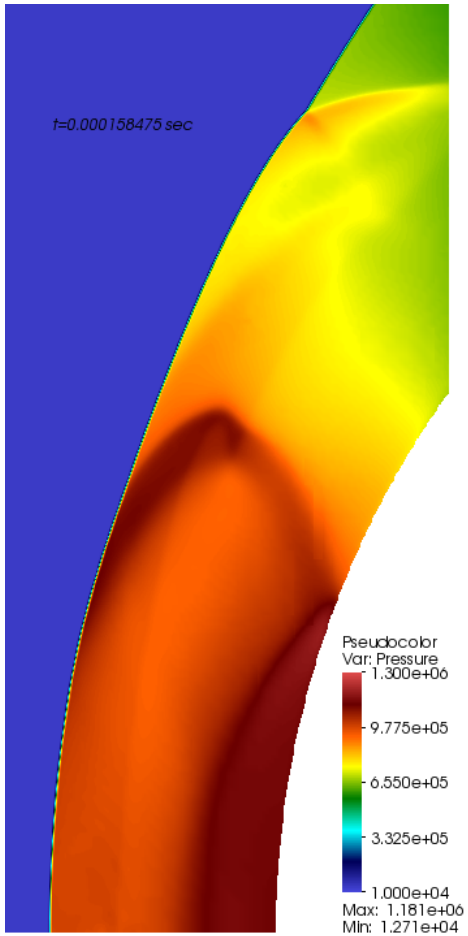

Oscillation mechanism

Schlieren of density

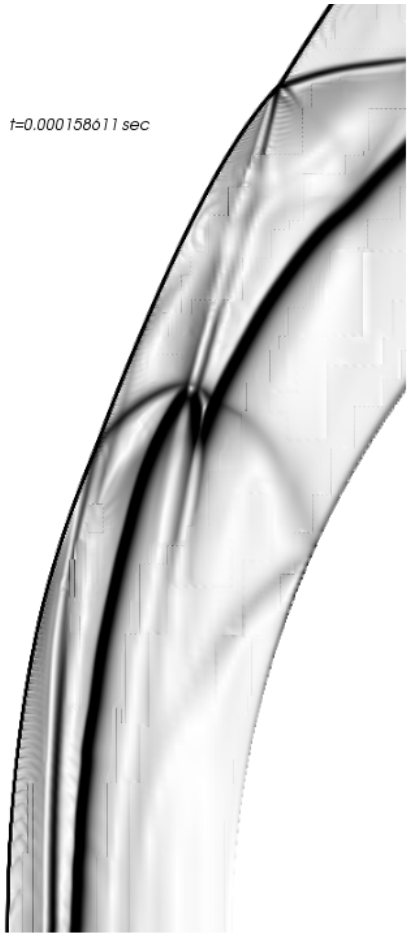

Temperature

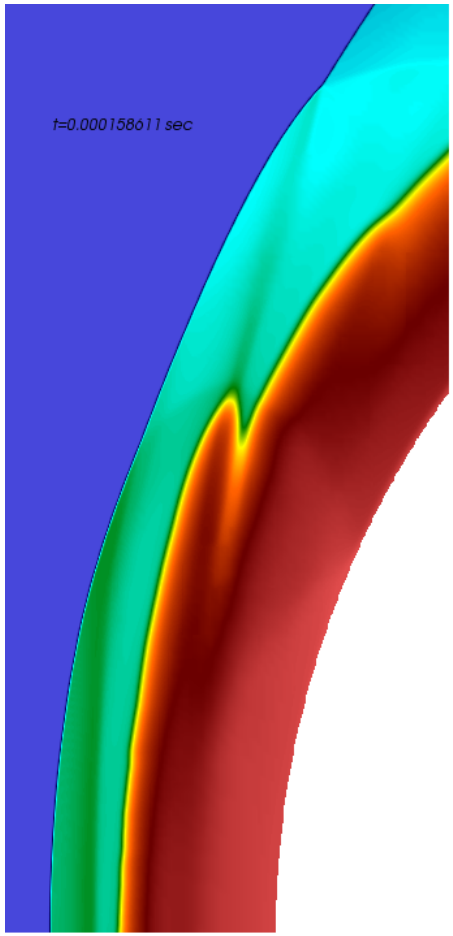

Mass fraction OH

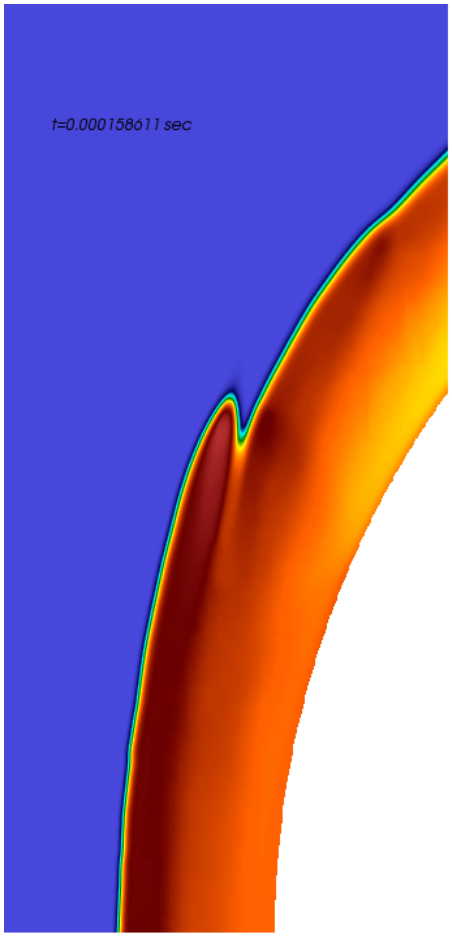

Pressure

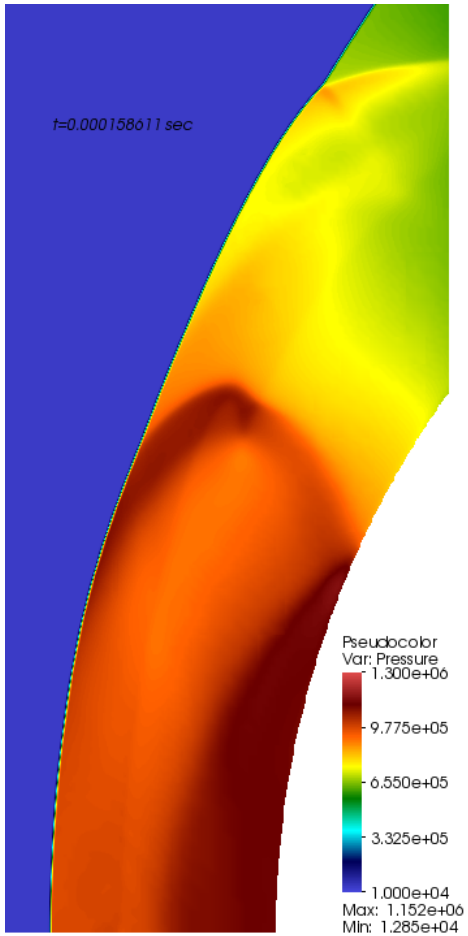

Oscillation mechanism

Schlieren of density

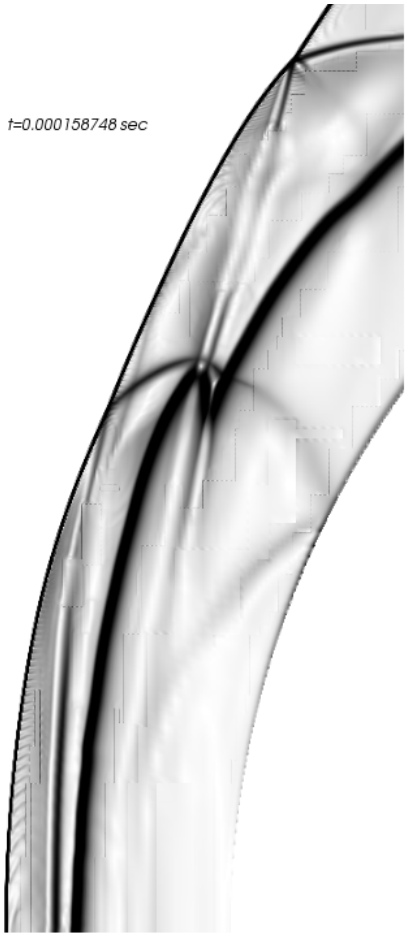

Temperature

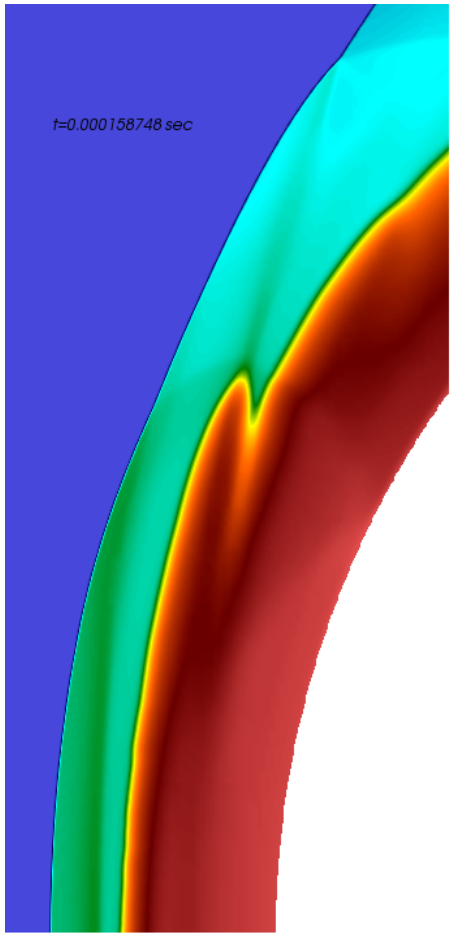

Mass fraction OH

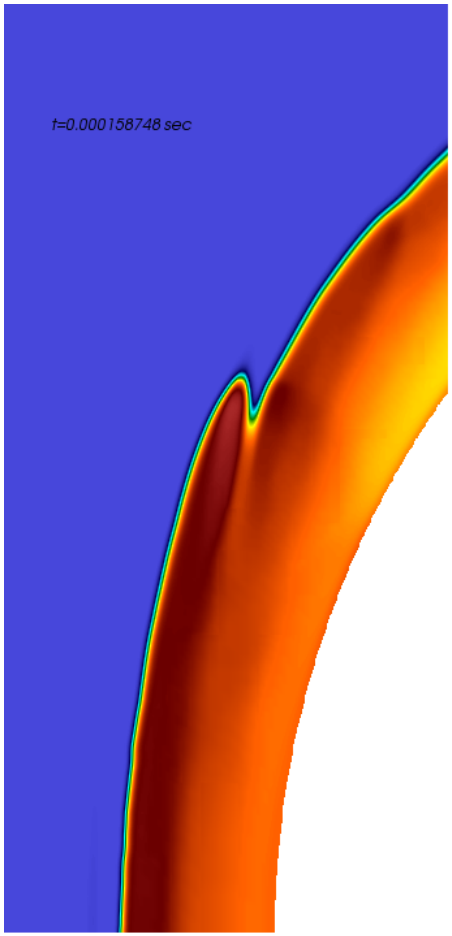

Pressure

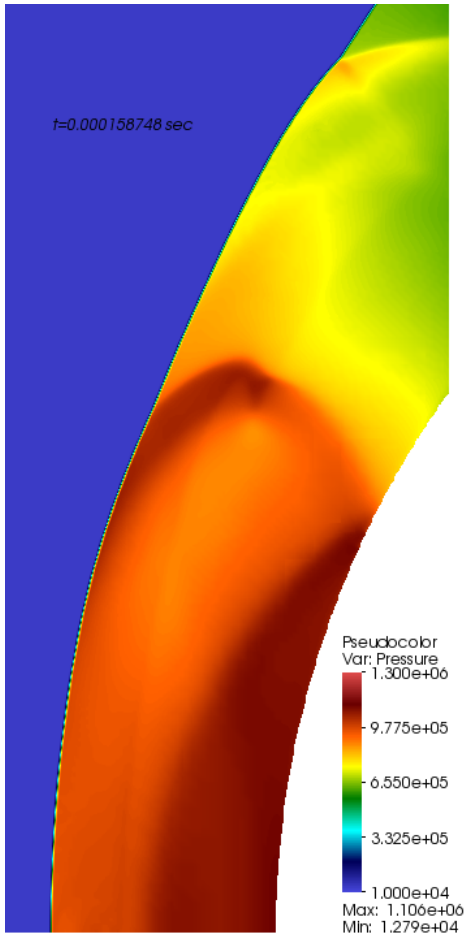

Oscillation mechanism

Schlieren of density

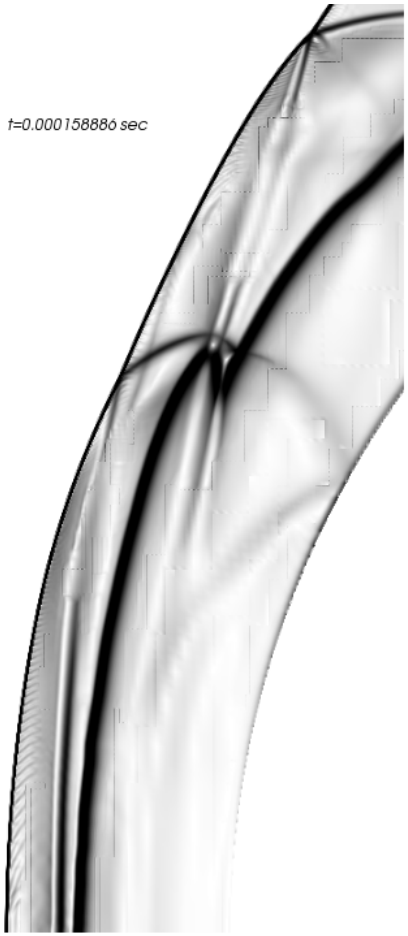

Temperature

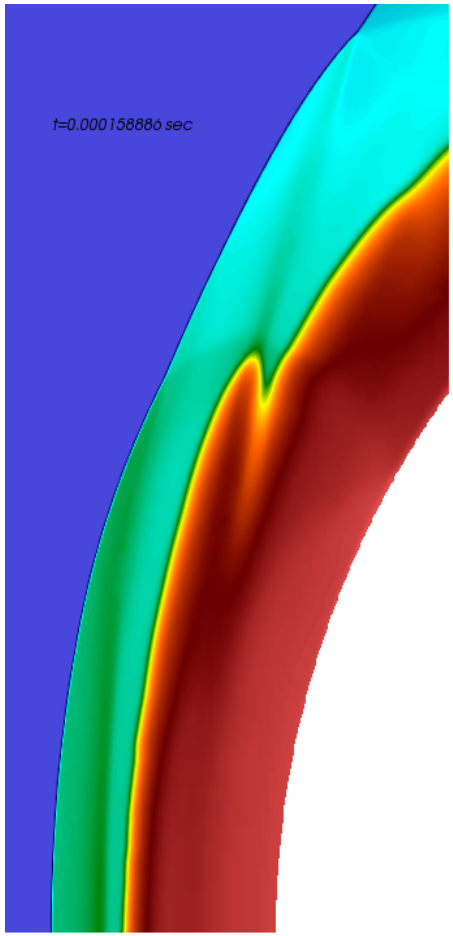

Mass fraction OH

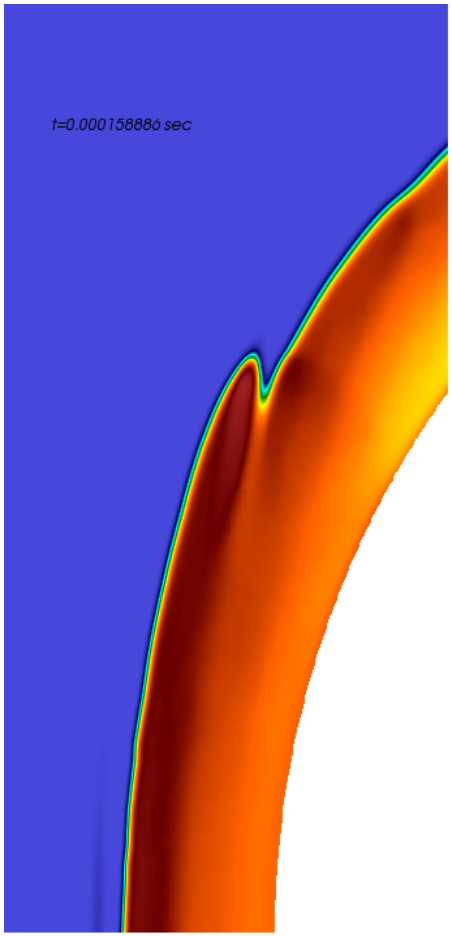

Pressure

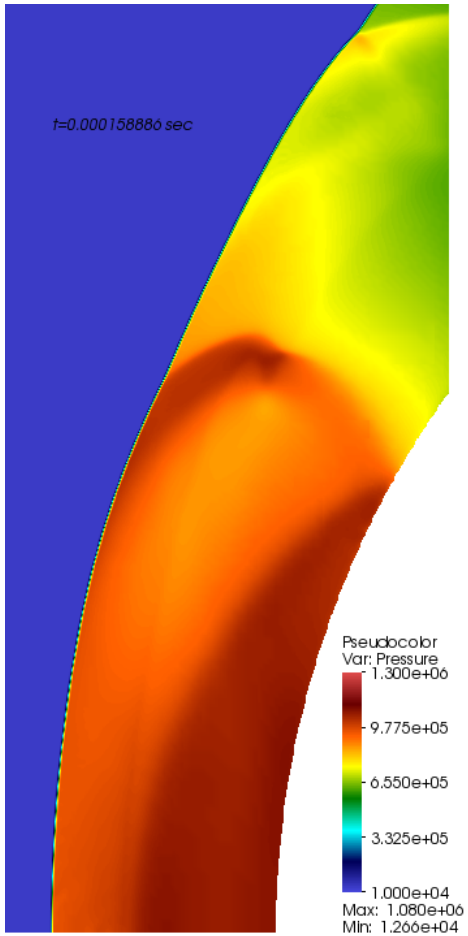

Oscillation mechanism

Schlieren of density

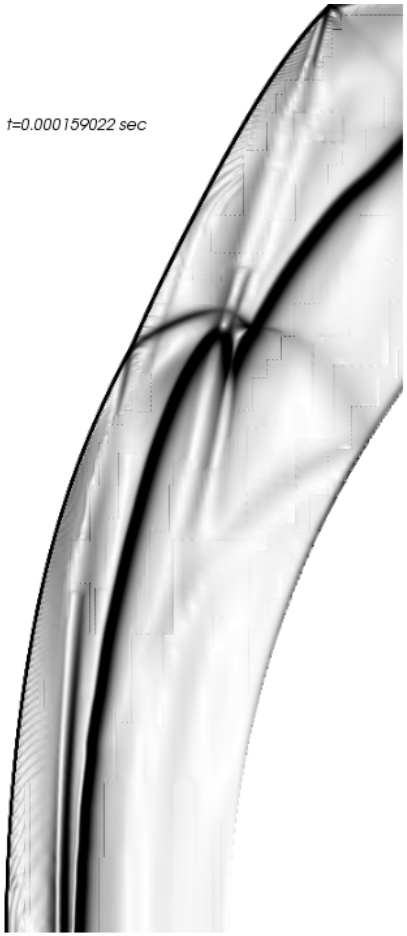

Temperature

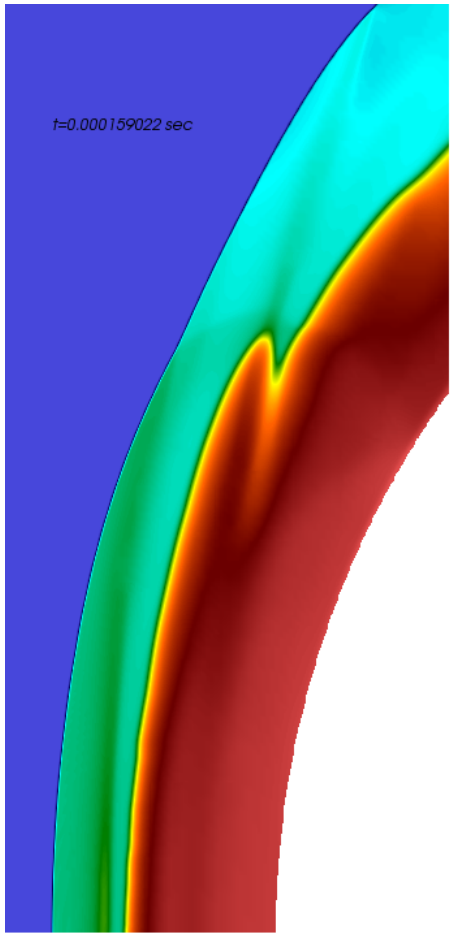

Mass fraction OH

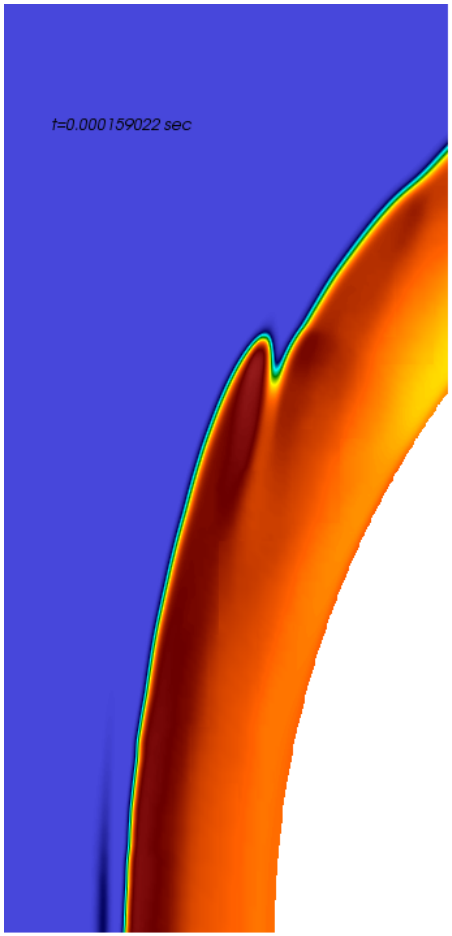

Pressure

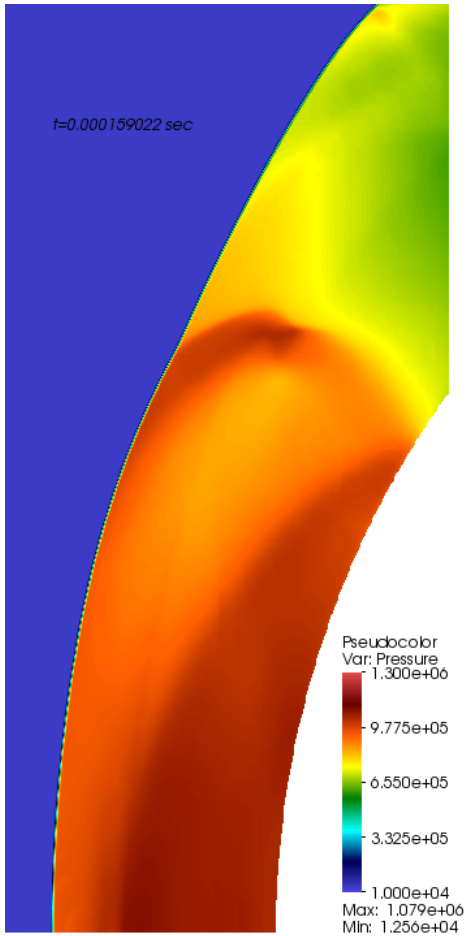

Oscillation mechanism

Schlieren of density

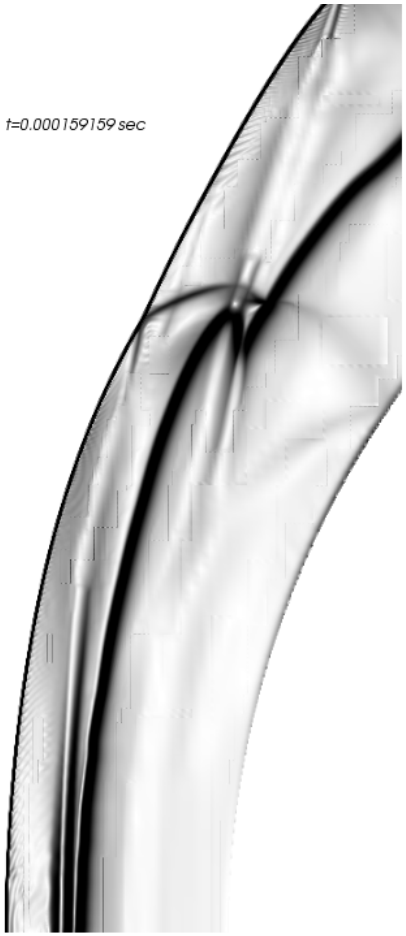

Temperature

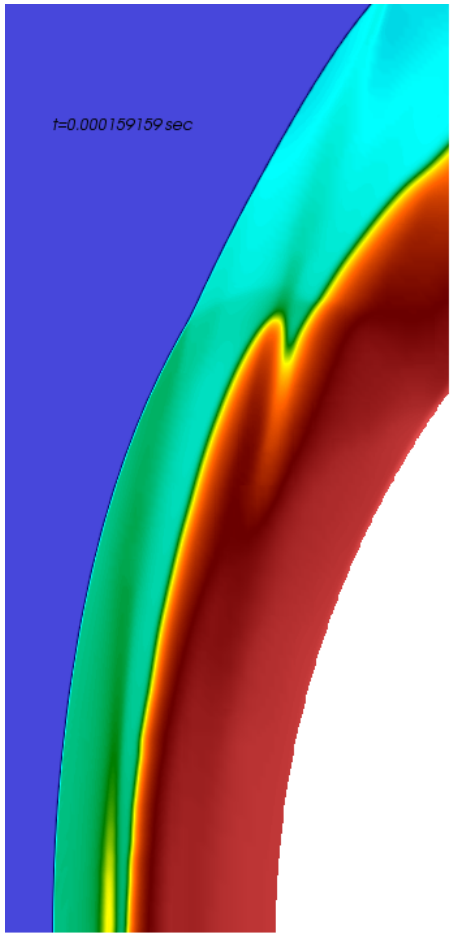

Mass fraction OH

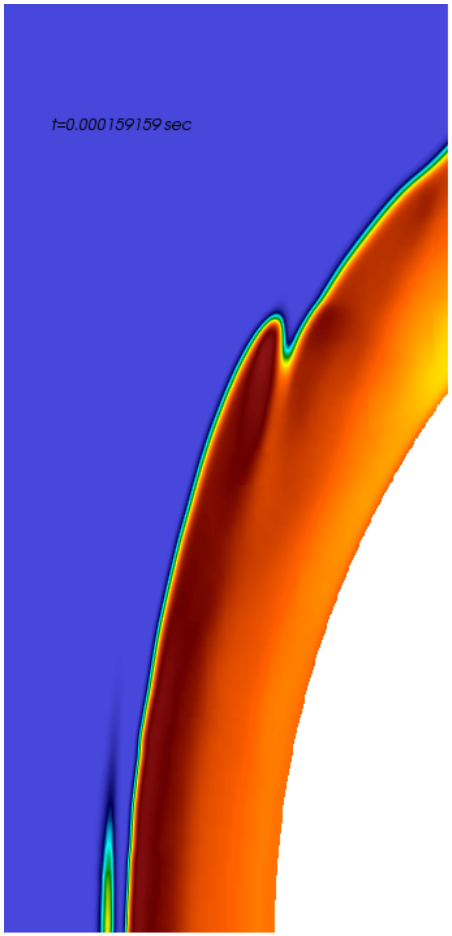

Pressure

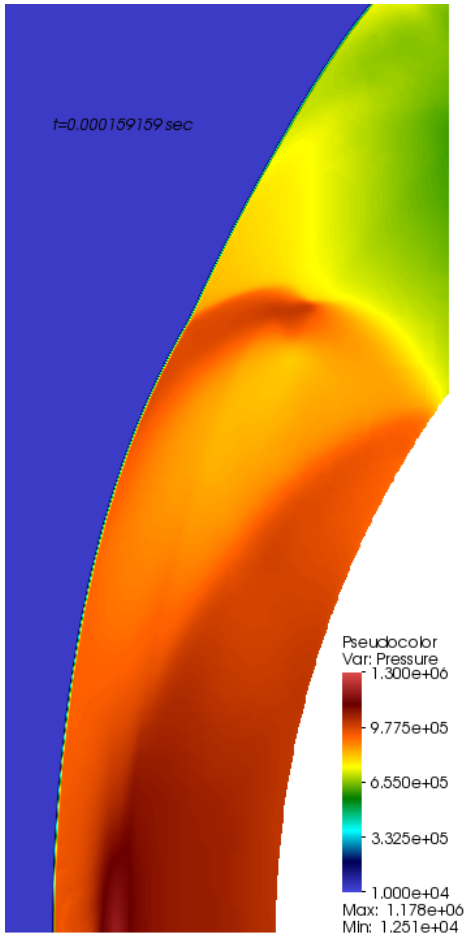

Oscillation mechanism

Schlieren of density

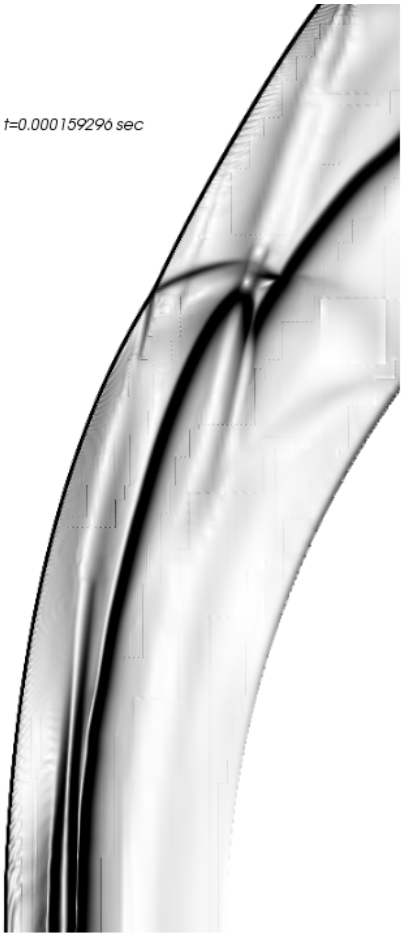

Temperature

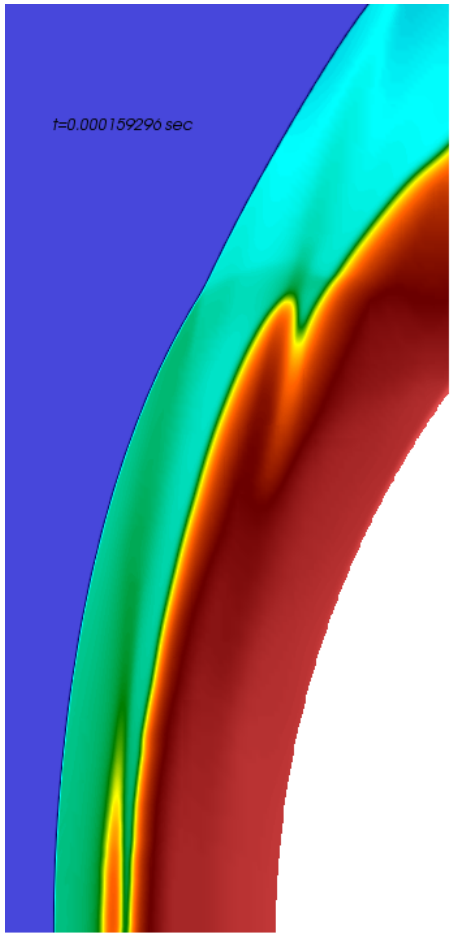

Mass fraction OH

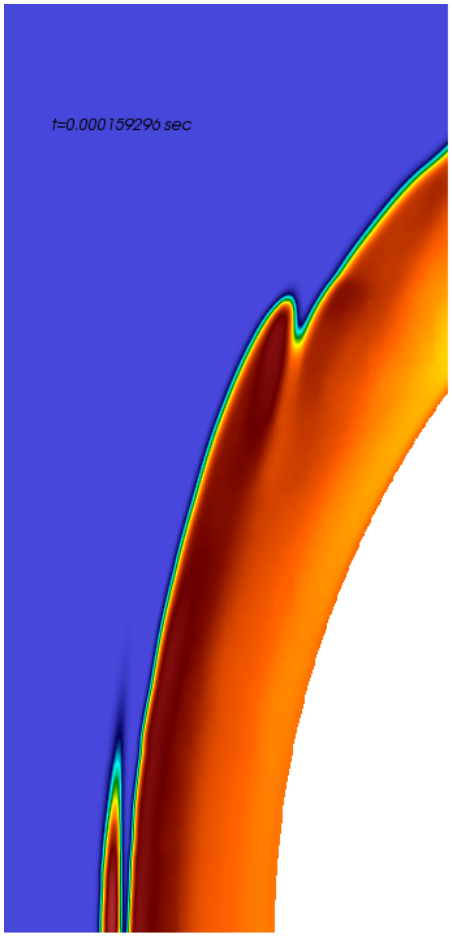

Pressure

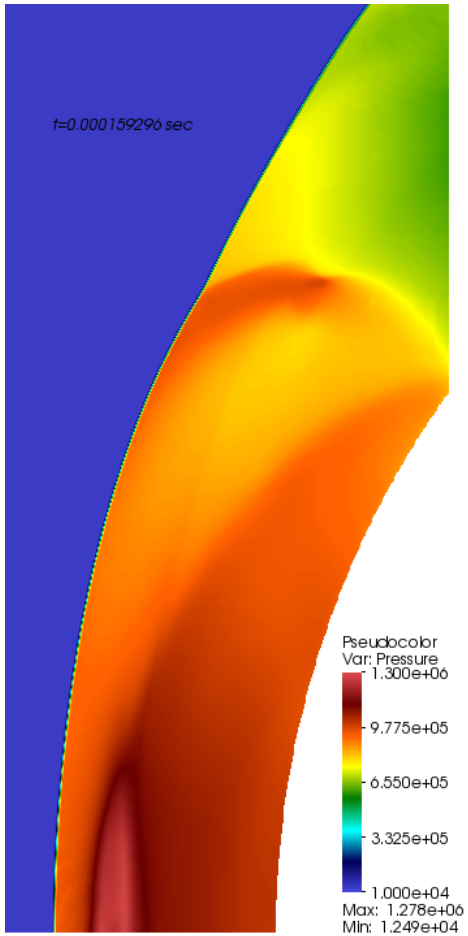

Oscillation mechanism

Schlieren of density

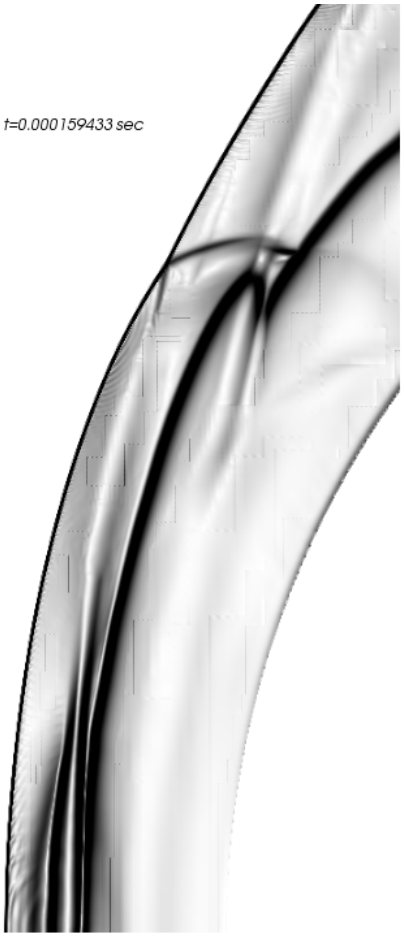

Temperature

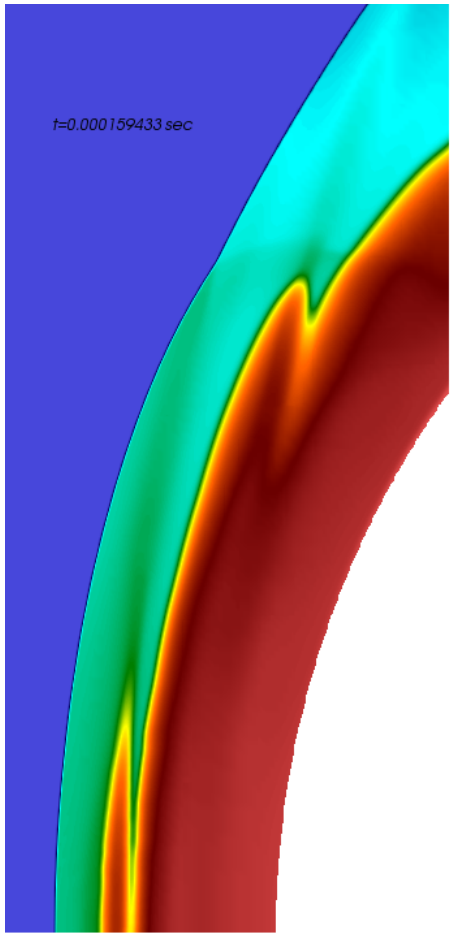

Mass fraction OH

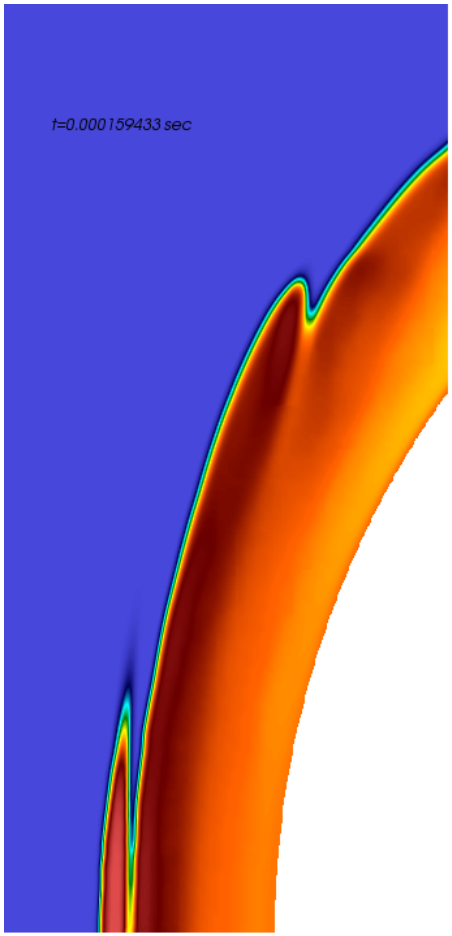

Pressure

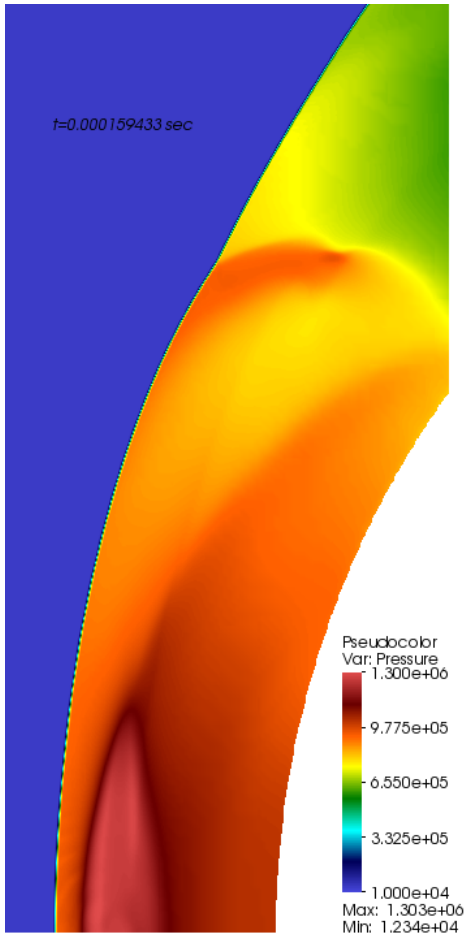

Oscillation mechanism

Schlieren of density

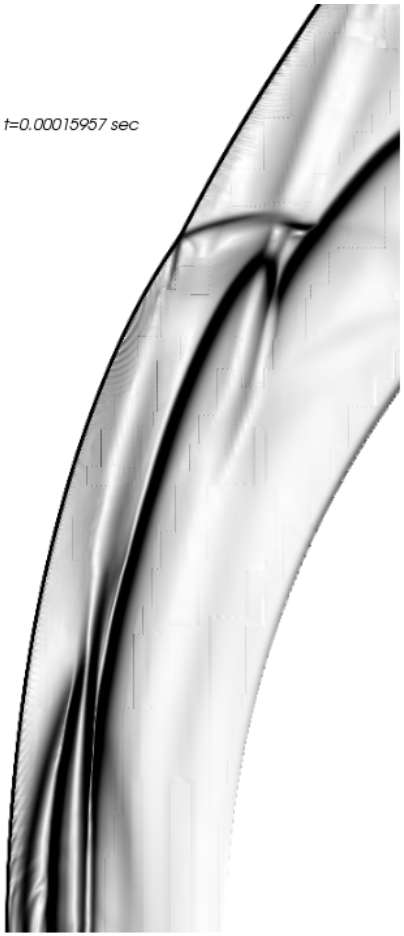

Temperature

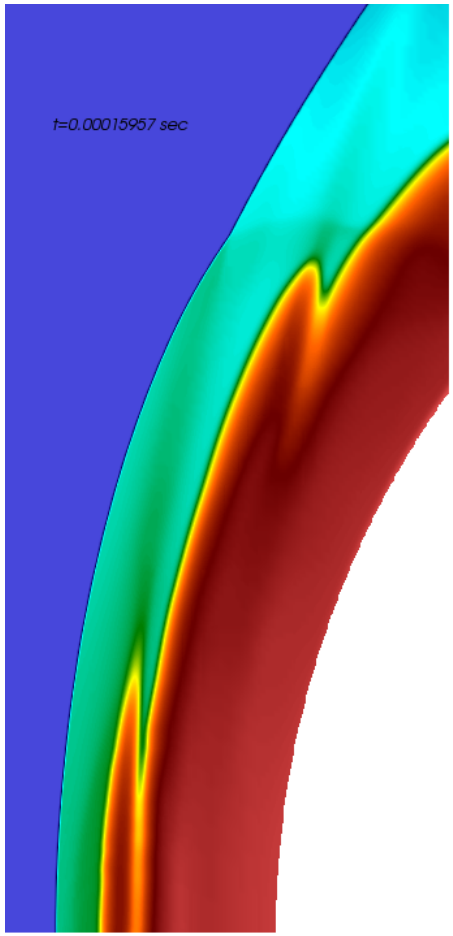

Mass fraction OH

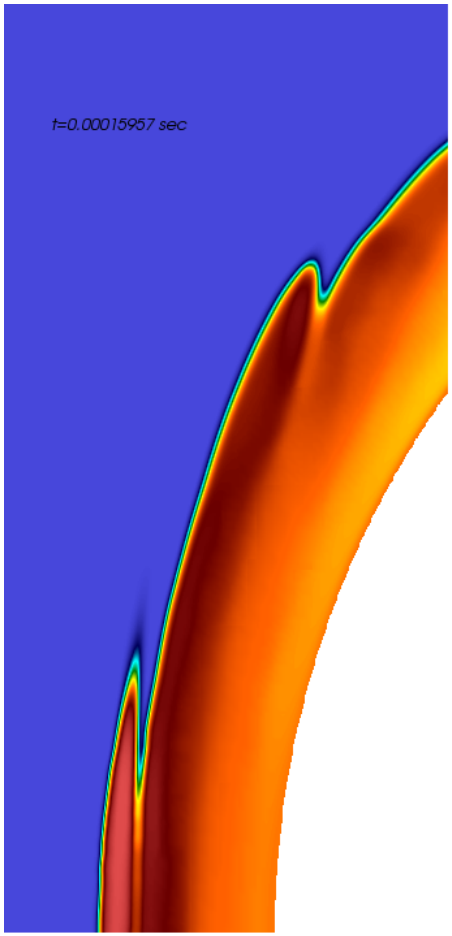

Pressure

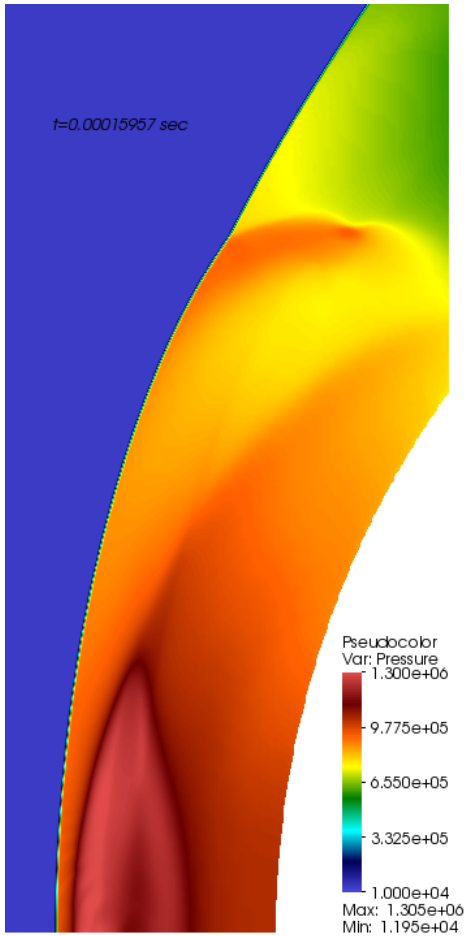

Oscillation mechanism

Schlieren of density

Temperature

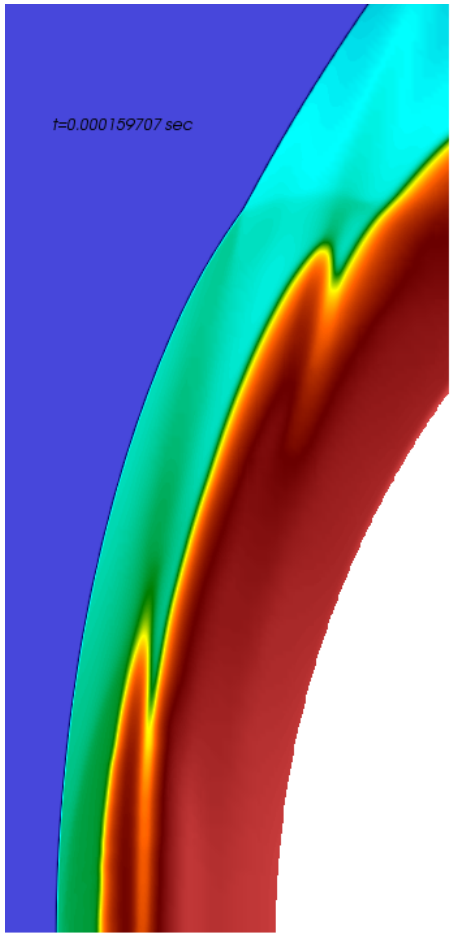

Mass fraction OH

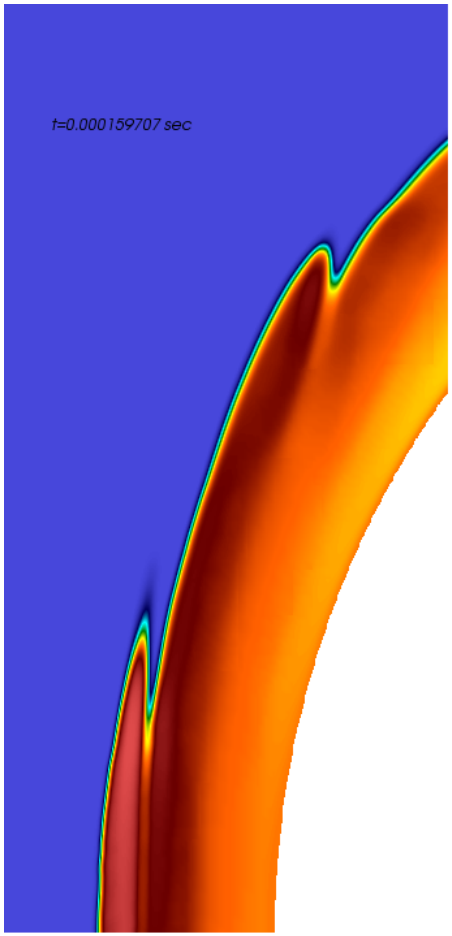

Pressure

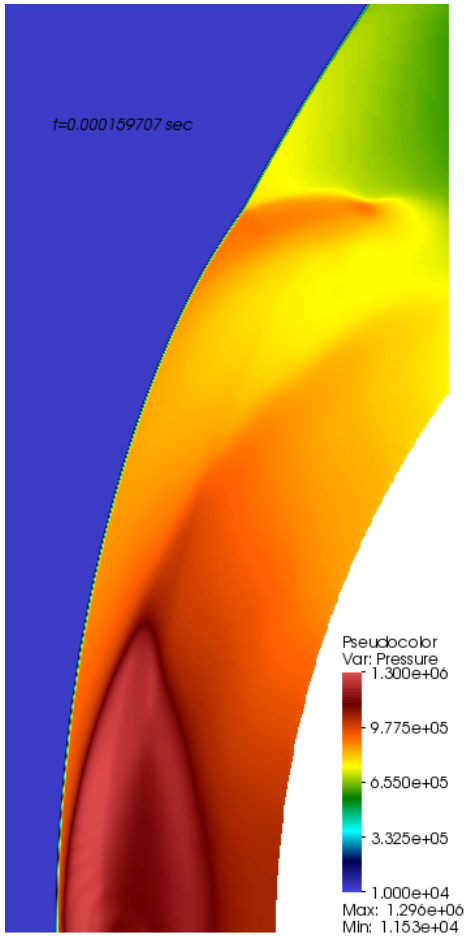

Oscillation mechanism

Schlieren of density

Temperature

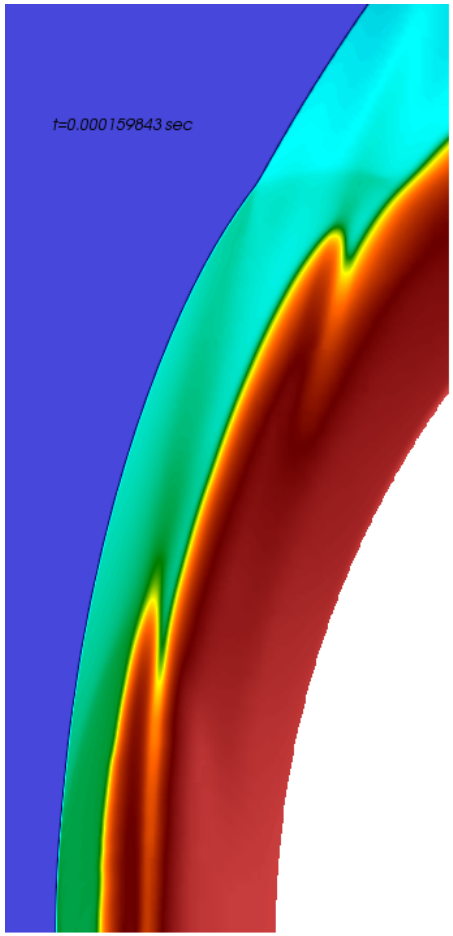

Mass fraction OH

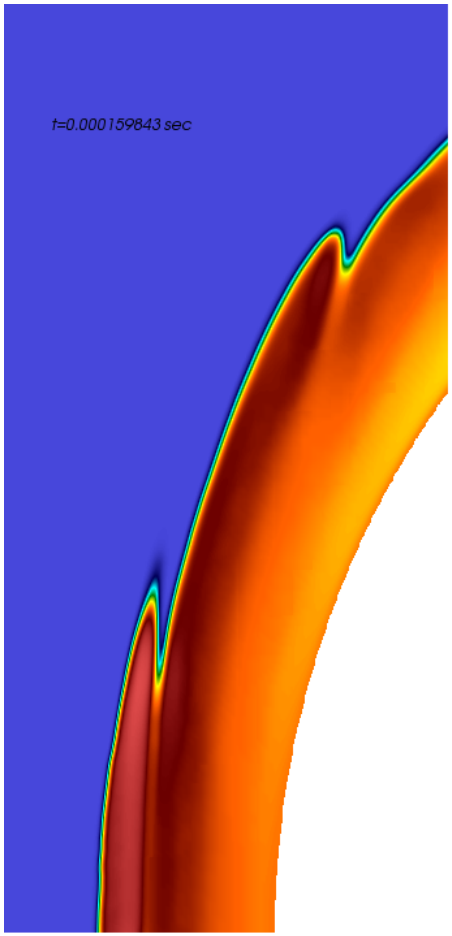

Pressure

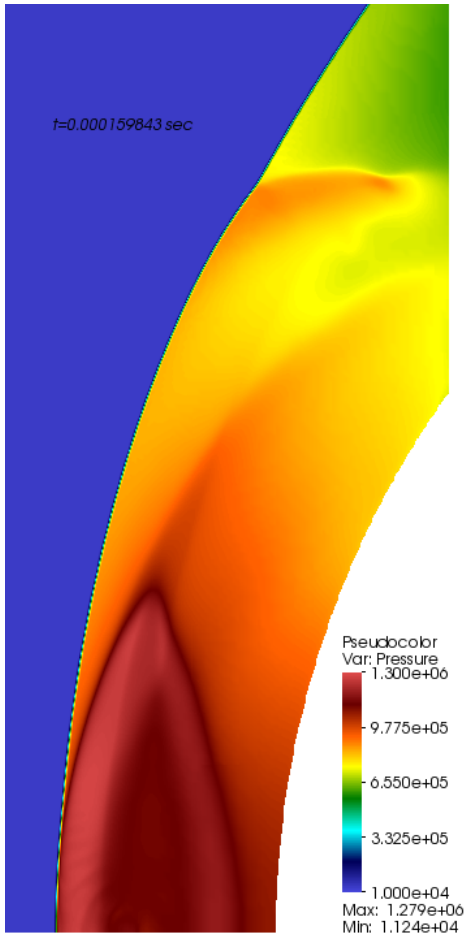

Oscillation mechanism

Schlieren of density

Temperature

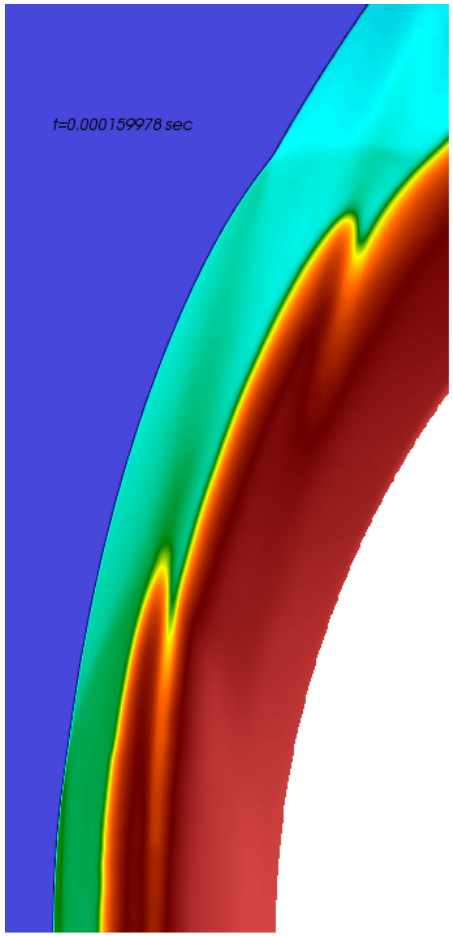

Mass fraction OH

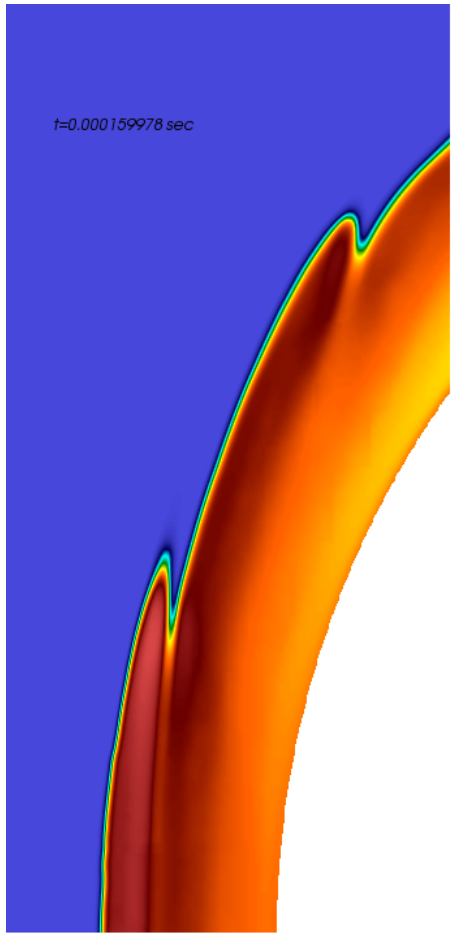

Pressure

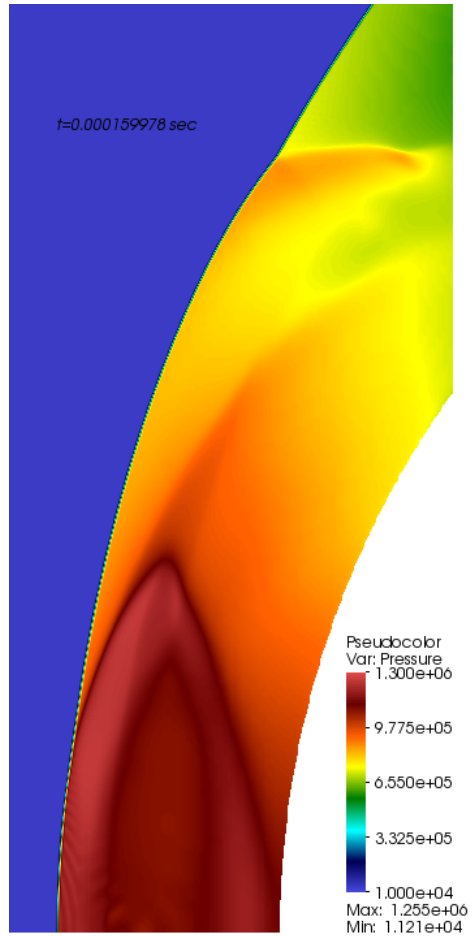

Oscillation mechanism

Schlieren of density

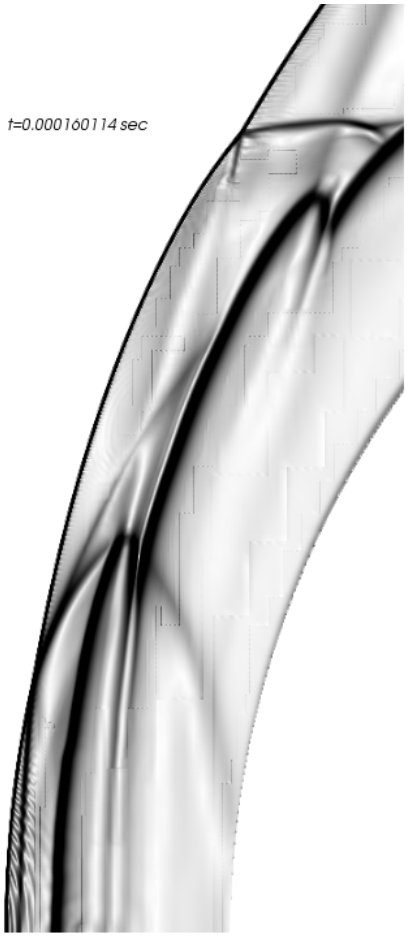

Temperature

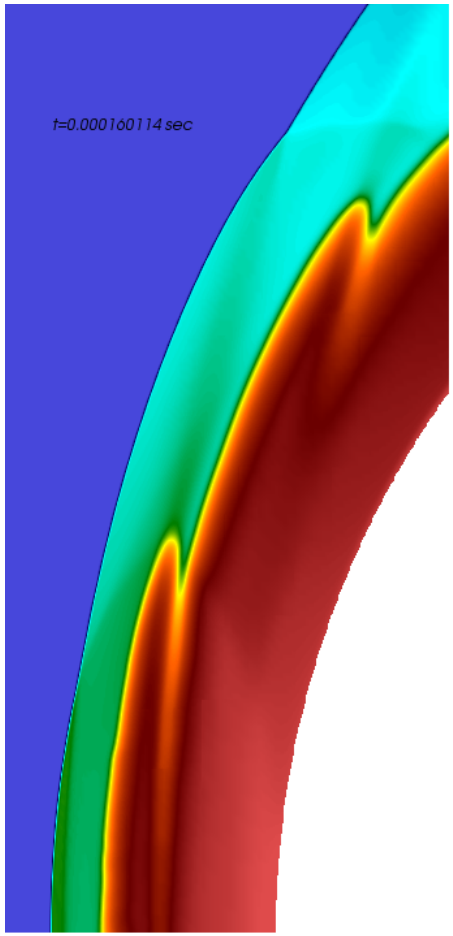

Mass fraction OH

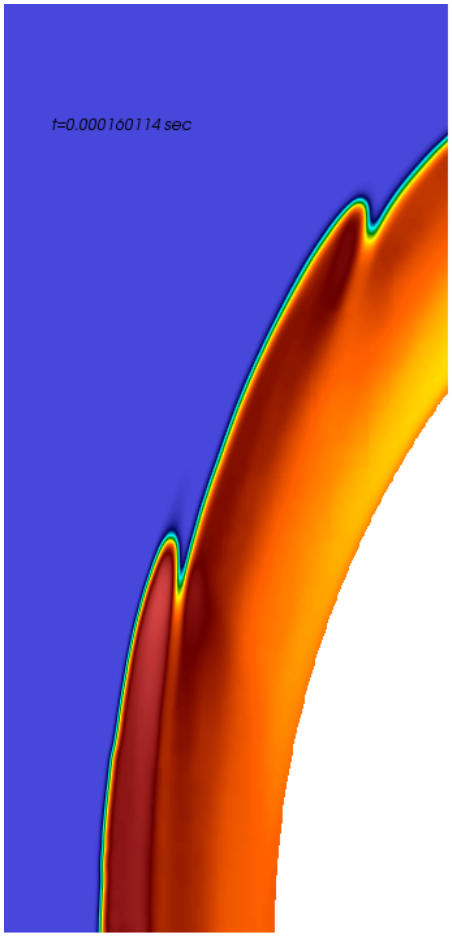

Pressure

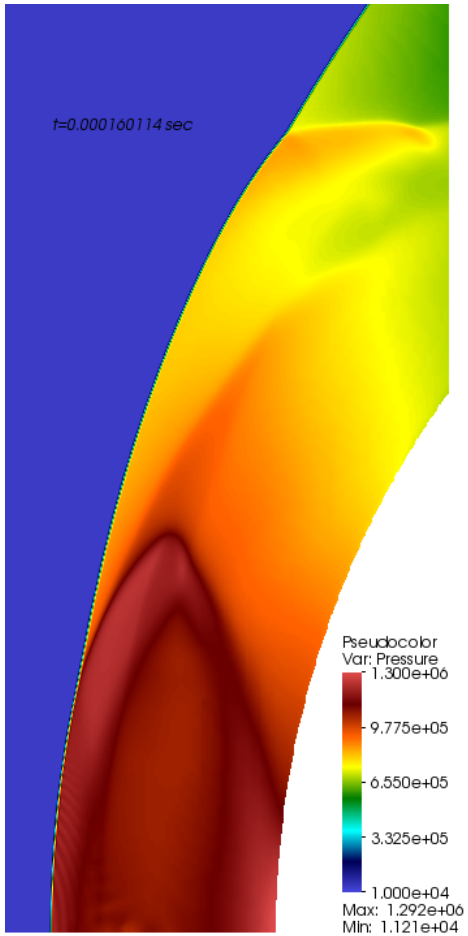

Oscillation mechanism

Schlieren of density

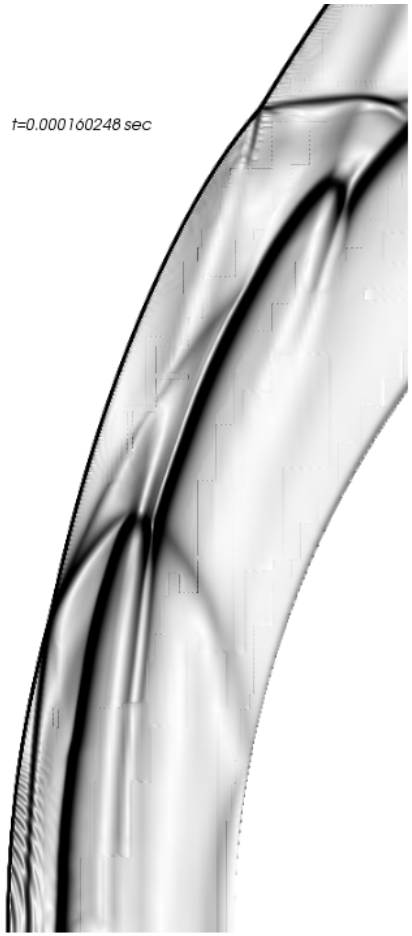

Temperature

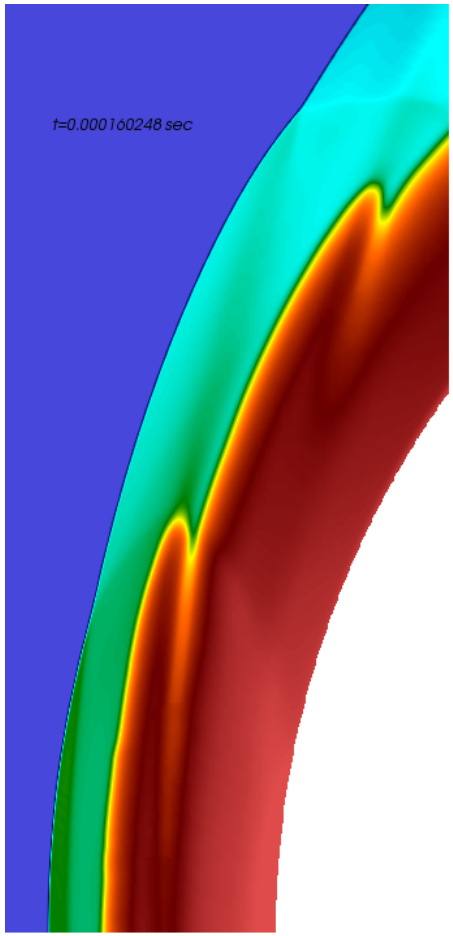

Mass fraction OH

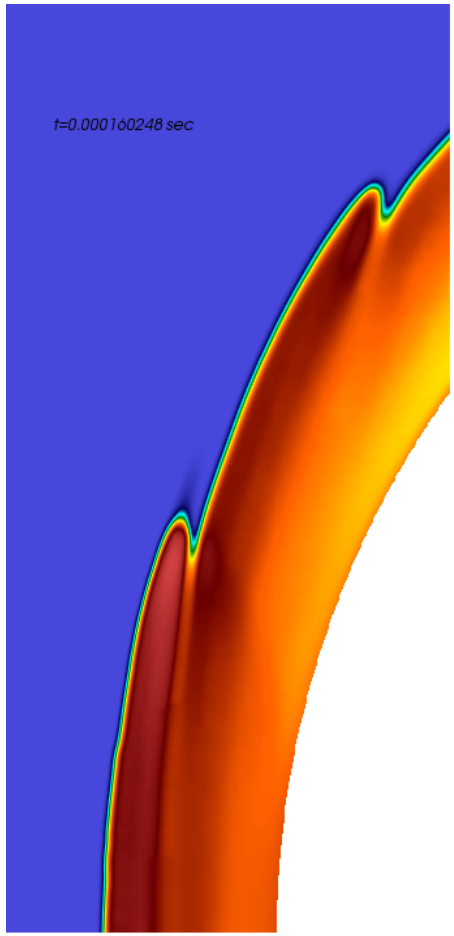

Pressure

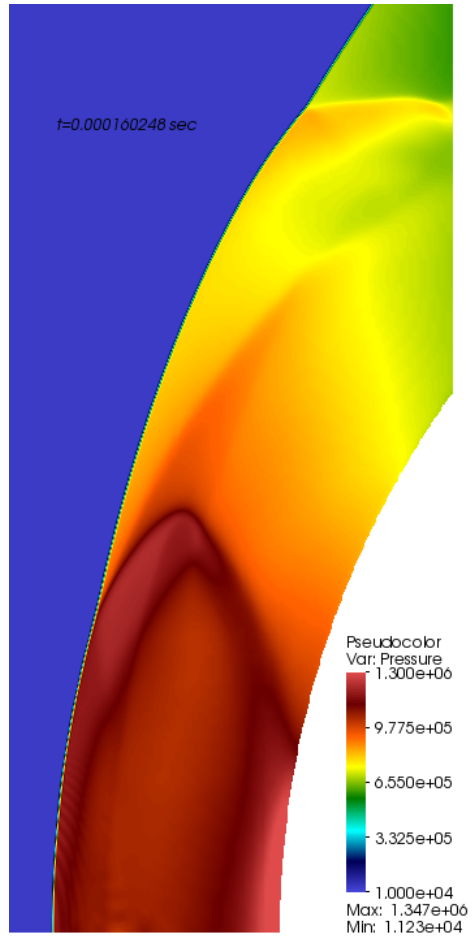

Oscillation mechanism

Schlieren of density

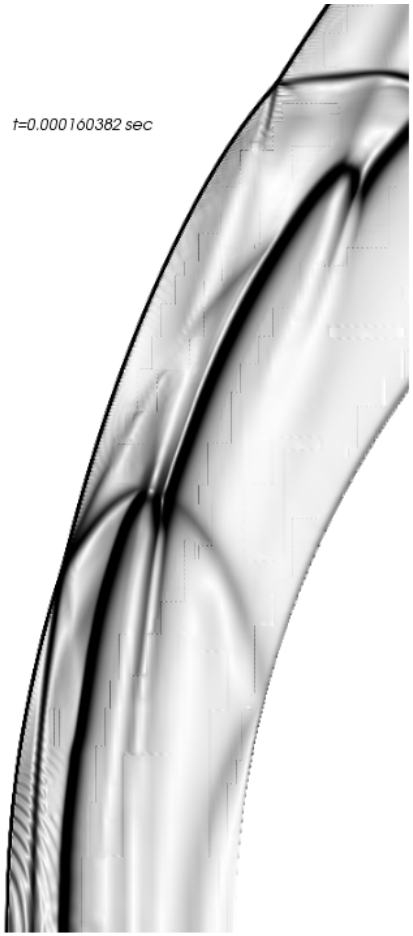

Temperature

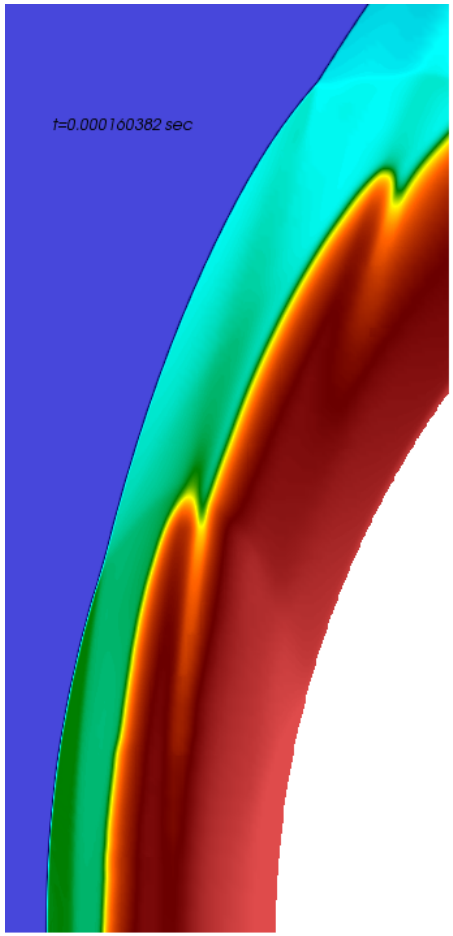

Mass fraction OH

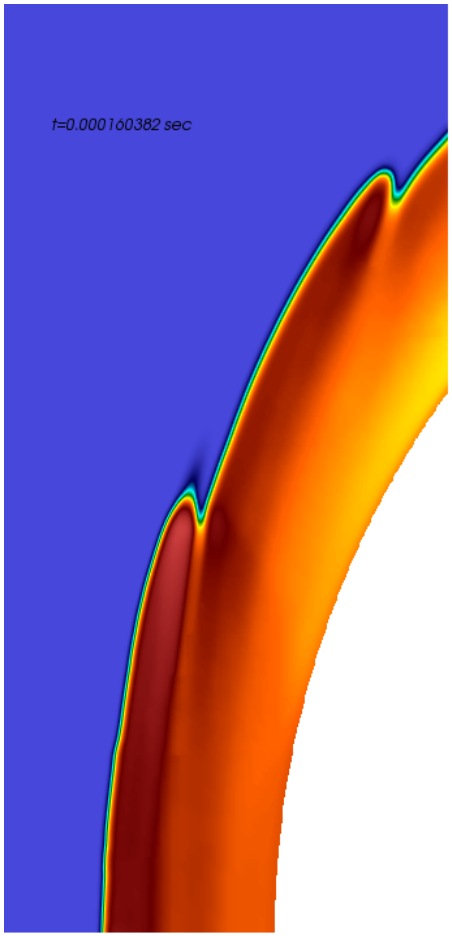

Pressure

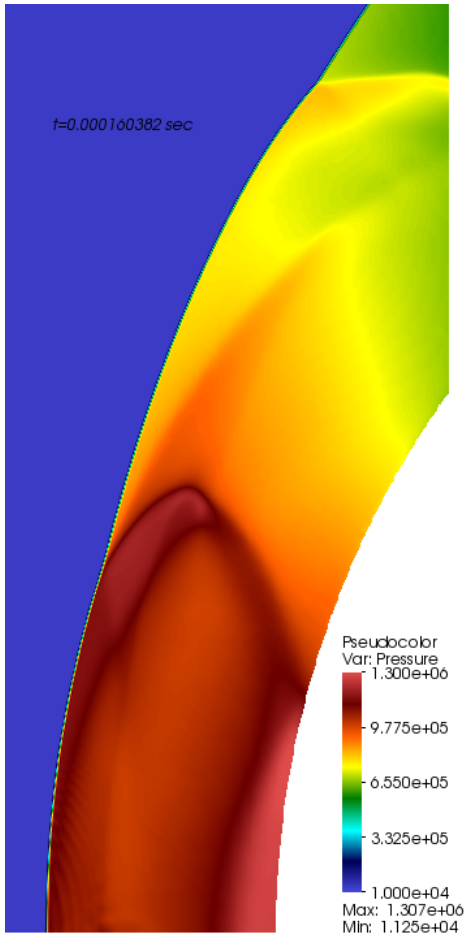

Oscillation mechanism

Schlieren of density

Temperature

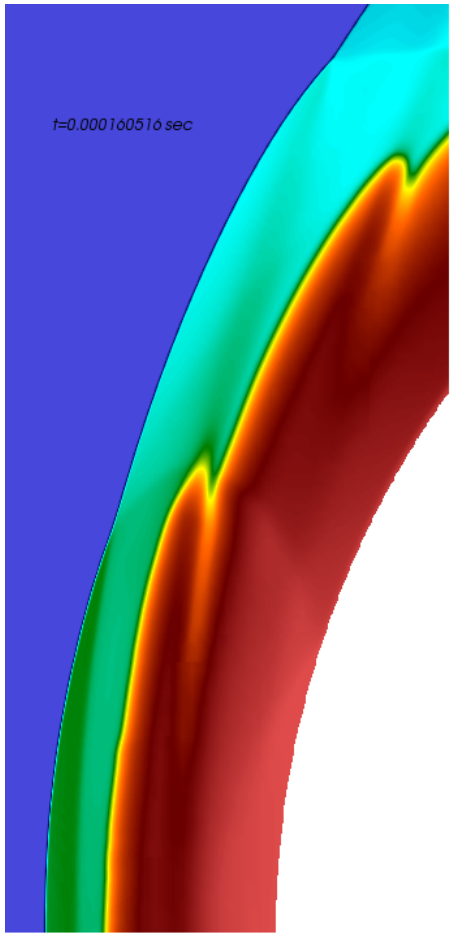

Mass fraction OH

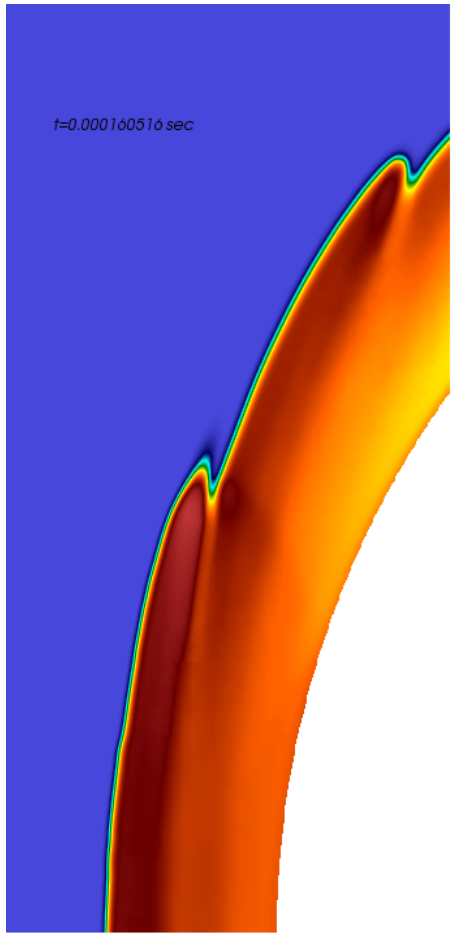

Pressure

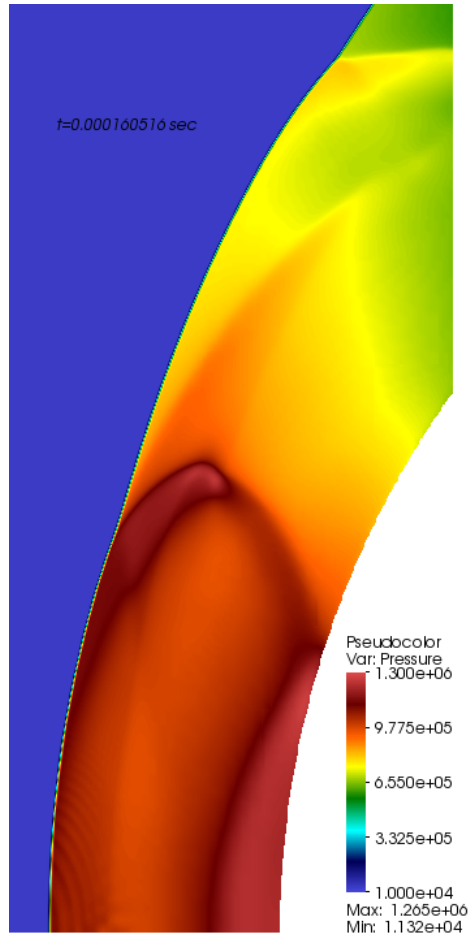

Oscillation mechanism

Schlieren of density

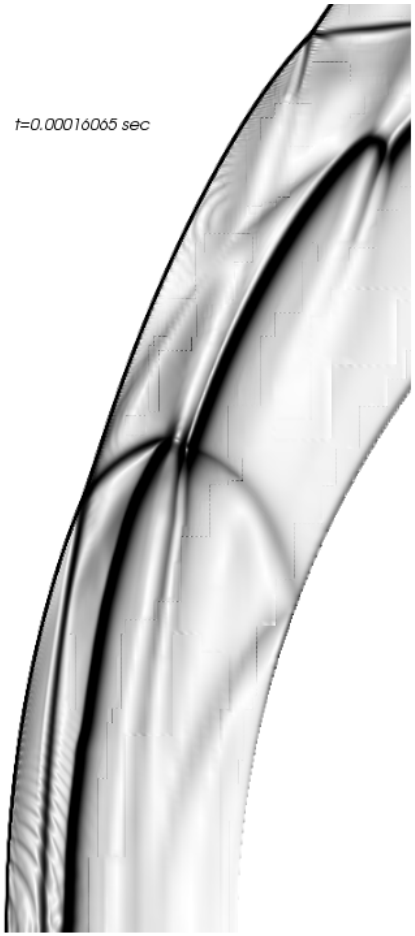

Temperature

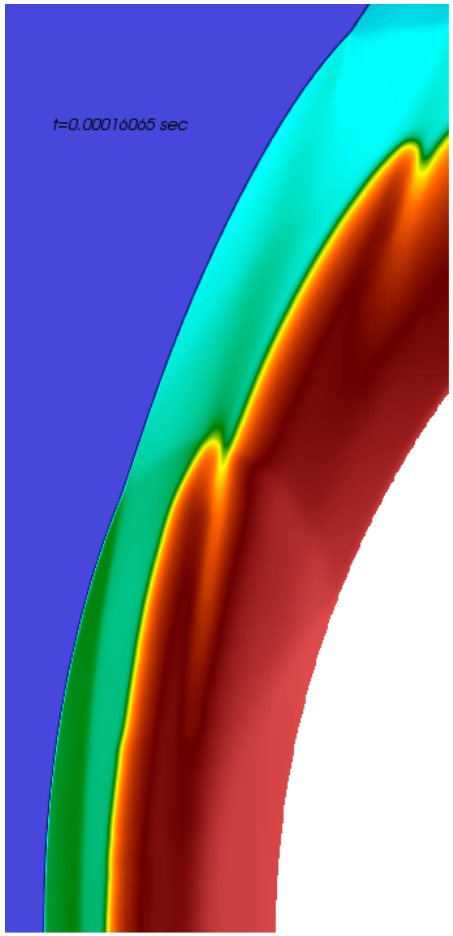

Mass fraction OH

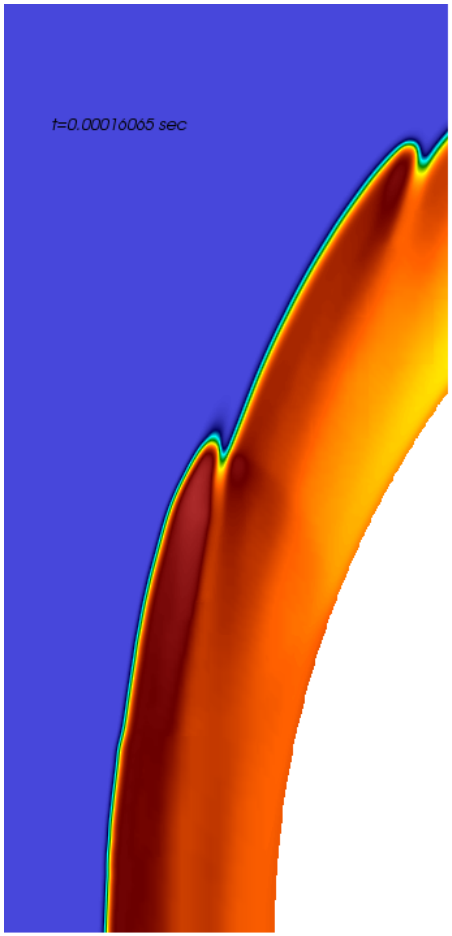

Pressure

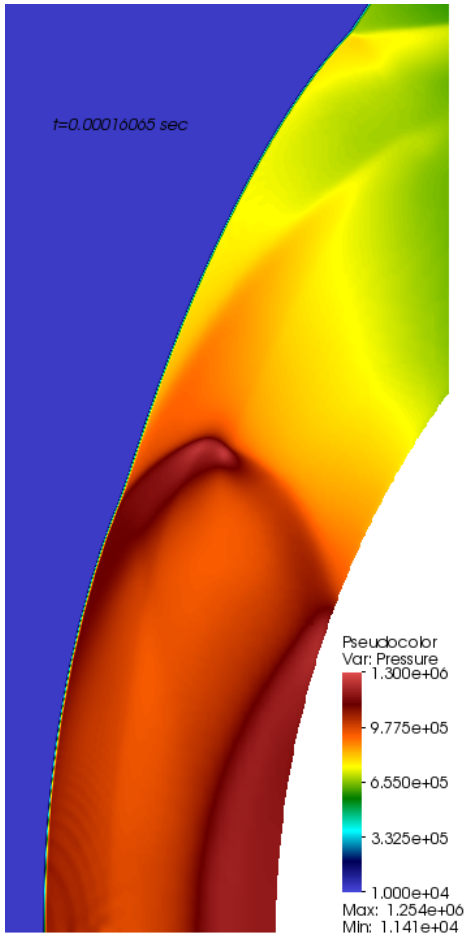

Oscillation mechanism

Schlieren of density

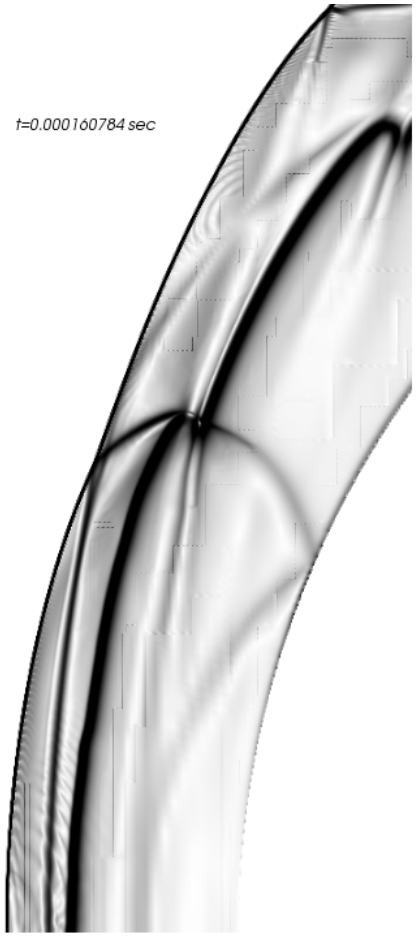

Temperature

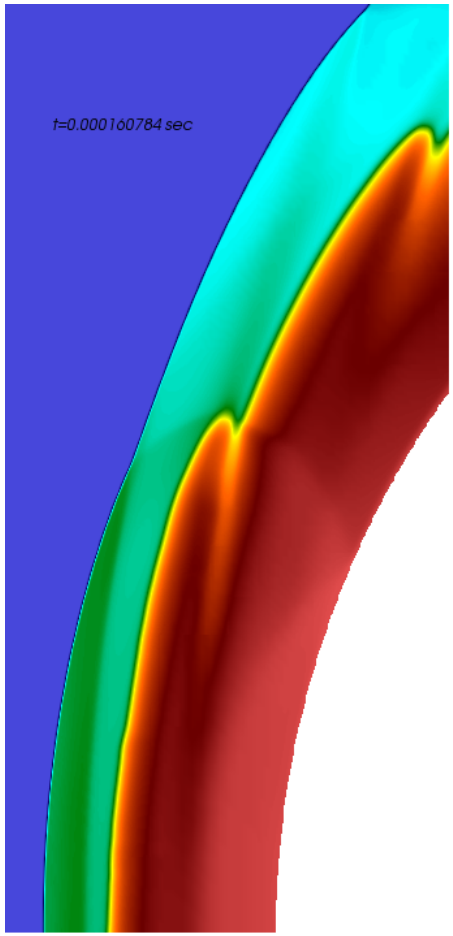

Mass fraction OH

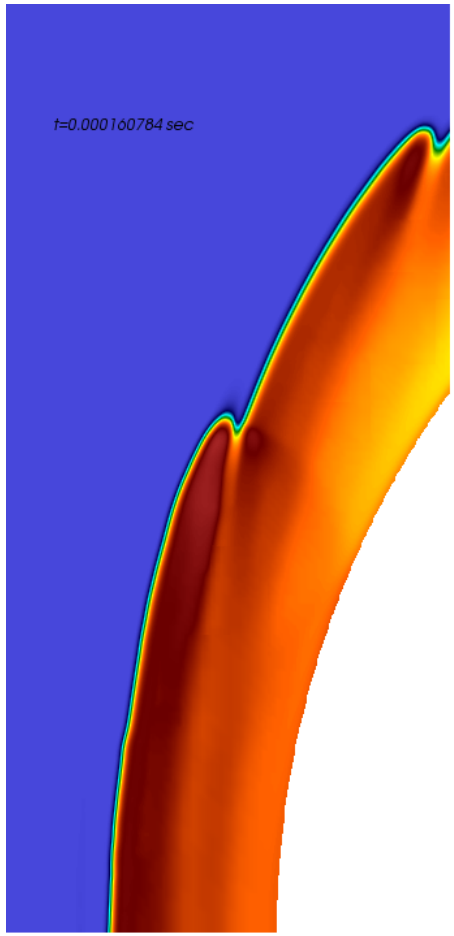

Pressure

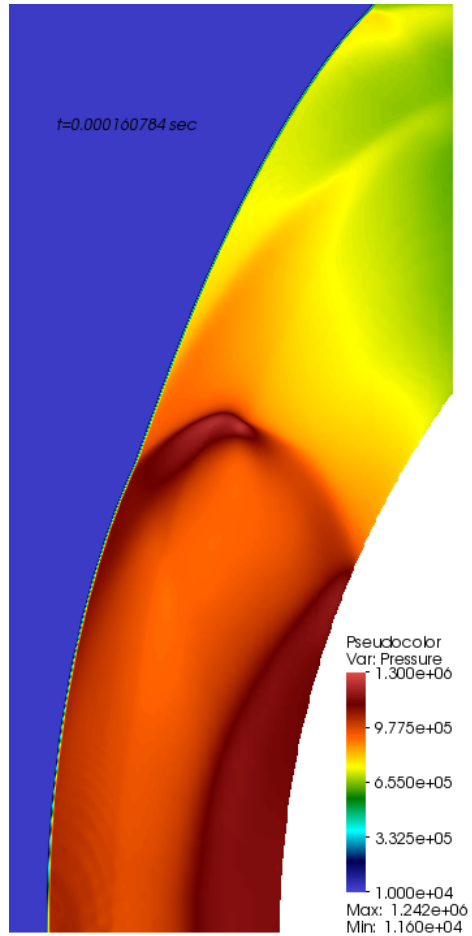

Oscillation mechanism

Schlieren of density

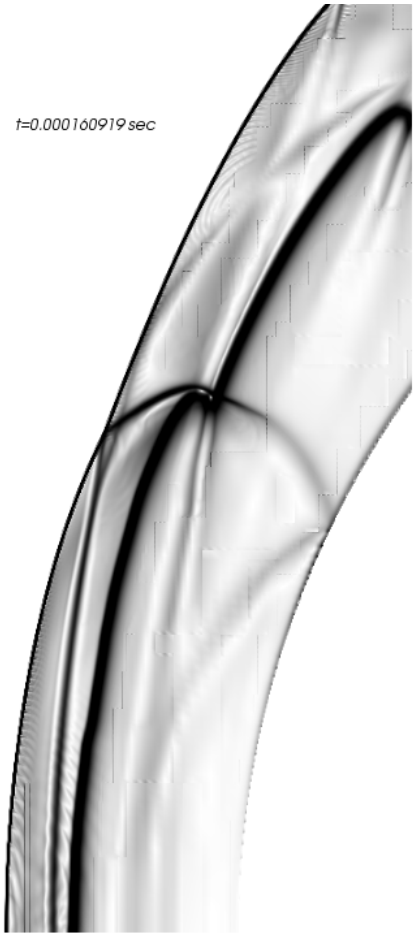

Temperature

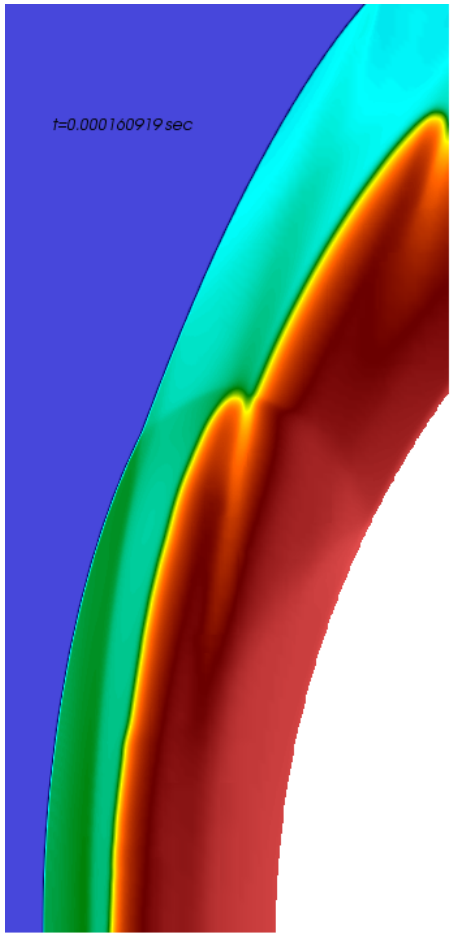

Mass fraction OH

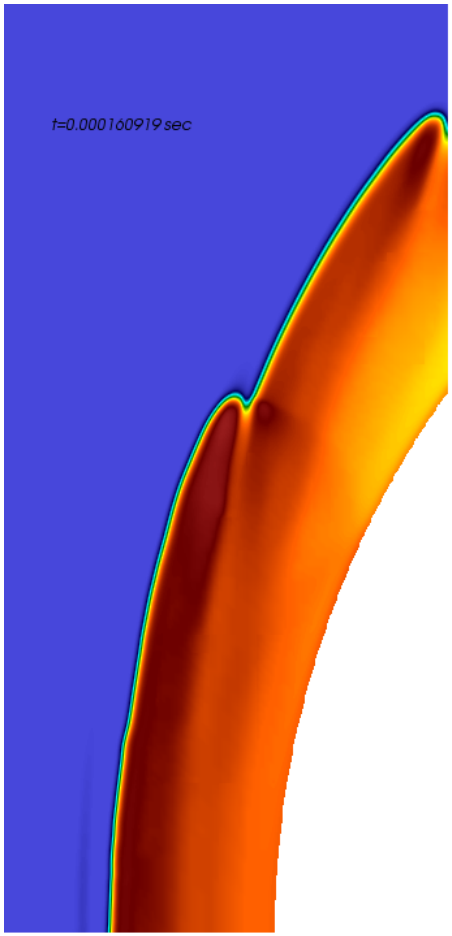

Pressure

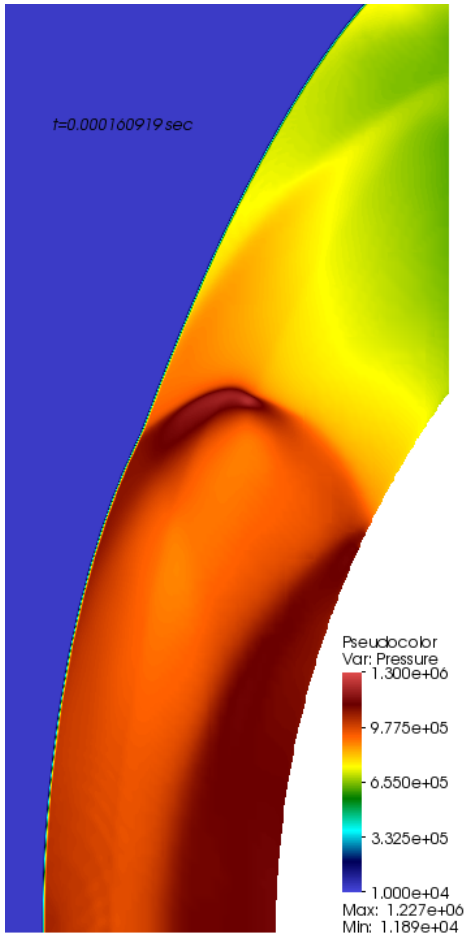

Oscillation mechanism

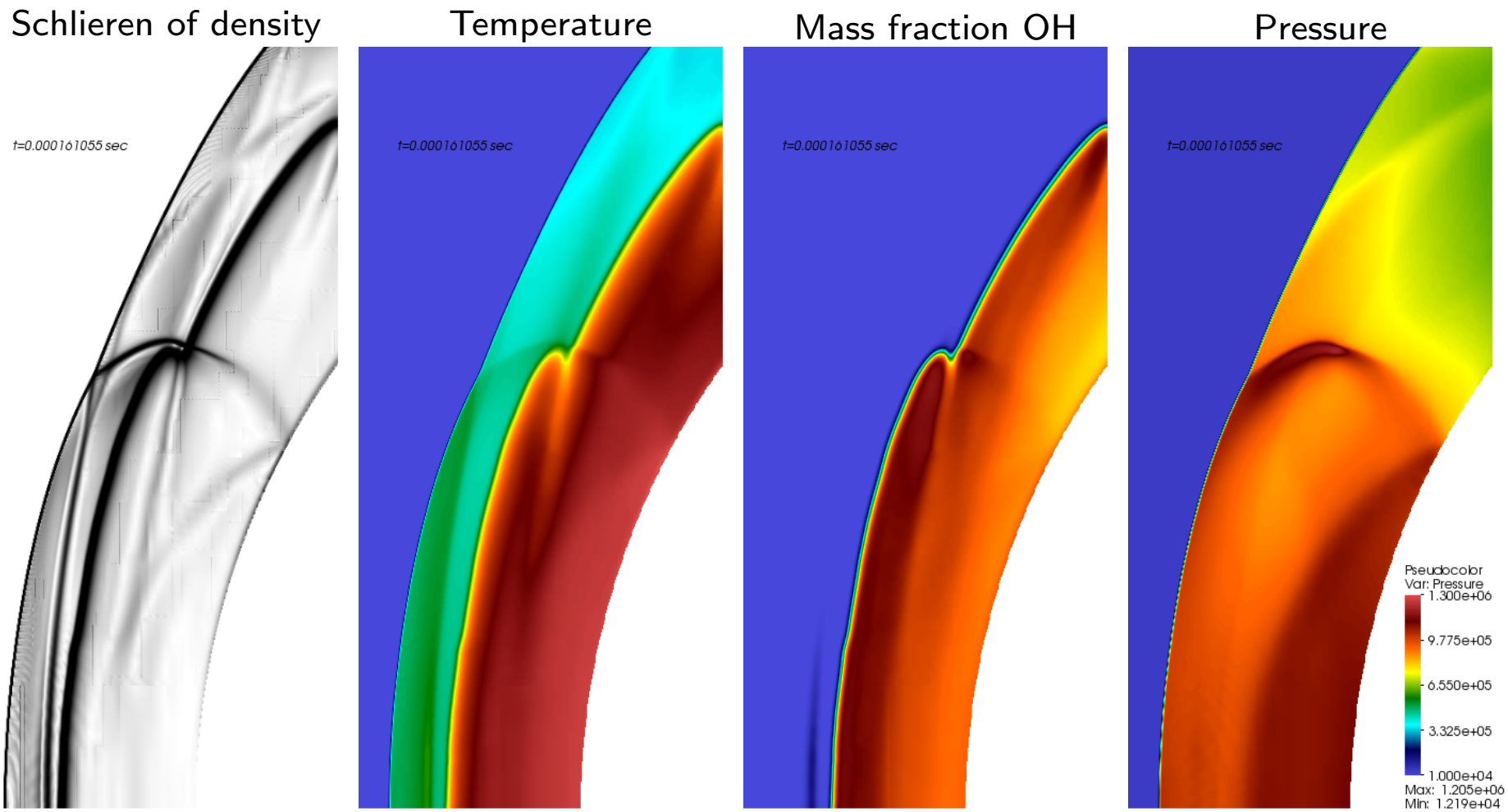

- Oscillation created by accelerated reaction due to slip line from previous triple point

Inviscid case – $M = 4.48$

- 4048 iterations with CFL=0.9 to $t = 170\,\mu\mathrm{s}$
- Oscillation frequency in last $20\,\mu\mathrm{s}$: $\sim 395\,\mathrm{kHz}$
- Experimental value: $\sim 425\,\mathrm{kHz}$

Schlieren plot of density

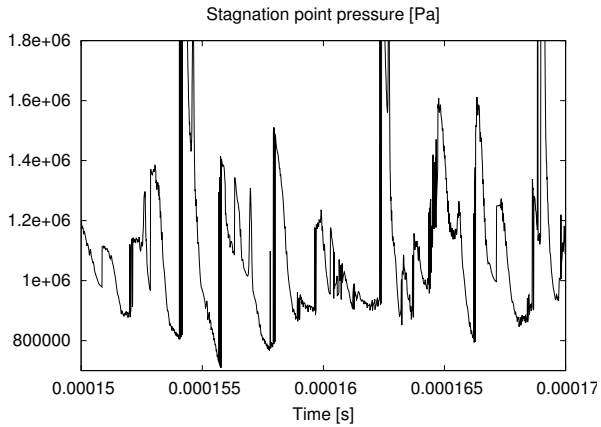

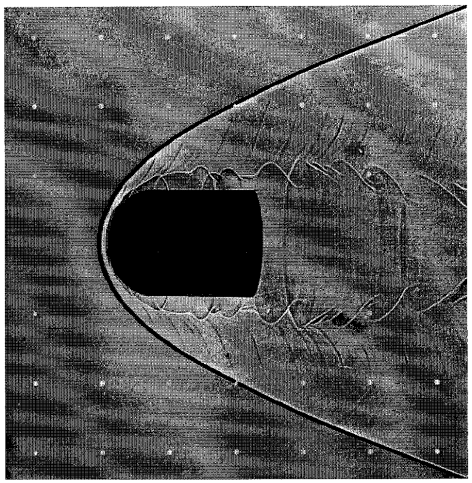

Perturbed oscillation mechanism

Schlieren of density

Temperature

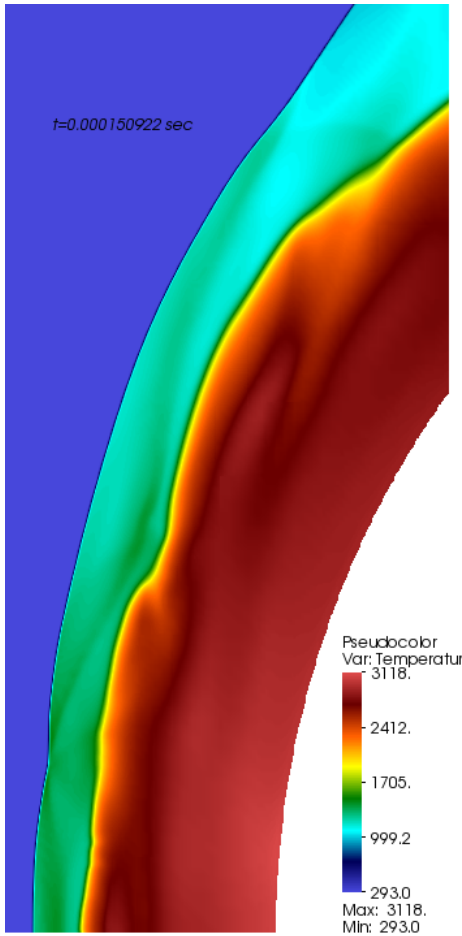

Mass fraction OH

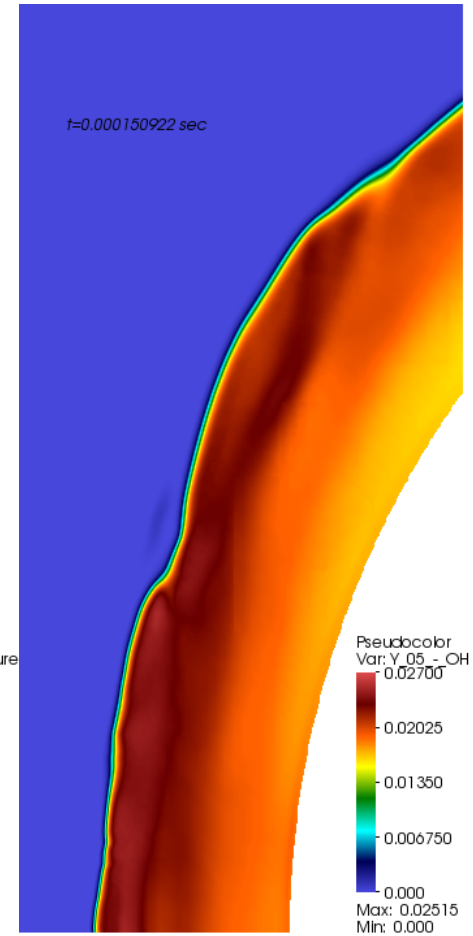

Pressure

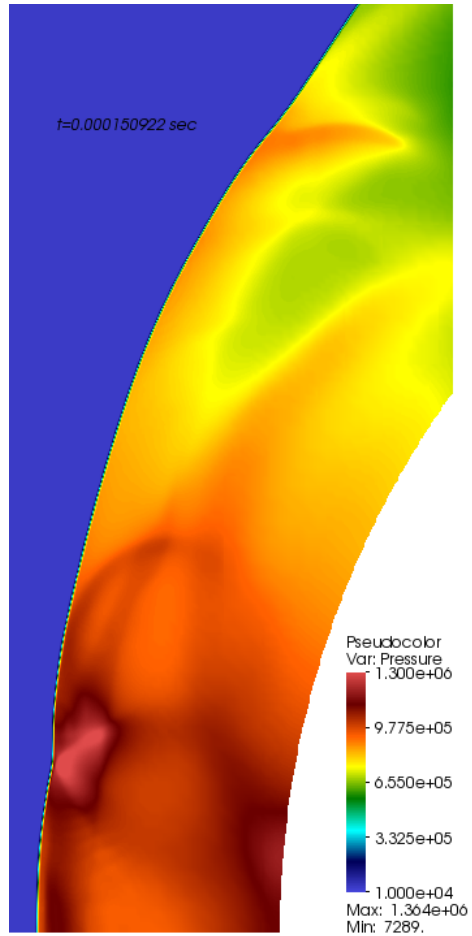

Perturbed oscillation mechanism

Schlieren of density

Temperature

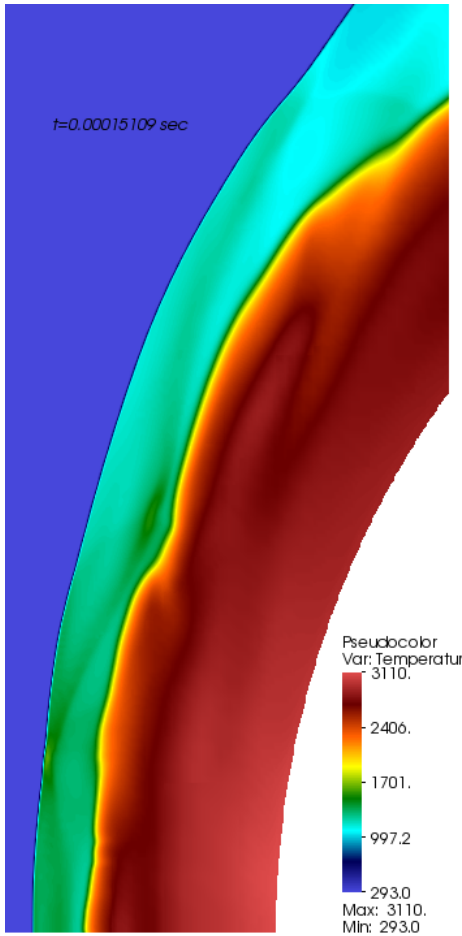

Mass fraction OH

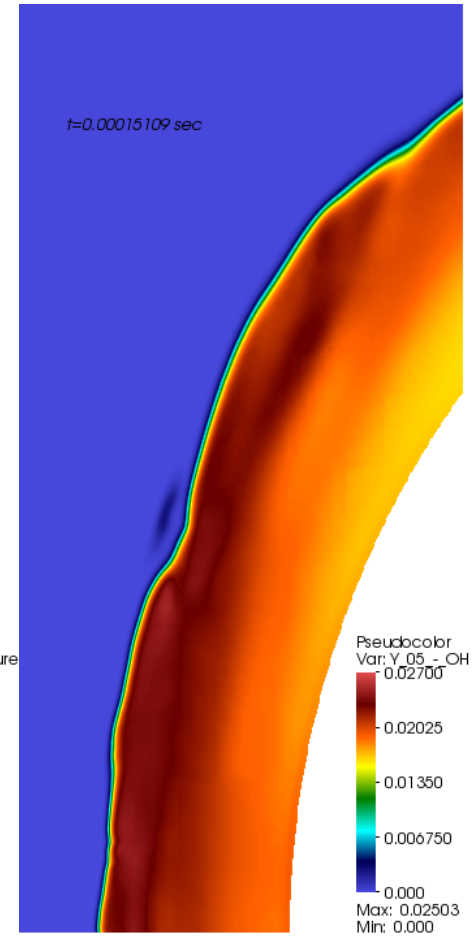

Pressure

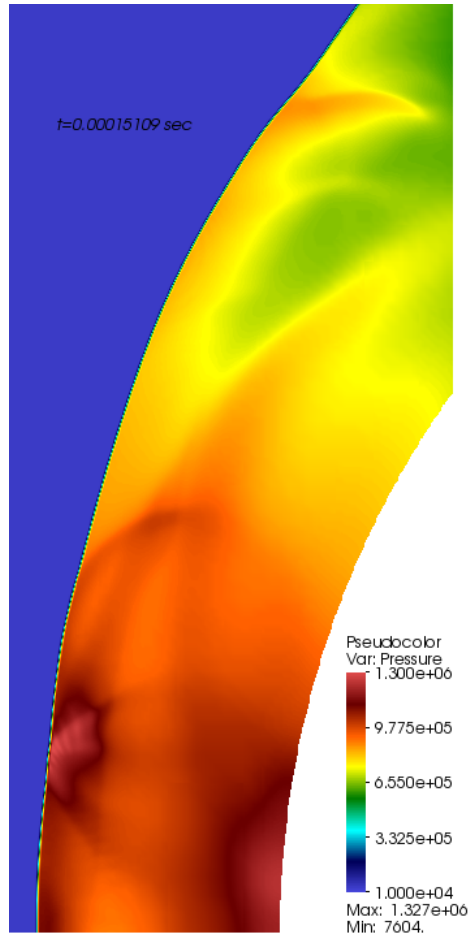

Perturbed oscillation mechanism

Schlieren of density

Temperature

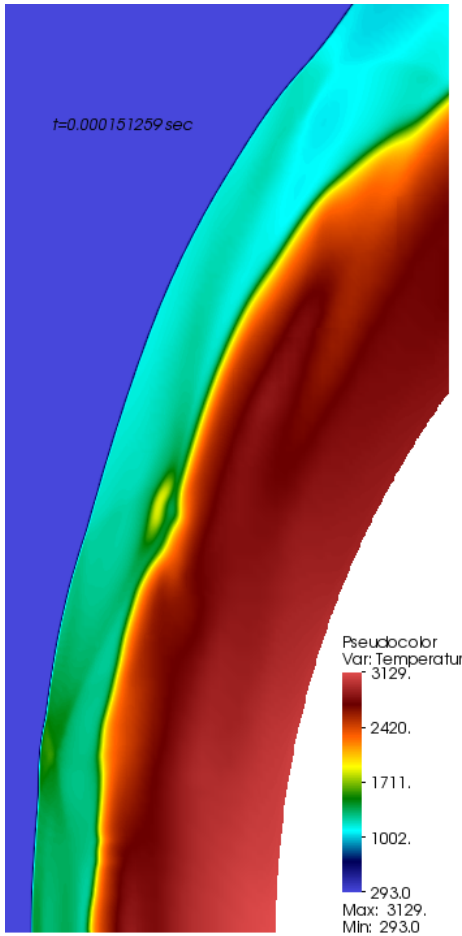

Mass fraction OH

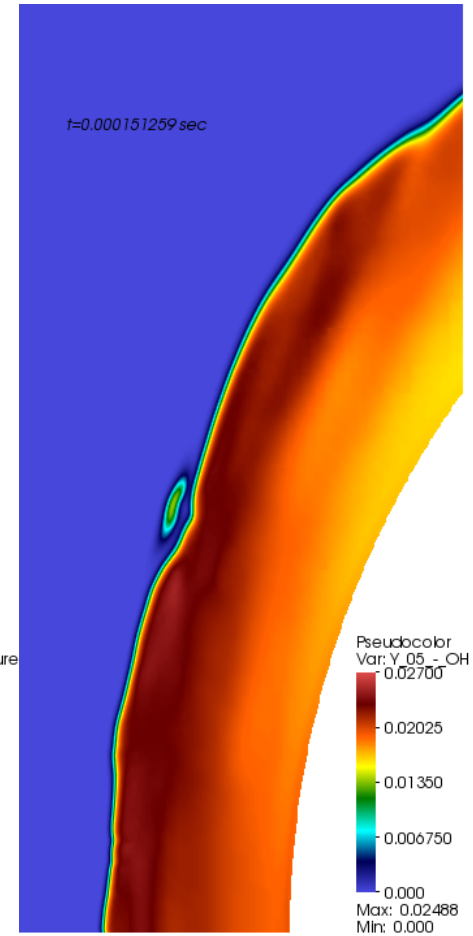

Pressure

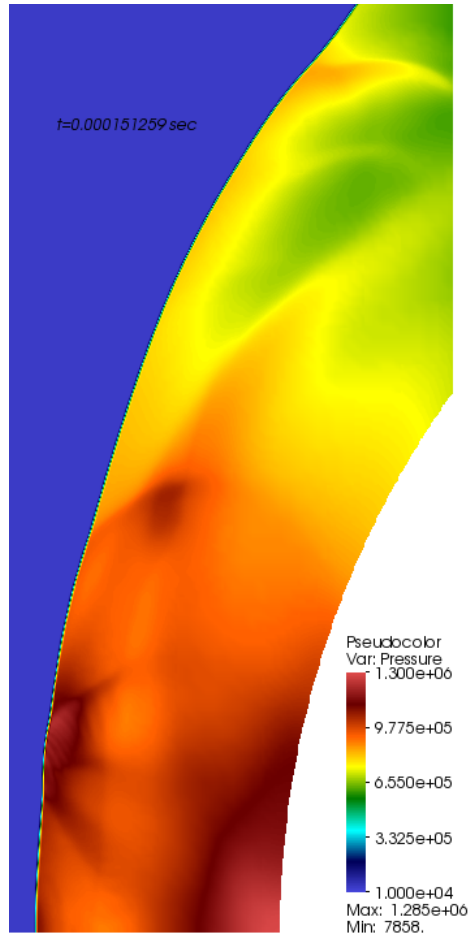

Perturbed oscillation mechanism

Schlieren of density

Temperature

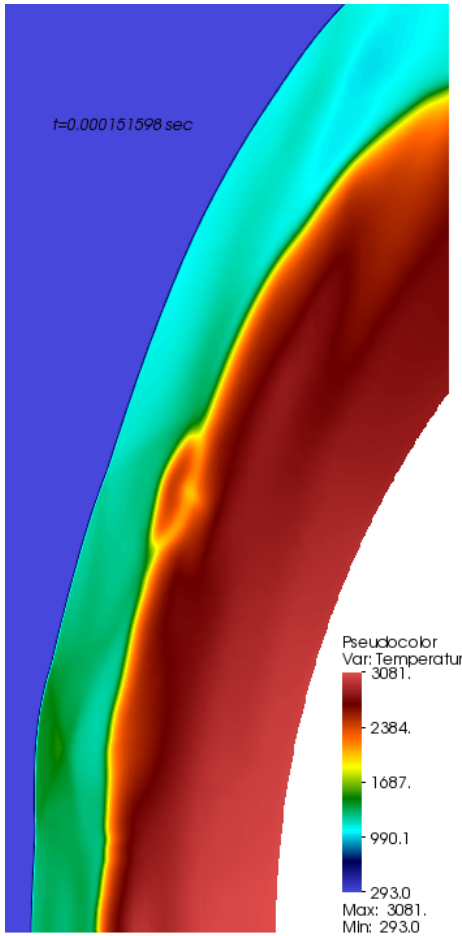

Mass fraction OH

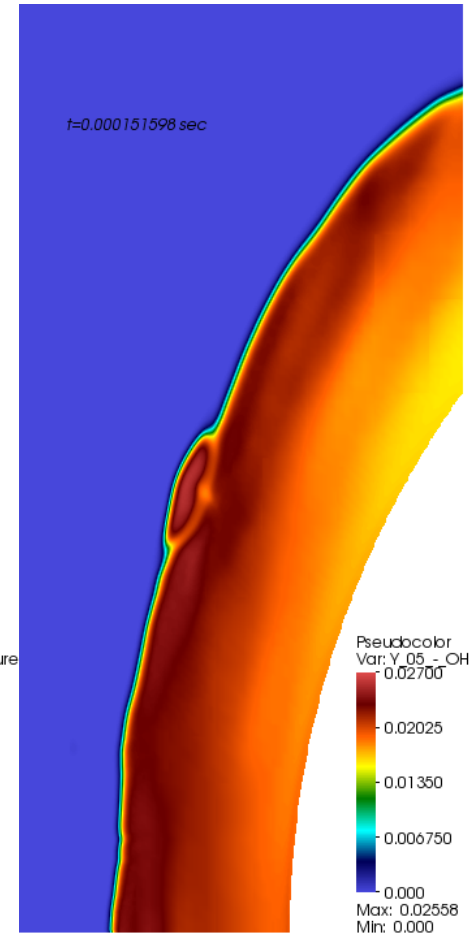

Pressure

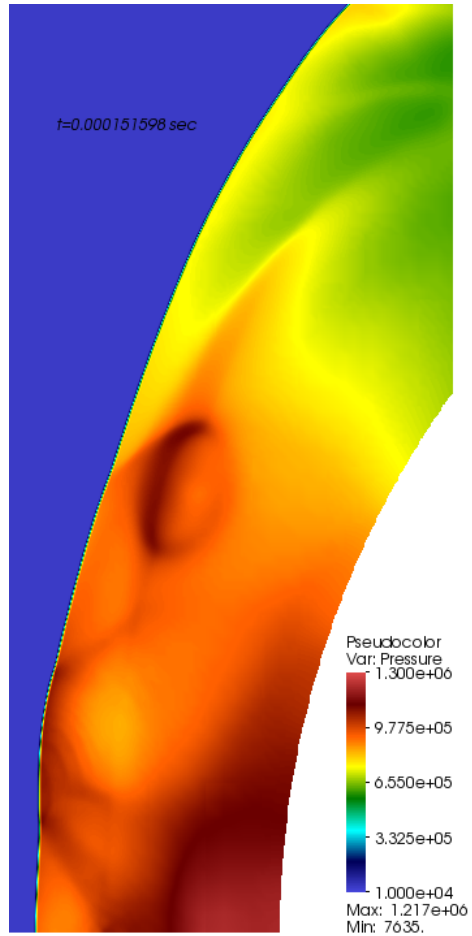

Perturbed oscillation mechanism

Schlieren of density

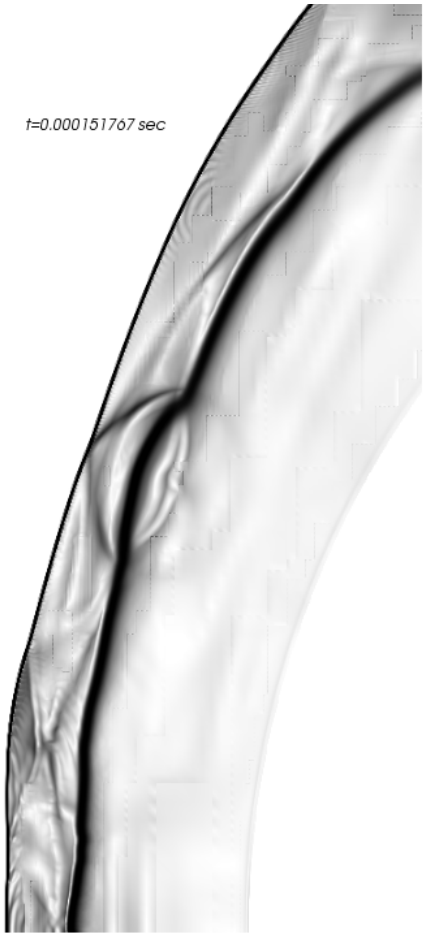

Temperature

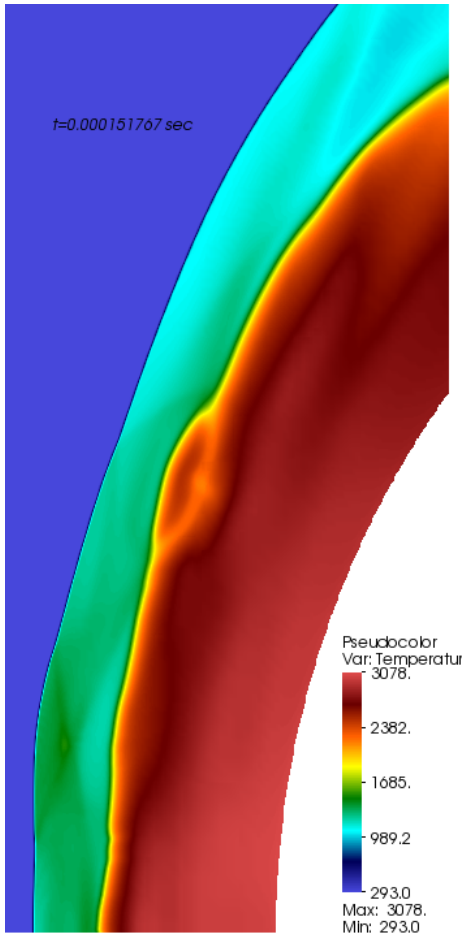

Mass fraction OH

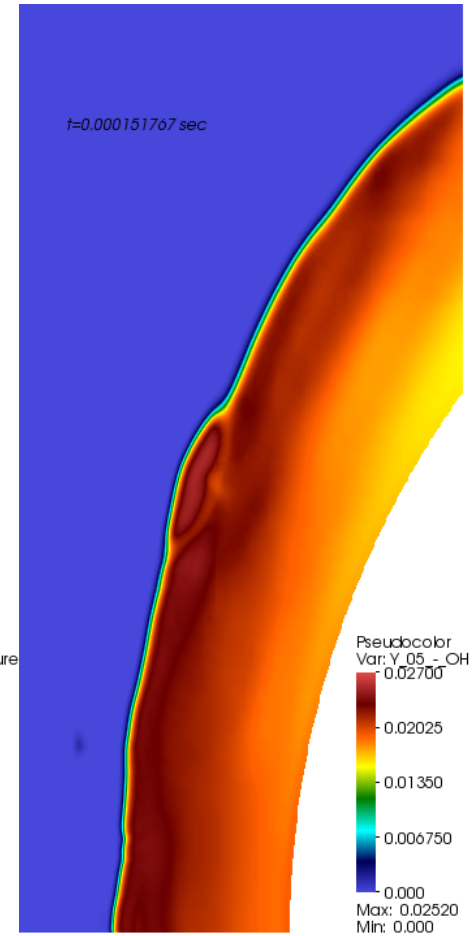

Pressure

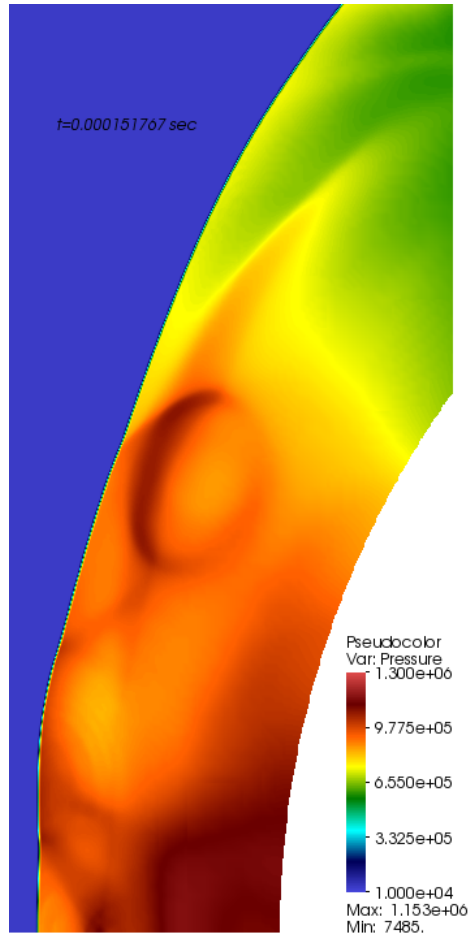

Perturbed oscillation mechanism

Schlieren of density

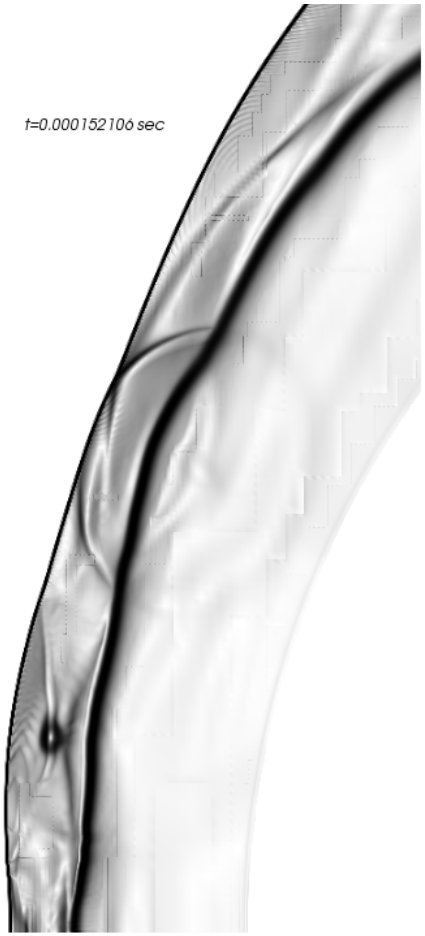

Temperature

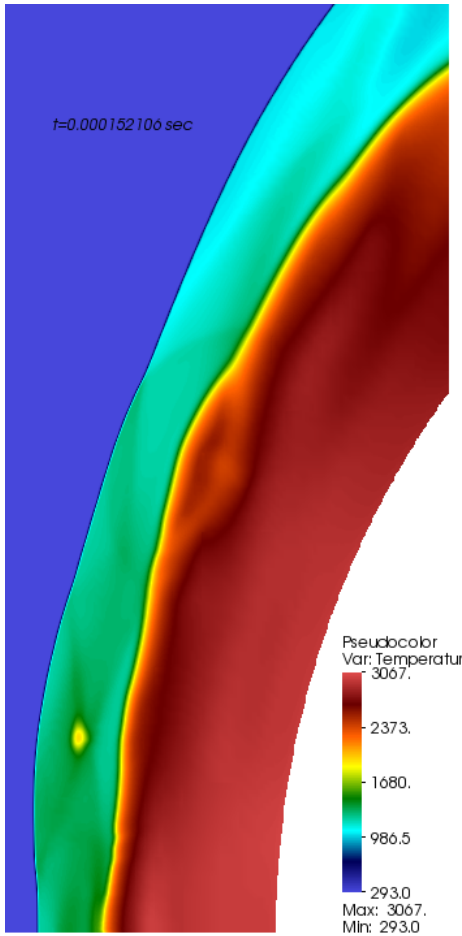

Mass fraction OH

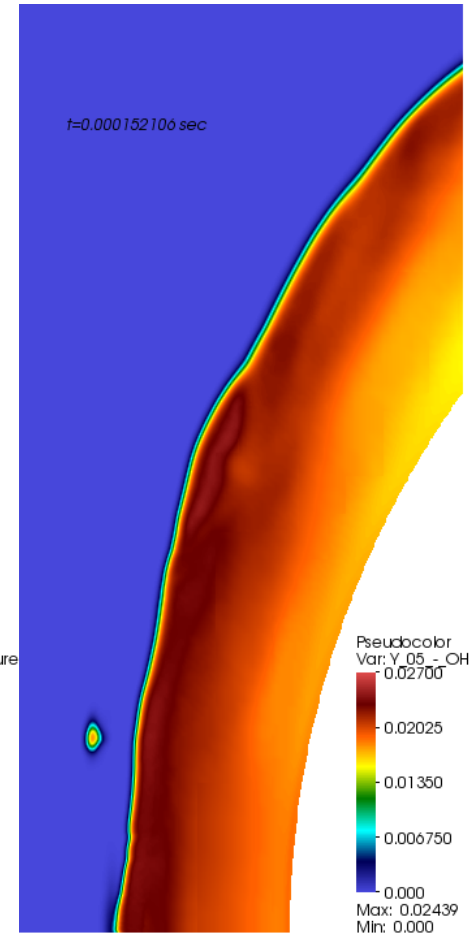

Pressure

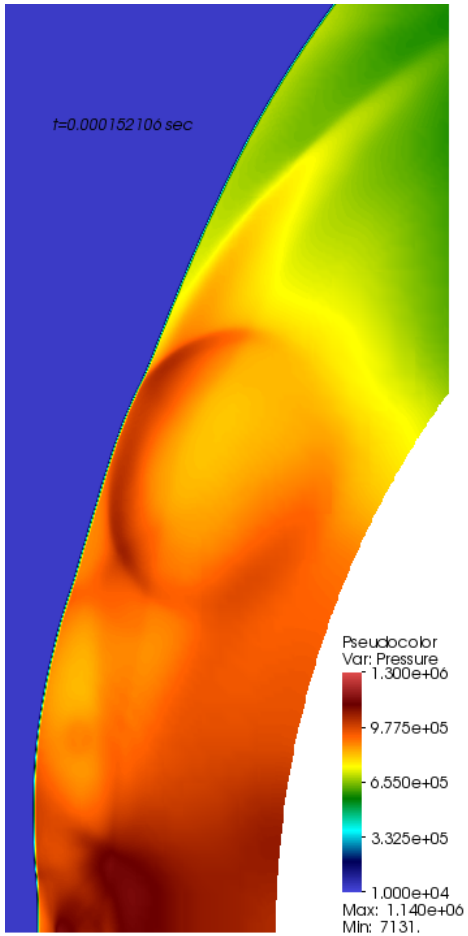

Perturbed oscillation mechanism

Schlieren of density

Temperature

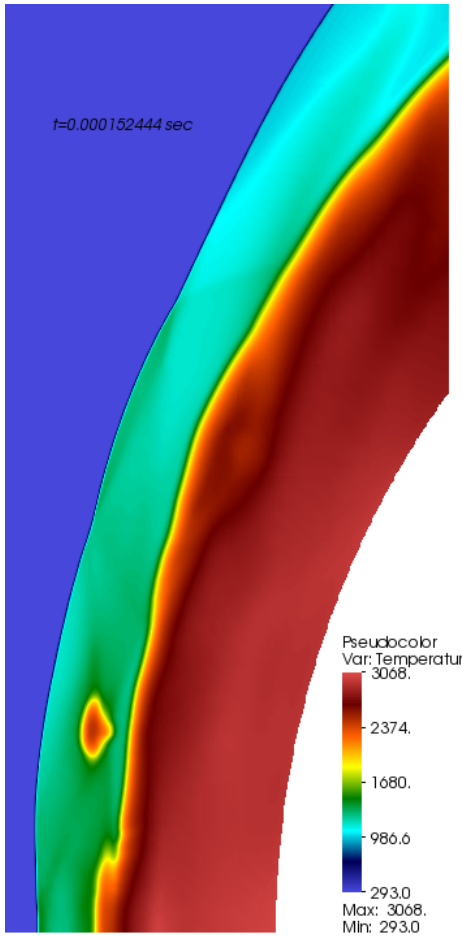

Mass fraction OH

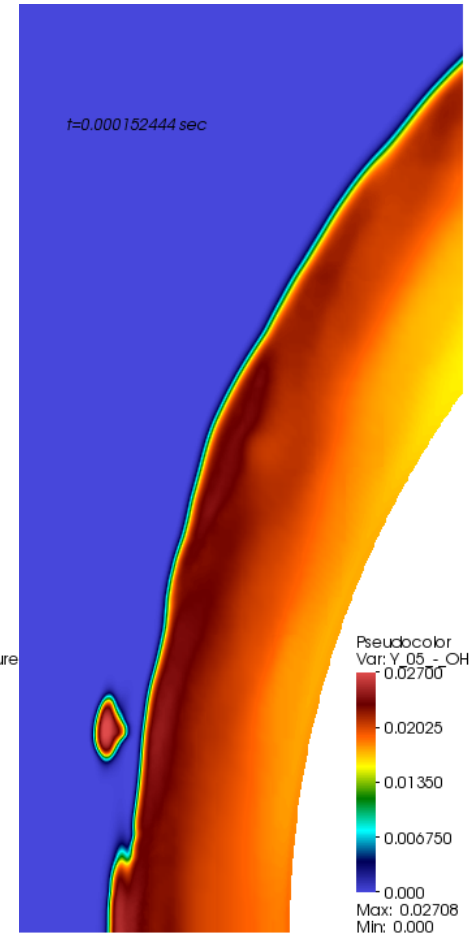

Pressure

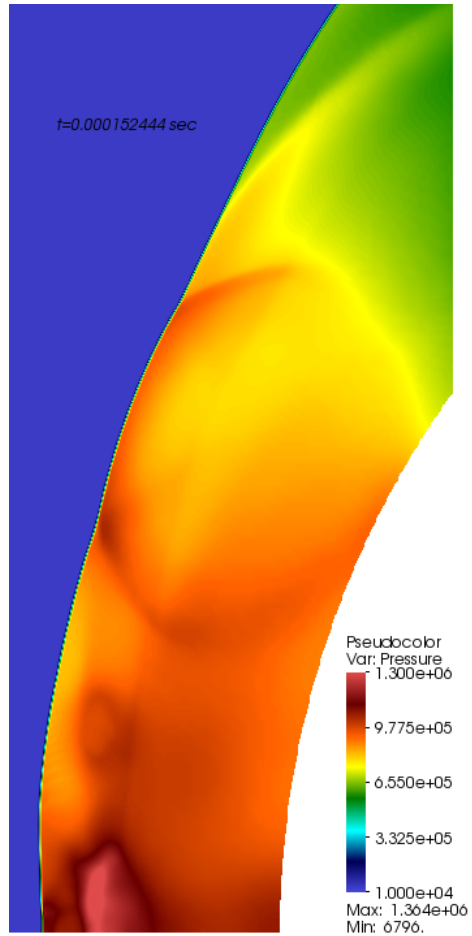

Perturbed oscillation mechanism

Schlieren of density

Temperature

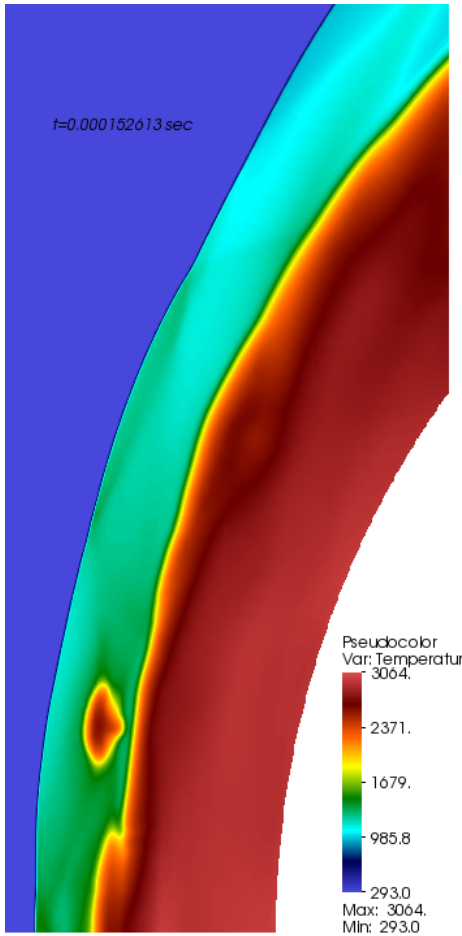

Mass fraction OH

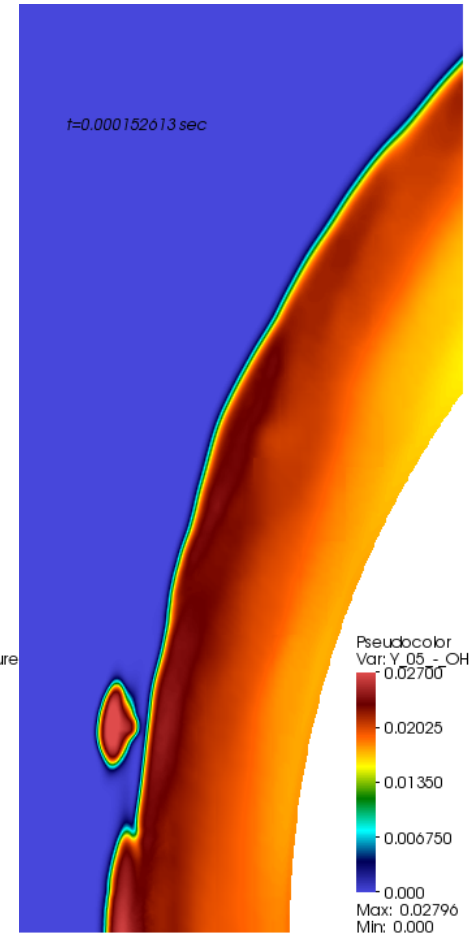

Pressure

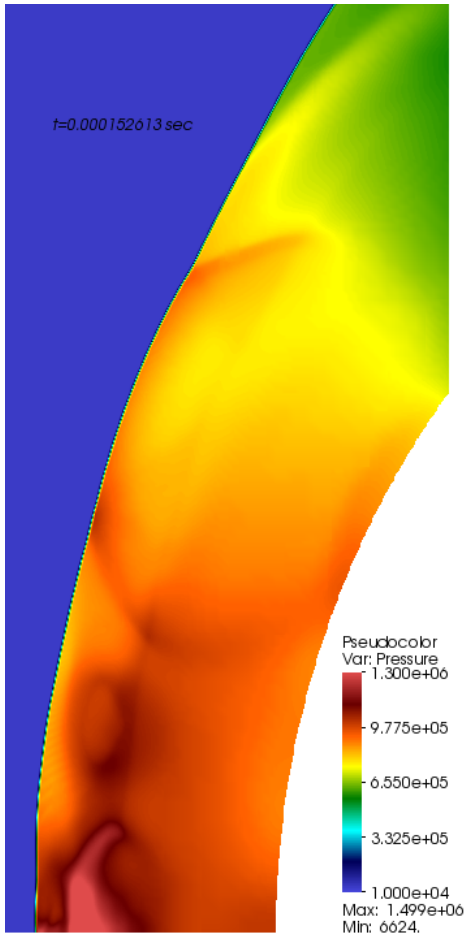

Perturbed oscillation mechanism

Schlieren of density

Temperature

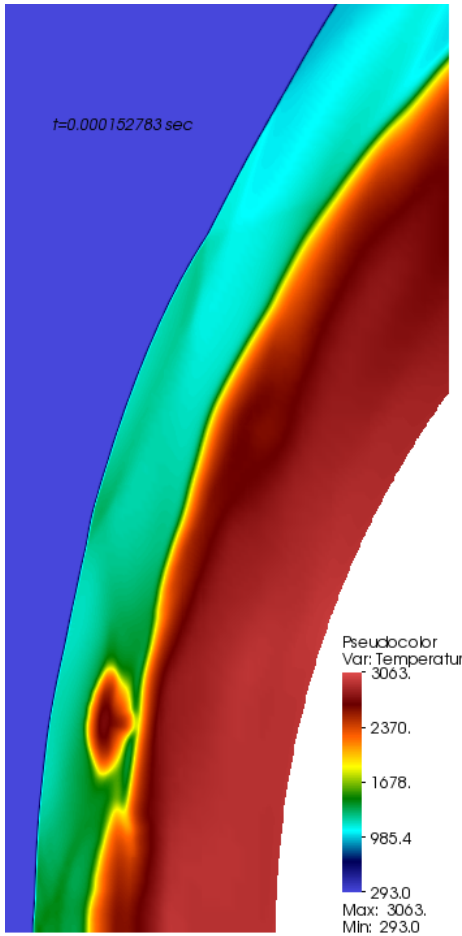

Mass fraction OH

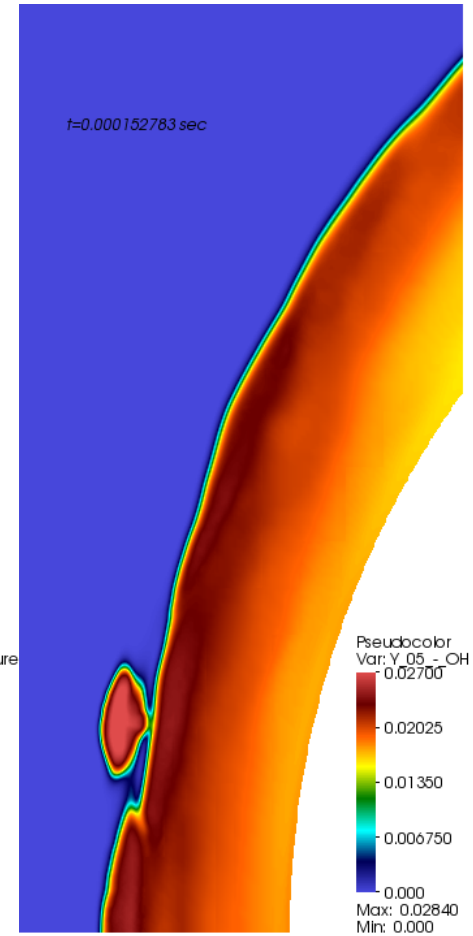

Pressure

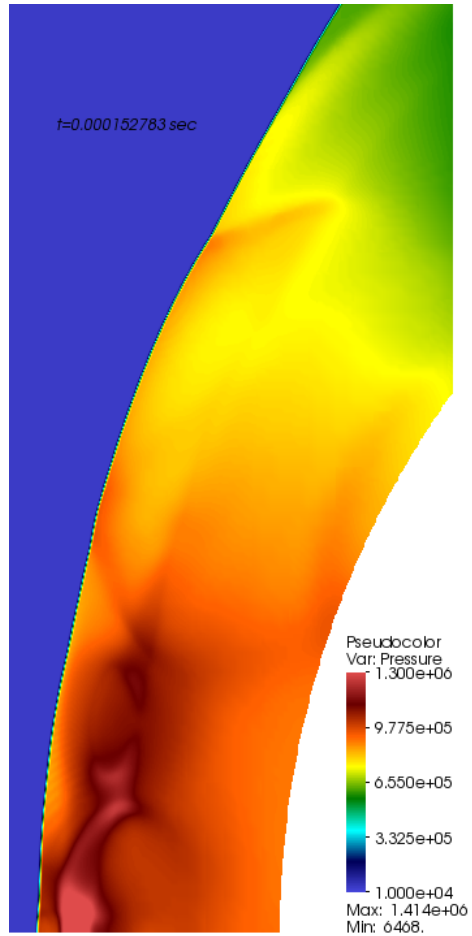

Perturbed oscillation mechanism

Schlieren of density

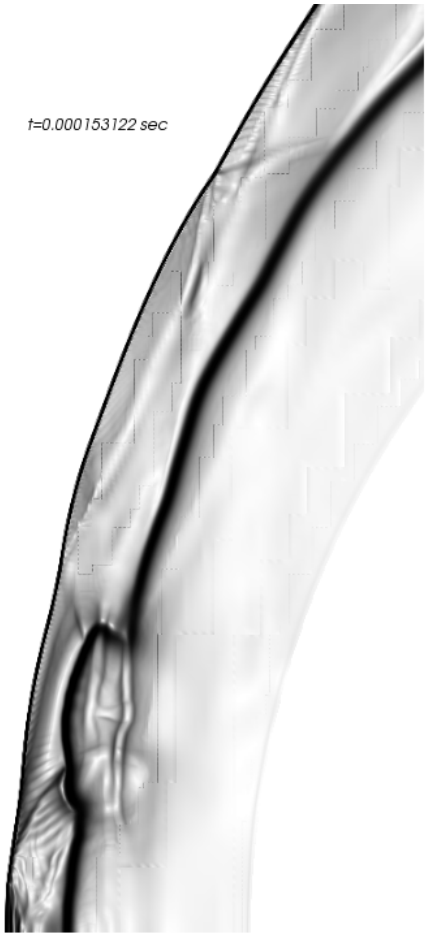

Temperature

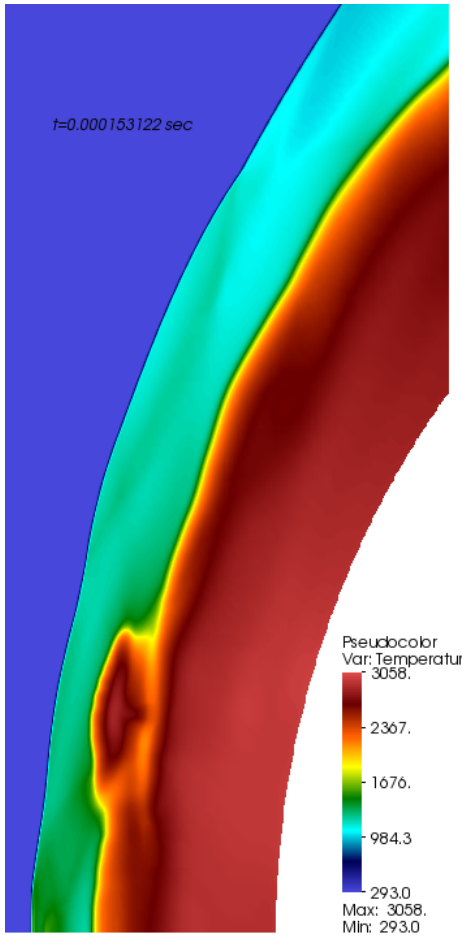

Mass fraction OH

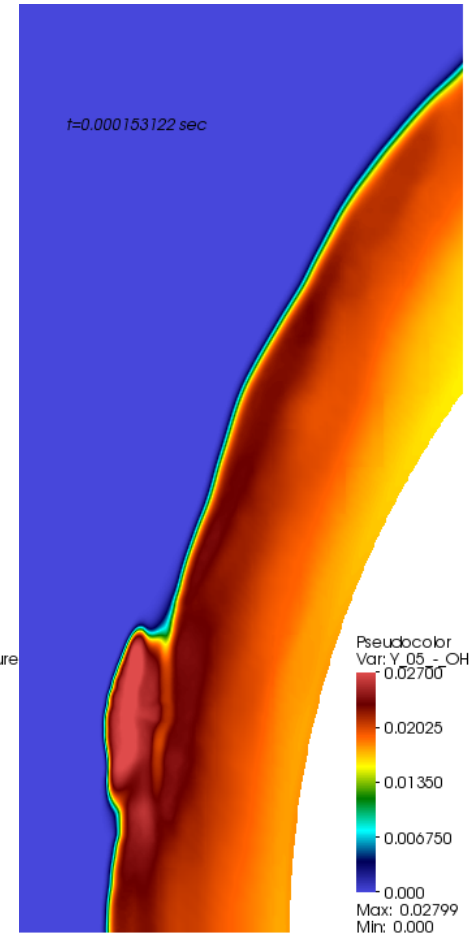

Pressure

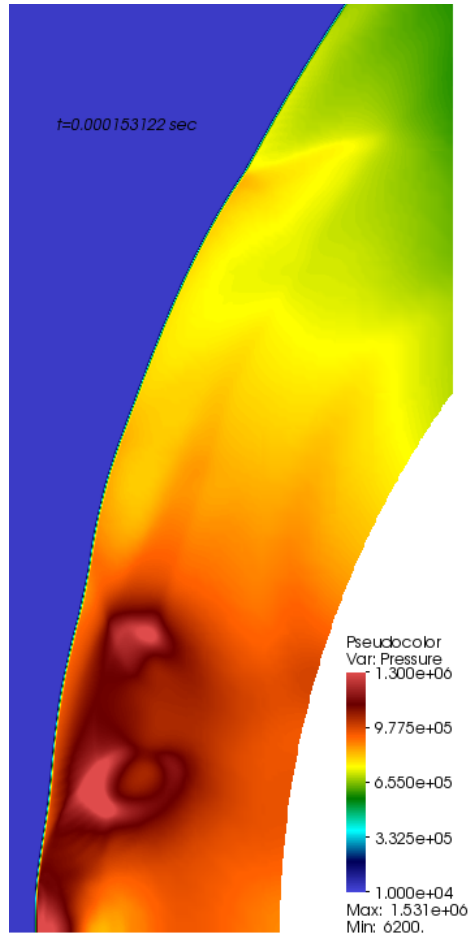

Perturbed oscillation mechanism

Schlieren of density

Temperature

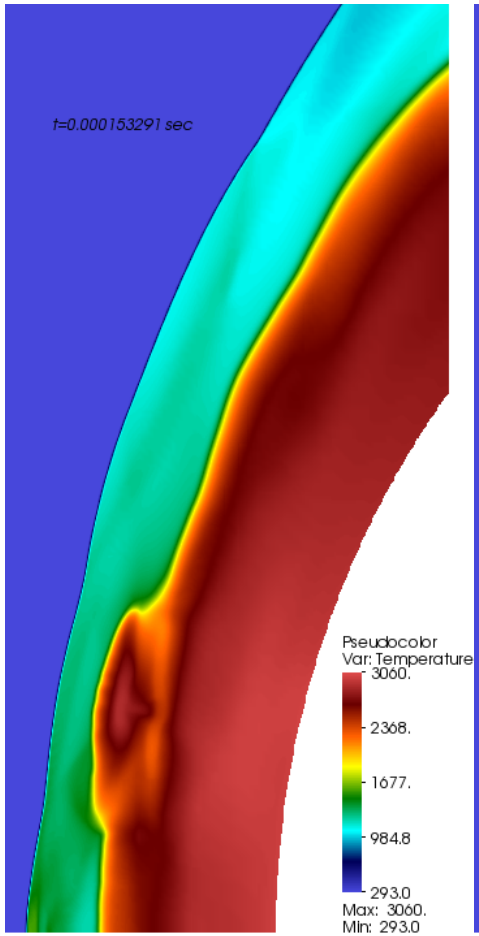

Mass fraction OH

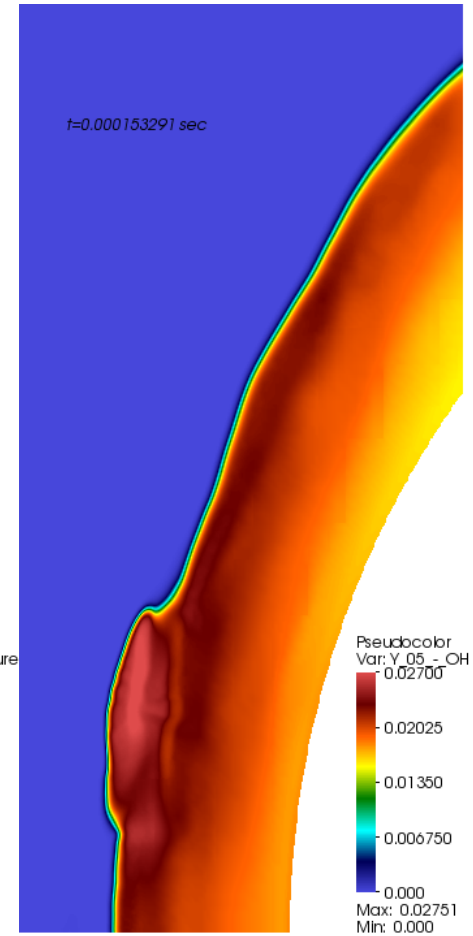

Pressure

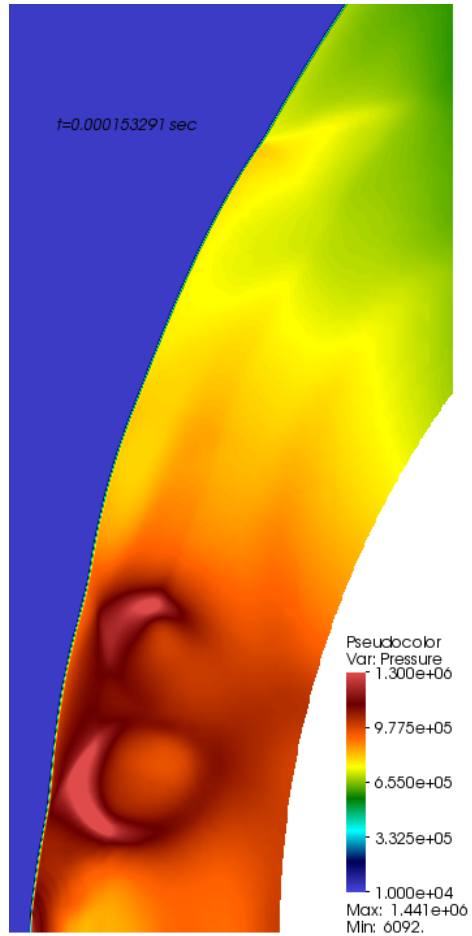

Perturbed oscillation mechanism

Schlieren of density

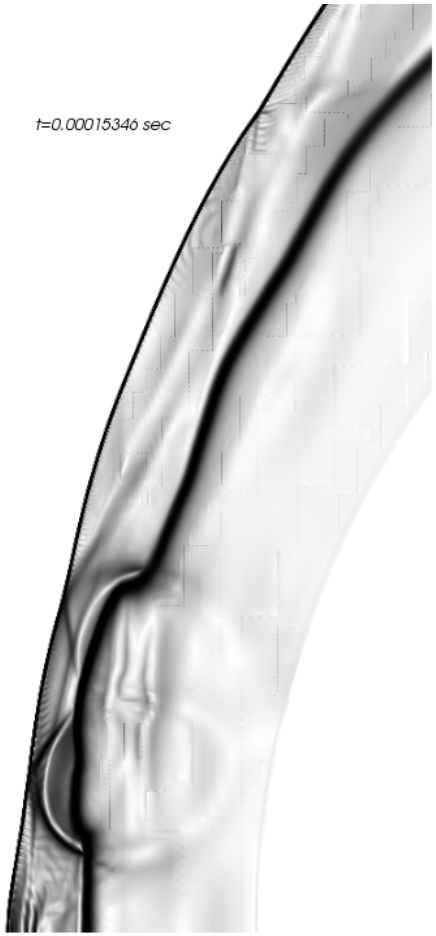

Temperature

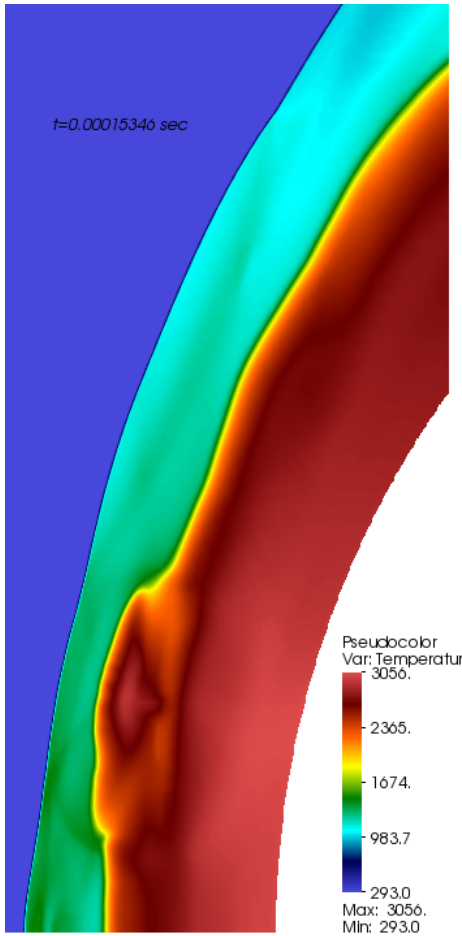

Mass fraction OH

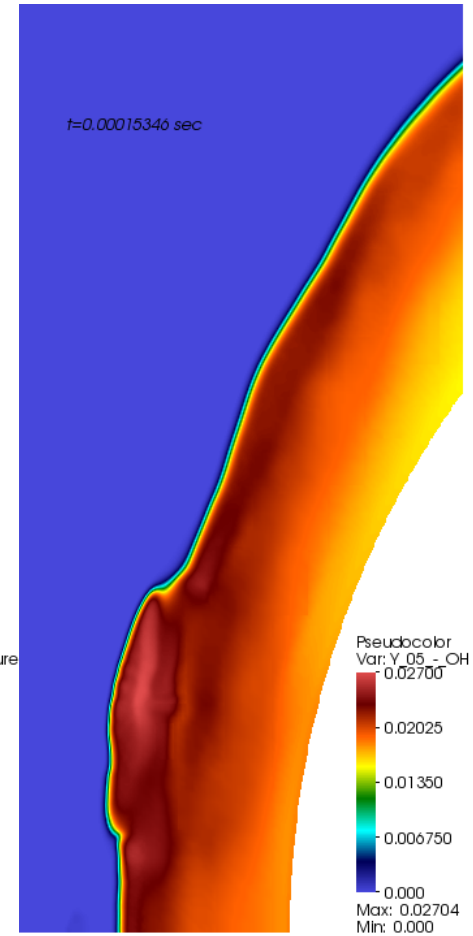

Pressure

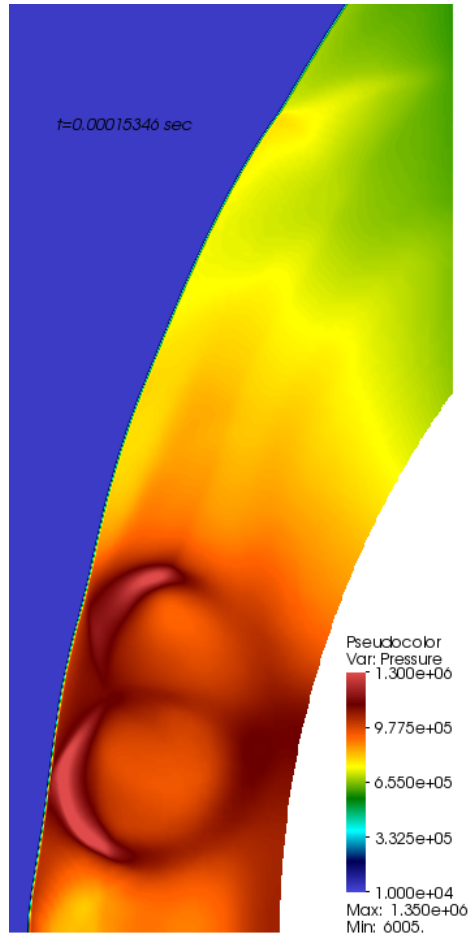

Perturbed oscillation mechanism

Schlieren of density

Temperature

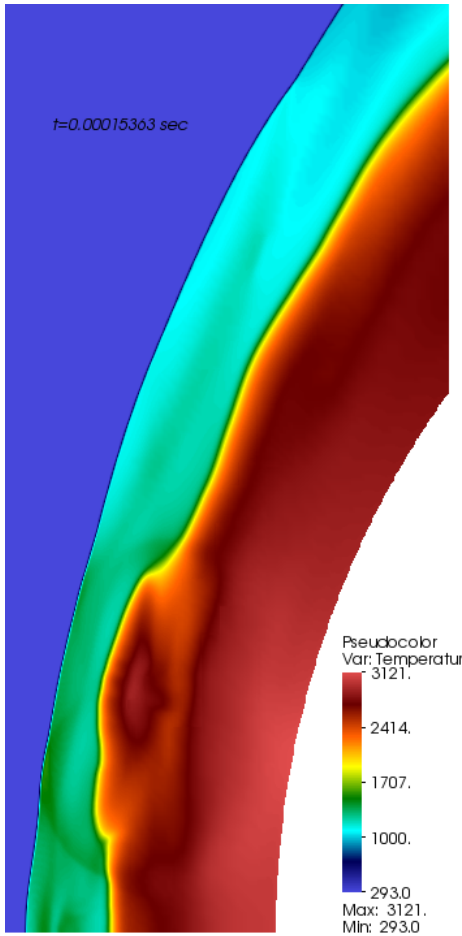

Mass fraction OH

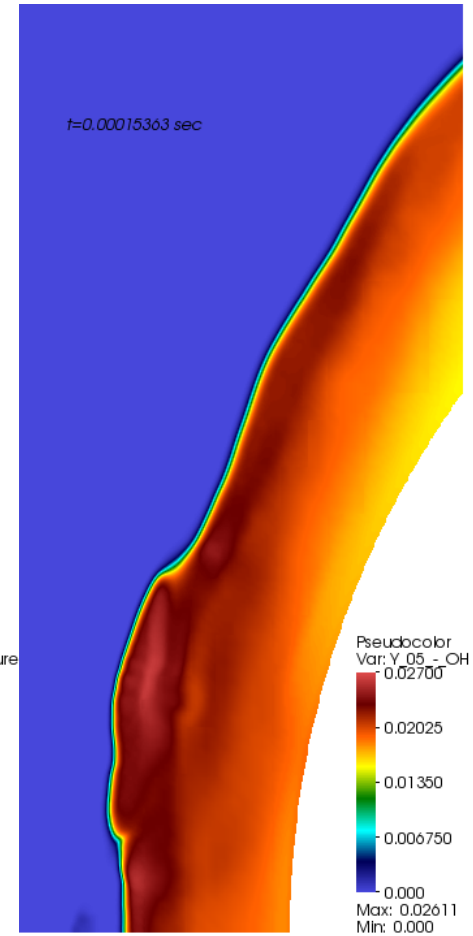

Pressure

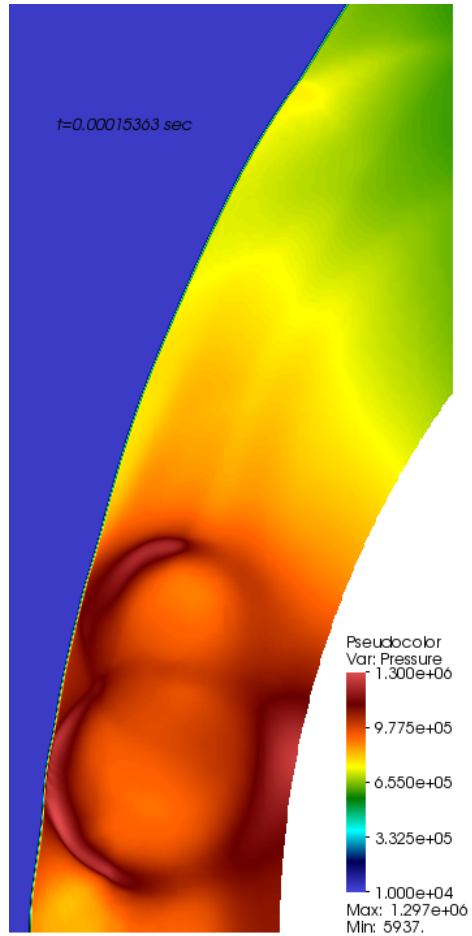

Perturbed oscillation mechanism

Schlieren of density

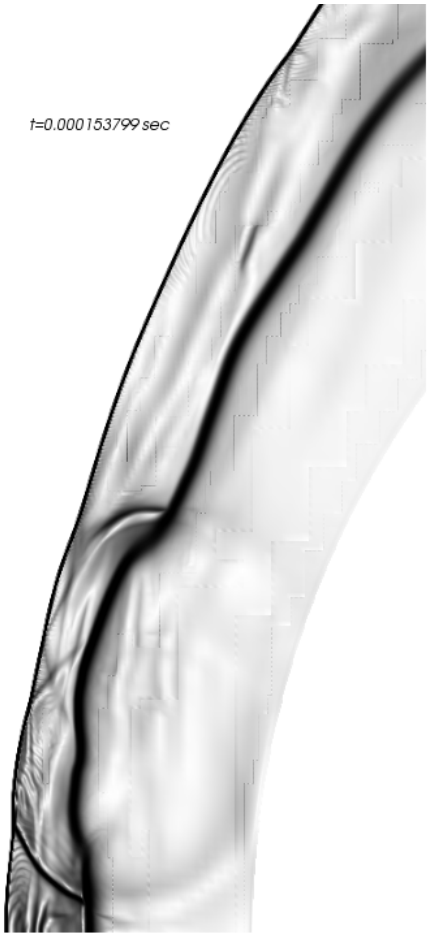

Temperature

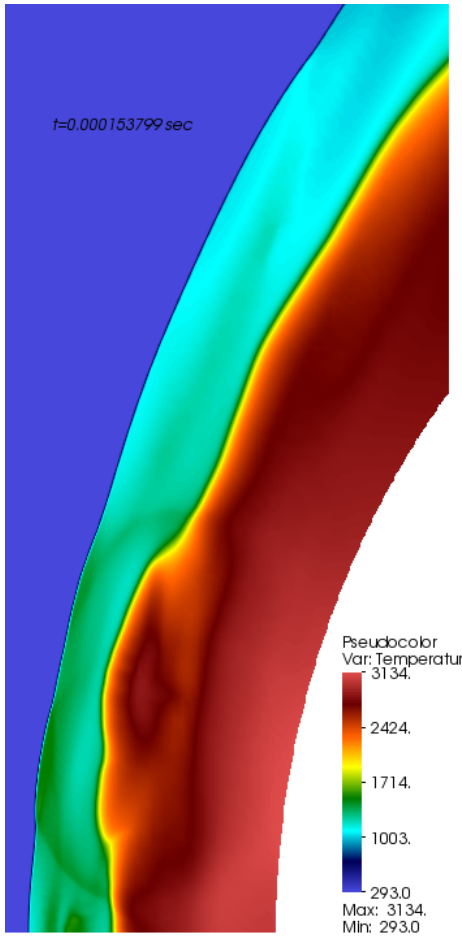

Mass fraction OH

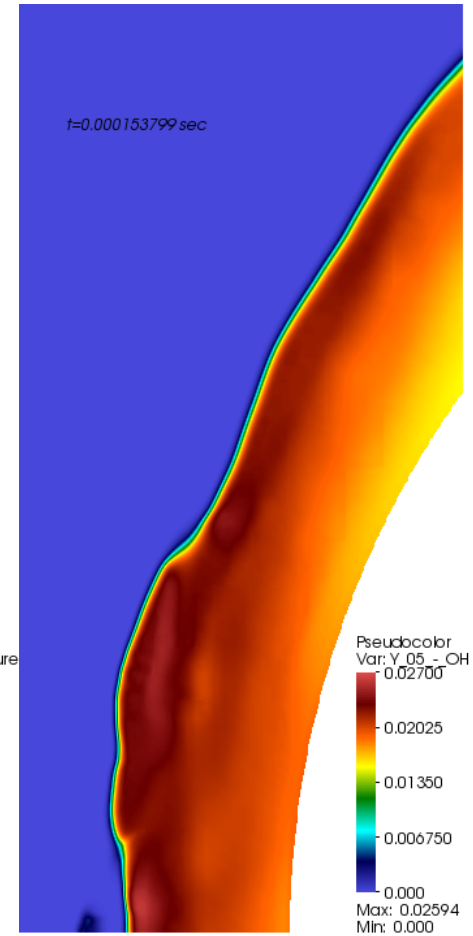

Pressure

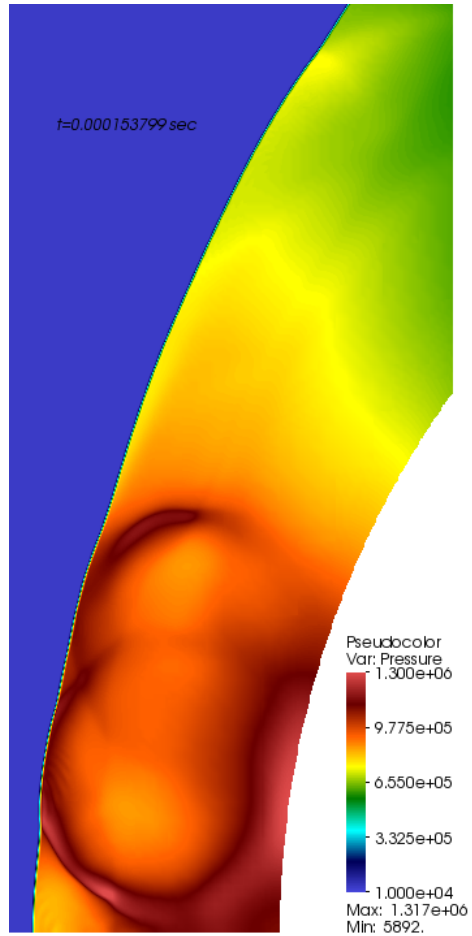

Perturbed oscillation mechanism

Schlieren of density

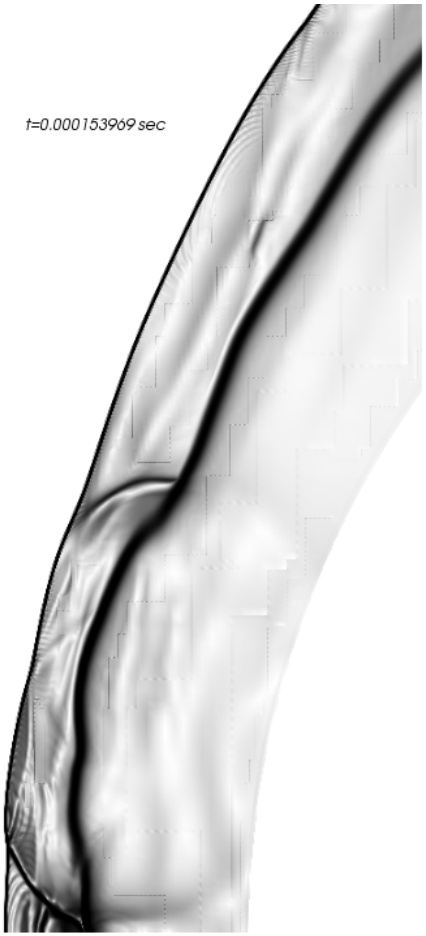

Temperature

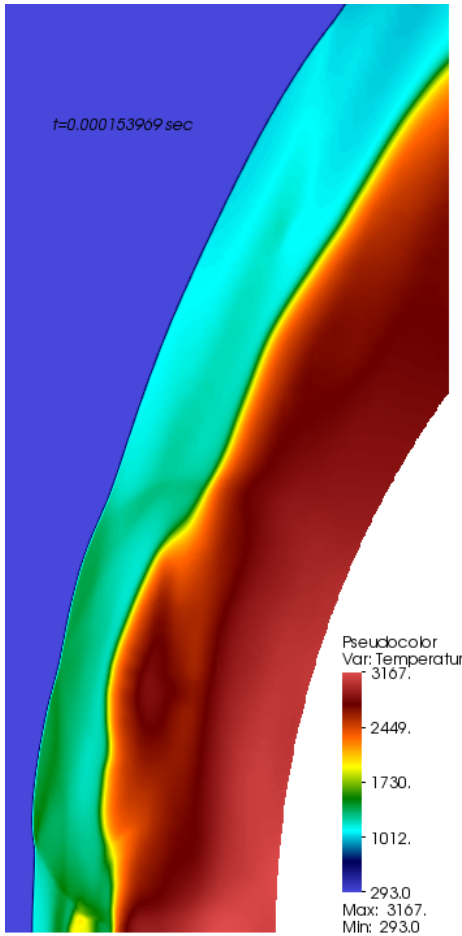

Mass fraction OH

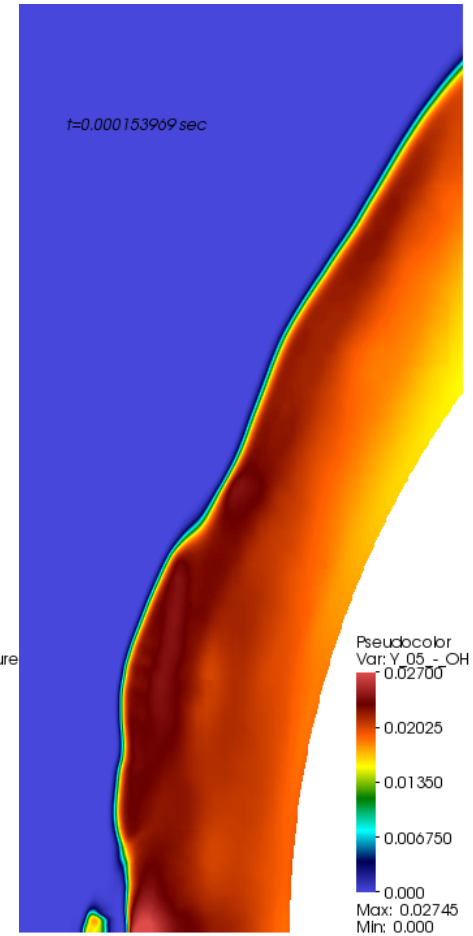

Pressure

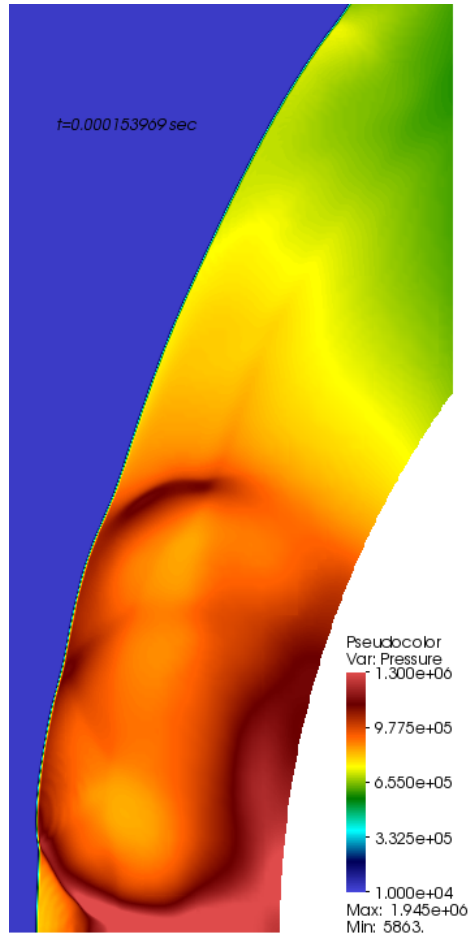

Perturbed oscillation mechanism

Schlieren of density

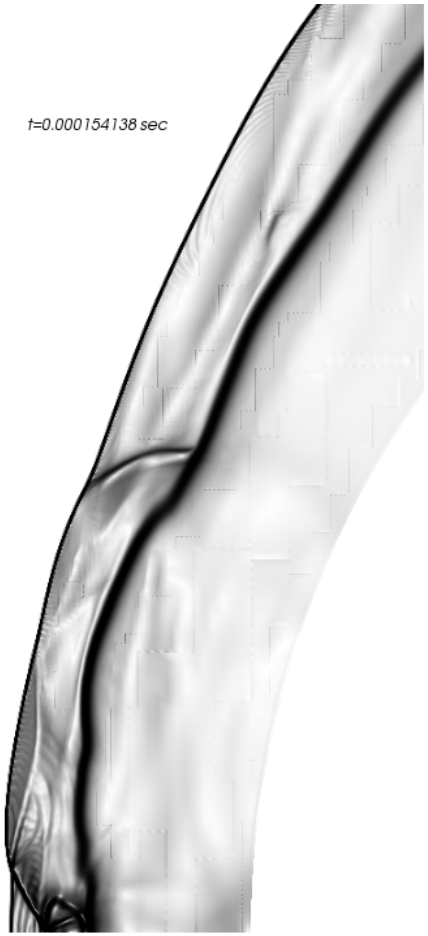

Temperature

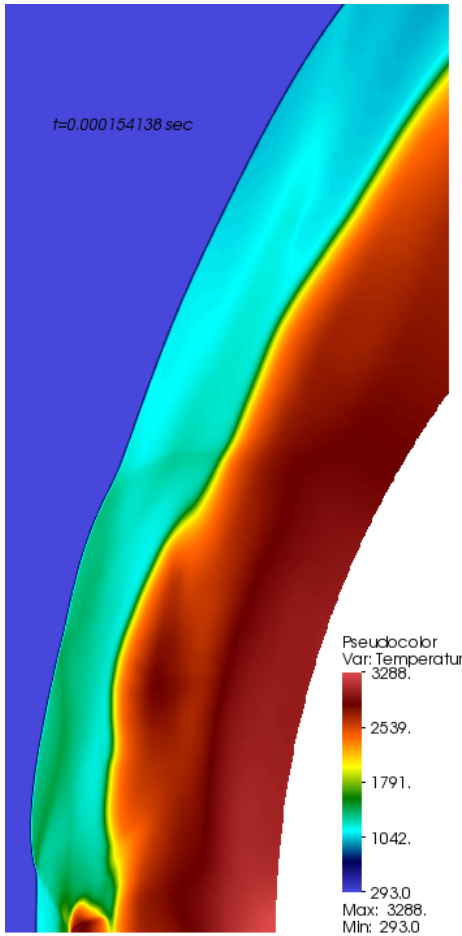

Mass fraction OH

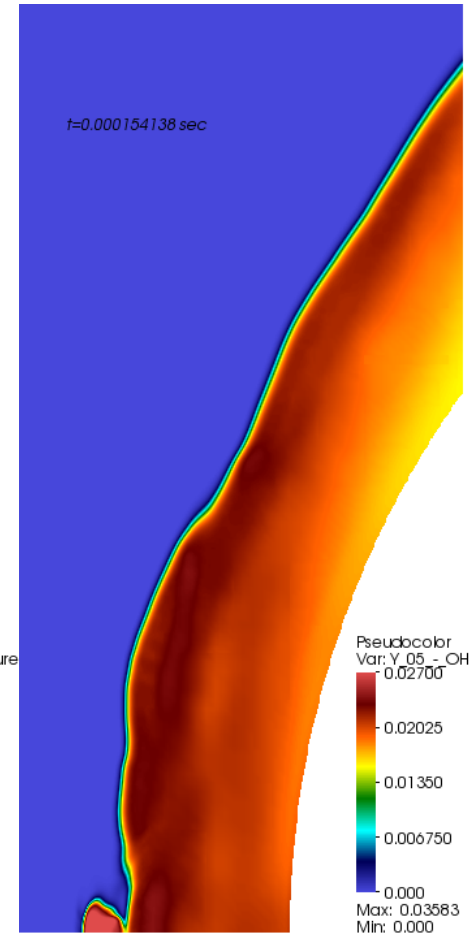

Pressure

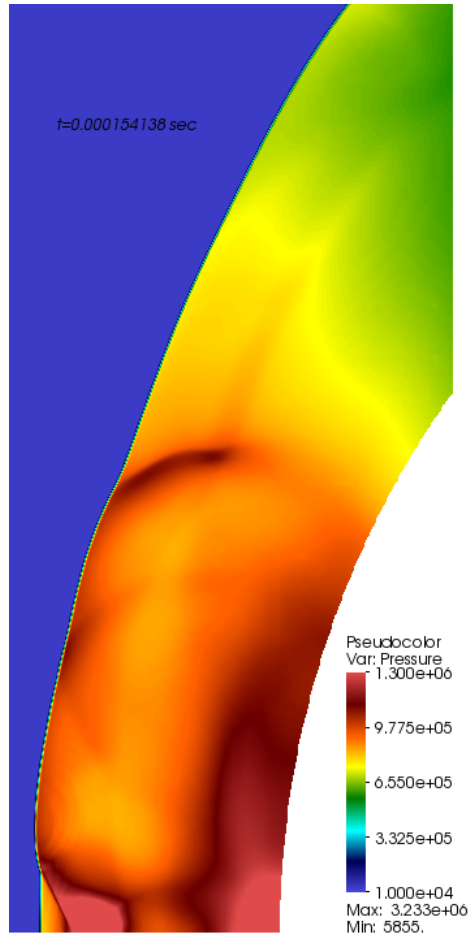

Perturbed oscillation mechanism

Schlieren of density

Temperature

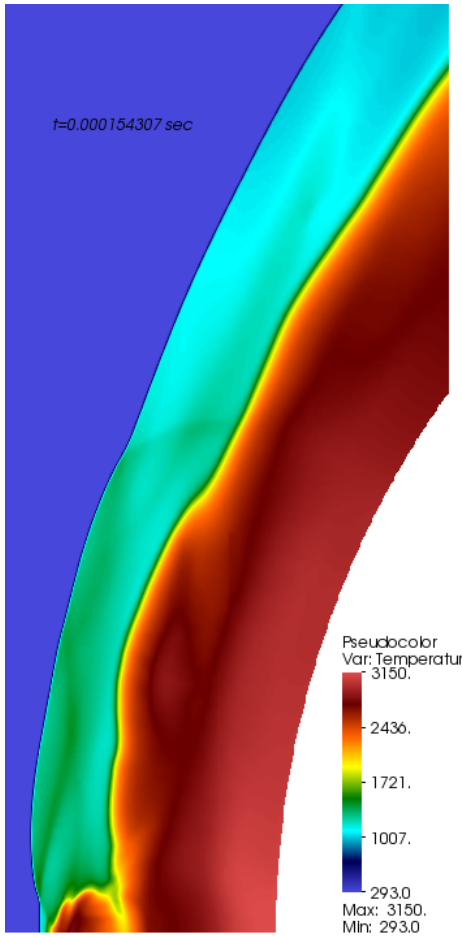

Mass fraction OH

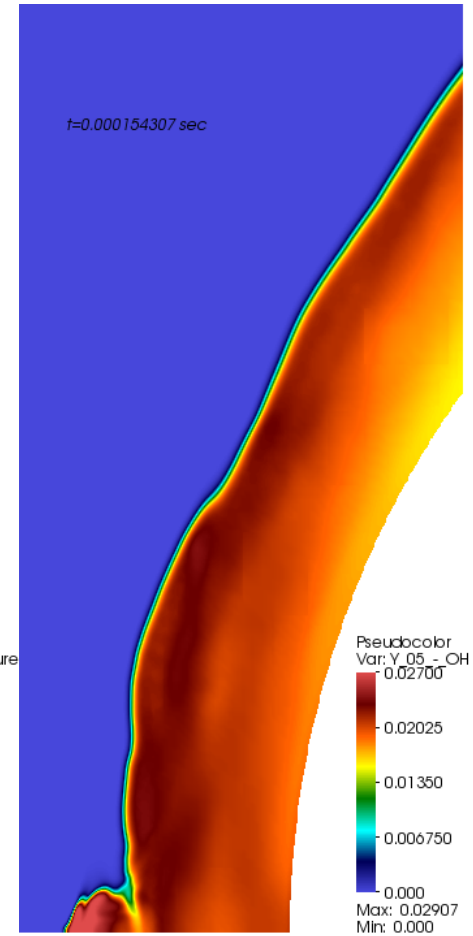

Pressure

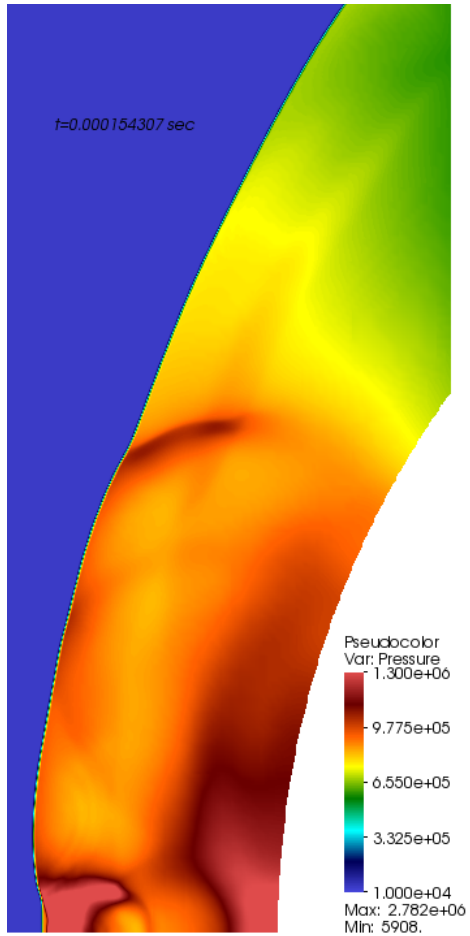

Perturbed oscillation mechanism

Schlieren of density

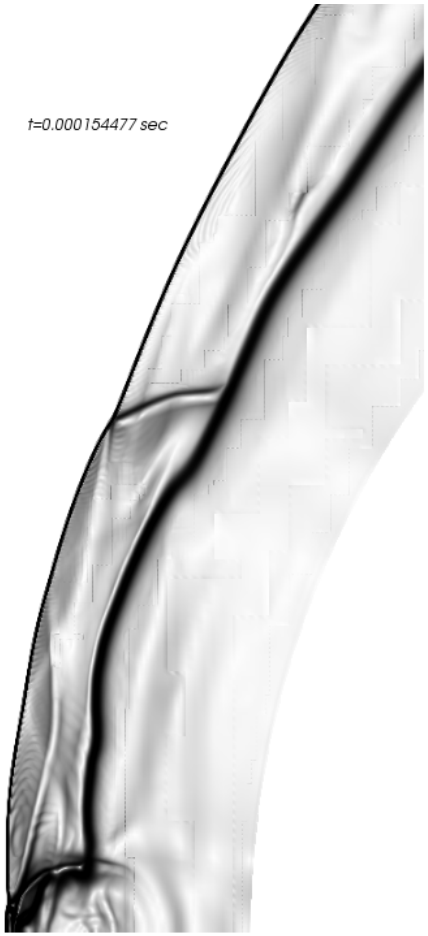

Temperature

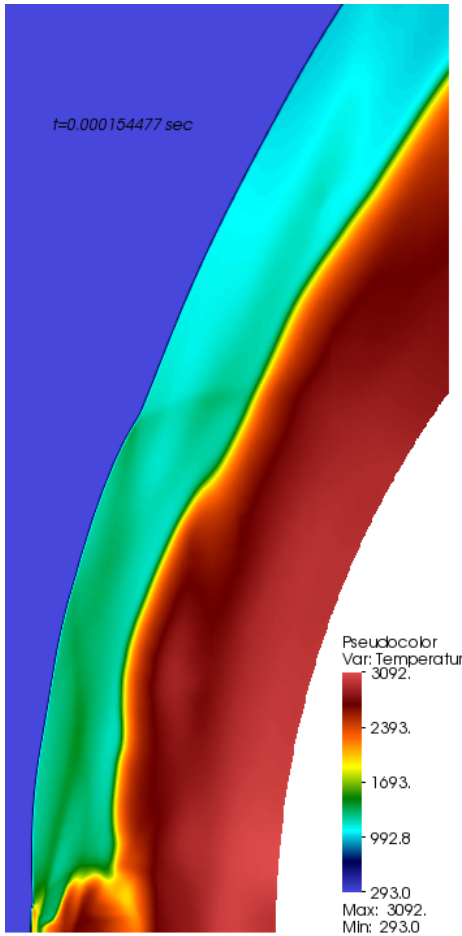

Mass fraction OH

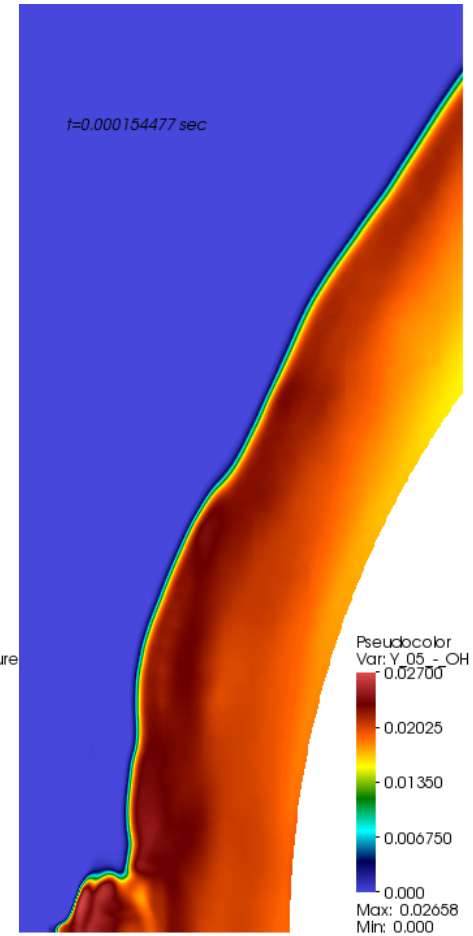

Pressure

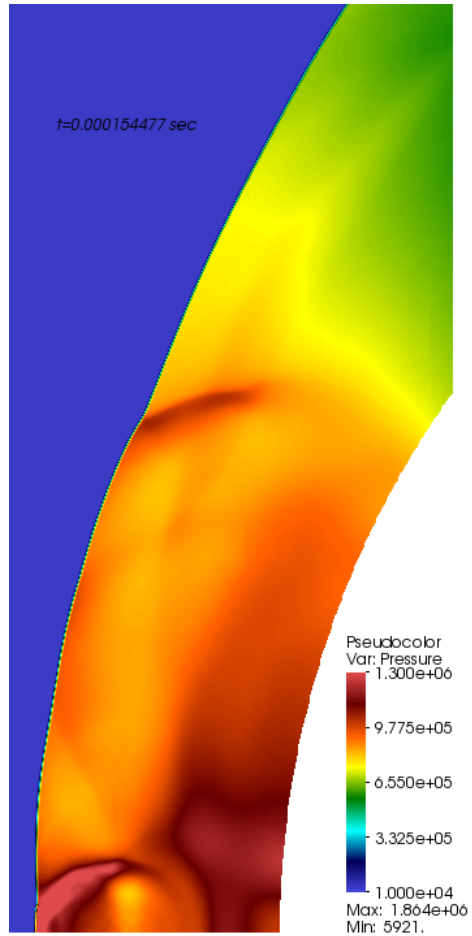

Perturbed oscillation mechanism

Schlieren of density

Temperature

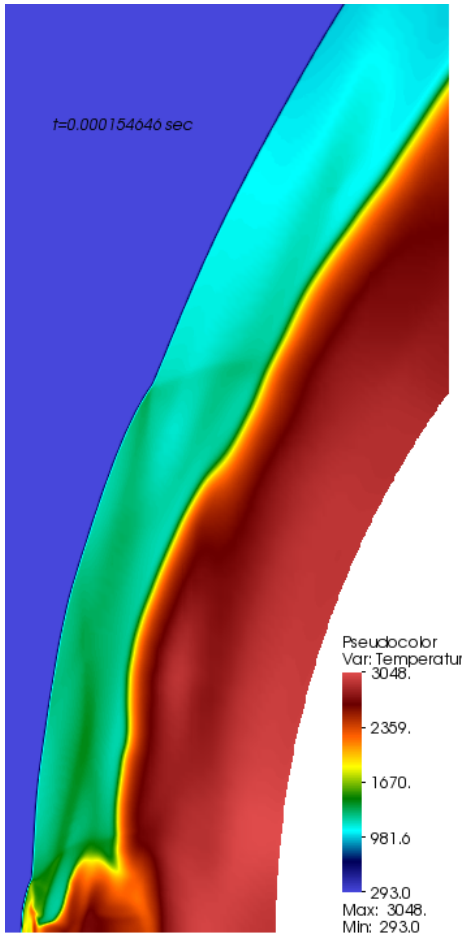

Mass fraction OH

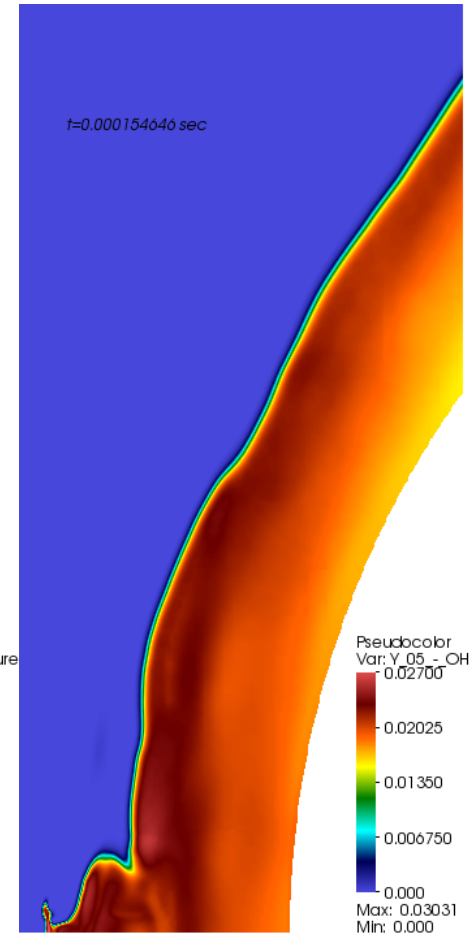

Pressure

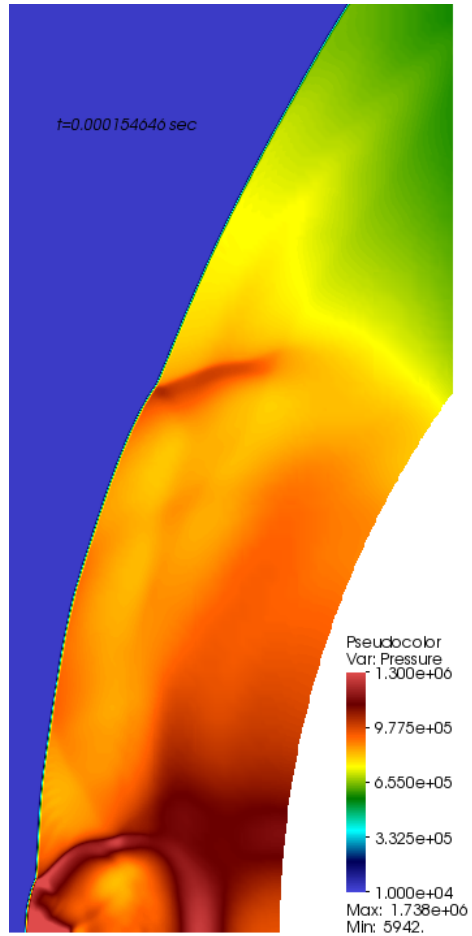

Perturbed oscillation mechanism

Schlieren of density

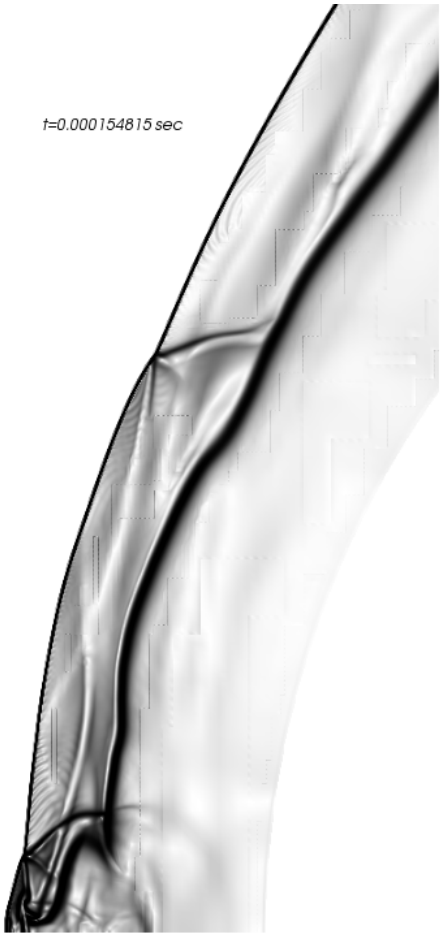

Temperature

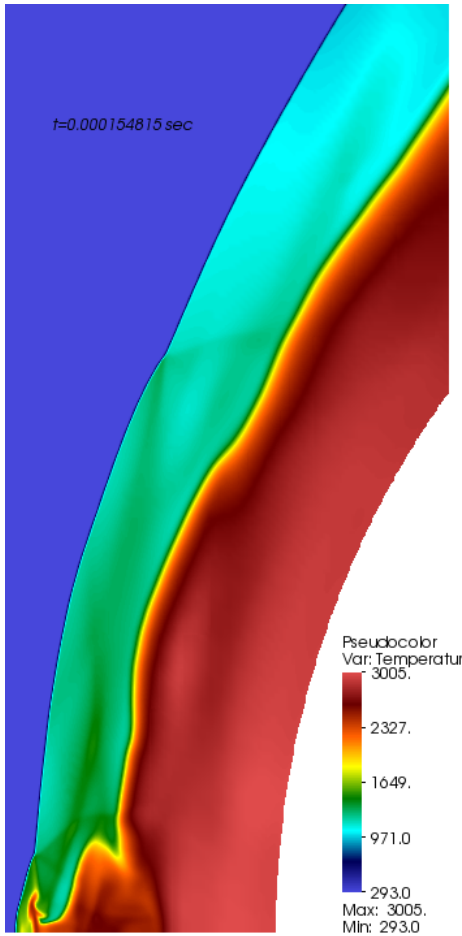

Mass fraction OH

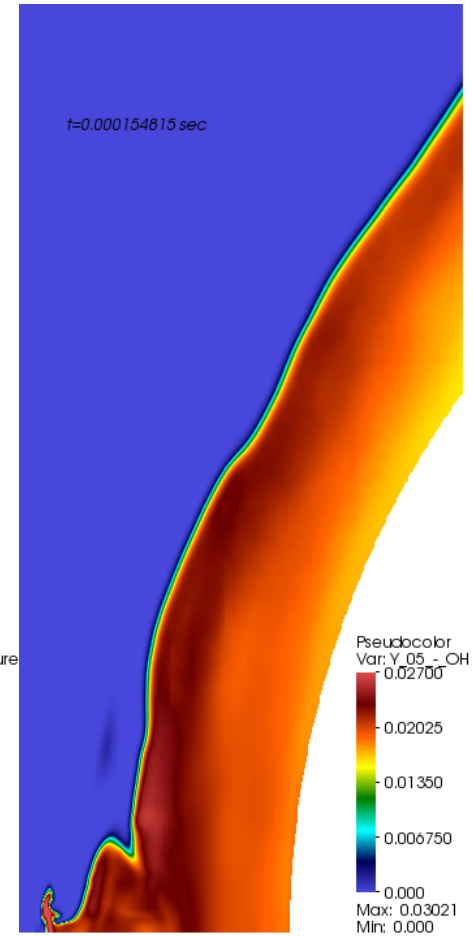

Pressure

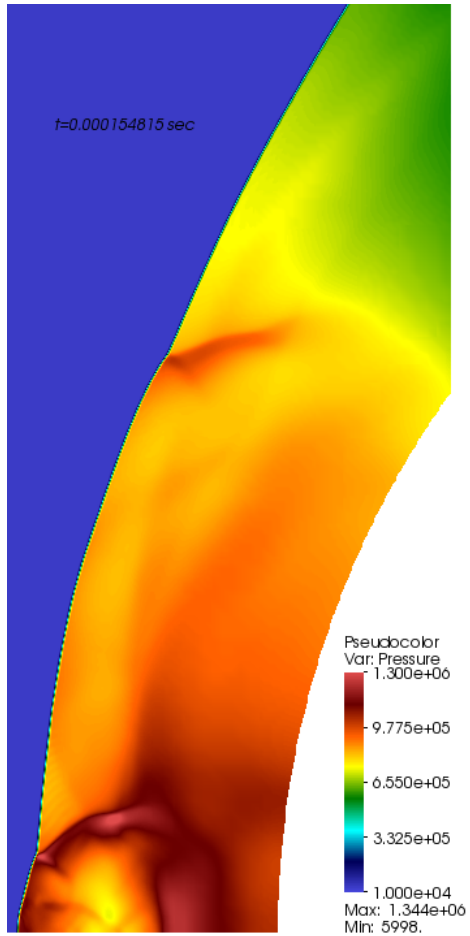

Perturbed oscillation mechanism

Schlieren of density

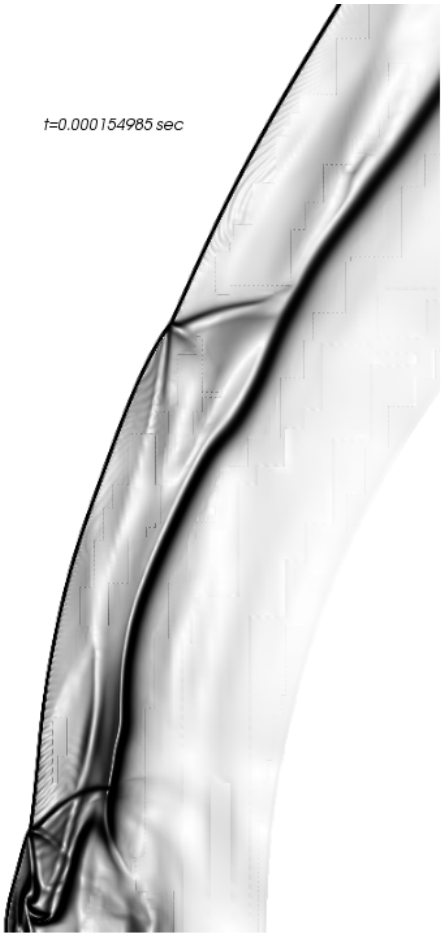

Temperature

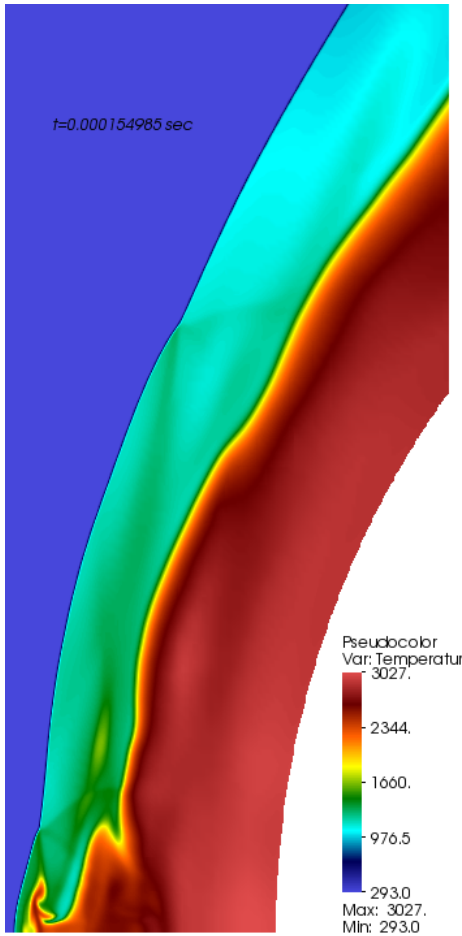

Mass fraction OH

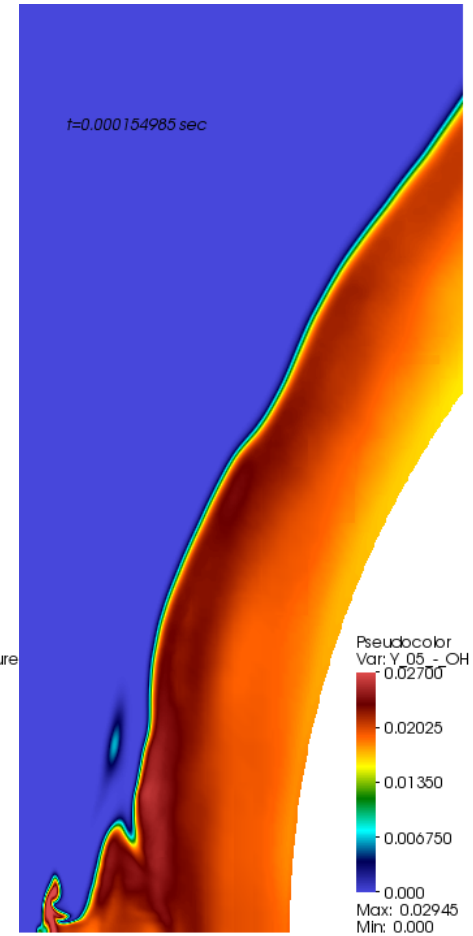

Pressure

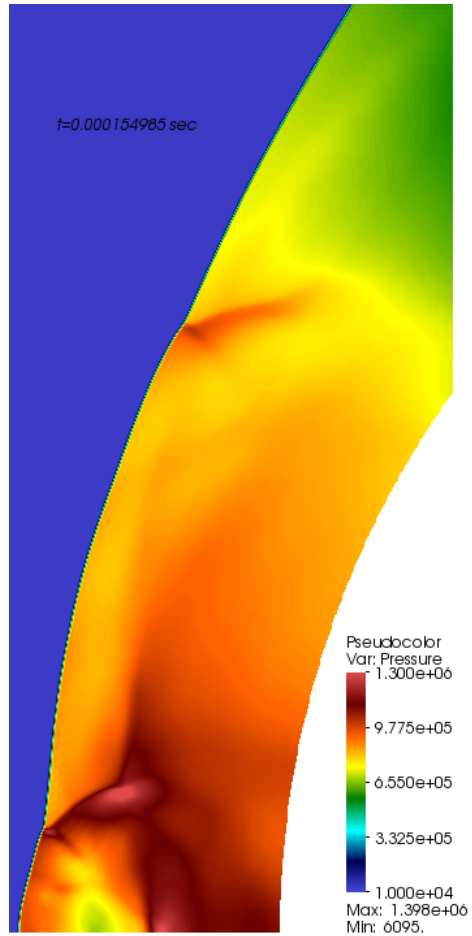

Perturbed oscillation mechanism

Schlieren of density

Temperature

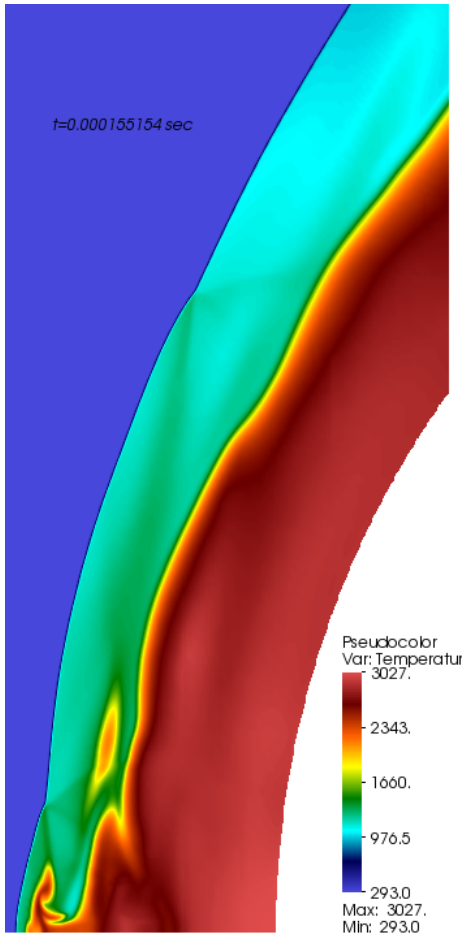

Mass fraction OH

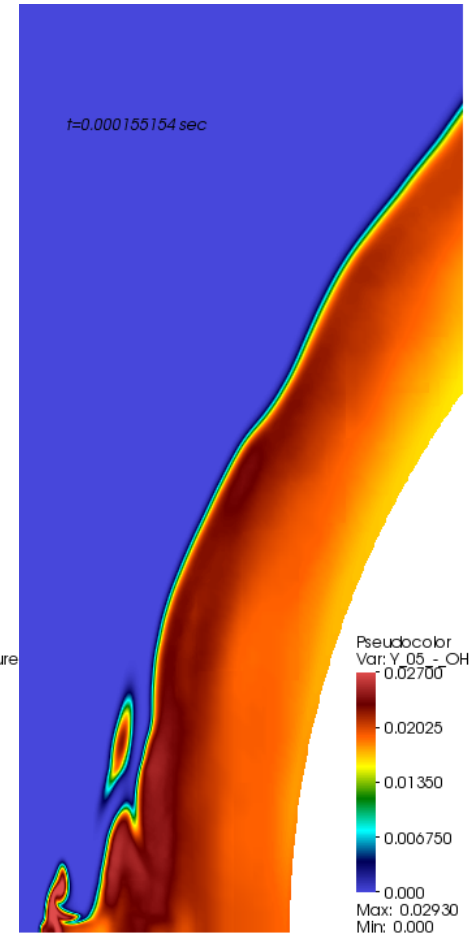

Pressure

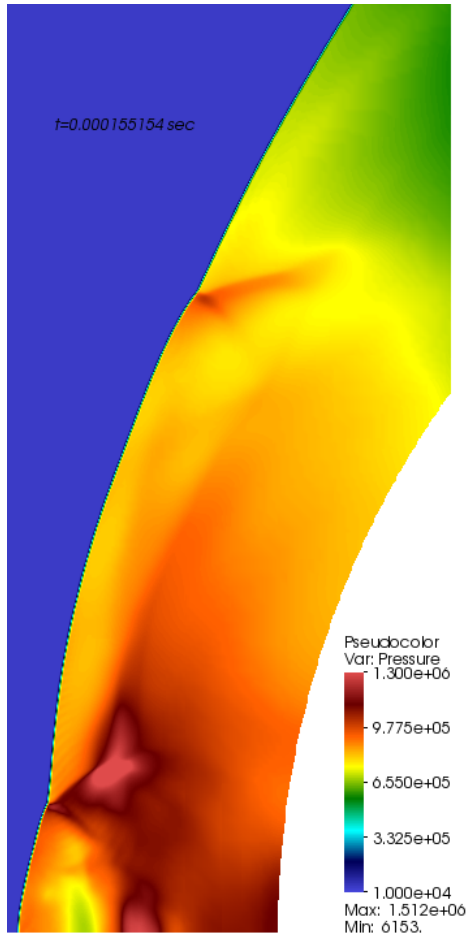

Perturbed oscillation mechanism

Schlieren of density

Temperature

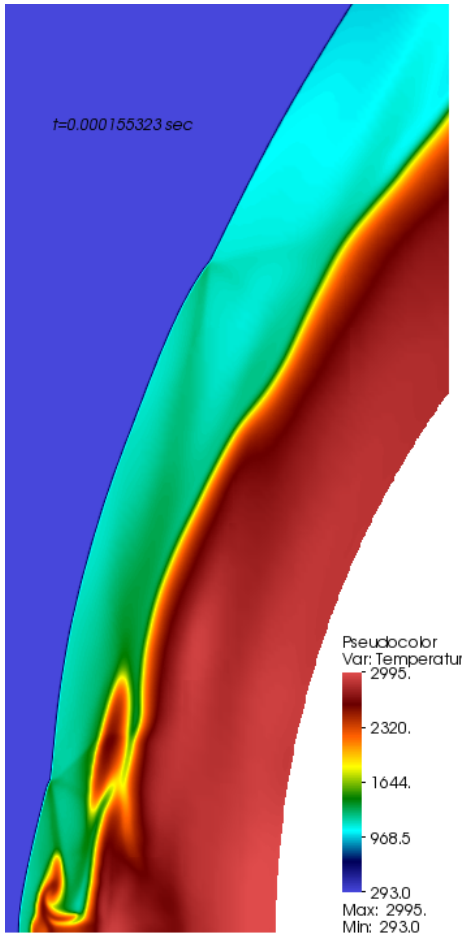

Mass fraction OH

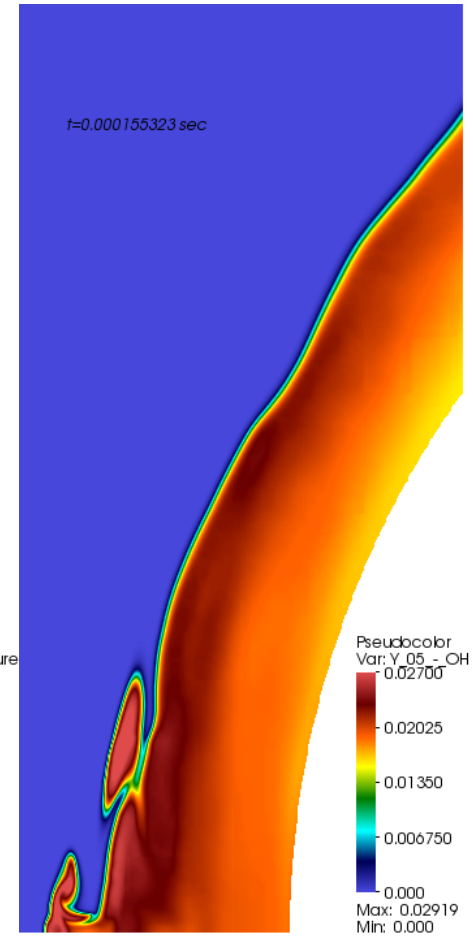

Pressure

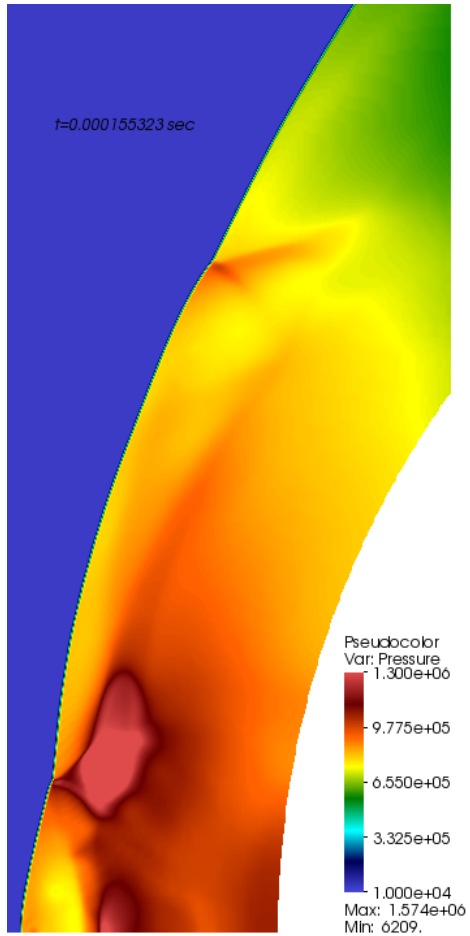

Perturbed oscillation mechanism

Schlieren of density

Temperature

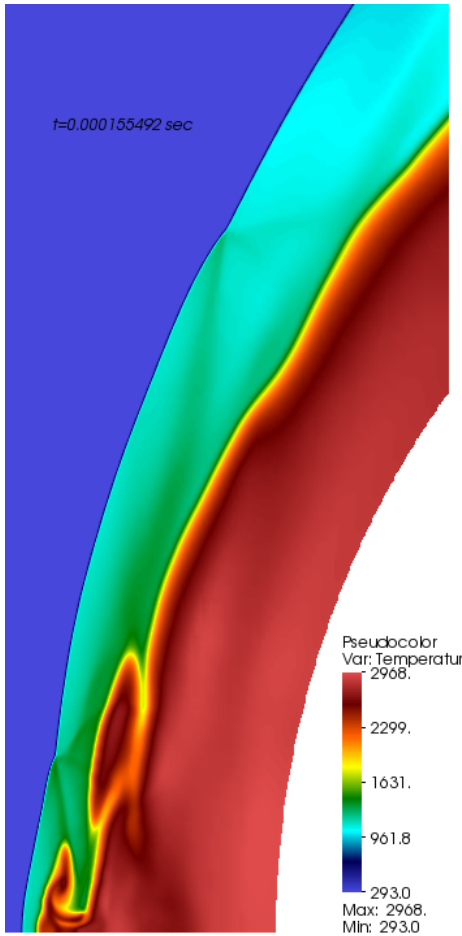

Mass fraction OH

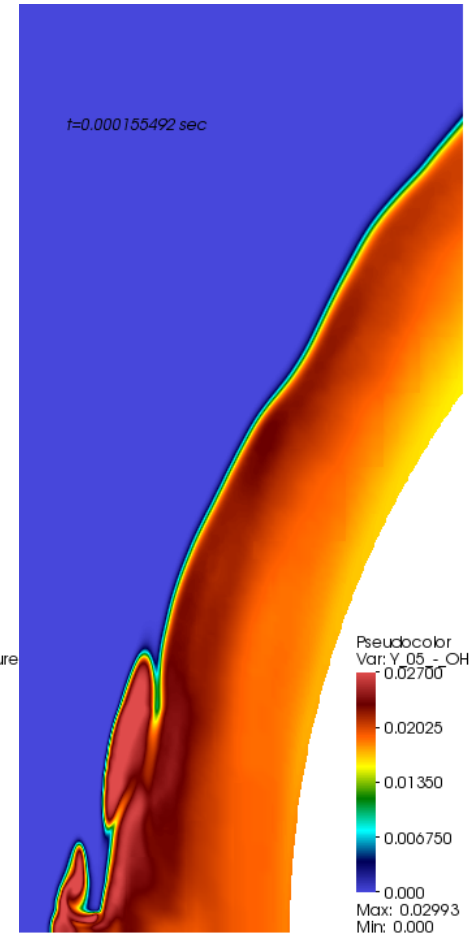

Pressure

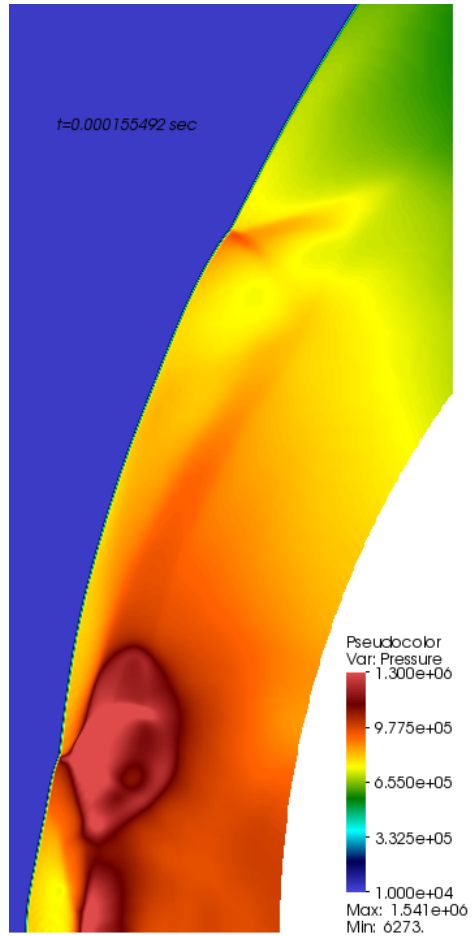

Perturbed oscillation mechanism

Schlieren of density

Temperature

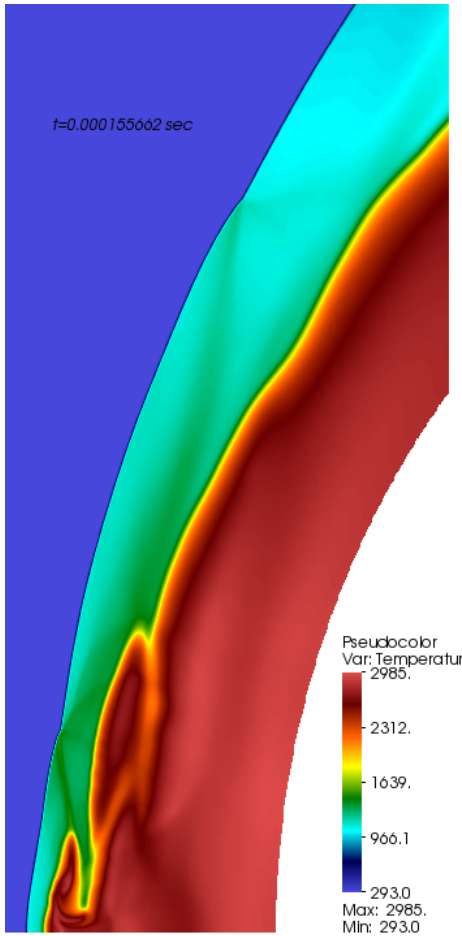

Mass fraction OH

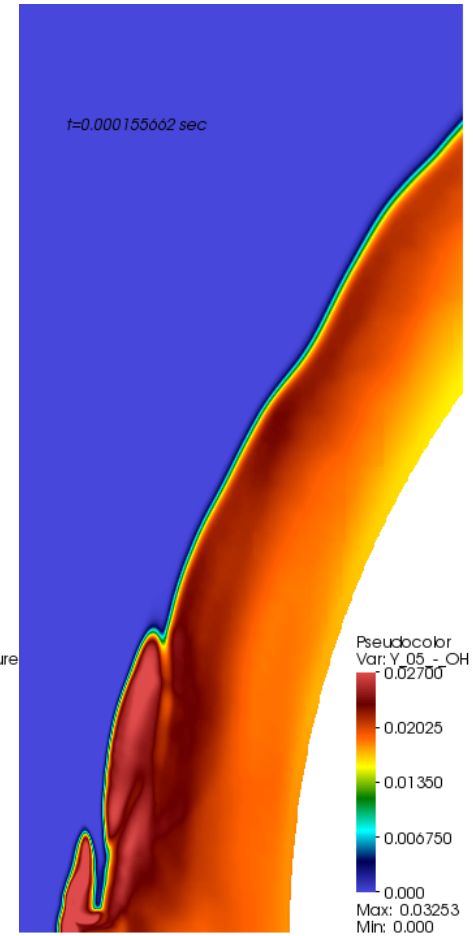

Pressure

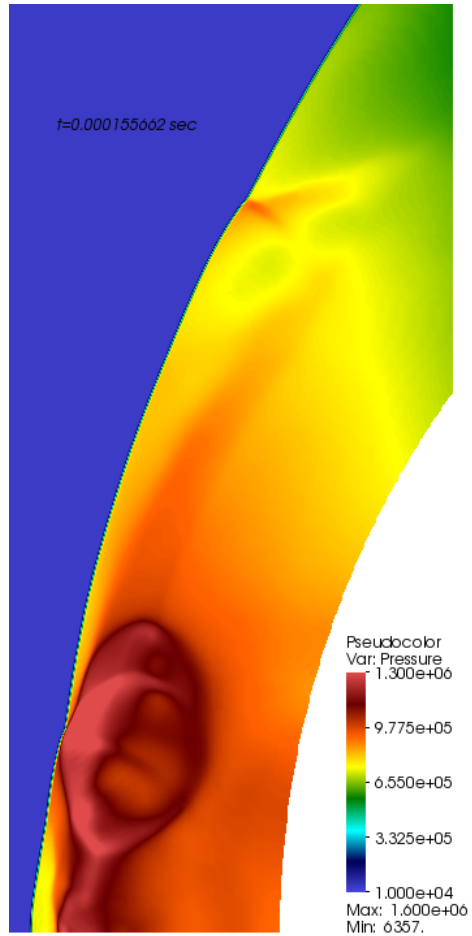

Perturbed oscillation mechanism

Schlieren of density

Temperature

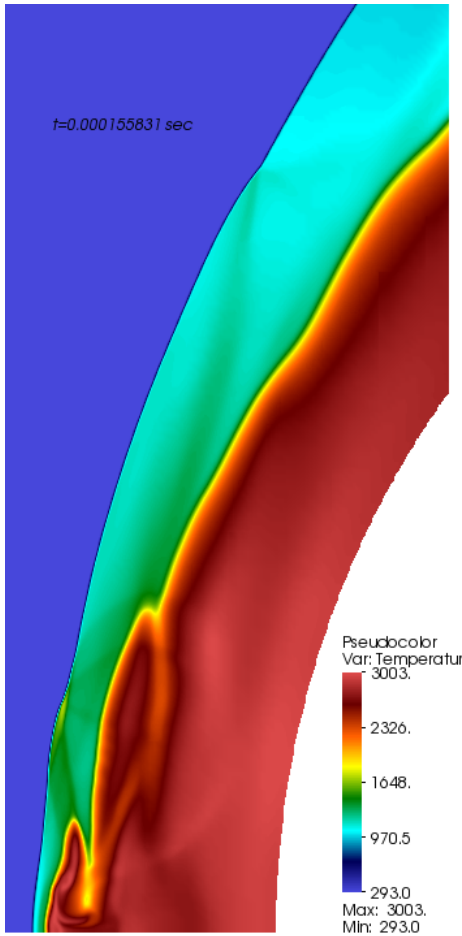

Mass fraction OH

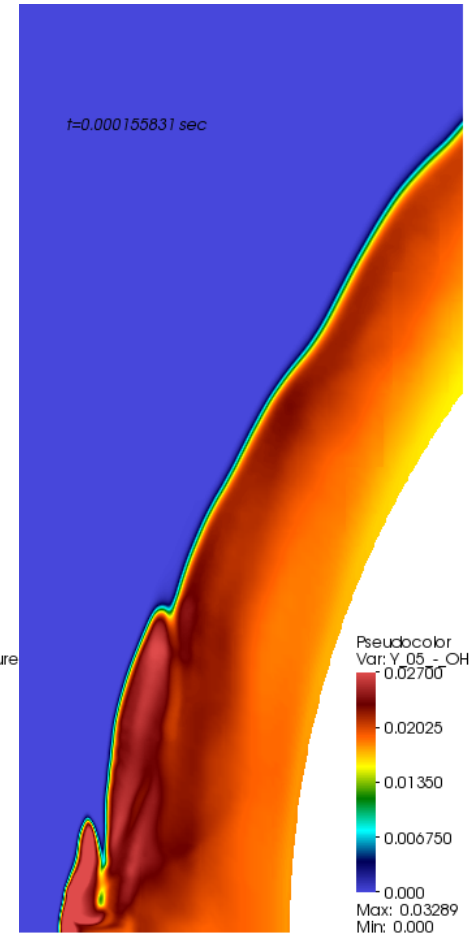

Pressure

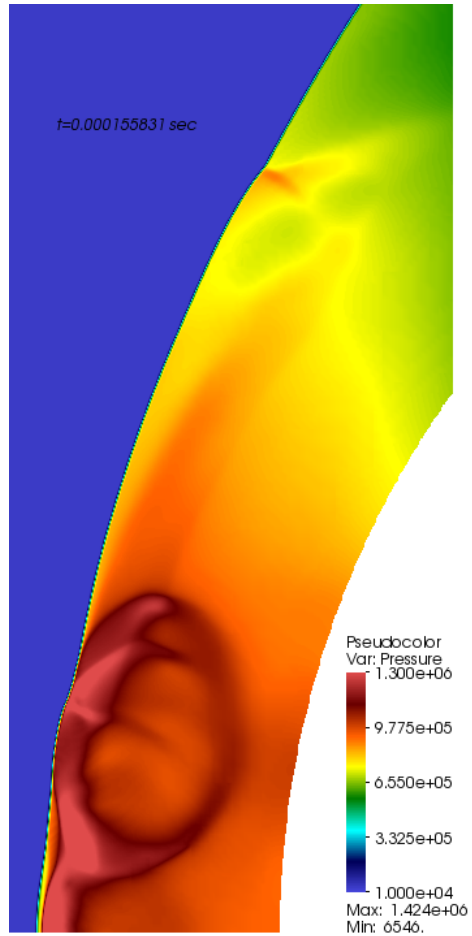

Perturbed oscillation mechanism

Schlieren of density

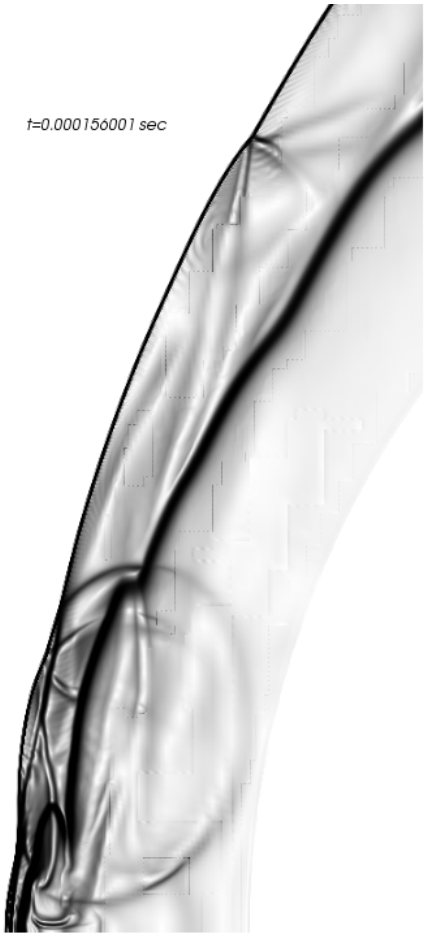

Temperature

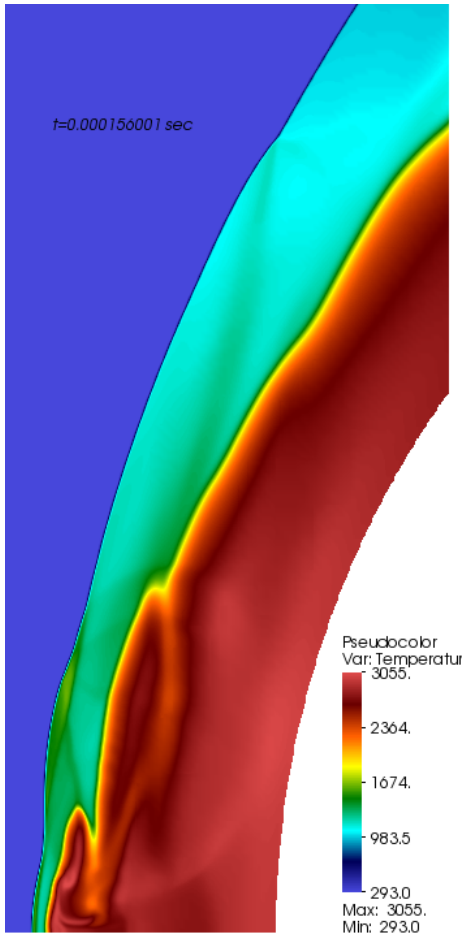

Mass fraction OH

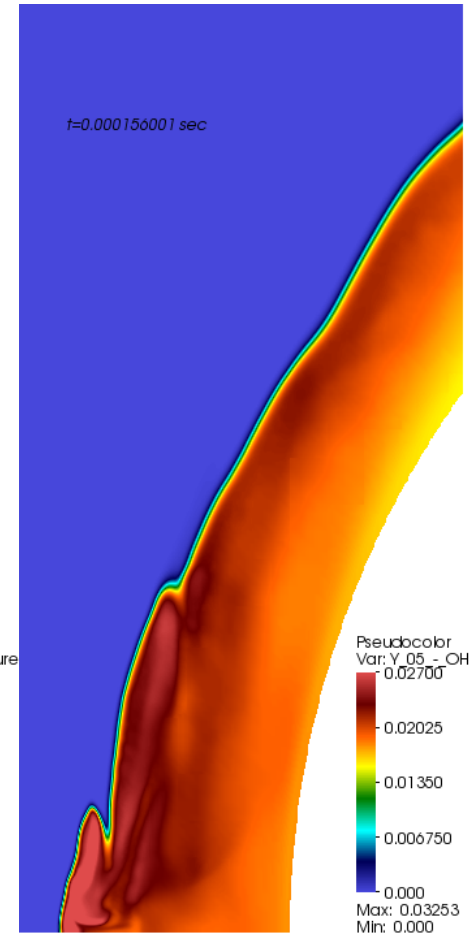

Pressure

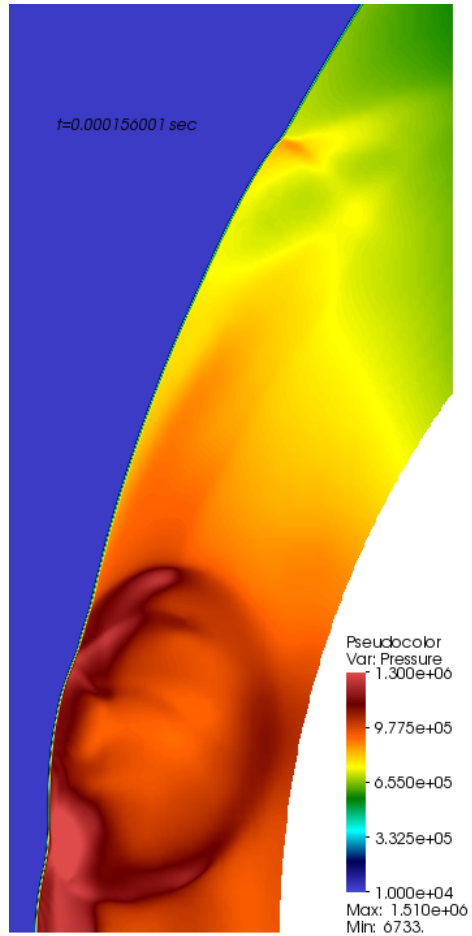

Perturbed oscillation mechanism

Schlieren of density

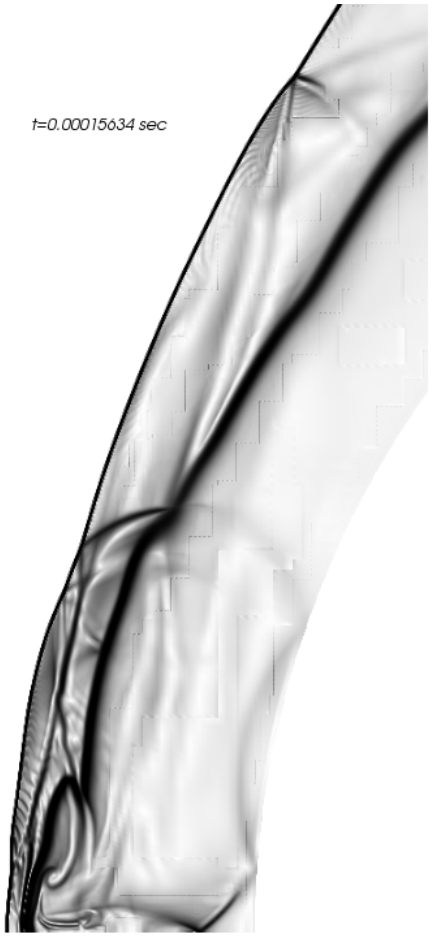

Temperature

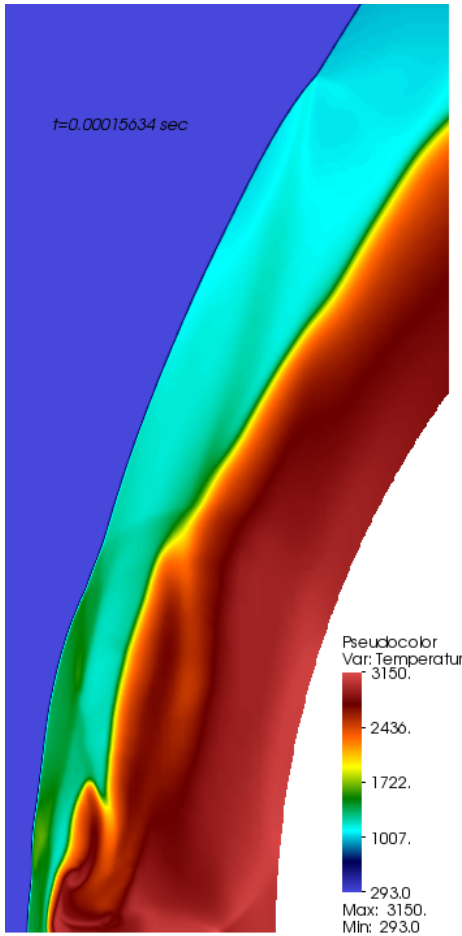

Mass fraction OH

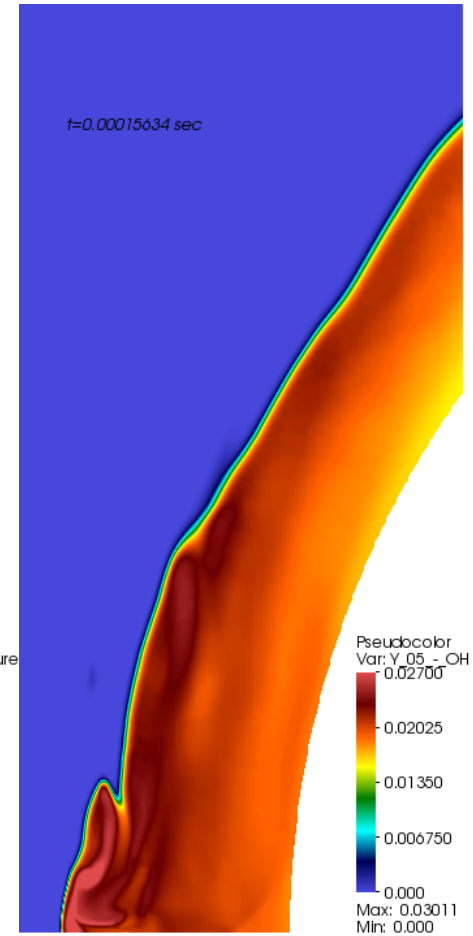

Pressure

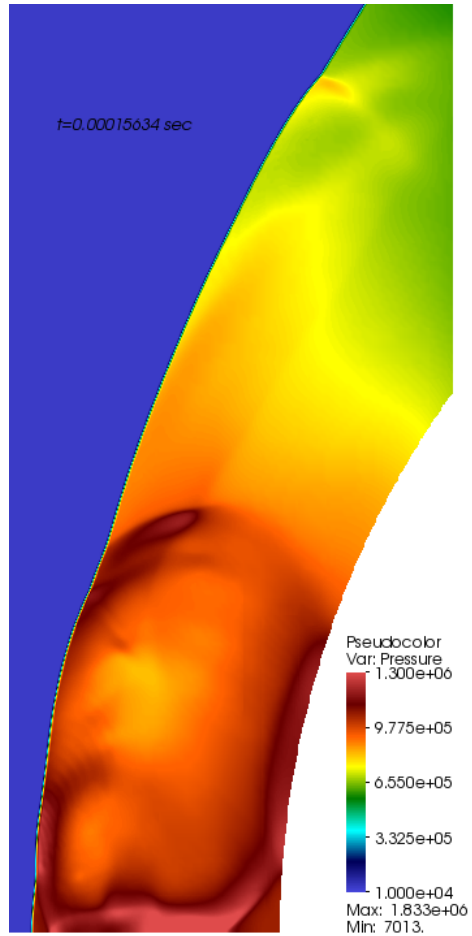

Perturbed oscillation mechanism

Schlieren of density

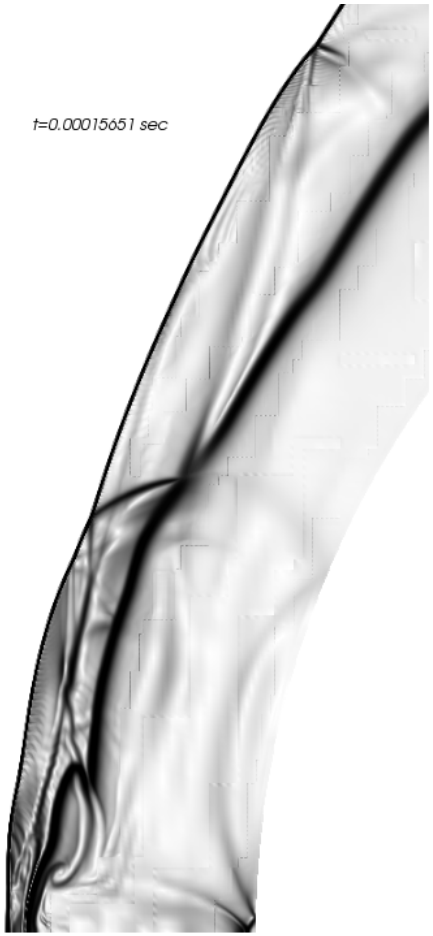

Temperature

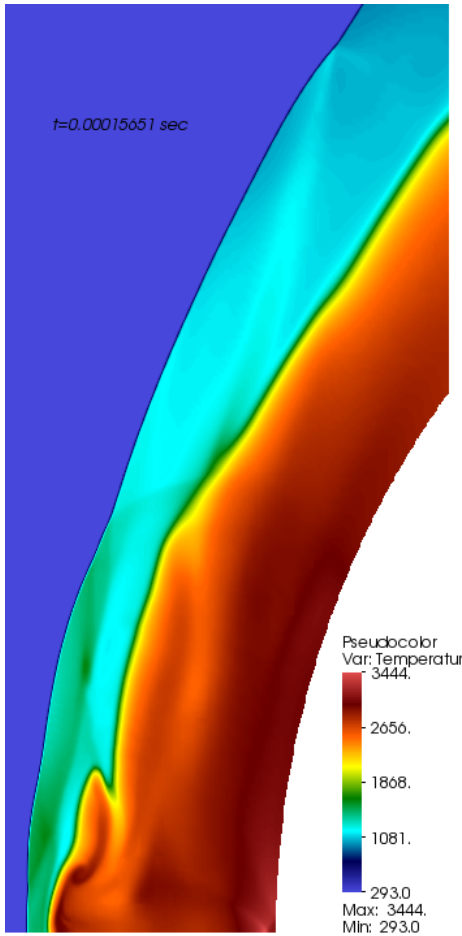

Mass fraction OH

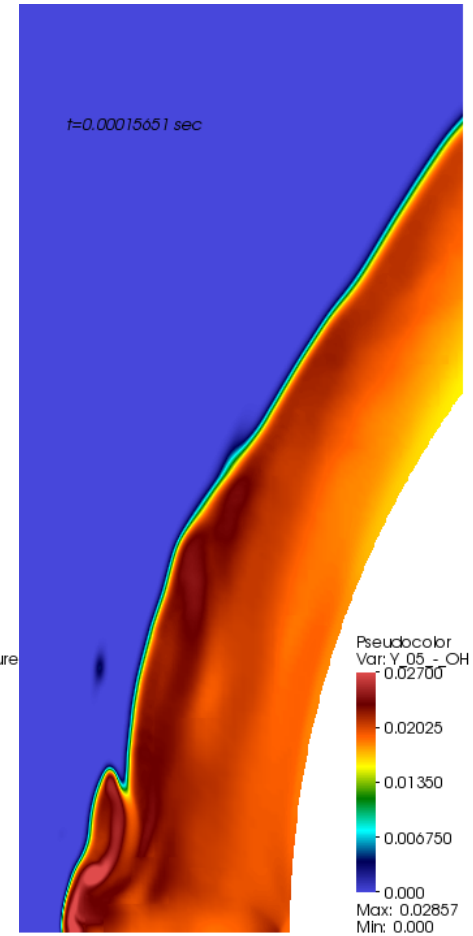

Pressure

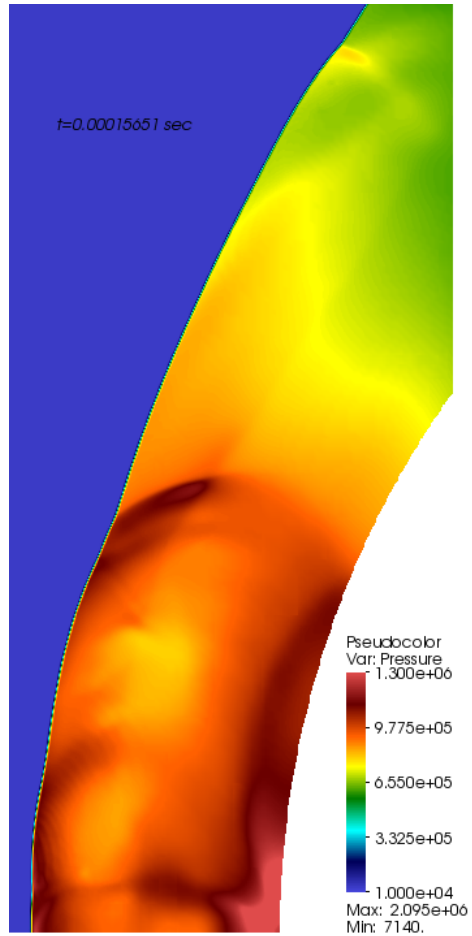

Perturbed oscillation mechanism

Schlieren of density

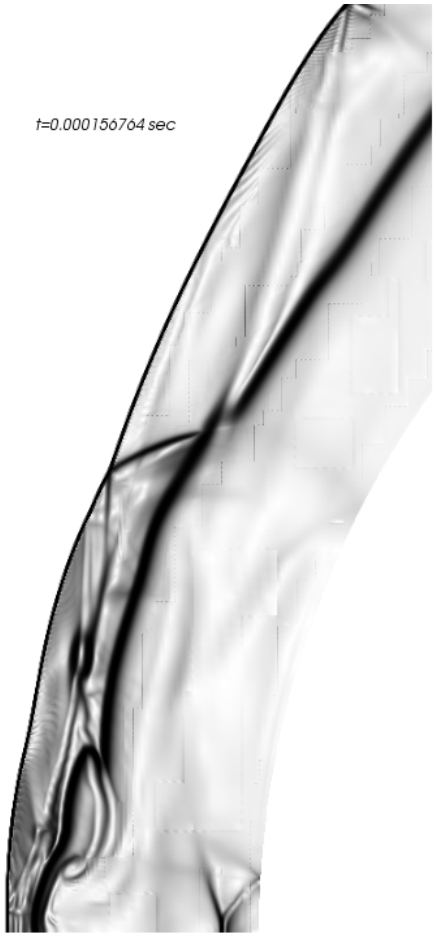

Temperature

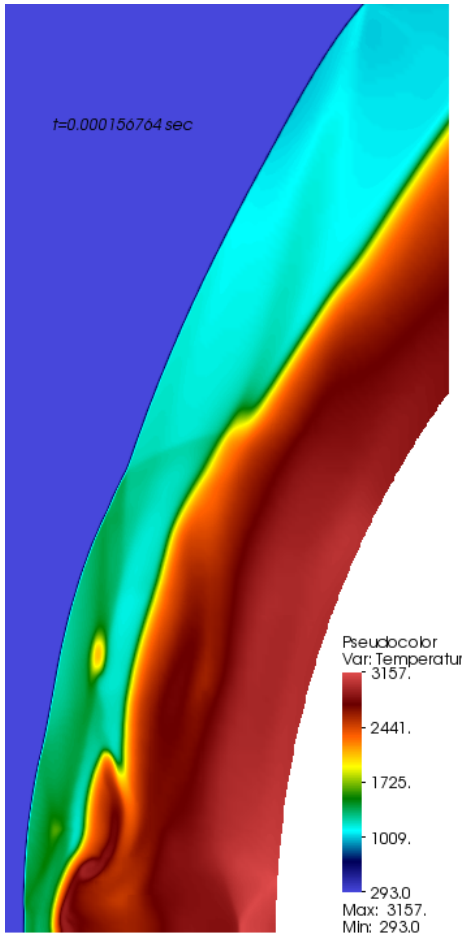

Mass fraction OH

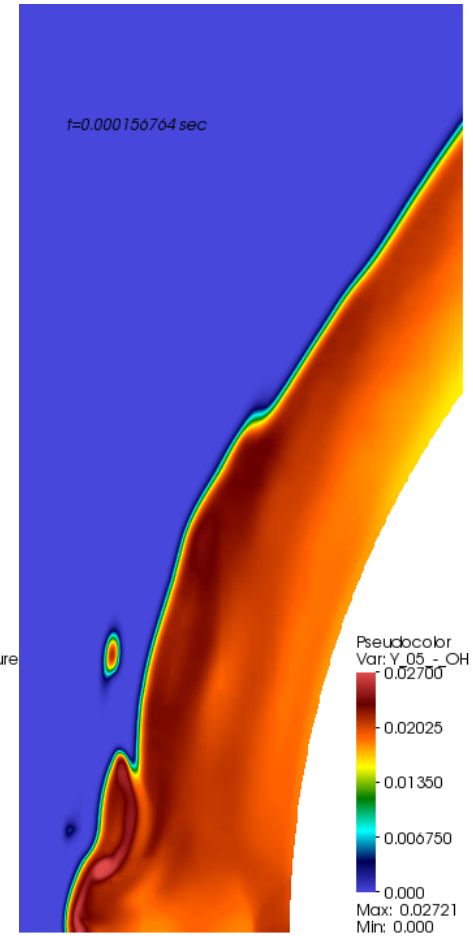

Pressure

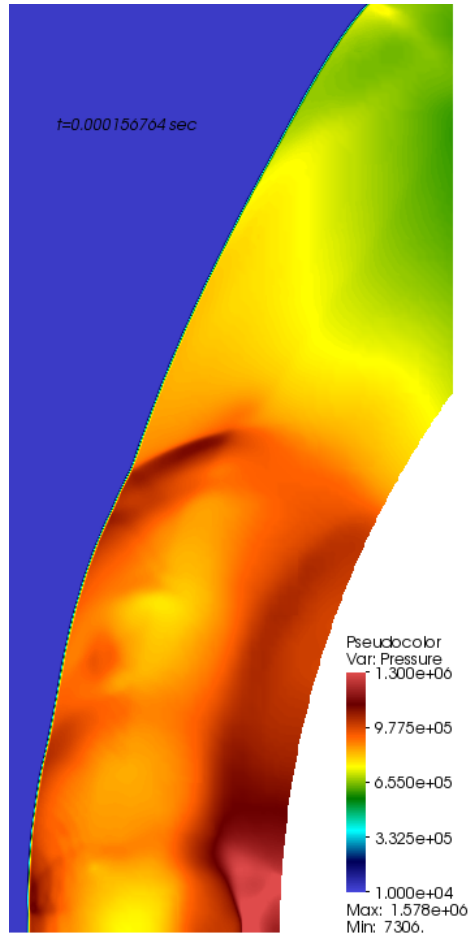

Perturbed oscillation mechanism

Schlieren of density

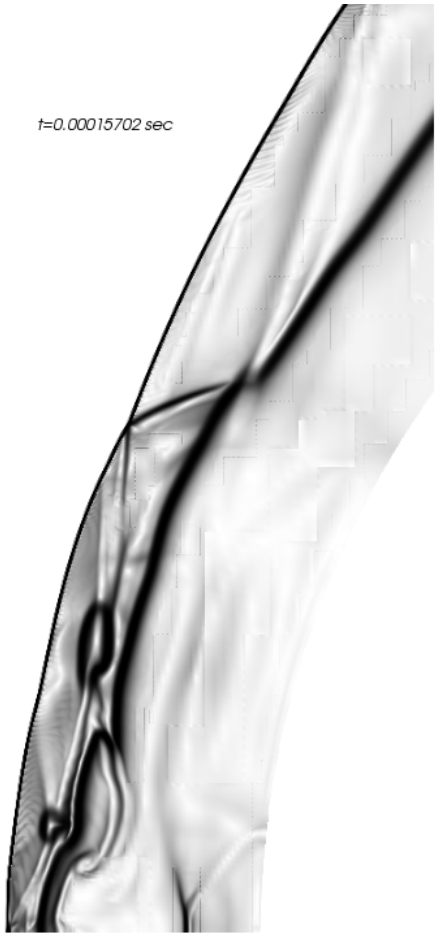

Temperature

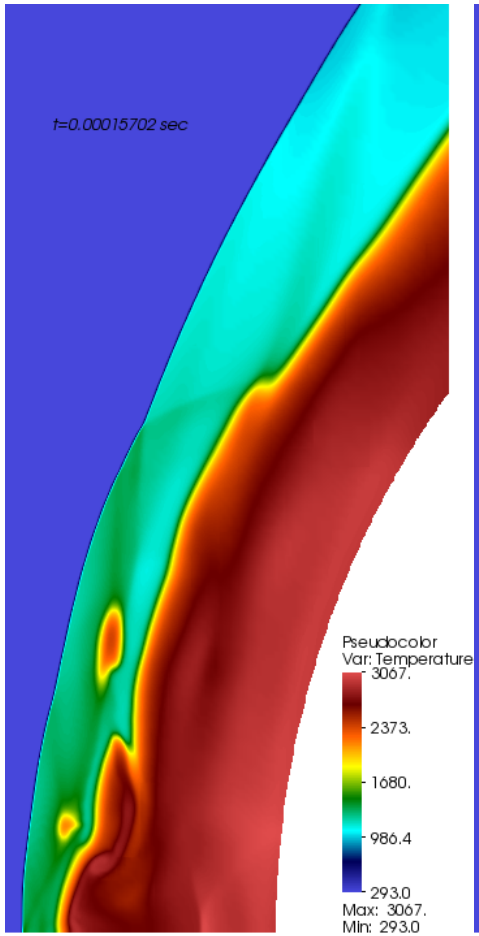

Mass fraction OH

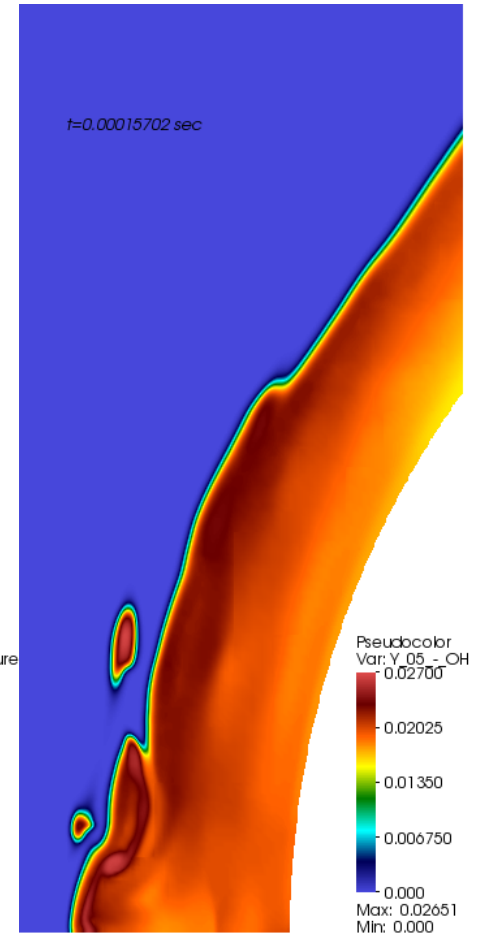

Pressure

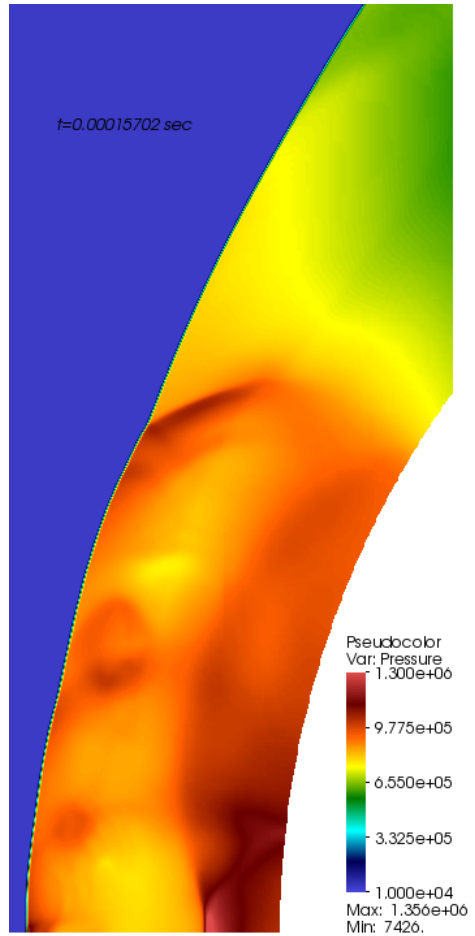

Perturbed oscillation mechanism

Schlieren of density

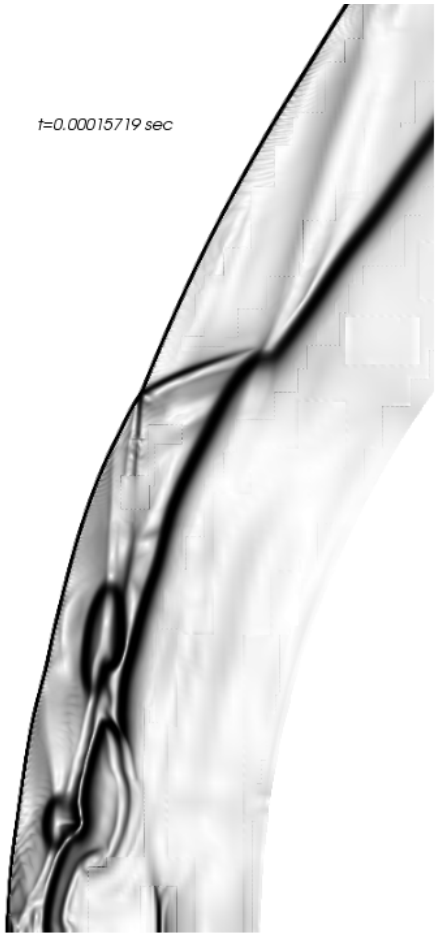

Temperature

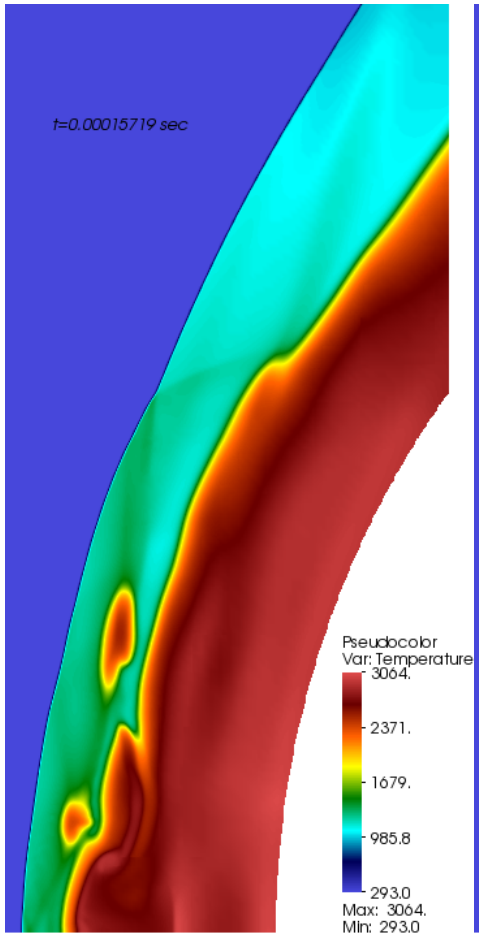

Mass fraction OH

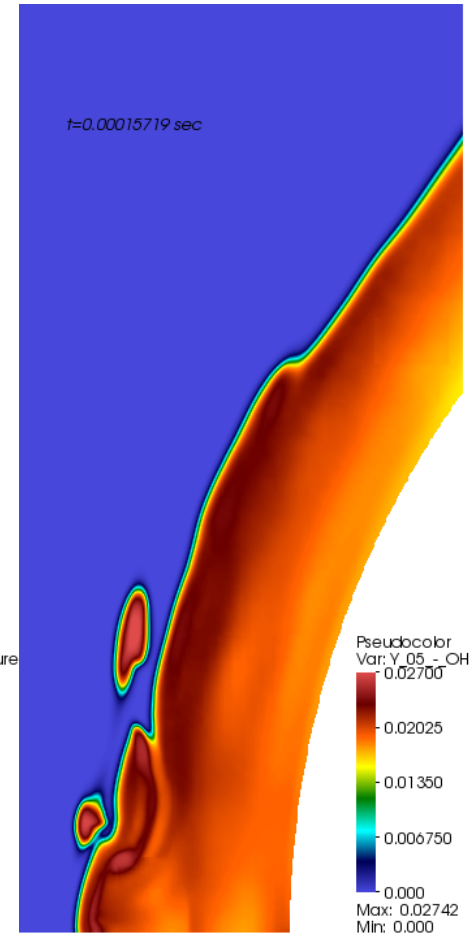

Pressure

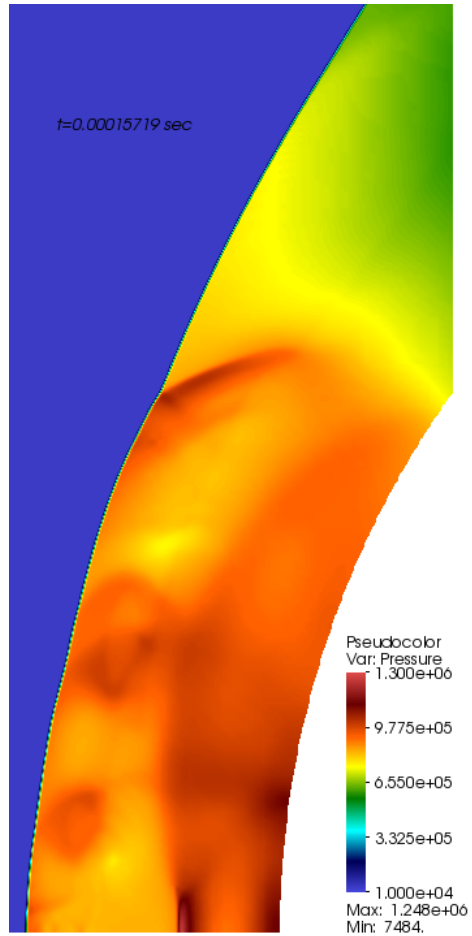

Perturbed oscillation mechanism

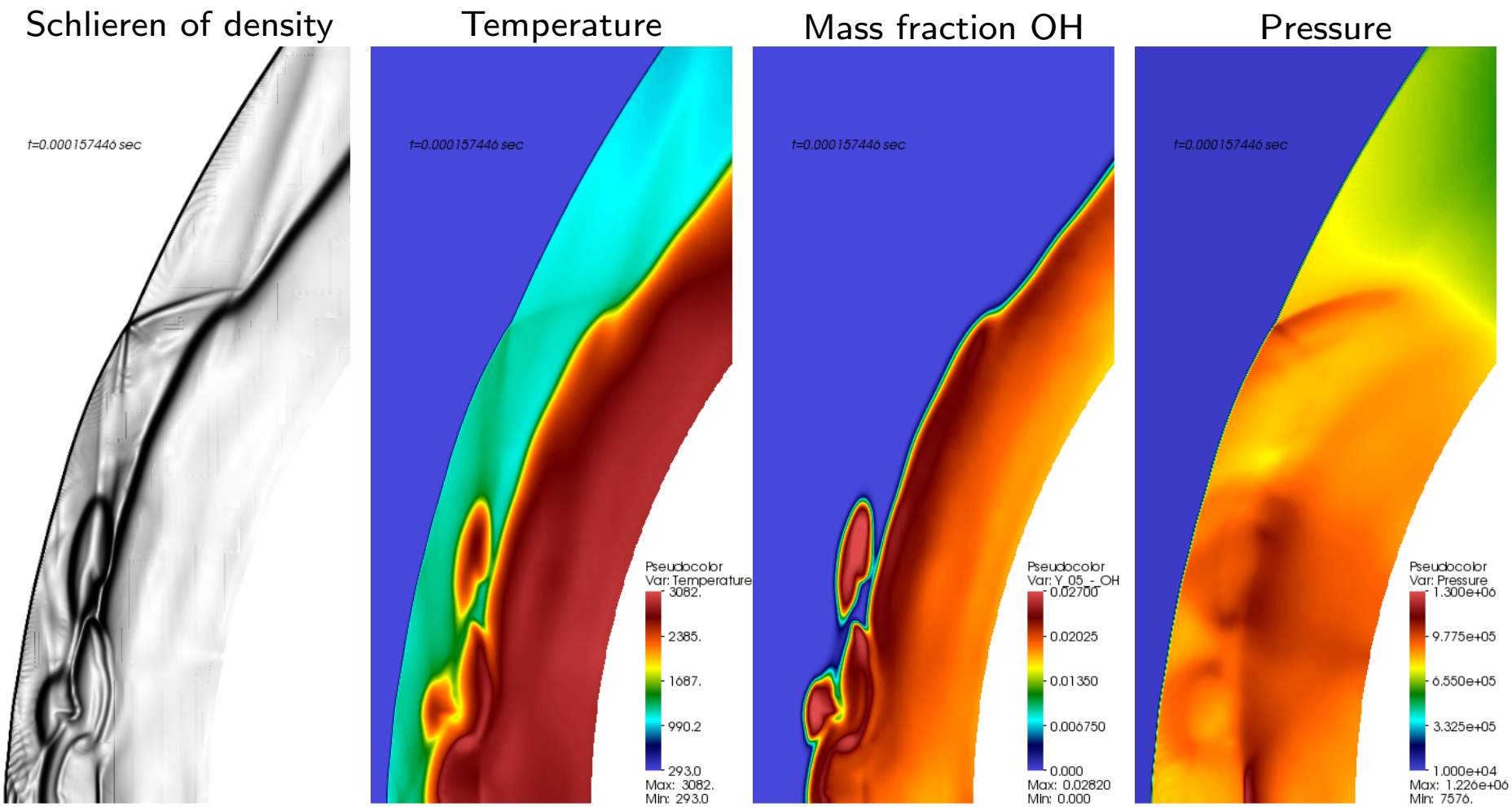

- Small perturbations can quickly create numerous triple points

Hybrid method

Convective numerical flux is defined as

$$\mathbf{F}^n_{inv} = \begin{cases} \mathbf{F}^n_{inv-WENO}, & \text{in } \mathcal{C} \\ \mathbf{F}^n_{inv-CD}, & \text{in } \overline{\mathcal{C}}, \end{cases}$$

Hybrid method

Convective numerical flux is defined as

$$\mathbf{F}^n_{inv} = \begin{cases} \mathbf{F}^n_{inv-WENO}, & \text{in } \mathcal{C} \\ \mathbf{F}^n_{inv-CD}, & \text{in } \overline{\mathcal{C}}, \end{cases}$$

- For LES: 3rd order WENO method, 2nd order TCD [Hill and Pullin, 2004]

Hybrid method

Convective numerical flux is defined as

$$\mathbf{F}^n_{inv} = \begin{cases} \mathbf{F}^n_{inv-WENO}, & \text{in } \mathcal{C} \\ \mathbf{F}^n_{inv-CD}, & \text{in } \overline{\mathcal{C}}, \end{cases}$$

- For LES: 3rd order WENO method, 2nd order TCD [Hill and Pullin, 2004]
- For DNS: Symmetric 6th order WENO, 6th-order CD scheme [Ziegler et al., 2011]

Hybrid method

Convective numerical flux is defined as

$$\mathbf{F}_{inv}^{n} = \begin{cases} \mathbf{F}_{inv-WENO}^{n}, & \text{in } \mathcal{C} \\ \mathbf{F}_{inv-CD}^{n}, & \text{in } \overline{\mathcal{C}}, \end{cases}$$

- For LES: 3rd order WENO method, 2nd order TCD [Hill and Pullin, 2004]
- For DNS: Symmetric 6th order WENO, 6th-order CD scheme [Ziegler et al., 2011]

Use WENO scheme to only capture shock waves but resolve interface between species.

Hybrid method

Convective numerical flux is defined as

$$\mathbf{F}^n_{inv} = \begin{cases} \mathbf{F}^n_{inv-WENO}, & \text{in } \mathcal{C} \\ \mathbf{F}^n_{inv-CD}, & \text{in } \overline{\mathcal{C}}, \end{cases}$$

- For LES: 3rd order WENO method, 2nd order TCD [Hill and Pullin, 2004]
- For DNS: Symmetric 6th order WENO, 6th-order CD scheme [Ziegler et al., 2011]

Use WENO scheme to only capture shock waves but resolve interface between species.

Shock detection based on using two criteria together:

1. Lax-Liu entropy condition $|u_R \pm a_R| < |u_* \pm a_*| < |u_L \pm a_L|$ tested with a threshold to eliminate weak acoustic waves. Used intermediate states at cell interfaces:

$$u_* = \frac{\sqrt{\rho_L}u_L + \sqrt{\rho_R}u_R}{\sqrt{\rho_L} + \sqrt{\rho_R}}, \quad a_* = \sqrt{(\gamma_* - 1)(h_* - \frac{1}{2}u_*^2)}, \ldots$$

Hybrid method

Convective numerical flux is defined as

$$\mathbf{F}^n_{inv} = \begin{cases} \mathbf{F}^n_{inv-WENO}, & \text{in } \mathcal{C} \\ \mathbf{F}^n_{inv-CD}, & \text{in } \overline{\mathcal{C}}, \end{cases}$$

- For LES: 3rd order WENO method, 2nd order TCD [Hill and Pullin, 2004]
- For DNS: Symmetric 6th order WENO, 6th-order CD scheme [Ziegler et al., 2011]

Use WENO scheme to only capture shock waves but resolve interface between species.

Shock detection based on using two criteria together:

1. Lax-Liu entropy condition $|u_R \pm a_R| < |u_* \pm a_*| < |u_L \pm a_L|$ tested with a threshold to eliminate weak acoustic waves. Used intermediate states at cell interfaces:

$$u_* = \frac{\sqrt{\rho_L}u_L + \sqrt{\rho_R}u_R}{\sqrt{\rho_L} + \sqrt{\rho_R}}, \quad a_* = \sqrt{(\gamma_* - 1)(h_* - \frac{1}{2}u_*^2)}, \ldots$$

2. Limiter-inspired discontinuity test based on mapped normalized pressure gradient θ_j

$$\phi(\theta_j) = \frac{2\theta_j}{(1+\theta_j)^2} \quad \text{with} \quad \theta_j = \frac{|p_{j+1} - p_j|}{|p_{j+1} + p_j|}, \quad \phi(\theta_j) > \alpha_{Map}$$

SAMR flux correction for Runge-Kutta method

Recall Runge-Kutta temporal update

$$\tilde{\mathbf{Q}}_j^{\upsilon} = \alpha_{\upsilon}\,\mathbf{Q}_j^{m} + \beta_{\upsilon}\,\tilde{\mathbf{Q}}_j^{\upsilon-1} + \gamma_{\upsilon}\,\frac{\Delta t}{\Delta x_n}\,\Delta\mathbf{F}^{n}(\tilde{\mathbf{Q}}^{\upsilon-1})$$

[Pantano et al., 2007]

SAMR flux correction for Runge-Kutta method

Recall Runge-Kutta temporal update

$$\tilde{\mathbf{Q}}_j^{\upsilon} = \alpha_{\upsilon}\,\mathbf{Q}_j^m + \beta_{\upsilon}\,\tilde{\mathbf{Q}}_j^{\upsilon-1} + \gamma_{\upsilon}\,\frac{\Delta t}{\Delta x_n}\Delta\mathbf{F}^n(\tilde{\mathbf{Q}}^{\upsilon-1})$$

rewrite scheme as

$$\mathbf{Q}^{m+1} = \mathbf{Q}^m - \sum_{\upsilon=1}^{\Upsilon}\varphi_{\upsilon}\,\frac{\Delta t}{\Delta x_n}\Delta\mathbf{F}^n(\tilde{\mathbf{Q}}^{\upsilon-1}) \quad \text{with} \quad \varphi_{\upsilon} = \gamma_{\upsilon}\prod_{\nu=\upsilon+1}^{\Upsilon}\beta_{\nu}$$

[Pantano et al., 2007]

SAMR flux correction for Runge-Kutta method

Recall Runge-Kutta temporal update

$$\tilde{\mathbf{Q}}_j^{\upsilon} = \alpha_{\upsilon}\mathbf{Q}_j^m + \beta_{\upsilon}\tilde{\mathbf{Q}}_j^{\upsilon-1} + \gamma_{\upsilon}\frac{\Delta t}{\Delta x_n}\Delta\mathbf{F}^n(\tilde{\mathbf{Q}}^{\upsilon-1})$$

rewrite scheme as

$$\mathbf{Q}^{m+1} = \mathbf{Q}^m - \sum_{\upsilon=1}^{\Upsilon}\varphi_{\upsilon}\frac{\Delta t}{\Delta x_n}\Delta\mathbf{F}^n(\tilde{\mathbf{Q}}^{\upsilon-1}) \quad \text{with} \quad \varphi_{\upsilon} = \gamma_{\upsilon}\prod_{\nu=\upsilon+1}^{\Upsilon}\beta_{\nu}$$

Flux correction to be used

1. $\delta\mathbf{F}^{1,l+1}_{i-\frac{1}{2},j} := -\varphi_1\mathbf{F}^{1,l}_{i-\frac{1}{2},j}(\tilde{\mathbf{Q}}^0)\,, \qquad \delta\mathbf{F}^{1,l+1}_{i-\frac{1}{2},j} := \delta\mathbf{F}^{1,l+1}_{i-\frac{1}{2},j} - \sum_{\upsilon=2}^{\Upsilon}\varphi_{\upsilon}\mathbf{F}^{1,l}_{i-\frac{1}{2},j}(\tilde{\mathbf{Q}}^{\upsilon-1})$
2. $\delta\mathbf{F}^{1,l+1}_{i-\frac{1}{2},j} := \delta\mathbf{F}^{1,l+1}_{i-\frac{1}{2},j} + \frac{1}{r_{l+1}^2}\sum_{\iota=0}^{r_{l+1}-1}\sum_{\upsilon=1}^{\Upsilon}\varphi_{\upsilon}\mathbf{F}^{1,l+1}_{v+\frac{1}{2},w+\iota}\left(\tilde{\mathbf{Q}}^{\upsilon-1}(t+\kappa\Delta t_{l+1})\right)$

[Pantano et al., 2007]

SAMR flux correction for Runge-Kutta method

Recall Runge-Kutta temporal update

$$\tilde{\mathbf{Q}}_j^{\upsilon} = \alpha_{\upsilon}\mathbf{Q}_j^m + \beta_{\upsilon}\tilde{\mathbf{Q}}_j^{\upsilon-1} + \gamma_{\upsilon}\frac{\Delta t}{\Delta x_n}\Delta\mathbf{F}^n(\tilde{\mathbf{Q}}^{\upsilon-1})$$

rewrite scheme as

$$\mathbf{Q}^{m+1} = \mathbf{Q}^m - \sum_{\upsilon=1}^{\Upsilon}\varphi_{\upsilon}\frac{\Delta t}{\Delta x_n}\Delta\mathbf{F}^n(\tilde{\mathbf{Q}}^{\upsilon-1}) \quad \text{with} \quad \varphi_{\upsilon} = \gamma_{\upsilon}\prod_{\nu=\upsilon+1}^{\Upsilon}\beta_{\nu}$$

Flux correction to be used

1. $\delta\mathbf{F}^{1,l+1}_{i-\frac{1}{2},j} := -\varphi_1\mathbf{F}^{1,l}_{i-\frac{1}{2},j}(\tilde{\mathbf{Q}}^0)\,, \qquad \delta\mathbf{F}^{1,l+1}_{i-\frac{1}{2},j} := \delta\mathbf{F}^{1,l+1}_{i-\frac{1}{2},j} - \sum_{\upsilon=2}^{\Upsilon}\varphi_{\upsilon}\mathbf{F}^{1,l}_{i-\frac{1}{2},j}(\tilde{\mathbf{Q}}^{\upsilon-1})$

2. $\delta\mathbf{F}^{1,l+1}_{i-\frac{1}{2},j} := \delta\mathbf{F}^{1,l+1}_{i-\frac{1}{2},j} + \frac{1}{r_{l+1}^2}\sum_{\iota=0}^{r_{l+1}-1}\sum_{\upsilon=1}^{\Upsilon}\varphi_{\upsilon}\mathbf{F}^{1,l+1}_{v+\frac{1}{2},w+\iota}\left(\tilde{\mathbf{Q}}^{\upsilon-1}(t+\kappa\Delta t_{l+1})\right)$

Storage-efficient SSPRK(3,3):

υ	α_{υ}	β_{υ}	γ_{υ}	φ_{υ}
1	1	0	1	$\frac{1}{6}$
2	$\frac{3}{4}$	$\frac{1}{4}$	$\frac{1}{4}$	$\frac{1}{6}$
3	$\frac{1}{2}$	$\frac{2}{3}$	$\frac{2}{3}$	$\frac{2}{3}$

[Pantano et al., 2007]

DNS of shear layer in detonation triple point

- Calorically perfect two-species model with $\gamma = 1.29499$ and $h_0 = 54,000\,\mathrm{J/mol}$ and one-step Arrhenius reaction with parameters $E_a = 30,000\,\mathrm{J/mol}$, $A = 6 \cdot 10^5\,\mathrm{s}^{-1}$, $W = 0.029\,\mathrm{kg/mol}$ $\longrightarrow$ 1d ZND theory predicts $d_{\mathrm{CJ}} = 1587.8\,\mathrm{m/s}$
- For dynamic viscosity, heat conductivity, and mass diffusion simple Sutherland models are used
- Distance $L(t) = d_{\mathrm{CJ}} \sin(\theta) t$ is used to define a Reynolds number as $\mathrm{Re} = \frac{\rho_0 a_0 L(t)}{\mu_0}$
- Viscous shear layer thickness, thermal heat conduction layer thickness, and mass diffusion layer thickness grow as $\delta_{\mathrm{visc}} \approx \sqrt{\frac{\mu}{\rho} t}$, $\delta_{\mathrm{cond}} \approx \sqrt{\frac{k_{\mathrm{ref}}}{\rho c_v} t}$, $\delta_{\mathrm{mass,i}} \approx \sqrt{\frac{D_i}{\rho} t}$
- Only shock thickness not resolved $\longrightarrow$ "pseudo-DNS"
- Computations with WENO/CD/RK3 use SAMR base mesh 320 $\times$ 160 and up to 8 levels refined by factor 2, domain: $40\,\mathrm{mm} \times 20\,\mathrm{mm}$
- Computations with MUSCL scheme use base mesh 590 $\times$ 352 and up to 7 levels refined by factor 2, domain: $40\,\mathrm{mm} \times 22\,\mathrm{mm}$

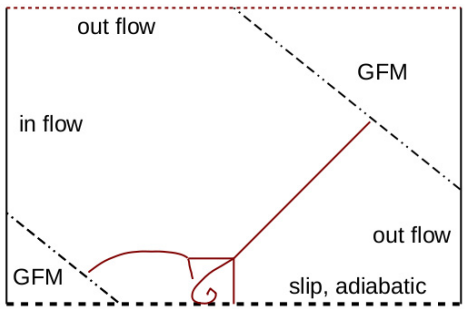

Setup

DNS of shear layer in detonation triple point

- Calorically perfect two-species model with $\gamma = 1.29499$ and $h_0 = 54,000\,\mathrm{J/mol}$ and one-step Arrhenius reaction with parameters $E_a = 30,000\,\mathrm{J/mol}$, $A = 6 \cdot 10^5\,\mathrm{s}^{-1}$, $W = 0.029\,\mathrm{kg/mol}$ $\longrightarrow$ 1d ZND theory predicts $d_{\mathrm{CJ}} = 1587.8\,\mathrm{m/s}$
- For dynamic viscosity, heat conductivity, and mass diffusion simple Sutherland models are used
- Distance $L(t) = d_{\mathrm{CJ}} \sin(\theta) t$ is used to define a Reynolds number as $\mathrm{Re} = \frac{\rho_0 a_0 L(t)}{\mu_0}$
- Viscous shear layer thickness, thermal heat conduction layer thickness, and mass diffusion layer thickness grow as $\delta_{\mathrm{visc}} \approx \sqrt{\frac{\mu}{\rho} t}$, $\delta_{\mathrm{cond}} \approx \sqrt{\frac{k_{\mathrm{ref}}}{\rho c_v} t}$, $\delta_{\mathrm{mass,i}} \approx \sqrt{\frac{D_i}{\rho} t}$
- Only shock thickness not resolved $\longrightarrow$ "pseudo-DNS"
- Computations with WENO/CD/RK3 use SAMR base mesh 320 $\times$ 160 and up to 8 levels refined by factor 2, domain: $40\,\mathrm{mm} \times 20\,\mathrm{mm}$
- Computations with MUSCL scheme use base mesh 590 $\times$ 352 and up to 7 levels refined by factor 2, domain: $40\,\mathrm{mm} \times 22\,\mathrm{mm}$

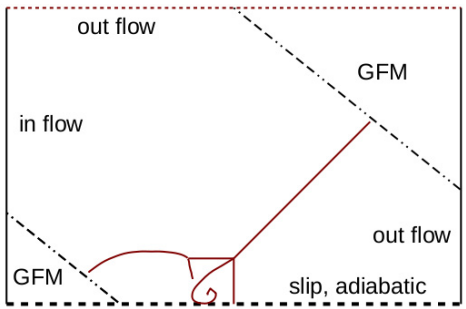

Setup

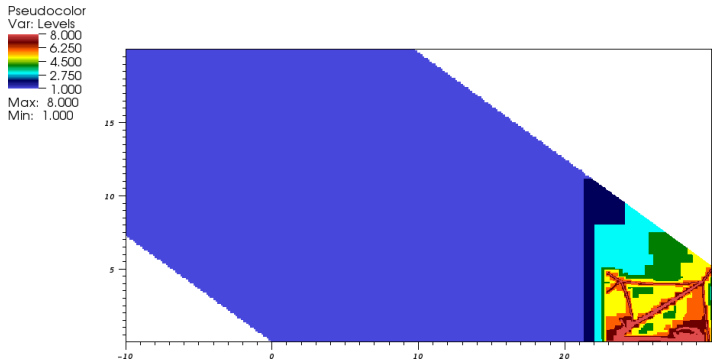

Refinement

DNS of shear layer in detonation triple point

- Calorically perfect two-species model with $\gamma = 1.29499$ and $h_0 = 54,000\,\mathrm{J/mol}$ and one-step Arrhenius reaction with parameters $E_a = 30,000\,\mathrm{J/mol}$, $A = 6 \cdot 10^5\,\mathrm{s}^{-1}$, $W = 0.029\,\mathrm{kg/mol}$ $\longrightarrow$ 1d ZND theory predicts $d_{\mathrm{CJ}} = 1587.8\,\mathrm{m/s}$
- For dynamic viscosity, heat conductivity, and mass diffusion simple Sutherland models are used
- Distance $L(t) = d_{\mathrm{CJ}} \sin(\theta) t$ is used to define a Reynolds number as $\mathrm{Re} = \frac{\rho_0 a_0 L(t)}{\mu_0}$
- Viscous shear layer thickness, thermal heat conduction layer thickness, and mass diffusion layer thickness grow as $\delta_{\mathrm{visc}} \approx \sqrt{\frac{\mu}{\rho} t}$, $\delta_{\mathrm{cond}} \approx \sqrt{\frac{k_{\mathrm{ref}}}{\rho c_v} t}$, $\delta_{\mathrm{mass,i}} \approx \sqrt{\frac{D_i}{\rho} t}$
- Only shock thickness not resolved $\longrightarrow$ "pseudo-DNS"
- Computations with WENO/CD/RK3 use SAMR base mesh 320 $\times$ 160 and up to 8 levels refined by factor 2, domain: $40\,\mathrm{mm} \times 20\,\mathrm{mm}$
- Computations with MUSCL scheme use base mesh 590 $\times$ 352 and up to 7 levels refined by factor 2, domain: $40\,\mathrm{mm} \times 22\,\mathrm{mm}$

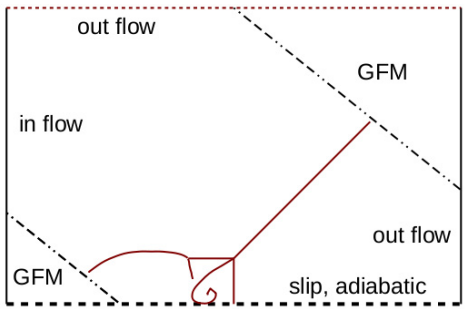

Setup

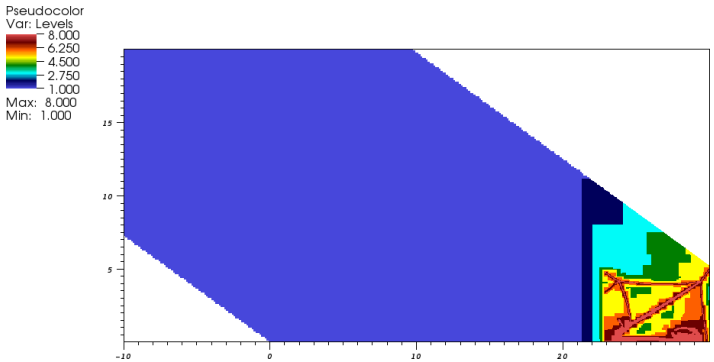

Refinement

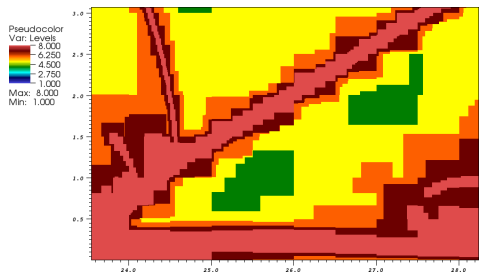

Enlarged

Computational results for shear layer

WENO/CD - 6 levels

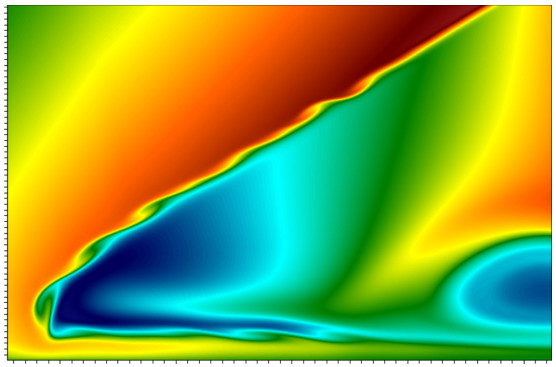

$\Delta x_{\min} = 3.91 \cdot 10^{-6}\,\mathrm{m}$

WENO/CD - 7 levels

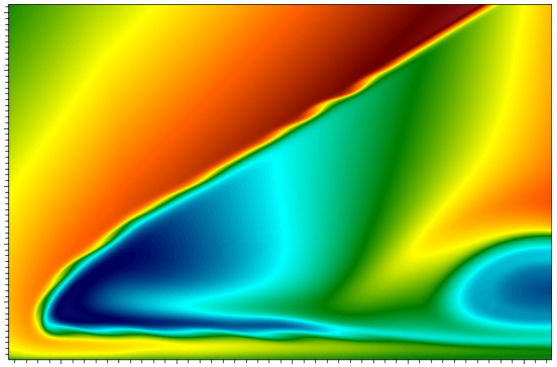

$\Delta x_{\min} = 1.95 \cdot 10^{-6}\,\mathrm{m}$

WENO/CD - 8 levels

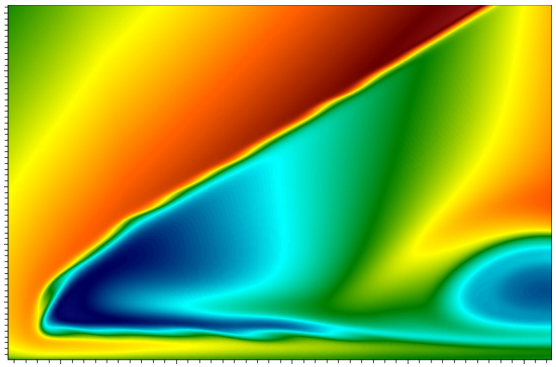

$\Delta x_{\min} = 9.77 \cdot 10^{-7}\,\mathrm{m}$

MUSCL - 7 levels

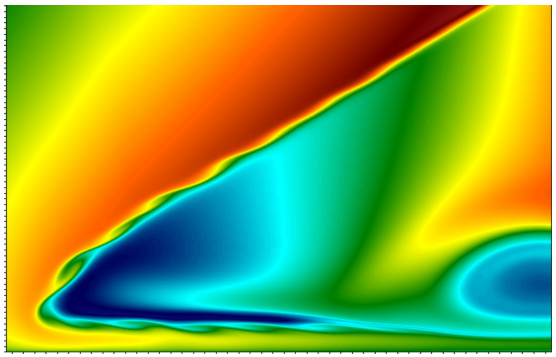

$\Delta x_{\min} = 1.05 \cdot 10^{-6}\,\mathrm{m}$

MUSCL - 7 levels - Euler

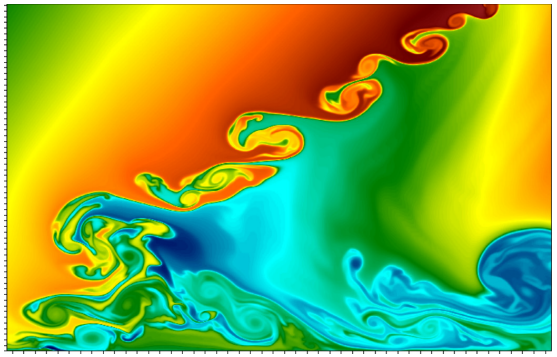

$\Delta x_{\min} = 1.05 \cdot 10^{-6}\,\mathrm{m}$

Usage of WENO for WENO/CD - 8 levels

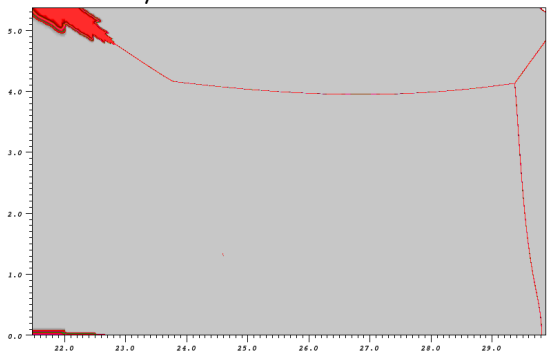

Computational results for shear layer

WENO/CD - 6 levels

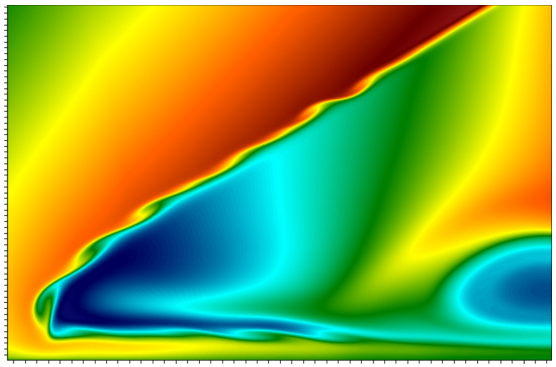

$\Delta x_{\min} = 3.91 \cdot 10^{-6}\,\mathrm{m}$

WENO/CD - 7 levels

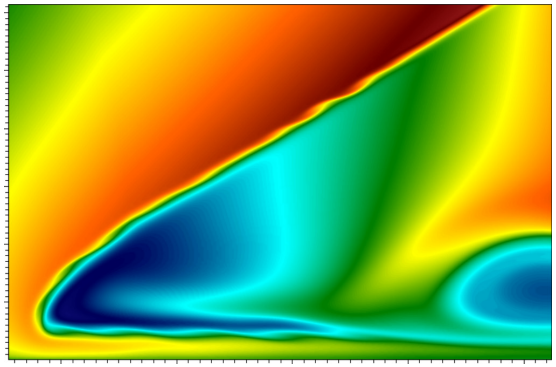

$\Delta x_{\min} = 1.95 \cdot 10^{-6}\,\mathrm{m}$

WENO/CD - 8 levels

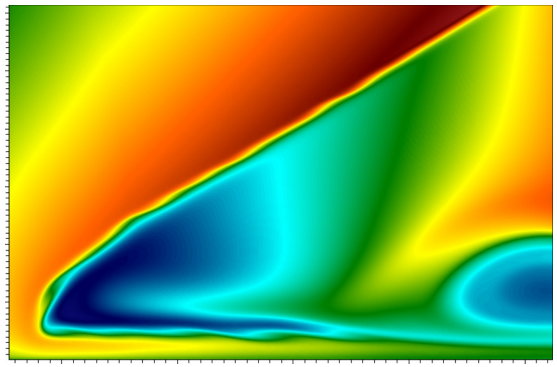

$\Delta x_{\min} = 9.77 \cdot 10^{-7}\,\mathrm{m}$

MUSCL - 7 levels

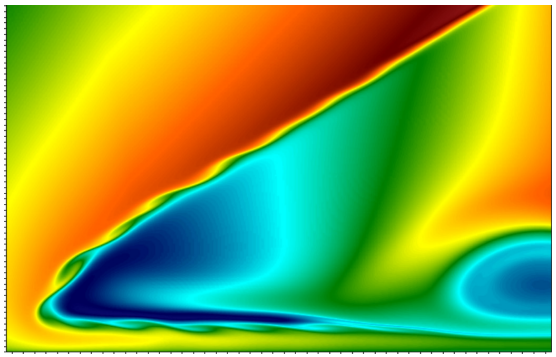

$\Delta x_{\min} = 1.05 \cdot 10^{-6}\,\mathrm{m}$

MUSCL - 7 levels - Euler

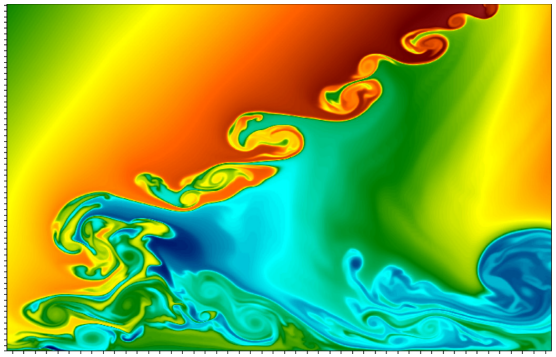

$\Delta x_{\min} = 1.05 \cdot 10^{-6}\,\mathrm{m}$

Usage of WENO for WENO/CD - 8 levels

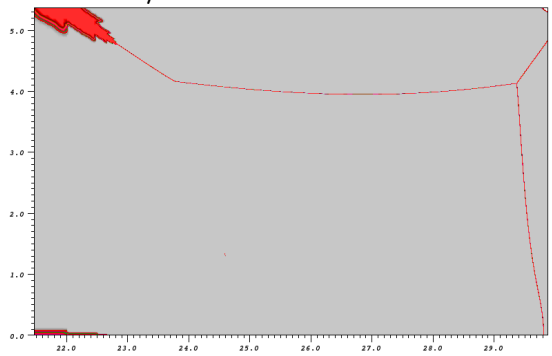

- WENO/CD/RK3 gives results comparable to 4x finer resolved optimal 2nd-order scheme, but CPU times with SAMR 2-3x larger

Computational results for shear layer

WENO/CD - 6 levels

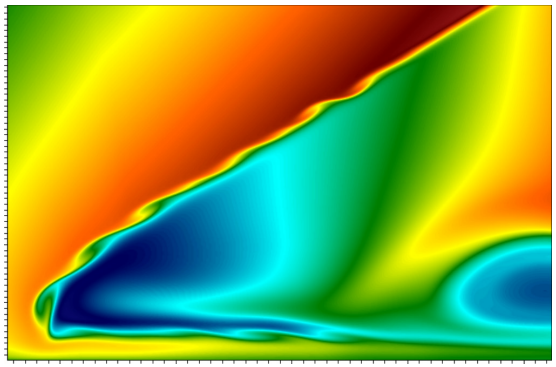

$\Delta x_{\min} = 3.91 \cdot 10^{-6}\,\mathrm{m}$

WENO/CD - 7 levels

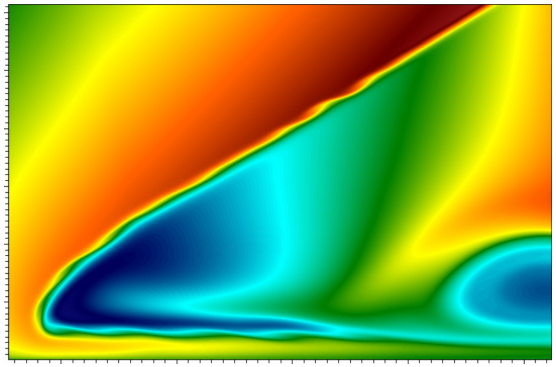

$\Delta x_{\min} = 1.95 \cdot 10^{-6}\,\mathrm{m}$

WENO/CD - 8 levels

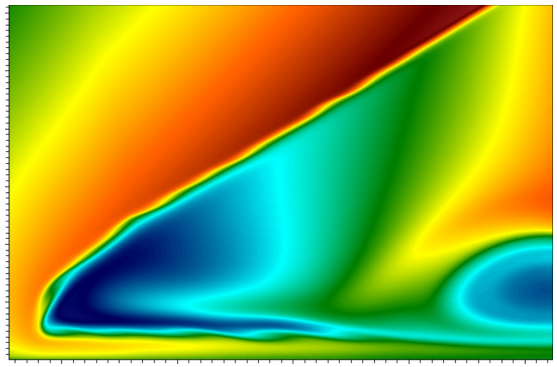

$\Delta x_{\min} = 9.77 \cdot 10^{-7}\,\mathrm{m}$

MUSCL - 7 levels

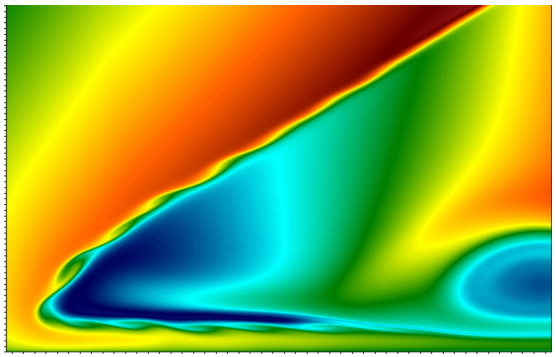

$\Delta x_{\min} = 1.05 \cdot 10^{-6}\,\mathrm{m}$

MUSCL - 7 levels - Euler

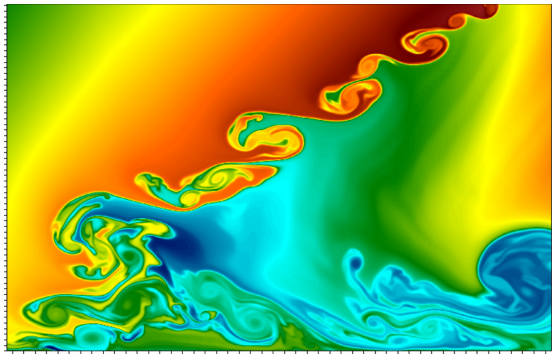

$\Delta x_{\min} = 1.05 \cdot 10^{-6}\,\mathrm{m}$

Usage of WENO for WENO/CD - 8 levels

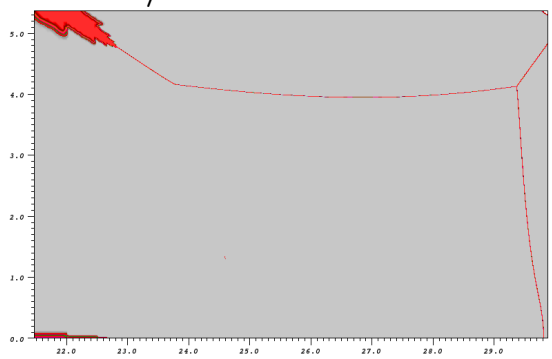

- WENO/CD/RK3 gives results comparable to 4x finer resolved optimal 2nd-order scheme, but CPU times with SAMR 2-3x larger
- Gain in CPU time from higher-order scheme roughly one order

Favre-averaged Navier-Stokes equations

$$\frac{\partial \bar{\rho}}{\partial t} + \frac{\partial}{\partial x_n}\left(\bar{\rho}\tilde{u}_n\right) = 0$$

$$\frac{\partial}{\partial t}\left(\bar{\rho}\tilde{u}_k\right) + \frac{\partial}{\partial x_n}\left(\bar{\rho}\tilde{u}_k\tilde{u}_n + \delta_{kn}\bar{p} - \tilde{\tau}_{kn} + \sigma_{kn}\right) = 0$$

$$\frac{\partial \bar{\rho}\bar{E}}{\partial t} + \frac{\partial}{\partial x_n}\left(\tilde{u}_n(\bar{\rho}\bar{E} + \bar{p}) + \tilde{q}_n - \tilde{\tau}_{nj}\tilde{u}_j + \sigma^e_n\right) = 0$$

$$\frac{\partial}{\partial t}\left(\bar{\rho}\tilde{Y}_i\right) + \frac{\partial}{\partial x_n}\left(\bar{\rho}\tilde{Y}_i\tilde{u}_n + \tilde{J}^i_n + \sigma^i_n\right) = 0$$

with stress tensor

$$\tilde{\tau}_{kn} = \tilde{\mu}\left(\frac{\partial \tilde{u}_n}{\partial x_k} + \frac{\partial \tilde{u}_k}{\partial x_n}\right) - \frac{2}{3}\tilde{\mu}\frac{\partial \tilde{u}_j}{\partial x_j}\delta_{in}\ ,$$

heat conduction

$$\tilde{q}_n = -\tilde{\lambda}\frac{\partial \tilde{T}}{\partial x_n}\ ,$$

Favre-averaged Navier-Stokes equations

$$\frac{\partial \bar{\rho}}{\partial t} + \frac{\partial}{\partial x_n}\left(\bar{\rho}\tilde{u}_n\right) = 0$$

$$\frac{\partial}{\partial t}\left(\bar{\rho}\tilde{u}_k\right) + \frac{\partial}{\partial x_n}\left(\bar{\rho}\tilde{u}_k\tilde{u}_n + \delta_{kn}\bar{p} - \tilde{\tau}_{kn} + \sigma_{kn}\right) = 0$$

$$\frac{\partial \bar{\rho}\bar{E}}{\partial t} + \frac{\partial}{\partial x_n}\left(\tilde{u}_n(\bar{\rho}\bar{E} + \bar{p}) + \tilde{q}_n - \tilde{\tau}_{nj}\tilde{u}_j + \sigma^e_n\right) = 0$$

$$\frac{\partial}{\partial t}\left(\bar{\rho}\tilde{Y}_i\right) + \frac{\partial}{\partial x_n}\left(\bar{\rho}\tilde{Y}_i\tilde{u}_n + \tilde{J}^i_n + \sigma^i_n\right) = 0$$

with stress tensor

$$\tilde{\tau}_{kn} = \tilde{\mu}\left(\frac{\partial \tilde{u}_n}{\partial x_k} + \frac{\partial \tilde{u}_k}{\partial x_n}\right) - \frac{2}{3}\tilde{\mu}\frac{\partial \tilde{u}_j}{\partial x_j}\delta_{in}\ ,$$

heat conduction

$$\tilde{q}_n = -\tilde{\lambda}\frac{\partial \tilde{T}}{\partial x_n}\ ,$$

and inter-species diffusion

$$\tilde{J}^i_n = -\bar{\rho}\tilde{D}_i\frac{\partial \tilde{Y}_i}{\partial x_n}$$

Favre-averaged Navier-Stokes equations

$$\frac{\partial \bar{\rho}}{\partial t} + \frac{\partial}{\partial x_n}\left(\bar{\rho}\tilde{u}_n\right) = 0$$

$$\frac{\partial}{\partial t}\left(\bar{\rho}\tilde{u}_k\right) + \frac{\partial}{\partial x_n}\left(\bar{\rho}\tilde{u}_k\tilde{u}_n + \delta_{kn}\bar{p} - \tilde{\tau}_{kn} + \sigma_{kn}\right) = 0$$

$$\frac{\partial \bar{\rho}\bar{E}}{\partial t} + \frac{\partial}{\partial x_n}\left(\tilde{u}_n(\bar{\rho}\bar{E} + \bar{p}) + \tilde{q}_n - \tilde{\tau}_{nj}\tilde{u}_j + \sigma^e_n\right) = 0$$

$$\frac{\partial}{\partial t}\left(\bar{\rho}\tilde{Y}_i\right) + \frac{\partial}{\partial x_n}\left(\bar{\rho}\tilde{Y}_i\tilde{u}_n + \tilde{J}^i_n + \sigma^i_n\right) = 0$$

with stress tensor

$$\tilde{\tau}_{kn} = \tilde{\mu}\left(\frac{\partial \tilde{u}_n}{\partial x_k} + \frac{\partial \tilde{u}_k}{\partial x_n}\right) - \frac{2}{3}\tilde{\mu}\frac{\partial \tilde{u}_j}{\partial x_j}\delta_{in}\ ,$$

heat conduction

$$\tilde{q}_n = -\tilde{\lambda}\frac{\partial \tilde{T}}{\partial x_n}\ ,$$

and inter-species diffusion

$$\tilde{J}^i_n = -\bar{\rho}\tilde{D}_i\frac{\partial \tilde{Y}_i}{\partial x_n}$$

Favre-filtering

$$\tilde{\phi} = \frac{\overline{\rho\phi}}{\bar{\rho}} \quad \text{with} \quad \bar{\phi}(\mathbf{x}, t; \Delta_c) = \int_\Omega G(\mathbf{x} - \mathbf{x}'; \Delta_c)\phi(\mathbf{x}', t)d\mathbf{x}'$$

Numerical solution approach

- Subgrid terms σ_{kn}, σ_n^e, σ_n^i are computed by Pullin's stretched-vortex model

Numerical solution approach

- Subgrid terms σ_{kn}, σ_n^e, σ_n^i are computed by Pullin's stretched-vortex model
- Cutoff Δ_c is set to local SAMR resolution Δx_l

Numerical solution approach

- Subgrid terms σ_{kn}, σ_n^e, σ_n^i are computed by Pullin's stretched-vortex model
- Cutoff Δ_c is set to local SAMR resolution Δx_l
- It remains to solve the Navier-Stokes equations in the hyperbolic regime
  - 3rd order WENO method (hybridized with a tuned centered difference stencil) for convection
  - 2nd order conservative centered differences for diffusion

Numerical solution approach

- Subgrid terms σ_{kn}, σ_n^e, σ_n^i are computed by Pullin's stretched-vortex model
- Cutoff Δ_c is set to local SAMR resolution Δx_l
- It remains to solve the Navier-Stokes equations in the hyperbolic regime
  - 3rd order WENO method (hybridized with a tuned centered difference stencil) for convection
  - 2nd order conservative centered differences for diffusion

Example: Cylindrical Richtmyer-Meshkov instability

- Sinusoidal interface between two gases hit by shock wave
- Objective is correctly predict turbulent mixing
- Embedded boundary method used to regularize apex
- AMR base grid $95 \times 95 \times 64$ cells, $r_{1,2,3} = 2$
- $\sim 70,000\,\mathrm{h}$ CPU on 32 AMD 2.5GHZ-quad-core nodes

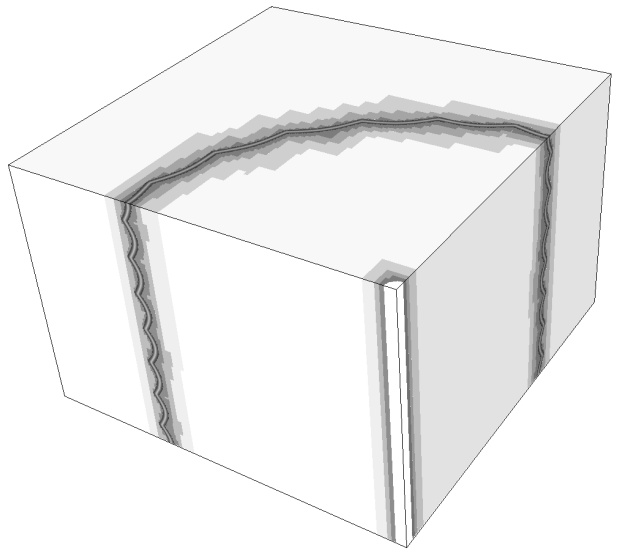

Planar Richtmyer-Meshkov instability

- Perturbed Air-SF6 interface shocked and re-shocked by Mach 1.5 shock
- Containment of turbulence in refined zones
- 96 CPUs IBM SP2-Power3
- WENO-TCD scheme with LES model
- AMR base grid $172 \times 56 \times 56$, $r_{1,2} = 2$, $10\,\mathrm{M}$ cells in average instead of $3\,\mathrm{M}$ (uniform)

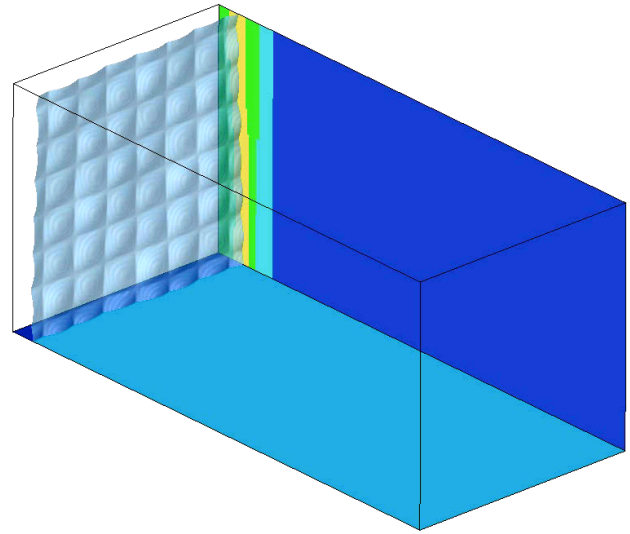

Task	2ms (%)	5ms (%)	10ms (%)
Integration	45.3	65.9	52.0
Boundary setting	44.3	28.6	41.9
Flux correction	7.2	3.4	4.1
Interpolation	0.9	0.4	0.3
Reorganization	1.6	1.2	1.2
Misc.	0.6	0.5	0.5
Max. imbalance	1.25	1.23	1.30

vtf/amroc/weno/applications/euler/3d/RM_AirSF6

Planar Richtmyer-Meshkov instability

- Perturbed Air-SF6 interface shocked and re-shocked by Mach 1.5 shock
- Containment of turbulence in refined zones
- 96 CPUs IBM SP2-Power3
- WENO-TCD scheme with LES model
- AMR base grid $172 \times 56 \times 56$, $r_{1,2} = 2$, $10\,\mathrm{M}$ cells in average instead of $3\,\mathrm{M}$ (uniform)

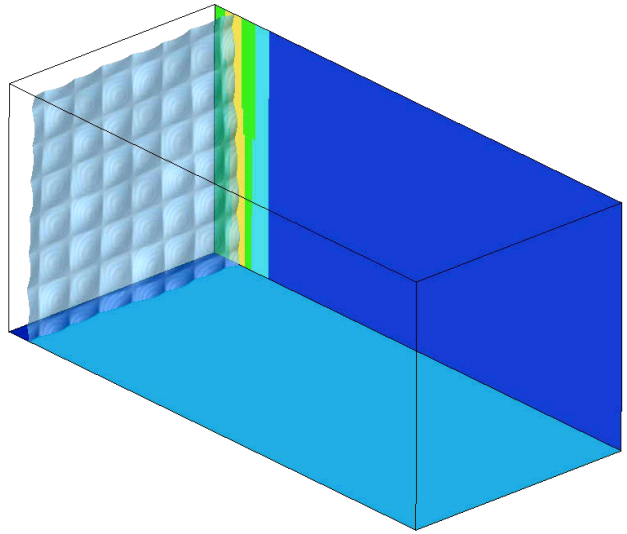

Task	2ms (%)	5ms (%)	10ms (%)
Integration	45.3	65.9	52.0
Boundary setting	44.3	28.6	41.9
Flux correction	7.2	3.4	4.1
Interpolation	0.9	0.4	0.3
Reorganization	1.6	1.2	1.2
Misc.	0.6	0.5	0.5
Max. imbalance	1.25	1.23	1.30

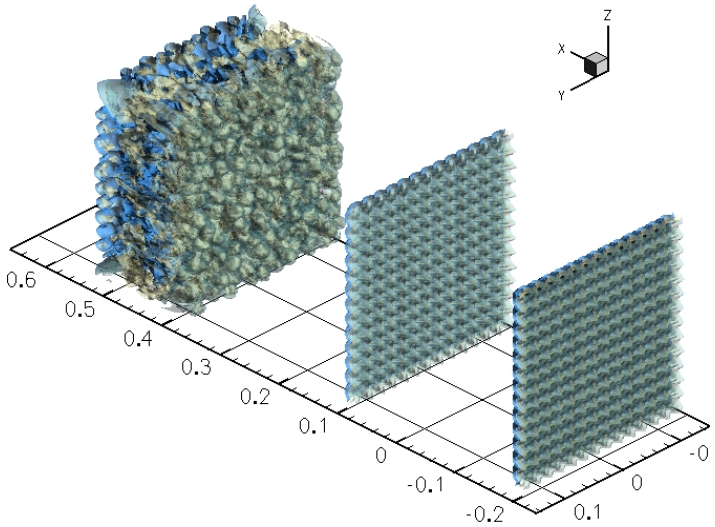

vtf/amroc/weno/applications/euler/3d/RM_AirSF6

References I

[Axdahl et al., 2011] Axdahl, E., Kumar, A., and Wilhite, A. (2011). Study of unsteady, sphere-driven, shock-induced combustion for application to hypervelocity airbreathing propulsio. In *Proc. 47th AIAA/ASME/SAE/SAEE Joint Propulsion Conference & Exhibit*.

[Ben-Dor, 2007] Ben-Dor, G. (2007). *Shock wave reflection phenomena*. Springer-Verlag, Berlin, Heidelberg, 2nd edition.

[Deiterding, 2011] Deiterding, R. (2011). High-resolution numerical simulation and analysis of Mach reflection structures in detonation waves in low-pressure $\mathrm{h_2} : \mathrm{o_2} : \mathrm{ar}$ mixtures: a summary of results obtained with adaptive mesh refinement framework AMROC. *J. Combustion*, 2011:738969.

[Hill and Pullin, 2004] Hill, D. J. and Pullin, D. I. (2004). Hybrid tuned center difference - WENO method for large eddy simulations in the presence of strong shocks. *J. Comput. Phys.*, 194(2):435–450.

[Jachimowski, 1988] Jachimowski, C. J. (1988). An analytical study of the hydrogen-air reaction mechanism with application to scramjet combustion. Technical Report TP-2791, NASA.

References II

[Lehr, 1972] Lehr, H. F. (1972). Experiments on shock-induced combustion. *Astronautica Acta*, 17:589–597.

[Pantano et al., 2007] Pantano, C., Deiterding, R., Hill, D. J., and Pullin, D. I. (2007). A low-numerical dissipation patch-based adaptive mesh refinement method for large-eddy simulation of compressible flows. *J. Comput. Phys.*, 221(1):63–87.

[Yungster and Radhakrishnan, 1996] Yungster, S. and Radhakrishnan, K. (1996). A fully implicit time accurate method for hypersonic combustion: application to shock-induced combustion instability. *Shock Waves*, 5:293–303.

[Ziegler et al., 2011] Ziegler, J. L., Deiterding, R., Shepherd, J. E., and Pullin, D. I. (2011). An adaptive high-order hybrid scheme for compressive, viscous flows with detailed chemistry. *J. Comput. Phys.*, 230(20):7598–7630.